TAL TECH

DOCTORAL THESIS

Accelerated Carbonation of Ca-rich Fly Ashes in Non-Cement Applications

Mustafa Cem Usta

TALLINNA TEHNIKAÜLIKOOL
TALLINN UNIVERSITY OF TECHNOLOGY
TALLINN 2023

TALLINN UNIVERSITY OF TECHNOLOGY
DOCTORAL THESIS
63/2023

Accelerated Carbonation of Ca-rich Fly Ashes in Non-Cement Applications

MUSTAFA CEM USTA

TAL TECH PRESS

TALLINN UNIVERSITY OF TECHNOLOGY
School of Engineering
Department of Materials and Environmental Technology
Laboratory of Inorganic Materials
This dissertation was accepted for the defence of the degree 23/10/2023

Supervisor:
Mai Uibu, PhD
School of Engineering
Tallinn University of Technology
Tallinn, Estonia

Co-supervisor:
Can Rüştü Yörük, PhD
School of Engineering
Tallinn University of Technology
Tallinn, Estonia

Opponents:
Associate Professor Päivö Kinnunen
Faculty of Technology
University of Oulu
Oulu, Finland

Professor Kalle Kirsimäe
Institute of Ecology and Earth Sciences
Department of Geology
University of Tartu
Tartu, Estonia

Defence of the thesis: 12/12/2023, Tallinn

Declaration:
Hereby I declare that this doctoral thesis, my original investigation and achievement, submitted for the doctoral degree at Tallinn University of Technology has not been submitted for doctoral or equivalent academic degree.

Mustafa Cem Usta

---
signature

European Union
European Regional
Development Fund

Investing
in your future

ISSN 2585-6898 (publication)
ISBN 978-9916-80-067-6 (publication)
ISSN 2585-6901 (PDF)
ISBN 978-9916-80-068-3 (PDF)
Printed by Koopia Niini & Rauam

TALLINNA TEHNIKAÜLIKOOL
DOKTORITÖÖ
63/2023

Kaltsiumirikka lendtuha kiirendatud karboniseerimine tsemendivabades rakendustes

MUSTAFA CEM USTA

TAL TECH
KIRJASTUS

Contents

List of publications

The list of author's publications, on the basis of which the thesis has been prepared:

I Usta, M. C., Yörük, C. R., Hain, T., Paaver, P., Snellings, R., Rozov, E., Gregor, A., Kuusik, R., Trikkel, A. & Uibu, M. (2020). Evaluation of new applications of oil shale ashes in building materials. *Minerals*, *10*(9), 765.

II Usta, M. C., Yörük, C. R., Uibu, M., Hain, T., Gregor, A., & Trikkel, A. (2022). CO_2 Curing of Ca-Rich Fly Ashes to Produce Cement-Free Building Materials. *Minerals*, *12*(5), 513.

III Usta, M. C., Yörük, C. R., Uibu, M., Traksmaa R., Hain, T., Gregor, A., & Trikkel, A. (2023) Carbonation and Leaching Behaviors of Cement-free Monoliths Based on High Sulphur Fly Ashes with Incorporation of Amorphous Calcium Aluminate. *ACS Omega* (accepted for publication).

Closely related publications and international conferences:

1. Yörük, C. R., Uibu, M., Usta, M. C., Kaljuvee, T., & Trikkel, A. (2020). CO_2 mineralization by burnt oil shale and cement bypass dust: effect of operating temperature and pre-treatment. *Journal of Thermal Analysis and Calorimetry*, *142*, 991–999. https://doi.org/10.1007/s10973-020-09349-9
2. Usta, M. C., Adegbile, A. M., Gregor, A., Paaver, P., Hain, T., Yörük, C. R., Uibu, M., & Trikkel, A. (2021). Performance evaluation of flue gas cured calcium rich fly ash based building blocks. *Proceedings of the 17th International Conference on Environmental* Science and Technology CEST2021. Springer. https://doi.org/10.30955/gnc2021.00333
3. Yörük, C. R., Usta, M. C., Uibu, M., Kaljuvee, T., & Trikkel, A. (2020, February). CO_2 mineralization by burnt oil shale and cement bypass dust: Effect of operating temperature and pre-treatment. *Graduate School of Functional Materials and Technologies Scientific Conference 2020*. Park Inn by Radisson Meriton Conference Spa Hotel, Tallinn.
4. Usta, M. C., Uibu, M., Yörük, C. R., Tamm, K., Kuusik, R., Trikkel, A., Gastaldi, D., & Canonico, F. (2021). Mineral sequestration of CO_2 from Vernasca Ca-looping demo system: Scale up to a pilot. *SSRN Electronic Journal*, 1–12. https://doi.org/10.2139/ssrn.3812245
5. Uibu, M., Usta, M. C., Tamm, K., Žuravljova, A., Kallas, J., Kuusik, R., & Trikkel, A. (2018, October). Mineral trapping of CO_2 for cement industry de-carbonization. In *Proceedings* of the 14th Greenhouse Gas Control Technologies Conference Melbourne (pp. 21–26).
6. Usta, M. C., Gregor, A., Hain, T., Yörük, C. R., Uibu, M., & Trikkel, A. (2021, May). Storage and use of CO_2 in oil shale ash based lightweight building materials. *International Conference on Accelerated Carbonation for Environmental and Material Engineering (ACEME)*.
7. Usta, M. C., Uibu, M., Yörük, C. R., Tamm, K., Kuusik, R., Trikkel, A., Gastaldi, D., & Canonico, F. (2021, May). Towards construction of CO_2 mineralization pilot in Vernasca cement plant. *International Conference on Accelerated Carbonation for Environmental and Material Engineering (ACEME)*.

Author's contribution to the publications

Contribution to the papers in this thesis are:

I The author contributed to the experiments, provided an interpretation of the results, and made minor contributions to the experimental setup.

II Designing and executing sophisticated experimental protocols, providing a nuanced interpretation of the derived data, and assuming a principal role in the scholarly composition of findings.

III Designing and executing sophisticated experimental protocols, providing a nuanced interpretation of the derived data, and assuming a principal role in the scholarly composition of findings.

Acknowledgements

I want to thank my supervisors, Mai Uibu and Can Rüştü Yörük, for their support, constructive feedback, and continued guidance, which made this thesis possible. I also wish to extend my gratitude to Can Rüştü Yörük, who, in addition to being my co-supervisor, has been my mentor throughout my PhD journey. Naturally, this work would not have been possible without the ongoing support from the rest of my colleagues at the Laboratory of Inorganic Materials. This research is funded by the CLEANKER project, which has received funding from the European Union's Horizon 2020 Framework Program under Grant Agreement No. 764816, and the Government of China (National Natural Science Foundation of China) under contract Nos. 91434124 and 51376105. This work is also partially supported by ASTRA's "TUT Institutional Development Program for 2016-2022," the Graduate School of Functional Materials and Technologies, and the Estonian Ministry of Education and Research (IUT33-19). Lastly, I want to thank my partner and family for continuously motivating me with words and acts of kindness throughout my studies. This thesis is dedicated to the memory of my father, who, above all, taught me the value of perseverance.

INTRODUCTION

One of the main greenhouse gases (GHG) released into the atmosphere by human activities, such as the burning of fossil fuels, is carbon dioxide (CO_2). In the last 170 years, highly concentrated anthropogenic activities have led to an atmospheric CO_2 concentration increase of over 47% since the pre-industrial levels of the 1850s (IPCC, 2019). Although the international community has already made significant efforts to mitigate the effects and reduce GHG emissions (Bodansky et al., 2015; Vicedo-Cabrera et al., 2018), the financial market continues to invest in fossil fuels. The continuous use of fossil fuels is predicted to increase by 2% annually until 2030, which would significantly increase the mitigating effort needed to keep global warming to 1.5 °C or below 2 °C (UNEP, 2020). One of the most important sectors in terms of CO_2 emissions is construction and cement industry. Cement companies are seeking for ways to employ more alternative cementitious substances without sacrificing performance and durability to meet the rising demand for cement and concrete and, at the same time, minimize CO_2 emissions and the depletion of primary resources. By 2050, if no measures are implemented, contribution of cement sector to world CO_2 emissions is anticipated to rise significantly from 6–7% to 25% or more (Provis et al., 2014).

In this context of today's scenario, it is critically important to develop not only alternative energy technologies but also technologies that will reduce existing and future anthropogenic CO_2 emissions. One such measure, advocated by the Intergovernmental Panel on Climate Change (IPCC, 2019) is the development of carbon capture and storage technologies (CCS). CCS technologies can be classified based on the capture processes which include pre-combustion, post-combustion, oxy-fuel combustion, and chemical looping. Post-combustion capture integrated with CO_2 utilization and storage include in-situ and ex-situ mineral carbonation technologies. In-situ mineral carbonation refers to geological CO_2 storage which is considered to be the most widely accepted large scale storage method (Garcia et al., 2010). In which, CO_2 can be stored in deep coal beds, saline aquifers as well as oil and gas reservoirs (Chiaramonte et al., 2011). However, In-situ storage has certain drawbacks and risks which include possibility of leakage and therefore requirement of accurate assessment of the capacity of the geological formation to store CO_2 and constant monitoring of injected CO_2. Moreover, finding suitable geological storage sites in every country can be very challenging (Zhang et al., 2017). Comparatively, ex-situ carbonation utilizing industrial alkaline solid wastes (IASW), incorporates CO_2 storage through chemical processes above ground between CO_2 and alkaline earth metals such as calcium and magnesium that exist in solid industrial residues (coal ash, oil shale ash, steel slags, cement kiln dust, wood ash). An important advantage of ex-situ IASW carbonation is that it tackles the problem of proper disposal and/or recycling of these potentially harmful industrial byproducts while providing avenues for value-added carbonate products which can be utilized in diverse industrial applications such as polymers, plastics, construction materials, adhesives (Eloneva et al., 2008).

The above-mentioned ex-situ mineral carbonation technology is particularly important in the context of Estonia. Energy sector in Estonia is primarily dependent on domestically extracted oil shale, followed by biofuels -primarily wood chips and marginal renewable resources and other fossil fuels. This heavy use of oil shale together with biomass as combustion fuel results in a considerable amount of CO_2 emission and the generation of potentially harmful ashes which requires safe disposal and taxation. Latest reports show that power generation using circulating fluidized bed (CFB) combustion creates a waste

ash stream changing between 3.5 to 7.2 million tons per year (Eesti Energia, 2021). It is known that these ashes having pozzolanic and latent hydraulic binding properties can be stabilized through accelerated carbonation (Kirsimäe et al, 2021; Uibu et al, 2016).

This study is of significant academic importance as it aligns directly with contemporary policy objectives regarding the utilization of industrial alkaline waste and global initiatives aimed at sequestering CO_2. It contributes to the reduction of harmful waste disposal, which is a key goal of the updated Estonian Environmental Strategy 2040. Additionally, the research supports mitigation efforts in the face of escalating climate change concerns. These efforts are a major component of recent global and regional commitments, including the Glasgow Climate Pact and the enhanced Paris Agreement from 2021, as well as the European Green Deal rolled out by the European Commission in 2021. Moreover, this study reinforces the EU's ambition to lead the transition towards a Circular Economy, as outlined in the New Circular Economy Action Plan from 2023.

In conclusion, the innovation of this doctoral research lies in its successful demonstration of the potential to upcycle oil shale fly ash, wood fly ash, and landfilled ash to produce fly ash based monoliths solidified via accelerated carbonation method. This study not only offers a feasible route for the utilization of fly ashes, but it also provides crucial insights into carbonation and leaching behaviours of ashes with encouraging results on immobilization of sulphates and heavy metals. This research therefore contributes significantly to the field, highlighting innovative waste management practices, while addressing pertinent environmental challenges.

LIST OF ABBREVIATIONS

CCUS	Carbon capture utilization and storage
CCS	Carbon capture and storage
CFBC	Circulating fluidized bed combustion
PF	Pulverized firing
FG	Flue gas
OSA	Oil shale fly ash
WA	Wood fly ash
LFA	Landfilled ash
NS	Niobium slag
XRD	X-ray diffraction
XRF	X-ray fluorescence
LOI	Loss on ignition
SEM	Scanning electron microscope
SSA	Specific surface area
BET	Absorption theory by S. Brunauer, P. H. Emmet and E. Teller
MIP	Mercury intrusion porosimetry
EDS	Energy Dispersive X-ray Spectroscopy
C2S	Dicalcium silicate
C3S	Tricalcium silicate
C3A	Tricalcium aluminate
C4AF	Tetra-calcium aluminoferrite
CSH	Calcium silicate hydrate
CAH	Calcium aluminate hydrate
CASH	Calcium aluminate silicate hydrate
CAS	Calcium aluminate sulphate
AFt	Ettringite
AFm	Monosulphate

1 LITERATURE OVERVIEW

Fossil fuels remain the primary global energy source, comprising over 80% of energy consumption (Hassan et al., 2021). Despite the growth in renewable energy, fossil fuel consumption has also risen, with energy from these sources increasing from 116,214 to 136,761 TWh in a decade. This reliance has escalated environmental concerns, notably CO_2 emissions from combustion of fossil fuels. In 2022, CO_2 emissions reached a record 36.8 Gt, a 0.9% increase (International Energy Agency [IEA], 2023), with over half from power and industrial sectors. Atmospheric CO_2 levels have surged from 280 ppm in 1750 to 420 ppm in 2022, largely due to increased fossil fuel use (National Oceanic and Atmospheric Administration, 2023). As a significant GHG, CO_2 intensifies climate change challenges, with potential impacts like melting ice caps, extreme weather events, and rising sea levels. The IPCC underscores the need to limit global warming to 2°C to prevent catastrophic outcomes (IPCC, 2021). With expected growth in global energy demand, relying solely on energy efficiency, renewable and nuclear sources, and afforestation will not sufficiently address GHG emission challenges.

Carbon capture utilization and storage (CCUS) is pivotal for reducing CO_2 emissions, but its energy demands can decrease power plant efficiency and increase fuel use. A study estimates capture costs at US$50-US$65 per ton CO_2 for specific coal power plants (Economic Research Institute for ASEAN, 2022). While CCUS is prevalent in industries like fertilizer production and natural gas processing, its adoption in sectors like steel and construction is nascent. Given limited alternatives, CCUS is vital for these sectors to curb emissions. Effective CO_2 reduction via CCUS requires long-term storage post-capture. One promising method is mineral carbonation of industrial solid residues. The annual production of alkaline solid waste from industries like coal power, cement, and steel is rising, often with environmental risks and CO_2 emissions. Yet, these residues can chemically bind CO_2, enabling ex-situ CO_2 mineralization, stabilizing waste, and repurposing them in construction, reducing raw material extraction. Despite proposed regulations and technologies, a significant CO_2 reduction breakthrough remains elusive. Challenges like energy use, transport costs, and environmental impacts must be tackled for CCUS to be a sustainable climate change solution.

This literature review delves specifically into the intersection of mineral carbonation and waste utilization, with a primary focus on their potential applications in building materials. While the broader realm of CCS encompasses a myriad of concepts and mineralization processes, this review narrows its scope to the utilization of industrial alkaline solid residues (mainly fly ash) in mineral carbonation. The aim is to understand how these residues, often viewed as waste, can be repurposed through mineral carbonation to create sustainable building materials. This targeted exploration is central to the thesis work, ensuring a comprehensive understanding of this niche within the larger CCS landscape.

1.1 Mineral carbonation

Mineral carbonation, also known as mineral CO_2 sequestration, is a method that aims to reduce CO_2 emissions by chemically transforming CO_2 into a thermodynamically stable product. This technique relies on the natural reaction between CO_2 and minerals containing metal oxides, forming insoluble carbonates (Aresta et al., 2019). Magnesium, iron, and calcium are the most commonly used elements in mineral carbonation processes due to their abundance in the Earth's crust and easy extraction from industrial

waste (Thonemann et al., 2022). The products generated through mineral carbonation can be commercialized, which helps reduce process costs. Since the 1990s, when mineral carbonation for CO_2 disposal was first proposed, various efforts have been made towards commercialization in relation to CCS schemes (Board, 2019).

Carbonation reactions (Eq. (1)) can occur either underground (in-situ) or above ground (ex-situ):

$$MO + CO_2 \rightarrow MCO_3 + \Delta H \quad (M: \text{alkaline earth metal}) \tag{1}$$

Because a carbon atom in a carbonate is in its lowest energy state, the carbonate reaction product is stable throughout geological timeframes. As a result, the carbonation reaction is exothermic, with the surplus energy (60–180 kJ/mol depending on the mineral reactant) being emitted as heat (Ellis et al., 2023).

In-situ mineral carbonation, also known as managed weathering or mineral trapping, is an accelerated weathering process (Hills et al., 2020). Natural rock formations containing silicates are considered the most suitable for in-situ mineral carbonation. In-situ reactions with silicate rocks can be represented as follows (Eq. (2)):

$$(Ca,Mg)SiO_3\ (s) + CO_2\ (g) \rightarrow (Ca,Mg)CO_3\ (s) + SiO_2\ (s) \tag{2}$$

Solid carbonates in nature can form through the weathering of serpentine ($Mg_3Si_2O_5(OH)$) or olivine (Mg_2SiO_4). This process involves the formation of carbonic acid via the dissolution and ionization of CO_2 in groundwater or rain, which subsequently breaks down into bicarbonate and hydrogen ions. Magnesium and calcium-bearing minerals can be broken down by bicarbonate, which acts as an acid buffer and forms magnesium or calcium carbonates. Weathering-induced carbonate formation binds around 300 million tons of CO_2 gas from the atmosphere (Baciocchi et al., 2022).

Ex-situ mineral carbonation is an above-ground process that uses mined alkaline minerals containing calcium or magnesium, such as olivine, serpentine, and wollastonite, or alkaline industrial residues like cement production residues, coal fly ash, wood (biomass) ash, steel slags, and construction waste (Rahmanihanzaki et al., 2022; Gerdemann et al., 2007). Although ex-situ carbonation processes may have high energy demands due to the solid reactant pre-treatment or activation, transport, mining, and usage of catalysts, the cost-effective techniques are always necessary (IPCC, 2021). Besides ex situ mineral carbonation is particularly important for closing the material loop in industrial production by chemically stabilizing industrial alkaline residues, which are typically disposed of in landfills (Wang et al., 2018). This method creates new opportunities for valorising industrial by-products while mitigating some of the environmental damage caused by industrial production. It is also a feasible option specifically for small and medium CO_2 emission sources where other CCS options are not available (Azdarpour et al., 2015).

The main routes through which the accelerated carbonation process occurs are as follows: first, dissolution of calcium hydroxide on the particle's surface; second, boundary layer influences, which involve the diffusion of particles across precipitation layers; third, transport mechanisms, which involve the movement of CO_2 and Ca^{2+} to and from the reaction sites; and fourth, pore-clogging and precipitation layers (Li et al., 2022). The slower conversion rate resulting from the waste's complex chemical composition is a key barrier to using industrial waste for extensive carbonation as well as utilization (Lu et al., 2022).

Currently, no comprehensive inventory of industrial alkaline streams exists that can serve as feedstock for ex-situ mineral carbonation as the technology is not widely utilized around the world yet (Yadav et al., 2021) While there are abundant natural silicate minerals worldwide that could be used for mineral carbonation, utilizing them for energy-intensive mineral carbonation processes is not yet feasible (Sanna et al., 2016).

1.1.1 Direct carbonation

Direct mineral carbonation can be classified into two categories based on different application methods: gas-solid carbonation and aqueous carbonation. Exemplary summary of ex-situ carbonation routes is shown as a diagram in figure 1 adapted from Azdarpour et al. (2015). Direct gas-solid carbonation, one of the least energy-intensive forms of mineral carbonation, has been studied with both natural minerals and industrial residues (Winnefeld et al., 2022; Song et al., 2019; Mazzella et al.,2016).

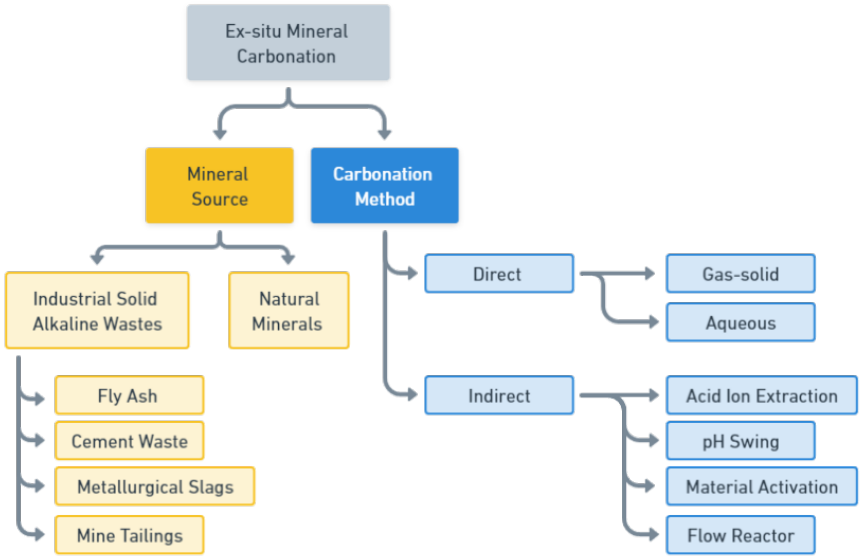

Figure 1. Diagram of ex-situ mineral carbonation routes.

Gas solid carbonation

Direct gas-solid carbonation is one of the most fundamental applications of mineral carbonation (Kusin et al., 2023; Saran et al., 2018). In theory, the formation of stable carbonates through the direct interaction between CO_2 gas and Ca and Mg-bearing minerals takes advantage of the energy released from the exothermic reaction (Woodall et al., 2019). Various reactions can occur depending on the available feedstock. Although some researchers have suggested that research in this area has not been as fruitful as they imagined due to costs and slow reaction kinetics (Moon et al., 2019; Monkman et al., 2006), modified applications continue to be developed. The direct gas-solid carbonation route using municipal solid waste fly ash is described by Eq. (3) and (4), which shows the overall carbonation chemistry (Gu et al., 2021).

$$Ca(OH)_2\ (s) + CO_2(g) \rightarrow CaCO_3(s) + H_2O(g) \quad (3)$$

$$CaO(s) + CO_2(g) \rightarrow CaCO_3(s) \quad (4)$$

Under normal atmospheric pressure, Du and his team (2021) looked at the instantaneous carbonation of semi-dry desulphurization waste. They found that the effectiveness of CO_2 absorption and carbonation led to the discovery of three distinct stages in the process. They proposed that the carbonation reaction was primarily constrained by three factors: CO_2 film diffusion, the carbonation reaction itself, and finally, the diffusion inside the product layer, using kinetic models of heterogeneous reactions to better understand the process. By adjusting a few key variables, the researchers were able to optimize the procedure: a gas flow rate of 300 mL/min with 15% CO_2, a temperature of 60 °C, a concentration of 100 g/L, a stirring speed of 400 rpm, and a concentration of 100 g/L. With these conditions, they managed an impressive 90 percent CO_2 storage in a rather small time (four hours) (Du et al., 2021).

1.1.2 Advancements in construction and waste management

Industrial alkaline solid wastes have the potential to sequester CO_2 due to a significant amount of calcium and/or magnesium content. Accelerated carbonation is an emerging technology gaining traction for its ability to utilize CO_2 in tandem with the valorisation of alkaline solid residues in the production of construction materials (Cizer et al., 2012). Early research into accelerated carbonation of industrial alkaline wastes started with the purpose of producing coherent structures (which they are further utilized in road construction) bonded by calcite crystals stabilizing harmful components in coal refuse piles (LaRosa, 1971).

Industrial by-products are often co-generated with CO_2 which makes the accelerated carbonation treatments easily accessible and cost-efficient, as a result this carbonation process may pose minimal environmental drawbacks (Bobicki et al., 2012). By-products of various industrial activities like metal processing, mining, coal combustion, PC production, and waste incineration include steel slag, mine tailings, fly ash, cement kiln dust, and air pollution control residues (Baena-Moreno et al., 2023). Different alkaline waste materials have been studied for their potential in carbonation, as documented by Teir et al. (2007, 2008), Huijgen et al. (2005), Lekakh et al. (2008), Schnabel et al. (2021), Rusanowska et al. (2023), Zhang et al. (2022), and Gu et al. (2021). Specifically, alkaline waste products like cement dust (Huntzinger et al., 2009; Pedraza et al., 2021), fly ashes (Back et al. 2008; Uibu et al., 2008; Senadeera et al., 2020; Miao et al., 2023), and concrete waste (Ghacham 2017; Nedunuri 2021; Kaliyavaradhan 2022) have been investigated for mineral carbonation. Utilization of these alkaline residues in building material applications is somewhat widely researched (Bernal et al., 2016). However, fewer studies focus on the role of accelerated carbonation in non-cement applications (Nielsen et al., 2017). This gap in the research landscape becomes especially pertinent when considering the widespread practice and potential in other sectors where the industrial alkaline wastes can be upcycled without the incorporation of traditional or alternative binders.

Diving deeper into the practical applications and implications of carbonation in these waste materials, Nielsen et al. (2020) embarked on an investigation exploring the parameters influencing strength development in monoliths crafted from steel slag, subjected to accelerated carbonation under mild operating conditions, such as 10–60 °C and 1.5 bar, and variable CO_2 concentrations (5–100%) within an autoclave. Their findings unveiled that the temperature plays a pivotal role in governing the solubility of CO_2 in the pore solution, revealing that elevated temperatures (60 °C) induced a less dense microstructure and curtailed strength development relative to their lower-temperature

counterparts. Moreover, a swift initial carbonation, spurred by high CO_2 concentration, was identified as being counterproductive to strength development, illuminating the delicate balancing act intrinsic to optimizing carbonation processes.

The monolith is mainly carbonation-strengthened, which refers to the fact that the particles of the powdered fly ash are mainly bonded to one another by means of the carbonate phases formed. Thus, the major binding phases are composed of the carbonates ($CaCO_3$) that are produced by accelerated carbonation process in the given method. In the current specification, "carbonation-strengthened" means that the carbonate phase or phases, generated by the relatively quick carbonation step, advantageously contribute to more than 60% of the monolith's final compressive strength. Additionally, hydration products undoubtedly affect strength development and continue to solidify the monoliths over a longer time as well.

The carbonation of supplementary cementitious materials has been under scientific scrutiny and reveals noteworthy potentials in reducing permeability of concrete and leaching possibilities when mixed with alkaline waste materials (Pu et al. 2023). A practical illustration of this can be seen in the stabilization of municipal solid waste incineration fly ash, especially those containing heavy metals, through accelerated carbonation (Liu et al., 2023). Several contradictory findings are often presented, for instance Moon and colleagues (2019) explored CO_2 uptake potential of steel slags and fly ash samples focusing on microstructural and mineralogical changes affecting their use in cement-based applications. It was found that for Ca-rich residues and cement mixes, initial hydration of the paste impedes CO_2 penetration. As a result, the hydration process dominates, significantly limiting the quantity of Ca components available for direct reaction with CO_2 in the early stages. The effect of precipitated $CaCO_3$ in pores of paste matrix on strength development was lower compared to the effect of silica gel formations.

Several studies have indicated that carbonation enhances the physical and chemical immobilization of various heavy metals within cementitious materials, including zinc, nickel, and arsenic (Grünhäuser Soares et al., 2021) and chromium (Wang et al., 2021). In terms of physical immobilization, the formation of $CaCO_3$ crystals during carbonation creates a denser concrete matrix, reducing its permeability and thereby physically entrapping and containing waste materials, preventing them from leaching into the surrounding environment. Solidification, defined as a chemical binding process, secures toxic waste material into solid forms by binding of waste at the molecular or ionic level, or restricts them from external exposure by encapsulating them. This process transforms potentially hazardous waste materials into comparatively safer solid materials prior to landfilling (Chen et al., 2021). Choosing an appropriate binder navigates a balance between economic and environmental aspects, with a higher content of calcium in the binder indicating a heightened potential for producing a carbonated product. Conversely, Kaja et al. (2021) highlight a challenge with this approach, noting that carbonation can increase leaching of certain metals such as vanadium and molybdenum. This occurs because the reaction of CSH gel (which hosts heavy metals in the hydrated steel slag) with CO_2 leads to the formation of calcite and amorphous silica, which can, in turn, lead to the increased release of heavy metals. Moreover, Librandi et al. (2019) present results that contradict previous findings concerning carbonation; they report a significant decrease in sulphate release from steel slags. This outcome diverges from a trend identified in an earlier study, wherein carbonation treatment applied to steel slag, derived from an Italian steelmaking plant, instigated an increase in sulphate concentrations (Librandi et al.,

2017). In light of these conflicting findings, it becomes imperative to comprehend the impacts of carbonation on sulphate containing industrial alkaline wastes and to discern their potential utility in the construction sector, ensuring the procedural and environmental efficacy of incorporating such materials into building practices.

While the scientific community explores these reactions in various waste materials, particular emphasis has been placed on two predominant industrial wastes: steel slags and fly ash (Liu, 2021). These materials not only present suitable matrices for carbonation studies but also represent significant waste streams on a global scale, with production volumes reaching approximately 750 and 420 Mt per annum for coal fly ash and steel slags respectively, and projections anticipating continued growth (World Steel Association, 2022; Yao et al., 2015). It is crucial to underscore that existing studies may harbour extensive variations and predominantly direct their focus towards steel slags, thereby not extensively exploring Class C fly ashes in a commensurate manner.

1.2 Fly ash

Fly ash generation is inversely correlated with energy usage and dependency on combustible solid fuel. As a result, China, the USA, and India are the three countries that create the most fly ash (Kanhar et al., 2020). A growth in energy consumption caused by China's rapidly developing industrial and construction sectors has resulted in an annual production of fly ash that surpassed 560 million tons in 2020 (Luo et al., 2021). Indian coal produces more ash per unit of coal burned because it is of poorer grade and has a greater ash concentration (30–45%) compared to imported coal (10–15%) (Yadav et al., 2022). India produced 230 million tons of fly ash in 2019–20, with a 41 percent usage rate (Vig et al., 2023). By 2025, this amount is anticipated to exceed 250 million tons (Ohja et al., 2022). According to the annual report of American Coal Ash Association (ACAA), the USA produced 26 million tons of fly ash in 2020, with a utilization rate of 60% (ACAA 2020). Future projections suggest a decrease in production and a yearly increase in utilization rate (Deonarine et al., 2023). Amid the COVID-19 pandemic, the global fly ash market was valued at US$5.482 billion in 2020 and is expected to have compound annual growth rate of 5.93% over the forecast period to reach a total market size of US$8.204 billion by 2027 (RAM, 2022).

The global energy landscape has been witnessing a shift towards unconventional resources, with oil shale and wood (forestry products) emerging as significant contributors (Kanger et al., 2022; Burger et al., 2017). Oil shale, a sedimentary rock abundant in organic content, and wood, a renewable resource, are both combusted to generate energy. Biomass, categorized as a renewable energy resource, plays a pivotal role in energy generation within the European Union. This shift is evident in the rising production of oil shale fly ash and wood fly ash. These ashes, while often perceived as waste, have unique properties that have sparked significant research interest and potential applications (Chai et al., 2022; Berber, 2020; Gunning et al., 2010).

Over 600 oil shale deposits have been identified in over 30 countries worldwide, and these are projected to produce a substantial amount of energy as the energy sector seeks diversification. (Alaloul et al., 2021). While exact figures on global production of energy from oil shale and wood are difficult to pinpoint due to the varied nature of deposits and diverse combustion technologies, it's evident that their contribution is growing steadily. This trend is in line with the global push towards diversifying energy sources and reducing carbon footprints.

Biomass accounted for about 60% of the EU's total renewable energy consumption (IEA, 2020). This makes it the largest source of renewable energy in the region. Resulting from the combustion process, wood fly ash is a by-product that contains valuable minerals and unburned carbon. Typically, for every tonne of wood combusted, about 1% to 1.5%, or 10 to 15 kg, results in wood fly ash (Ates et al., 2023). Its pozzolanic properties, similar to those of oil shale fly ash, make it a suitable supplementary cementitious material (SCM) in concrete mixtures. Beyond concrete, wood fly ash has been explored as a filler in the production of composite materials, bricks, and ceramics (Martínez-García et al., 2022). However, it's essential to ensure the ash is free from contaminants (particularly heavy metals) and to understand its chemical composition thoroughly, as these factors can influence its behaviour and compatibility in various building applications (Fořt et al., 2020).

In contrast, coal, once a dominant energy source, now accounts for 26.8% of the global energy supply, as reported by the International Energy Agency (IEA, 2021). Its by-product, coal fly ash, constitutes between 60 and 88% of the waste from coal and lignite combustion in power plants (Panda et al., 2020). Municipal solid waste, another contributor to the energy mix, also produces ash residues, but its share is comparatively smaller (Bhagat et al., 2023). As the world continues to explore sustainable energy solutions, the focus on oil shale and wood as viable alternatives is poised to grow.

A steady rise is anticipated each year in the production of fly ash, the predicted yearly global production is close to 1 billion tons (Sultana et al., 2021). Despite efforts to reuse fly ash in several sectors, including agriculture (in soil amelioration) (Banaszkiewicz et al., 2022; Chen et al., 2022; Turkane et al., 2022), construction (as supplementary cementitious material in cement composites, brick production, and the construction of roads and dams) (Zdeb et al., 2023; Da silva et al., 2022; Patil et al., 2022), the 3/4th of global production is still dumped in landfills (Kelechi et al., 2022). Fly ash disposal poses environmental risks due to the dispersion of airborne particles and the leaching of harmful substances into the soil and waterways (Mathapati et al., 2022). These dangers are well known and are shown by Dindi et al. (2019) in Figure 2 as well.

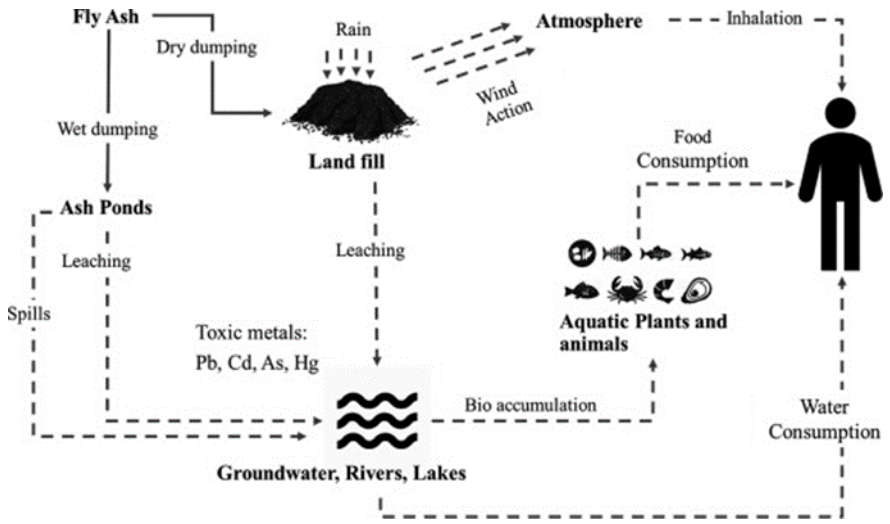

Figure 2. Pathways of Fly Ash Contamination (Dindi 2019)

1.2.1 Fly ash characteristics

Fly ash's distinct physical and chemical properties determine the applications. While these properties can vary based on the solid fuel type (e.g., oil shale, wood) and production conditions, certain traits are consistent across all fly ashes, enabling their use in the construction sector (Das et al., 2023). Comprising a blend of organic (1–9%) and inorganic (90–99%) components, fly ash's composition includes both amorphous (30–84%) and crystalline (17–63%) elements (Mudasir et al., 2022). These particles, predominantly below 75 m in size (Li et al., 2022), vary in composition, with unburned carbon found in coarser particles and finer particles primarily consisting of alumino-silicate glass.

Particle size can be influenced by the dust collection system. For instance, older plants using only mechanical collectors produce coarser fly ash than those with electrostatic precipitators (Rafieizonooz et al., 2022). Fly ash's colour varies based on the content of unburned carbon and iron, ranging from reddish-brown to black (Becerra-Duitama et al., 2022). Factors like the parent coal or burner type can influence the unburned carbon content, with bituminous coals and low-NO_x burners often resulting in higher percentages due to inefficient combustion (Rafieizonooz et al., 2022).

The chemical makeup of fly ash supports a wide range of recycling prospects. With components like silica, alumina, and unburned carbon, fly ash can serve as a precursor for materials like silica, zeolite, or activated carbon, which can act as cost-effective CO_2 adsorbents (Dindi et al., 2019). Fly ashes produced by varied source fuels exhibit varied chemical compositions, suggesting that not all have identical reactive characteristics. Alkaline earth metals in oxide forms, such as magnesium, aluminium, iron, calcium, sulphur, and silicon dominate fly ash compositions (Zahedi et al., 2019). The chemical composition's variation is attributed to the combustion process and the fuel source (Yadav et al., 2021), with differences observed in fly ashes from sources like coal, petroleum coke, lignite, and peat-wood. Trace elements in fly ash vary based on the fuel used (Ohenoja et al., 2020). Despite the US Environmental Protection Agency's (EPA) 2014 ruling that fly ash isn't classified as hazardous waste, certain elements, and ionic salts in fly ash, such as mercury, sulphate, etc. can pose environmental risks (EPA 2015).

The pozzolanic behaviour of oil shale and wood fly ashes are explained by the content of lime, silicate, and aluminate phases as well as iron oxide and amorphous silica (Kalpokaitė-Dičkuvienė et al., 2023; Berra et al., 2019). When these phases come into contact with calcium hydroxide (lime) in the presence of water, they undergo pozzolanic reactions to form cementitious compounds like calcium silicate hydrate (CSH) (Carević et al., 2019). On the other hand, the hydraulic property of certain ashes arises from the presence of calcium-rich phases (lime and portlandite), which can directly react with water to form cementitious compounds without the need for an external source of calcium hydroxide (Uibu et al., 2021; Risannen et al., 2019). In essence, while the pozzolanic nature of ashes is driven by their silica and alumina content, their hydraulic behaviour is influenced by calcium-rich phases. Fly ashes with high calcium content can also aid in CO_2 capture by producing $CaCO_3$ (Yousuf et al., 2020). The carbonation of free lime happens faster compared to calcium silicates (Liendo et al., 2022). The reason for the faster carbonation rate of free lime is its inherent chemical reactivity with carbon dioxide to form calcium carbonate (Eq. (4)). It is the main process responsible for strength development of aerial lime binders (Rodriguez-Navarro et al., 2023).

Calcium silicates, on the other hand, such as dicalcium silicate (C_2S) and tricalcium silicate (C_3S), have distinct carbonation pathways necessitate the presence of moisture,

which plays a crucial role in the reaction. The reaction of hydrated calcium silicate with CO_2 results in the decalcification of the CSH phases, resulting in silicate polymerization and, ultimately the formation of a calcium-modified amorphous SiO_2 gel and calcium carbonate (Steiner et al., 2020). Fly ash is also beneficial as catalyst support in CO_2 utilization reactions (Popova et al., 2020).

1.2.2 Applications of fly ash in building materials

Fly ash in concrete

Construction projects are paying close attention to fly ash, also a by-product of circulating fluidized bed combustion (CFBC), as a potential partial replacement for ordinary Portland cement (OPC) in concrete applications. Research has shown that fly ash can be successfully used as a cementitious component in blended cement applications for different purposes in different concentrations, exhibiting promising outcomes (Afroz et al., 2023; Liu et al., 2021; Carro-López et al., 2019; Zhao et al., 2018; Chen et al., 2017). For concrete used in buildings such as walls, parking lots, and pavements, the range is 15 to 35 wt. % and can even exceed 70 wt. %; for autoclaved aerated concrete it can reach up to 80 wt. % (Alterary et al., 2021). To ensure optimal performance, the recommended limit for OPC replacement by fly ash is generally suggested to be below 20% (Chi et al., 2016). However, studies have shown that fly ash acts as an excellent cement substitute when used as a 25% or even 30% cement replacement, maintaining compressive strengths comparable to reference samples (De Maeijer et al., 2020; Herath et al., 2020). Remarkably, even with a 40% cement replacement ratio, the compressive strengths of mortar samples using fly ash were as high as 88% of the control sample's strength (Risannen et al., 2017).

CFBC fly ash generally has self-cementing properties because it contains reactive phases like active aluminosilicate, anhydrite, and lime in the presence of water. These active phases could produce hydration products like ettringite (AFt) and CSH whether it is being added to cement or used as a raw ingredient (Wu et al., 2022; Xun et al., 2020). 20–30 weight percent of cement replacement was explored by Glinicki et al. (2019), with the primary hydration products being CSH and crystalline ettringite. Due to the cementitious property attained by these products, after 28 days of curing, flexural strengths of 5.2–6.4 MPa and compressive strengths of 35.9–53.3 MPa were attained.

Additionally, instead of using gypsum as a sulphate donor in Portland clinker, CFBC fly ash has been used as a cheap alternative because of its high anhydrite content (Hanisková et al., 2016; Shen et al., 2013). Portland cement and CFBC fly ash can be combined in different ways, depending on whether they are mixed directly (Lin et al., 2017), mixed after mechanical activation (Carro-López et al., 2019), or in conjunction with other substances (Zhang et al., 2022).

For industrial applications, particularly in the cement industry, fly ashes are generally categorized into two chemical types: Class C and Class F. As per the American Society for Testing Materials standard ASTM C618 [ASTM 2013], Class F is defined as ash containing more than 70 wt.% SiO_2+Al_2O_3+Fe_2O_3, while Class C contains between 50 and 70 wt.% of these compounds. Other chemical and physical requirements for Classes C and F include SO3 (5%), moisture (3%), Na2O (1.5% optional), particle size (34%, 5% on average value retained on 45 mm), and loss on ignition (LOI) (6% and up to 12% for Class F based on performance). However, the classification systems for fly ash in Canada, Russia, and the European Union differ from the US, and there is currently no international classification system (Vassilev et al., 2007). Furthermore, the American standard ASTM C618 and the

European standard EN 450-1 (European Committee for Standardization, 2012), which govern the use of fly ashes in the building industry, forbid the use of FBC or biomass fly ashes as a partial cement replacement material. The EN 450-1 standard is applicable to ashes produced by pulverized combustion, but only if the coal concentration is greater than 60%. When coal and pure wood are combusted together, this barrier is lowered to more than 50%. Future modifications to the laws governing the use of fly ash in concrete may limit its usage to fly ashes that satisfy the physical and chemical requirements specified in the ASTM C 618 or EN 450-1 standards (see Table 1). Therefore, the use of fly ash as cement replacement can currently be measured against these limit values.

Table 1. Fly ash classification according to European and American standards.

Property	**EN 450-1 Limit Value (%)**	**ASTM C 618 Limit Value (%)**
LOI at 950 °C	A < 5, B < 7, C < 9	< 6
Sum of SiO_2, Al_2O_3, Fe_2O_3	> 70	F > 70, C > 50
Chloride	< 0.1	-
Sulphate as SO_3	< 3	< 5
Free CaO	< 1.5	-
Total alkalis (Na_2O + K_2O)	< 5	-
MgO	< 4	-
P_2O_5	< 5	-
Fineness (45 µm)	S < 12, N < 40	< 34
Activity index 28 days	> 75	-

While the initial setting time of mortars increases and the compressive strength decreases with an increasing amount of cement replacement by fly ash, various studies have reported higher strength, faster hydration, and higher temperatures due to heat release during the initial hours of hydration (He et al., 2021; du Toit et al., 2022; Jianming et al., 2019). The pozzolanic reaction, where (mainly Class F) fly ash reacts with calcium hydroxide to form CSH, is slower than the hydration of Portland cement (Vanoutrive et al., 2022). By replacing a portion of the cement with fly ash, the amount of clinker reacting with water is reduced, which can lead to a decrease in the rate of the hydration reactions and thus extend the setting time. This can reduce the water demand for achieving a particular slump (workability), which can lead to a reduction in water-to-cement ratio. A lower water-to-cement ratio generally results in stronger and more durable concrete. Additionally, the filler effect of finer fly ash can reduce water requirement, and subsequently, limestone particle surfaces serve as heterogeneous nucleation sites, lowering the energy barrier and speeding up the precipitation of hydration products from the pore solution (Dai et al., 2021). This effect is more pronounced with finer fly ash because of its greater surface area, leading to faster cement hydration in the initial stages. Moreover, alkaline components (mainly Class C fly ashes with higher alkali content) can accelerate the hydration of cement, potentially reducing the setting time (Snellings et al., 2016). Alkali ions in cement can function as catalysts for hydration reactions by increasing the solubility of cementitious phases. Elevation of the pH of the pore solution also promotes silicate phase dissolution, accelerating CSH formation. Enhanced dispersion of cement and fly ash particles by alkali ions, reducing agglomeration and enhancing available surface area for hydration can result in acceleration of the overall hydration process. The water requirement of cement tends to increase when fly

ash is added; however, this can be mitigated through grinding (Dave et al., 2014; Turgut et al., 2019). The free lime (f-CaO) content of fly ash has been found to contribute to the increased water requirement (Nayak et al., 2022).

Compared to conventional pulverized firing (PF), fly ash derived from CFBC processes has a finer particle size with a higher irregular shape and surface area, resulting in higher porosity and air permeability in fly ash-containing pastes (Wang et al., 2016). Finer particles have typically lower activation energy, which can lead to faster initial pozzolanic and hydraulic reactions and potentially a quicker contribution to strength development.

Apart from partial OPC replacement, fly ash has been explored in various concrete applications. Studies have investigated the utilization of fly ash in concrete, producing aggregates suitable for lightweight concrete (Nadesan et al., 2017; Majhi et al., 2021). Furthermore, fly ash has been successfully used in the preparation of aerated concrete and roller-compacted concrete (RCC). Aerated concrete, characterized by its porous structure, lightweight properties, lower thermal conductivity (Chaipanich et al., 2015), and sound absorption properties (Shi et al., 2019) can be produced using fly ash (Song et al., 2015; Wu et al., 2020). Wu et al. (2020) investigated the addition of 18% fly ash to autoclaved aerated concrete. CSH gel and tobermerite were the main hydration products, and the blocks had compressive strengths of 7.3–12.8 MPa with bulk densities of 824.0–910.2 kg/m^3 after 36 h of curing in climate-controlled autoclaves. The use of fly ash in roller-compacted concrete has shown enhanced long-term flexural strength and reduced setting time (Aghaeipour et al., 2020).

The research focusing on aerated concrete and alkali-activated composites, which are typically composed of lime, cement, gypsum, and sand, with aluminium powder added as a pore-forming agent (Pozniak et al., 2021). The inclusion of fly ash in this mix has been proven successful, enhancing the material's overall performance (Qu et al., 2022; Šebestová et al., 2020). The aluminium in the mixture reacts with portlandite to release hydrogen gas, resulting in the formation of numerous tiny bubbles uniformly distributed throughout the matrix (Kumar et al., 2022). This process contributes to the unique properties of aerated concrete, making it an ideal choice for wall materials.

On the other hand, the alkali-activation of fly ashes, particularly CFBC fly ashes, has been less extensively studied compared to PF fly ashes. Despite this, existing research suggests that CFBC fly ashes could serve as suitable precursors for alkali-activated materials, although this often requires the use of co-binders or pre-treatment of the fly ash (Hao et al., 2022, Chindaprasirt et al., 2019; Hui-Teng et al., 2021; Nath et al., 2020; Zhuang et al., 2016; Chen et al., 2022; Gökçe et al., 2020; Farhan et al., 2019).

The crystalline nature of CFBC fly ashes tends to lower their reactivity in alkali-activation (Pour et al., 2022). However, studies have shown that it is possible to achieve compressive strengths of 10–30 MPa (Han et al., 2022; Lete et al., 2015), which is sufficient for most mortar- and paste-type applications. Studies even achieved 50 MPa when the fly ash content was 10–20 wt.% and high percentage of the binder was slag-based (Kim et al., 2019). This indicates the potential of fly ash in the production of cement-free, alkali-activated composites, contributing to more sustainable construction practices. Wu et al. (2015) presented the feasibility of fly ash as an alkali-activator for steel slags; they concluded that the optimum mixing ratio of fly ash and steel slag was 30%:70%, respectively, reaching up to 31 MPa compressive strength.

Furthermore, the addition of fly ash as a cement replacement has shown a significant reduction in chloride ion penetration in concrete, indicating its potential for corrosion mitigation (Hosan et al., 2022; Wongkeo et al., 2014; Hussain et al., 1994). Similarly fly

ashes in concrete mixes are known to have lower expansion due to external sulphate attack compared to OPC. Sulphate attack resistance in sodium sulphate is increased with an increase in cement substitution with low-calcium fly ash (more than 10%), a pattern not seen with high-calcium fly ash (Elahi et al., 2021). The accessible alumina sulphate ratio in the hydrating fly ash cement paste is a better indicator of sulphate attack performance than oxide content alone (Elahi et al., 2021, Zhang et al., 2022).

Additionally, fly ash-containing pastes tend to expand due to the presence of ettringite (Aft), with grinding processes preferred for achieving higher strength and sharp expansion development (Chen et al., 2017). Autoclave curing or limiting the content of total SO_3 to below 3.5% has been suggested to control the volume stability of fly ash cementitious systems (Chen et al., 2017; Wang et al., 2013). It has also been observed that fly ash-containing pastes have a higher polycarboxylate superplasticizer adsorption capacity, leading to lower fluidity in the cementitious system (Özen et al., 2022).

The utilization of fly ash, whether as a cement replacement or in various concrete applications, offers the potential to reduce cement usage, decrease costs, and minimize CO_2 emissions in concrete production. By exploring methods such as aerated concrete or roller-compacted concrete using fly ash, efficient recycling of fly ash and sustainable concrete production can be achieved.

Non-cement applications of fly ash

CFBC fly ash, has garnered attention in the construction industry due to its innate capacity to harden upon contact with water, functioning similarly to cement (Wu et al., 2022). This unique property, combined with its low carbon footprint and favourable engineering characteristics, has spurred interest in its use in alkali-activated non-clinker binders or geopolymers (Gartner et al., 2018; Maddalena et al., 2018; Mehta et al., 2016; Li et al., 2020; Sun et al., 2022).

Research by Telesca et al. (2015) displayed the potential of CFBC fly ash in the production of construction components based on ettringite. After a curing period of 15 hours, a commendable compressive strength of around 5.5 MPa was achieved. Optimal outcomes were achieved when the hydration was conducted between 55–70 °C. Outside this range, notably below 55 °C or above 70 °C, there was a distinguished reduction in ettringite formation. This was attributed to a slower reaction rate at lower temperatures and ettringite breakdown at higher temperatures. Chen et al. (2022) further delved into the optimal CaO and SO_3 content for fly ash-based geopolymers prepared at room temperature, highlighting the influence of these components on the reaction products. Relative to the original fly ash-based geopolymer, there is an increment in reaction products when the CaO and SO_3 levels are raised. This leads to the formation of a minor quantity of calcium silicate hydrate gel and coinciding ettringite. As a result, the geopolymer's microstructure is enhanced, producing a minor swelling effect that boosts its mechanical properties and offsets its drying shrinkage.

The reactivity of fly ash systems can be enhanced with the introduction of chemical activators. Pacewska et al. (2013) observed that high-calcium fly ash exhibited its activity earlier than its low-calcium counterpart. The addition of sodium hydroxide (NaOH) further boosted this reactivity, promoting the dissolution of silicate and aluminate phases in the fly ash. This dissolution facilitates the formation of an aluminosilicate gel, which can react with calcium ions to produce the primary binder in alkali-activated fly ash systems, the calcium-aluminosilicate hydrate (C-A-S-H) gel.

Li et al. (2012) confirmed the self-cementing properties of CFBC ash, achieving a compressive strength of 11.4 MPa after 28 days without chemical modifiers. With

modifications, this strength was nearly doubled to 22.4 MPa. Kledyński et al. (2017) emphasized the role of sulphate ion availability in water binding in fly ash-slag based pastes, noting the contribution of fly ash to the early hydration stages. The primary hydration products include the CSH phases and ettringite, with smaller quantities of aluminates (CAH) and aluminosilicates (CASH). The findings indicate that the examined combinations of fly ash and slag can be viewed as clinker-free binders.

Several studies, including those by Illikainen et al. (2014) and Ohenoja et al. (2016-a), have highlighted the importance of soluble calcium, aluminium, and sulphate in the ashes, emphasizing their impact on the self-cementing compressive strength of fly ash. The latter study particularly underscored the significance of the Ca/Al ratio in the fly ash, with an optimal ratio yielding strengths exceeding 9 MPa.

In conclusion, the unique properties of fly ash, combined with ongoing research, present promising avenues for its application in sustainable construction practices.

1.3 Utilization potential of fly ashes from Estonia through accelerated carbonation

Oil shale is a low-quality fossil resource that can be combusted in thermal power plants to generate heat and electricity or pyrolyzed to recover shale oil (Yang et al., 2020). Several European countries are still heavily dependent on fossil fuels to produce electricity, with Estonia leading the way with a total mining volume of 12.1 million tons in 2019 (Paiste et al., 2019).

Kukersite oil shale with varying concentrations of organic, carbonate, and terrigenous material has been extracted in Estonia for almost a century (Bauert et al., 1997). The content of organic matter varies between 10% and 60% and is mostly composed of kerogen, but also contains a few percent of bitumen. Processing oil shale leaves more than 50% of solid waste (ash), which has a limited secondary usage. The annual oil shale mining output in the past five years has been at the level of 12–15 Mt and about 80% of mined oil shale is burned in thermal power plants for electricity and heat generation using PF or CFBC technologies with temperatures reaching about 1300 °C and 700–850 °C, respectively (Leben et al., 2021). As a result of high dependence on oil shale, significant amounts of ash (7 to 8 Mt) are produced in Estonia (Lees et al. 2022).

In Estonia, the utilization of oil shale ash and wood ash is not only an economically viable solution due to potential savings from reduced landfill fees and waste-related taxes but also offers significant environmental and health benefits by mitigating the adverse effects of waste accumulation and promoting sustainable construction practices. The products derived from oil shale ash can be used in ash-based cement, binding agents, autoclave-strengthened ash bricks, glass ceramics, heat-insulating materials, road construction, and substitutes for chalk in rubber fillings (Kaljuvee et al., 2021; Paiste et al., 2016; Trikkel et al., 2008). Similarly, there has been a growing interest in studying wood ash due to the rise in wood combustion in Europe (Martinez-Garcia et al., 2022). Wood ash offers a viable alternative for partially substituting binders and kaolin in geopolymer formation (Ohenoja et al., 2016-b). Wood ash incorporation enhances workability, porosity, and drying shrinkage while providing an eco-friendly use for these wastes, thereby mitigating potential environmental pollution, and promoting circularity (Danraka et al., 2019; Sigvardsen et al., 2021; Tamanna et al., 2020).

The Solidification/cementation of fly ash-based non-clinker concretes is controlled by complex concurrent systems involving hydration, pozzolanic, and carbonation reactions

(Pihu et al., 2012; Pihu et al., 2019; Zhao et al., 2022). Hydration, setting, and hardening processes of fly ash-based binders have specific characteristics that are influenced by the firing temperature (about 800 °C in CFB boilers and 1400 °C in PF boilers which is not used under this study) and dust cooler type and filter type (Raado et al., 2014). Setting times were assessed to evaluate how long the samples remained in a plastic state to find out both the workability of the ashes as well as binding properties related to hydration without accelerated carbonation.

Burnt oil shale was researched previously to determine the composition, specifications, and conformance criteria for ash-based mineral binders (Raado et al., 2011; Uibu et al., 2016). These tests were conducted in accordance with the standards EVS-EN 196, EVS-EN 459-2:2010, and EVS 636:2002 for the production of composite cement (Raado et al., 2014; Uibu et al., 2016). It was found that the composition of residual material can vary based on the thermal treatment process (direct combustion, retorting etc.) and the nature of the fuel used. Owing to the decomposition of carbonate during the thermal treatment the ash produced in power plants can be rich in reactive free CaO (15–20%) (Leben et al., 2020). Typically the content of Al_2O_3 ranges between 2–10.5%, which is an increasing trend in finer fractions (Pihu et al., 2012). Fe_2O_3 content could be notably high, averaging 4.3%, with a gradual increase from the bottom ash to more than 5% in ash collected from electrostatic precipitators (Paiste et al., 2016). The sulphur content can vary between 1–5% and is highest in the INTREX ash of CFB boilers, where almost complete SO_2 removal from flue gases occurs (Konist et al., 2020).

Studies on oil shale ash conducted in the past (Kuusik et al., 2012; Liira et al., 2009; Pihu et al., 2012) have demonstrated that the solidification/cementation of oil shale ash mainly governed via the formation of secondary Ca-rich hydrate phases as well as hydration of free lime (CaO), secondary Ca(Mg)-silicate minerals, non-crystalline Al–Si phases and, anhydrite ($CaSO_4$). Portlandite, which is crucial for both cementitious reactions and carbonation, is created during hydration of free lime (Eq. (5).

$$CaO(s) + H_2O(l) \rightarrow Ca(OH)_2(s) \quad (5)$$

Portlandite and $3CaO.2SiO_2.3H_2O$ are created by the hydration of secondary calcium silicates (C_2S) (Eq. (6)). In turn, $Ca(OH)_2$ can react with hydrated active silicates to form CSH (Eq. (7) (Samadi et al., 2015)).

$$2Ca_2SiO_4 + 4H_2O \rightarrow 3CaO.2SiO_2.3H_2O + Ca(OH)_2 \quad (6)$$

$$Ca(OH)_2 + H_4SiO_4 \rightarrow Ca^{2+} + H_2SiO_4^{2-} + 2H_2O \rightarrow CaH_2SiO_4 \cdot 2H_2O \quad (7)$$

Historically, the hydraulic transport and landfilling of oil shale ash have been identified as the most feasible methods in terms of economic and technical considerations (Pihu et al., 2019). However, this approach raises several environmental challenges that are complex to address. Currently, nearly 300 Mt of landfilled ash is stored in such deposits (Leben et al., 2021). In oil shale-fuelled power plants, a hydraulic ash handling system is employed. Ash from CFBC and PF boilers is combined with water at a 1:20 ratio and pumped to an ash field for settling (Kuusik et al., 2012). The ash fields are constructed from hydrated ash layers, which vary in density, strength, and size. Calcium oxide, while highly reactive with other minerals and gases at elevated temperatures, does not fully react during combustion due to limited residence time, leaving a notable portion unreacted in the ash (Pihu, 2012). In a system dominated by $Ca(OH)_2$, minerals like $3CaO{\cdot}Al_2O_3$ and anhydrite engage in reactions with water and $Ca(OH)_2$ over days or weeks (Paiste, 2017). Another significant reaction that takes place within the initial

weeks or months is the creation of ettringite (Paaver et al., 2021). This formation aids in the crystallization of ash sediments and helps utilize pore water. When there is an abundance of water, the determining factor for ettringite formation is the available quantity of $CaSO_4$ (Leben et al., 2021). However, the influence of belite, K-feldspar, K-mica/clay minerals, and the glass phase in forming new minerals and altering pore water chemistry becomes apparent over longer durations, spanning months to years (Pihu et al., 2019). Long-term chemical reactions in the ash plateau, especially the crystallization of the K-containing glass phase and interactions between $Ca(OH)_2$ and K-rich minerals, lead to the formation of new Ca-silicates and Ca-aluminosilicates (Paaver et al., 2019). Additionally, belite undergoes hydration in these prolonged reactions. The process of CO_2 diffusion-controlled carbonation of sedimentary deposits is known to be slow. In addition, this process is further impeded in the upper strata of ash deposits due to the effective precipitation of calcite and other secondary minerals (Leben et al., 2021). These minerals progressively occupy the pore spaces, thereby causing a reduction in the porosity of the deposits. This demonstrates that the majority of ash deposits in landfills maintain their CO_2 binding capacity, making them a promising feedstock for accelerated carbonation.

1.4 Motivation and aim of the study

Amidst the pressing global challenge of climate change, largely driven by escalating CO_2 emissions, industrial activities, especially fossil fuel-based energy production, stand as significant contributors. Concurrently, these sectors generate substantial solid waste. Similarly in Estonia's energy sector, predominantly dependent on indigenous carbonaceous fossil fuels like oil shale, presents a context for research on circularity. The co-combustion (oil shale – biomass) and retorting activities yield substantial quantities of alkaline solid residues, encompassing oil shale fly ash (OSA), wood fly ash (WA), and landfilled oil shale ash (LFA). The advent of novel combustion regimes and technologies, notably CFBC, has engendered shifts in the phase composition of ashes. Such compositional shifts may pose challenges to the optimal utilization of fly ash in building materials. As a result of this conventional utilization applications have been progressively sidelined, emphasizing the pressing need to identify and investigate alternative strategies for fly ash utilization, both at the national and global scales.

Notwithstanding, scholarly discourse suggests that harnessing this potential necessitates a nuanced comprehension of their chemical composition, CO_2 mineralization potential, and viable building material applications. A particular area of ambiguity lies in the mechanisms underpinning the self-cementing processes of fly ash, especially the behaviour of various phases under diverse conditions. The scientific literature reveals discernible gaps concerning the operational parameters for CO_2 mineralization of C-class fly ash and which can be recycled in building materials.

This thesis centrally explores the characteristics of monoliths constructed from fresh and land filled OSA as well as WA through accelerated carbonation processes and aligns its findings with the most recent advancements in the field of carbonated materials. Initially, the study delves into the self-cementing properties of contemporary oil shale ashes, to characterize the chemical and physical properties of ashes while evaluating the reactions contributing on the strength development of mortars containing ash alone. Subsequent evaluations focus on the carbonation behaviour of compacted ashes to study the mechanism of carbonation reaction, extent of carbonation and reaction stages. The impact of various process parameters (temperature, gas pressure, CO_2 concentration)

is investigated emphasizing the CO_2 uptake and compressive strength of monoliths. Additionally, the study aims to elucidate the carbonation caused microstructural and mineralogical changes and evaluate environmental properties, emphasizing sulphate leaching, through the incorporation of high sulphur fly ashes.

The overarching objective of this research is to provide scientific basis for the effective and sustainable use of ash materials in non-cement construction and building practices while concurrently achieving the mitigation of CO_2 emissions.

2 EXPERIMENTAL

2.1 Materials

The ash samples collected for this study include distinct types of OSA, WA and LFA. These are common by-products from Estonia's power and heat generation sectors, representing the abundant residues from circulating fluidized bed (CFB) combustion operations and biomass co-firing applications.

Initially, six different ash streams from Estonian power plants were selected for the performance testing of self-cementitious properties. A single stream of ash from Eesti power plant was selected in the formulation of clay bricks.

For carbonated monoliths initially single stream of Auvere power plant electrostatic precipitator ash was selected (See Paper I, Chapter 2).

For further elaborate study on the substantive topic of cement-free monoliths through accelerated carbonation OSA from Auvere power plant and WA from Utilitas district heating plant as well as LFA from accumulated ash plateau were selected (See Paper II, Section 2.1).

For the incorporation of high sulphur fly ash in carbonated monoliths high sulphur containing streams of OSA and WA is selected similarly from streams of Auvere power plant and Utilitas district heating plant. Additionally, calcium aluminate-bearing niobium slag (NS, as ground sample) is obtained from NPM Silmet niobium process plant. (See Paper III, Section 2.1)

2.2 Methods

This scientific study utilizes a range of methods for the thorough examination and characterization of selected waste streams. These methods focus on the determination of key characteristics of the samples, including their physical properties, chemical and mineralogical composition, thermal decomposition behaviour, and leaching characteristics. A summary of these methods, along with the instruments used in each study, has been presented in table 2 below. The table is organized to outline the specific methods with a brief description of the procedure or analysis, and the instrument(s) used to conduct each respective method. The objective of employing these diverse techniques is to gain a comprehensive understanding of the samples, providing a foundation for further research and applications. Further description of the characterization methods and specific instruments can be found in the methods sections of Paper I–III.

Table 2. List of methods and corresponding equipment.

Method	Instrument(s) Used
Mean Sampling and Size Fractioning	Sieves
Particle Size Distribution (PSD) Measurement	Horiba Laser Scattering instrument (LA-950V2)
Specific Surface Area (SSA) Measurement	Kelvin 1042 sorptometer (Costech Microanalytical SC)
Free Lime and Carbon Content Determination	ELTRA CS 580 Carbon Sulphur Determinator Ethylene glycol method of free CaO (Reispere, 1966)
Pore Size Distribution and Porosity Measurement	POREMASTER-60-17 porosimeter (Quantachrome Instruments)
Chemical and Mineralogical Characterization	X-ray fluorescence (XRF) (Bruker S4 Pioneer), X-ray diffraction (XRD) with Rigaku, SmartLab SE
Thermogravimetric Analysis (TGA)	Setaram Labsys 2000 thermoanalyser
Microstructural Analysis	Scanning Electron Microscope (SEM) ZEISS Evo MA 15 with an EDX analyser
Compressive Strength Measurement	Toni TechnikD-13355
Leaching Test	GFL 3025 overhead shaker
Conductivity and pH Measurement	Mettler Toledo SevenGo Duo Pro pH/Cond meter SG23
Ion Determination	Lovibond Spectro direct spectrometer
Heavy Metal Determination	Agilent 4210 Microwave Plasma Atomic Emission Spectrometer (MP-AES)

2.3 Sample preparation and experimental setup

For the evaluation of cementitious properties, pastes (ash, sand, and water) were formulated with a water-to-ash ratio of 0.7 and an ash-to-sand ratio of 0.33 (Paper I, Section 2.1.3). These pastes were subsequently cast into prismatic moulds and underwent a curing process in a climate chamber (at >95% RH and 20±2 °C) for a duration of 28 days. Following this, their flexural and compressive strengths were evaluated in accordance with EN 196-1:2016. In a parallel study focused on sintered clay bricks aiming for optimum sand to OSA replacement, clay bricks were meticulously prepared with press moulding (Paper I, Section 2.2.2). Various tests were executed including measurements of density, water absorption, flexural and compressive strength, and thermal conductivity tests while assessing quality and durability.

For the completion of the thesis work, over two hundred distinct samples were formulated, encompassing 100% OSA, 100% WA as well as mixed designs (Paper II, Section 2.3), and the incorporation of NS into both OSA and WA (elaborated in Paper III, Section 2.2.1). LFA was exclusively integrated for an initial assessment, evaluating its potential for a mix design in conjunction with OSA and WA at a 50/50 ratio (Paper II,

section 2.3). For each sample group, a minimum of four cylindrical specimens were prepared, and the mean strength values, derived from these specimens, were presented in the results corresponding to each tested parameter.

In the preliminary preparation step, ash samples were mesh sieved (≤200μm) then hydrated with specific liquid-to-solid ratios (0.15–0.25) w/v for different ashes. This ensured a necessary moisture content for all samples prior to curing, measured using an MB23 moisture analyser.

The samples were uniformly blended with deionized water, using a semi-batch Eirich EL1 type intensive mixer at a consistent rotation speed of (600 rpm) for a duration of 20–30 minutes. After mixing and preliminary wetting, all ashes (powder) were allowed to hydrate and cure, in sealed and vacuumed containers at room temperature between 12–24 hours.

Following this phase, the samples were compacted using a hydraulic press and stainless-steel mould into cylindrical monoliths of 20 mm diameter and 20±1 mm height. Special attention was given to the uniform preparation in terms of compaction pressure of samples as compaction was performed manually.

NS powder, in its dry form, was incorporated into the ash powders after the first hydration period. The NS powder together with the hydrated ash powders were mixed for 10 minutes considering the given rapid hydration and hardening characteristics of NS as typical calcium aluminate-bearing slags.

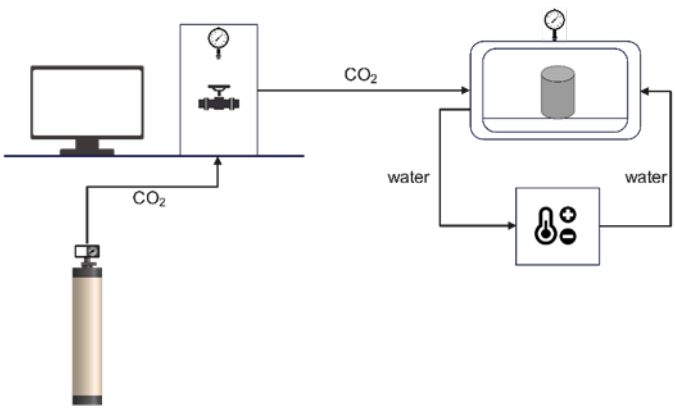

Figure 3 Scheme of the experimental set-up for the accelerated carbonation system (comprising CO2 gas cylinder, computer, temperature regulator, gas flow controller and curing chamber).

It's noteworthy that the NS powder exhibits lower workability and compressibility compared to the ash samples, influencing the compaction ability of the final blend. The impact of compaction pressure on the final product performance was evaluated by applying two different pressures (150±10 and 300±10 kg/cm^2). Accelerated carbonation curing was conducted in an automated carbonation system (Fig. 3), which includes a 400 mL stainless-steel jacketed pressure vessel, a temperature controlling apparatus (Circulator C-400) and gas flow controller (Buchi press-flow gas controller-bpc) for monitoring CO_2 gas usage (Fig. 4).

Varied experimental conditions were carried out, and simultaneous comparative tests were undertaken in periods of 2 hours of carbonation curing conditions, to study the impacts of differing curing temperatures (25, 50, 75 °C), typical flue gas (FG) CO_2

concentration (15%CO_2/6%O_2/N_2) versus 100% CO_2, and varying gas pressures (5, 10, and 15 bar). A consistent CO_2 concentration during (FG) curing was ensured by implementing a sequence of flushing and refilling every 20 minutes. Additionally, to control humidity throughout all tests, a potassium iodide saturated solution was utilized, which helped to maintain relative humidity (RH) between 61–68% at different curing temperatures.

Figure 4 Experimental setup comprising gas monitoring device, computer, CO_2 gas cylinder and climate-regulated autoclave.

3 RESULTS AND DISCUSSIONS

3.1 Characterization of fly ashes from diverse sources

3.1.1 Chemical characterization

X-ray fluorescence analysis has shown that calcium and silicon are the primary components of all ash samples (OSA, WA, and LFA), collectively making up 59–64% of the total composition (for detailed chemical composition please see Paper I and II). Further insights into the mineralogical composition of these ashes were provided by X-ray diffraction analysis (Paper I and II). It was found that both OSA and WA contain a significant amount of free lime (17–20%) and a smaller proportion of portlandite (1.4–3%), both of which are key reactants in accelerated carbonation and hydration processes. The NS, used as an additive, contains calcium aluminates with a small amount of NbO_5 remaining in the slag (Gorkunov & Munter, 2007).

In the context of cement production, the presence of C_3S (alite), C_2S (belite), C_3A (aluminate), C_4AF (ferrite) in clinkers is essential for the development of concrete strength. These materials react vigorously with water, forming a cement paste in the final product. The term “pozzolan” in the building industry refers to all materials that react with lime and water to produce calcium silicate and aluminate hydrates. These pozzolans, which constitute 22–45% of the samples, are rich in reactive silica or alumina plus silica. C_2S is found in 13.9% of OSA and 4.1% of WA, respectively.

However, LFA exhibits a different mineralogical profile. The hydration of CaO in the presence of natural water in LFA leads to the formation of $Ca(OH)_2$, accounting for 18% of the total composition. Additionally, the C_2S in LFA undergo hydration, resulting in the formation of CSH (tobermerite, thaumasite, afwillite), which makes up 45% of the phase composition. This transformation occurs due to the reaction of atmospheric water with the ash constituents in the disposal area.

High percentages of sulphate in cement can lead to internal sulphate attack, a deterioration mechanism that can significantly compromise the structural integrity of concrete. As such, ASTM C618 stipulates that the sulphate content of fly ash used in concrete should not exceed 5% SO_4^{-2}. However, the selected fly ashes have an elevated sulphate content, In OSA, anhydrite is the main sulphate-containing phase, while in WA, arcanite is the predominant sulphate phase. This was a deliberate investigation in the under-researched area of high-sulfur fly ash utilization to determine how accelerated carbonation affects leaching properties.

A common standard for the unburned carbon content in fly ash used in concrete is less than 3%. The restriction on unburned carbon content for fly ash to be used in construction is a critical issue and allowed values can vary based on the intended use and local building codes. The predominant form of carbon present in the ashes used under this research is mineral CO_2. In OSA, the total inorganic carbon content amounts to 1.25%, whereas in WA, it constitutes 2.65% (Paper III, Section 2.2.3).

In terms of heavy metal content of studied C-class fly ashes, WA typically exhibited higher levels compared to OSA. Specifically, elements such as zinc, manganese, copper, and barium are present in WA. In contrast, NS is deficient in these trace elements. While OSA contains heavy metals like zinc, lead, nickel, chromium, and barium, their concentrations are notably lower than those found in WA (Paper III, Table 4).

3.1.2 Physical characterization

Particle size distribution and specific surface area

The efficiency and capacity of carbonation tend to increase with decreasing particle size of fly ash (Li et al., 2022). This is primarily due to two factors: firstly, smaller particles have a larger specific surface area (SSA), which promotes carbonation reactions, and secondly, a smaller particle size facilitates the release of metal ions such as Ca^{2+} and Mg^{2+}.

PSD analysis of the samples indicated that the OSA samples, with mean particle sizes ranging from 17.97 µm to 21.96 µm, have slightly smaller particle sizes compared to the WA sample, which has a mean particle size range of 26.8–54.6 µm (Table 3). Despite this, the surface area of WA can be higher than that of the OSA samples. This is likely due to the presence of unburned carbon in the WA sample, which can increase the specific surface area by providing more active sites for chemical reactions and adsorption.

In contrast, the LFA sample has a significantly larger mean particle size of 79.25 µm, and the NS sample has an even larger mean particle size of 99.87 µm. The larger particle size of NS sample is likely due to its high-temperature production processes, which can cause melting and pore blocking, resulting in lower specific surface areas. The specific surface area of the NS sample, as measured by the BET method, is notably lower than that of the fly ash samples.

Table 3. Mean particle size (d_{50}) and BET surface areas of the samples (For more details please see Paper I and II).

	d_{50} (µm)	BET SSA (m^2/g)
OSA	17.9-25.3	3.1-6.2
WA	26.8-54.6	3.2-9.8
LFA	79.25	1.8
NS	99.87	0.34

3.2 Evaluation of ash suitability for targeted applications

3.2.1 Self-cementing properties of OSA

The binding capability is influenced by the chemical makeup and granularity of the ashes, especially the presence of unbound CaO, portlandite, Ca/Mg silicates, and SO_3 (De Maeijer et al., 2020). The self-cementing capability of ashes, characterized by coarser particle sizes tends to be suboptimal. An evaluation of the self-cementing attributes of all the examined ashes is presented in Paper I. It is evident that samples with an elevated SSA and higher contents of lime and portlandite (approximately 14–23%) as well as, Ca-Mg silicates (C_2S), and C_4AF (approximately 15–22%) that engage in hydraulic or pozzolanic reactions yield superior self-cementing properties. Well-known hydration reactions of the major compounds which are commonly found in cement clinker as well as in the fly ash samples are given below (Eq. 8–13).

$$2(3CaO{\cdot}SiO_2) + 6H_2O \rightarrow \rightarrow 3CaO{\cdot}2SiO_2 \cdot 3H_2O + 3Ca(OH)_2 \quad (8)$$

This reaction produces CSH and CH. The CSH produced exhibits a Ca/Si ratio approximately 1.5 with a water content of 3 mol (Hoskova et al., 2009). However, during C_3S hydration, both the Ca/Si ratio and water content can undergo variations (Naber et al.,

2019). The reaction is exothermic and is responsible for the initial set and early strength of the cement paste.

When tricalcium aluminate (C_3A) interacts with water and is accompanied by gypsum, it leads to the formation of ettringite (Eq. (9)) with a hexagonal-prism shape which can encapsulate certain heavy metals (Cr) and/or sulphates. This subsequently transforms into monosulphate (Eq. (10)) with a pseudo-hexagonal plate structure (Hoskova et al., 2009).

$$3CaO{\cdot}Al_2O_3 + 3CaSO_4 \cdot 2H_2O + 26H_2O \rightarrow \rightarrow 3CaO{\cdot}Al_2O_3 \cdot 3CaSO_4 \cdot 32H_2O \quad (9)$$

$$3CaO{\cdot}Al_2O_3 \cdot 3CaSO_4 \cdot 32H_2O + 2(3CaO{\cdot}Al_2O_3) + 4H_2O \rightarrow 3(3CaO{\cdot}Al_2O_3 \cdot CaSO_4 \cdot 12H_2O) \quad (10)$$

Ettringite formation during hydration of cementitious systems plays a dual role in cementitious structures. On the positive side, ettringite contributes to initial set and strength development, densifies the microstructure by filling void spaces, and can immobilize potentially harmful ions, enhancing concrete durability (Wolf et al., 2019). However, its formation isn't without challenges. Delayed ettringite formation can lead to internal cracking, especially if concrete is exposed to high curing temperatures (Kothari et al., 2022). External sulphate sources can instigate sulphate attack, causing deterioration. Additionally, excessive ettringite formation can induce expansion and cracking, and in some cases, increase the porosity of the cement paste, compromising strength and durability. Proper understanding and management of these aspects are crucial for optimal concrete performance (Colman et al., 2023).

Based on the findings of Xue et al. (2022), C_4AF undergoes full hydration to form $C_3(A,F)H_6$ [35], as depicted in Eq. (12). The hydration of C_4AF can lead to the formation of a hydrated garnet, and the observation that iron can interchangeably take the place of aluminium aligns with the conclusions drawn by Rose et al. (2006).

$$2(2CaO{\bullet}SiO_2) + 4H_2O = 3CaO{\bullet}2SiO_2{\bullet}3H_2O + Ca(OH)_2 \quad (11)$$

The reaction for C_2S (Eq. (11)) is slower than that of C_3S and contributes to the later strength of the cement paste (Hoskova et al., 2009).

Hydration of C_4AF in the presence of water:

$$3(4CaO{\cdot}Al_2O_3{\cdot}Fe_2O_3) + 30H_2O \rightarrow 2(3CaO{\cdot}Al_2O_3{\cdot}6H_2O) + 2(3CaO{\cdot}Fe_2O3{\cdot}6H_2O) + Fe(OH)_3 + Al(OH)_3 \quad (12)$$

Hydration of C_4AF in the presence of gypsum:

$$4CaO{\cdot}Al_2O_3{\cdot}Fe_2O_3 + CaSO_4{\cdot}2H_2O + 11H_2O \rightarrow 3CaO{\cdot}(Al_2O_3,Fe_2O_3){\cdot}CaSO_4{\cdot}12H_2O + Ca(OH)_2 \quad (13)$$

When gypsum levels surpass 20%, the diffraction peak of $C_3(A,F)H_6$ is no longer observed, suggesting that $C_3(A,F)H_6$ interacts with gypsum to produce AFm (monosulphate) (Eq. (13)) (Xue et al., 2022). In a different study Matschei et al (2007), the same AFm phase is also identified as one of the components that can encapsulate SO_4^{2-} at ambient temperatures.

Anhydrite, one of the principal sulphur-bearing components of OSA, is significant because, in the presence of $Al(OH)_3$, it serves as a major precursor to ettringite which provides additional self-cementation (Freidin et al., 1998; Leben et al., 2019; Uibu et al., 2016). The Aft phase (ettringite) is known to form rapidly in cement composites containing fly ash (Hewlett & Liska, 2019).

Ettringite and CSH gels, which will be examined in greater detail in section 3.3.4 in relation to triadic utilization of fly ash, niobium slag, and CO_2, are likely to be responsible for the strength development.

Compared to the 2015 (Uibu, 2016) data on the ashes of the same energy block presented in Appendix 1, 2018-2019 is the contents of free lime and Ca-Mg-silicates in the ashes are higher and the calcite content is lower. Most of the studied mixes demonstrated noticeably short setting times. This is tentatively related to the quick hydration of free CaO. The setting time and compressive strength values observed in most of the ash samples are suboptimal, potentially constraining the integration of ash with cement in contemporary applications – a prevalent methodology. While commercially available cement mixed designs incorporate approximately 10–15% of OSA, this proportion is notably diminutive when compared with the annual ash production volume. The setting times of certain ash specimens (APP-EPA) are close to the recommended ranges, and the 28-day compressive strength of the mortar is up to 14.1 MPa (Paper I, Figure 5,6). In general, the variation in both composition and binder properties is quite large from year to year: the 28-day compressive strength varies between 6.9–14.1 MPa. It is understood that APP-EPA stands as an ash variety which can be recognized as an independent potential binder. Conversely, the other examined ashes necessitate supplementary physical or thermal pretreatments to render them suitable for incorporation into similar applications. Such waste classifications, for example, might be reassessed as integral components for compound binders comprising diverse constituents.

3.2.2 Integrating OSA into clay bricks

This investigation presented a case analysis, endeavouring to evaluate the prospective incorporation of ashes within the ceramic sector. The principal research objective centred on the systematic exploration of ash integration; however, the empirical outcomes yielded were not particularly promising.

The inclusion of distinct compounds within the ash partially replacing the sand, including $Ca(OH)_2$, Ca and Mg carbonates, and to a certain extent, Ca-sulphate, exerts a significant impact on the brick's microstructural characteristics. This effect is evidenced by the emission of H_2O, CO_2, and SO_2, stemming from decomposition reactions intrinsic to ash. These reactions are in addition to the typical processes observed, such as clay mineral dehydroxylation, quartz inversion, crystallization, and the vitreous phase reactions.

The inclusion of ash in bricks increased porosity, affecting their mechanical properties negatively and resulting in a decreased compressive strength (~20 MPa compared to the reference's ~30 MPa). Besides the inclusion of ash in bricks increased the water absorption, ash-included bricks absorbed 2.5 times more water than the reference bricks (Paper I, Table 7 and Figure 9).

Nevertheless, thermal conductivity in clay bricks, influenced by porosity and solid constituent properties, is crucial for building insulation and energy performance; notably, ash-included bricks displayed 50% enhanced insulation compared to reference bricks (Paper I, Table 7 and Figure 9).

The SEM images show enhanced particle interlocking and uniformity in the reference brick microstructure, while the presence of carbonate and sulphates in ash reduces the interlocking, influenced by $CaCO_3$ and $CaSO_4$ decomposition, and confirms findings on waste additives as pore-formers in literature (Dos Reis et al, 2020) (Paper I, Figure 10). The Phase composition highlights the significant presence of plagioclase (Ca-feldspar) in ash included bricks, resulting from the reaction of CaO with clay aluminosilicates, and notes partial anhydrite persistence post-sintering (Paper I, Table 8).

3.2.3 Preliminary tests for accelerated carbonation

C-class fly ash, characterized by its higher lime and portlandite content, exhibits exceptional suitability for accelerated carbonation processes. This distinction becomes even more pronounced when contrasted with its limited utilization potential compared to class F fly ash in conventional applications such as blending with cement, clay brick manufacturing, self-cementing applications, and geo-polymer formulations [Mishra et al., 2023]. Prior research on ash utilization under this thesis revealed limited potential, emphasizing the need for alternative binder-free methodologies. The ash chosen for initial testing, due to its high lime and portlandite content coupled with its fine particle size from electrostatic precipitation filters, seems better suited for the intended carbonation process.

The formation of carbonates leads to an increase in the solid volume and a decrease in porosity within the monoliths. These carbonates function as main binding phases, creating robust links between reactive particles and aiding in pore occlusion.

Compressive strength tests on the compacted monoliths have yielded promising results, with strengths reaching up to 40 MPa (Paper I, Table 9). Accelerated carbonation studies of these compacted monoliths indicate that the synergy of compaction and carbonation presents a valuable method for waste repurposing. This method not only strengthens cement-free monoliths stabilizing fly ash, but also effectively sequesters CO_2. Given these findings, a thorough examination of the microstructure of the carbonated monoliths is crucial to understanding the fundamental mechanisms of the carbonation reaction and to further optimize the process parameters, enhancing the performance of the carbonated products.

Based on the preliminary analysis results of accelerated carbonation in cement-free fly ash monoliths, it became evident that a deeper understanding of the carbonation reaction mechanism is essential. The behaviour of the products is influenced by a variety of factors, as will be demonstrated in the following sections. In light of this, section 3.3 goes into great detail on the observation of the various process variables that may have an impact on these phases.

3.3 Carbonation of fly ash monoliths

3.3.1 Variables affecting CO_2 uptake and compressive strength

Effect of compaction pressure

The green density that can be attained at a specific compaction pressure depends on the compressibility of fly ash and similar powdered alkaline residues (Singh et al., 2021). Particle size, chemical composition as well as density, hardness, and shape of the particles all play a role in compressibility (Koley et al., 2011). Because the pores formed during the compaction are virtually between the particles, a powder with a smooth glassy surface has a higher compressibility compared to a particle with a less regular shape (Shee-Ween et al., 2021). Due to the increased probability of irregular particle's tendency to fold on itself, lower green density can develop with powders consisting less regular shaped particles. This porosity cannot be remedied by further compaction (Sudha et al., 2020).

The physical characteristics of the compacted bodies and the mechanical performance of the resulting monoliths are influenced by the compaction force during the preparation of the monoliths. When the compaction pressure is increased, the porosity and permeability of the solid compact diminish (Hills & Pollard, 1997), which results in a

stronger structure and greater strength since internal gaps are closed. Additionally, it should be emphasized that adequate amount of water is required for optimum particle compaction and interconnectivity in the monoliths(Liu et al., 2023). In contrast, the decreased gas permeability caused by refined porosity prevents CO_2 from penetrating the inner surfaces of compressed substances (Siddique et al., 2020). As a result, the physical restrictions on CO_2 permeability, diffusivity, and solubility can have a negative impact on the effectiveness of the carbonation sourced strength development process by causing less amount of $CaCO_3$ to crystallize.

According to the compressive strength and CO_2 uptake values of carbonated OSA and WA monoliths, the above-mentioned phenomenon is present to a certain extent (Paper II, figure 5–6).

At the applied compaction pressure ranges, the potential detrimental effect of higher compaction pressure on CO_2 uptake ability of both fly ash monoliths is less than 2 wt. % which is thought to be primarily related to refined porous structure. Higher compaction pressure (between 150 kg/cm_2 and 300 kg/cm^2) is seen to increase compressive strength in all prepared samples. Average compressive strength increases by 63% in OSA monoliths and 71 % in WA monoliths as a result of increased compaction pressure. The average density of OSA monoliths increased from 1595 kg/m^3 to 1720 kg/m^3, while WA monoliths increased in density from 1830 kg/m^3 to 1970 kg/m^3.

Additionally, two distinct kinds of mixed design monoliths were created, one with a composition of 50% OSA and 50% LFA (designated by M1) and the other with a composition of 50% WA and 50% LFA (designated by M2) (Paper III, Fig. 7). M1 monoliths have a CO_2 uptake level of 13.1% and an average compressive strength of 9.2 MPa. This suggests that, in comparison to 100% OSA monoliths, LFA is marginally enhancing CO_2 uptake while decreasing the compressive strength of the samples. M2 monoliths have a CO_2 uptake level of 12.3%t and an average compressive strength of 10.4 MPa. Similar trends are seen between M2 monoliths and 100% WA monoliths when it comes to strength and CO_2 uptake levels. Compressive strength and CO_2 uptake levels are comparable for both kinds of mixed designs. Comparing LFA monoliths to OSA (1595 kg/m^3) and WA (1830 kg/m^3) monoliths, LFA monoliths have a lower total density (1340 kg/m^3). Increased density of 1470 kg/m^3 due to higher compaction pressure of 300 kgf/cm^2, which may indicate potential use of LFA for low density construction material applications. Based on the constituents, mixed designs show a median density. The average density of the M1 is 1380 kg/m^3, while that of the M2 monoliths is 1420 kg/m^3 (Paper II, Table 4). An overview of the average results for compressive strengths and CO_2 uptakes is concisely illustrated in Figure 13, located in Appendix 4, providing a snapshot of the detailed graphical representations and data to guide the ensuing discussion.

As can be seen, characteristics vary along with the compaction pressure applied during monolith preparation, which play a pivotal role in determining the physical properties and mechanical performance of the resulting monoliths. Higher compaction pressures generally lead to increased strength and density in the samples, but which can also reduce CO_2 uptake due to refined porosity.

Effect of gas pressure and CO_2 concentration

Carbon dioxide gas pressure and concentration are some of the variables influencing the rate of CO_2 absorption as well as relevant strength gain because of their effect on the physisorption process at the interface between the solid and the gas reactant (Jamil et al., 2023; Nielsen et al., 2020). Upon analysis of the CO_2 uptake rates and compressive strengths of OSA and WA monoliths, the influences of both CO_2 gas pressure and CO_2

concentration on these parameters were discerned. The final levels of CO_2 uptake as well as a rise in compressive strength in both OSA and WA monoliths coincide with the increase in gas pressure from 5 to 15 bar (Paper II, figure 8–9). Increase in carbonation rate could be explained by the increased gas penetration of CO_2 into the compact at high pressures, which supports the magnitude of carbonation reaction. As the pressure increases, the number of gas molecules (in this case, CO_2) in the system also increases. This leads to a higher probability of these molecules interacting with the pore surface of the fly ash monoliths, thereby increasing the amount of CO_2 adsorbed. This phenomenon is particularly relevant if the fly ash monoliths have a porous structure with micro and mesopores, which are known to enhance gas adsorption. Due to pore refinement and porosity reduction brought on by the carbonate precipitation, the compressive strength of the monoliths increases as the partial pressure of CO_2 gas increases (Humbert & Castro-Gomes, 2019). For OSA, the CO_2 uptake shows a 7.5% increase from 5 bar to 10 bar and a 6.1% increase from 10 bar to 15 bar. The compressive strength for OSA increases by 7.9% from 5 bar to 10 bar and by 15.5% from 10 bar to 15 bar.

For WA, the CO_2 uptake increases by 14.6% from 5 bar to 10 bar and by 8.5% from 10 bar to 15 bar. The compressive strength for WA shows a more significant increase of 31.7% from 5 bar to 10 bar and 25.6% from 10 bar to 15 bar. Although increasing CO_2 pressure was advantageous for CO_2 diffusion and solubility, high pressure can cause significant $CaCO_3$ precipitations on the sample's surface, generating a passivated layer that clogs the pores and reduces CO_2 diffusion (Zhong et al., 2021). There will also be a point at which pressure increase does not significantly boost uptake any further. This is because the fly ash monoliths only have a limited number of adsorption sites depending on porous structure, which will eventually be saturated, and the system will reach equilibrium.

It is also recognized that the amounts of total CO_2 uptake will differ depending on the degree to which CO_2 gas permeates cementitious materials under high and low CO_2 concentration levels. When curing with a 100% CO_2 concentration, the CO_2 uptake values for OSA and WA are respectively 10.8% and 9.4%. At the FG curing (16% CO_2), the CO_2 uptake values for OSA and WA are reduced to 7.6 % and 7.9 %, respectively (Paper II, figure 10). Samples cured in 100% CO_2 have higher compressive strengths than samples cured in FG, which is consistent with lower CO_2 uptakes. OSA monoliths have better compressive strength values than WA monoliths because they include more Ca-Mg silicates, which participate in hydraulic or pozzolanic processes. Longer curing times allow FG curing to achieve CO_2 uptake values that are on par with 100% CO_2 curing.

When cured in various CO_2 concentrations, the CO_2 absorption and compressive strength of fly ash monoliths, both OSA and WA, exhibit comparable changes. For OSA, when cured in 100% CO_2, the CO_2 uptake is 10.8%, which decreases by 29.6% to 7.6% when cured in model FG with 16% CO_2. The compressive strength also decreases from 22.1 MPa in 100% CO_2 to 16.1 MPa in FG, a decrease of 27.1%.

Similarly, for WA, the CO_2 uptake decreases from 9.4% in 100% CO_2 to 7.9% in FG, a decrease of 16%. The compressive strength also decreases from 13.5 MPa in 100% CO_2 to 10.2 MPa in FG, a decrease of 24.4%.

These changes indicate that both CO_2 uptake and compressive strength of fly ash monoliths decrease when the concentration of CO_2 in the curing environment is reduced from 100% to 16%. This suggests that higher CO_2 concentrations may enhance the initial reaction rates for carbonation process, leading to higher CO_2 uptake and related

compressive strength. However, at lower CO_2 concentrations, the carbonate conversion rate may be reached over longer times, and eventually, it may even exceed the carbonate conversion rate at greater CO_2 concentrations (Nielsen et al., 2020).

Effect of temperature

The accelerated carbonation process is influenced by temperature elevations through various intricate mechanisms including reaction kinetics, diffusion rates, solubility of CO_2, moisture evaporation and microstructure evolution (von Greve-Dierfeld et al., 2020; Wu et al., 2022; Yadav & Mehra, 2021). Previous investigations have reported that the temperature increase during carbonation directly affects the solubility of CO_2, the rate at which components dissolve, and the structure and mineralogy of the carbonates (Liu et al., 2016; Luo et al., 2021; Nielsen et al., 2020). At higher temperatures, calcium is more quickly released from the matrix, CO_2 diffusion is enhanced but the water evaporation is hastened, and the aqueous solubility of CO_2 is reduced (Zhong et al., 2021). For the carbonation of portlandite, while higher temperatures might accelerate the rate of reaction (kinetic control), the extent of carbonation might be less favourable compared to lower temperatures (thermodynamic control) (von Greve-Dierfeld et al., 2020). Temperature plays a crucial role in determining the thermodynamic stability of calcium carbonate polymorphs that form during the carbonation process, with calcite being the most stable among them. (Liendo et al., 2022).

Through an examination of the correlation between temperature and both CO_2 uptake levels and compressive strength, the influence of temperature was systematically assessed (Paper II, Fig. 11–12). For OSA, the CO_2 uptake increases from 9.1% at 25 °C to 11.2% at 50 °C, an increase of 23.1%. However, the increase in CO_2 uptake from 50 °C to 75 °C is smaller, at 5.4%. Whereas, the compressive strength increases from 22.1 MPa at 25 °C to 24.8 MPa at 50 °C, an increase of 12.2%, but then decreases to 21.6 MPa at 75 °C, a decrease of 12.9% from the peak at 50 °C. While higher temperatures elevate CO_2 uptake levels for OSA monoliths, they do not correspondingly enhance strength development, indicating that higher CO_2 uptake does not necessarily guarantee increased strength. The secondary reaction between CSH, $Ca(OH)_2$, and CO_2, which results in high-intensity calcium carbonate crystal and lowers the calcium-silicon ratio (c/s) of CSH, can favourably affect the strength development monolith up to 50°C (Duan et al., 2020). CSH with a lower ratio of C/S has better mechanical properties, and the accumulation of calcium carbonate particles reduces the porosity and increases the density of the monolith (Duan et al., 2020; Lodeiro et al., 2010; Qian et al., 2018; Shaikh & Supit, 2014). Therefore, the compressive strength of the monolith will improve. Between 50 °C to 7 5°C, a decrease in the compressive strength can be attributed to disintegration of CSH as well as increased lack of water availability at higher temperatures affecting homogeneity of hydration and carbonation reactions. High temperatures can cause the double-chain silicate anion structure of CSH to break, which will inhibit the growth of combined strength (Fang & Chang, 2015). It is well known that excessive carbonation can degrade the micro-mechanical property of CSH (Liu et al., 2022).

Similarly, for WA, the CO_2 uptake shows a significant increase from 8.5% at 25 °C to 13% at 75 °C, an overall increase of 52.9%. However, the compressive strength decreases from 14.7 MPa at 25 °C to 13.2 MPa at 75 °C, a decrease of 10.2%. The experiment conducted at the lowest temperature (25 °C) registered the highest compressive strength, even though it had less CO_2 bound to the monoliths. This implies that for WA, the impact of temperature on carbonation strengthening is more pronounced. Considering that WA possesses a lower concentration of active silicates relative to OSA, it can be deduced that

carbonates exert a more pronounced impact on strength development than hydration products when compared with OSA. Despite higher temperatures prompting a faster initial reaction rate for both WA and OSA, this accelerated carbonation could potentially lead to the formation of weaker carbonate structures. These less robust structures contribute less effectively to strength development, suggesting that a balance between reaction speed and structural integrity is crucial for optimal strength. The influence of temperature on the stability of carbonates is further elaborated in the section dedicated to thermal analysis. In line with findings from similar studies, the uptake of CO_2 tends to increase with temperature, peaking at around 60 °C, particularly at lower pressures (Bertos et al., 2004). Given that the carbonation reaction is exothermic, it is advisable to cap the temperature at 333 K to maintain optimal conditions (Mazzella et al., 2016).

3.3.2 Thermal analysis

TGA was employed to investigate the thermal decomposition and mass reduction behaviour of both uncarbonated and carbonated samples meanwhile CO_2 uptake levels were also evaluated. This analytical technique provided insights into the various phases of mass reduction associated with the evaporation of water, dehydration of components ($Ca(OH)_2$, ettringite, CSH etc.), and release of CO_2 from $CaCO_3$.

The TGA and DTG curves of uncarbonated samples reveal three main phases of mass reduction with smaller steps in between (Paper II, Figure 13-14; Paper III, Figure 3). The initial mass loss step can be linked to the evaporation of water and the ensuing dehydration of both crystalline and amorphous components, including ettringite, which can continue up to 140 °C, as well as CSH or calcium-aluminate-(silicate) hydrate (CA(S)H) (Juenger et al., 2019; Scrivener et al., 2018). In the uncarbonated OSA, a slightly more pronounced peak of ettringite decomposition is observed between 100–130 °C compared to carbonated and NS-added samples. Similarly, in the WA, decomposition around 80 °C was less in NS added samples compared to carbonated and uncarbonated samples (Paper III, Figure 3). This suggests that CO_2 curing either slowed the formation of AFt, CSH, and CAH or induced their phase change. In both samples, the mass loss between 200–370 °C can be attributed to CSH decomposition as well as the ongoing decomposition of monosulphate which is formed after ettringite decomposes (Kurdowski, 2014). The subsequent phase is marked by the dehydration of $Ca(OH)_2$, which occurs up to 500 °C, as illustrated by Eq. (14). The final mass loss step is defined by the release of CO_2 resulting from the decomposition of $CaCO_3$, a process that unfolds between 550–900 °C, (Paper II, III).

$$Ca(OH)_2 \leftrightarrow CaO(s) + H_2O(g) \quad \Delta H\ 298K = -104\ kJ/mol \tag{14}$$

$$CaCO_3(s) \leftrightarrow CaO(s) + CO_2(g) \quad \Delta H\ 298K = +178\ kJ/mol \tag{15}$$

In carbonated samples, primarily two stages of mass reduction are observed – the evaporation of water and the release of CO_2 from $CaCO_3$. The loss of water from $Ca(OH)_2$ is not substantial due to its carbonation, as shown in Eq. (16), (Paper II, III), with the exception of OSA carbonated at 25 °C. The Mass Spectrometry (MS) curves of OSA monoliths that were cured at 75 °C corroborate the findings from the TGA curves.

$$Ca(OH)_2(s) + CO_2(g) \rightarrow CaCO_3(s) + H_2O(g) \quad \Delta H\ 298K = -113\ kJ/mol \tag{16}$$

The third stage of mass loss in uncarbonated samples reveals that both types of ash already contain $CaCO_3$ in their initial states, prior to hydration and carbonation. Consequently, the net absorption of CO_2 is determined by deducting the CO_2-related mass loss from the uncarbonated minerals from the total CO_2-related mass loss in carbonated samples.

The samples demonstrated a CO_2 uptake of 9.1% for OSA and 8.5% for WA (Paper II, figure 11) when cured at a temperature of 25 °C.

The net CO_2 uptake of the 100% OSA sample is 12.2% and NS added OSA sample is 11.7%. 100% WA sample and NS added WA samples are 7.8% and 5.4% respectively (Paper III, figure 2). The lower CO_2 uptake of NS-added samples can be explained by the rapid hydration of calcium aluminates altering pore structures, resulting in less available surface area and a lower percentage of portlandite, which is the main phase contributing to carbonation, due to the replacement of ash with NS. Yet, these findings indicate that there is a minor negative impact of NS on the carbonation of selected ashes.

The influence of the curing temperature is evident in both the TGA/DTG curves, which clearly demonstrate an increase in CO_2 uptake with rising curing temperatures of 25, 50, and 75 °C.

The thermal stability of the newly formed $CaCO_3$ can be assessed by examining the TG/DTG curves.

The onset temperatures, which represent the beginning of $CaCO_3$ decomposition in carbonated samples, are slightly lower compared to uncarbonated ones. For OSA, these temperatures are 520 °C for curing temperatures of 25, 50, and 75 °C, and 580 °C for the initial sample (Paper II, figure 13). For WA, the temperatures are 510 °C for curing temperatures of 25, 50, and 75 °C, and 580 °C for the initial sample (Paper II, figure 14).

These findings align with those of several other researchers who have reported lower thermal decomposition temperatures for $CaCO_3$ when it occurs in a less crystalline form of calcite (Karunadasa et al., 2019). This could indicate a variation in the thermal stability of the newly formed crystalline and amorphous $CaCO_3$ phases at temperatures above room temperature under the given curing conditions (Du et al., 2018). This could also be due to the inefficient transformation of amorphous $CaCO_3$ into calcite, which typically forms more stable structures at room temperature (Ihli et al., 2014). However, it's also known that the thermal stability of amorphous calcium carbonate can eventually increase and spontaneously crystallize.

3.3.3 Kinetic analysis

The properties of the initial ash, along with the conditions to which they are exposed during the sample preparation processes, profoundly influence the reaction kinetics and overall CO_2 uptake in the accelerated carbonation of OSA and WA monoliths. Formerly mentioned initial characteristics include SSA, composition of the mix, porosity, and free water content of the compacted monoliths. Surface area, porosity and to an extent free water content are also dependent on the compaction pressure. In general, carbonation process parameters include CO_2 gas pressure/concentration, curing temperature, and relative humidity. The curing temperature as a main process parameter has been taken into account within the section in order to obtain relevant kinetic curves of the carbonation stages of OSA and WA.

Methodology of preparation of the monoliths has been explained in 2.3 (Sample preparation and experimental setup chapter). Based on the above-mentioned

experimental equipment simultaneous gas monitoring was conducted at different curing temperatures (25–50–75 °C), capturing data every 5 seconds over a 2-hour carbonation period for the monoliths. The collected experimental data is illustrated in figure 5–6 (reproduced from Paper II, Figures 15–16). These figures depict the kinetic curves of CO_2 consumption at varying temperatures.

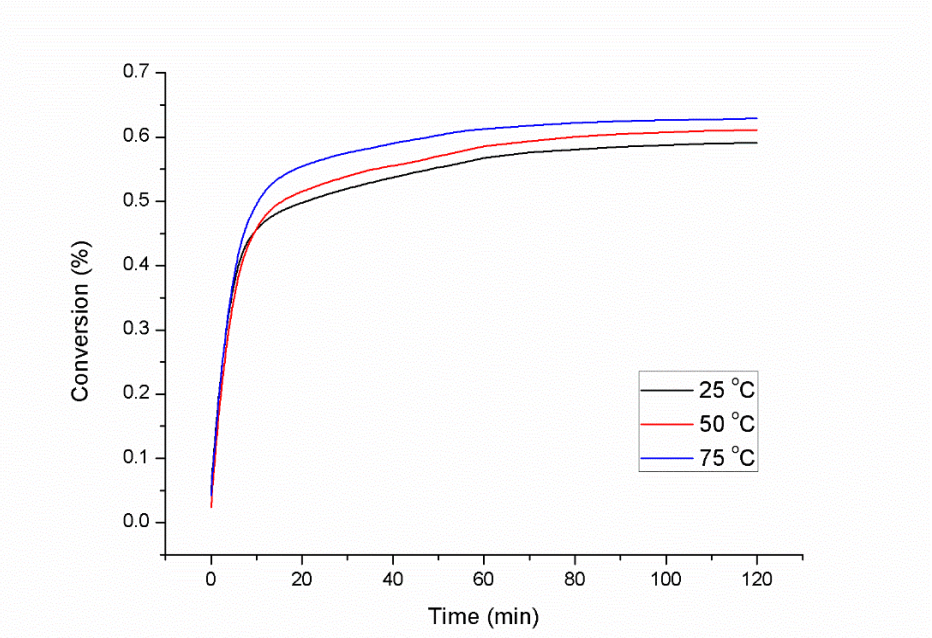

Figure 5. Simultaneous CO_2 uptake profiles of OSA compacts subjected to curing at temperatures of 25°C, 50°C, and 75°C.

The carbonation reaction in both OSA and WA monoliths is initially rapid, a phenomenon attributable to the open porous surfaces and ample physically bound water in the open pore structures of the samples, which facilitates a swift onset of carbonation. Following this phase, the reaction rate slows due to diffusion constraints through the product layer as carbonation advances from the exterior surface into the internal spaces.

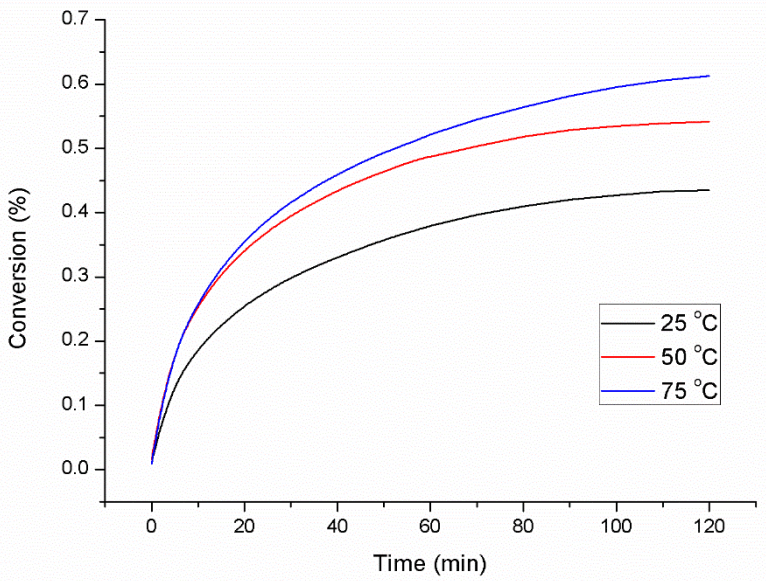

Figure 6. Simultaneous CO_2 uptake profiles of WA compacts subjected to curing at temperatures of 25°C, 50°C, and 75°C.

Moreover, the initial rapid carbonation reaction can also impact particle temperatures due to exothermic nature of the reaction, potentially speeding up the evaporation of physically bound water. This could impose a limit on the diffusion of CO_2 and the formation of carbonic acid. While the initial phase of the carbonation reaction does not exhibit a clear temperature dependency, an increase in temperature does have a positive/or visible effect on CO_2 absorption, particularly during the diffusion-controlled phase of OSA.

The trend of CO_2 consumption in terms of carbonation rate differs slightly in WA compared to OSA and varies with temperature. The beneficial effect of rising temperature on the rate of WA carbonation is more noticeable, indicating a more kinetic-controlled reaction, even in the initial stages of carbonation. A temperature increase extends the duration of the rapid carbonation phase, allowing WA to react for a longer period before transitioning to a more diffusion-controlled stage.

The CO_2 absorption values derived from gas monitoring results corroborate the total CO_2 absorption values identified in thermal analysis. After two hours of curing, the final conversion values range from 0.58 to 0.64 for OSA and 0.43 to 0.62 for WA. CO_2 binding efficiency calculated based on theoretical maximal CO_2 uptake capacity which is shown in Eq. (4) in Paper II. Graph extrapolation suggests that full conversion can be achieved after 11 hours for OSA and 13 hours for WA.

Well-known reaction-order models were assessed as described by Li et al., (2020) and Khawam et al. (2006). It's established that the carbonation of Ca-Mg silicates exhibits reduced reactivity under alkaline conditions in comparison to $Ca(OH)_2$, with potential pH drops to around 10, based on equilibrium calculations (Nam et al., 2012). Consequently, the total CO_2 sequestration during carbonation is determined based on the most reactive ash phases, namely CaO and $Ca(OH)_2$, excluding Ca-Mg silicates (Eq. 4, Paper II).

Carbonation reaction in the monolith can be summarized by following order of intermediate reactions (Eq. 17-23):

Hydration of calcium oxide (lime) to produce calcium hydroxide (slaked lime):

$$CaO(s) + H_2O(l) \rightarrow Ca(OH)_2(s) \quad \Delta H = -65.27 \tag{17}$$

Dissolution of carbon dioxide in water to form carbonic acid:

$$CO_2(g) + H_2O(l) \rightarrow H_2CO_3(aq) \qquad \Delta H = 66.55 \text{ kJ/mol} \tag{18}$$

Dissociation of carbonic acid into bicarbonate ions:

$$H_2CO_3(aq) \rightarrow H^+(aq) + HCO_3^-(aq) \quad \Delta H = 1412.7 \text{ kJ/mol.} \tag{19}$$

Further dissociation of bicarbonate ions into carbonate ions:

$$HCO_3^-(aq) \rightarrow H^+(aq) + CO_3^{2-}(aq) \quad \Delta H = 15.48 \text{ kJ/mol} \tag{20}$$

Dissolution of calcium hydroxide:

$$Ca(OH)_2(s) \rightarrow Ca^{2+}(aq) + 2OH^-(aq) \quad \Delta H = -980.83 \text{ kJ/mol} \tag{21}$$

Reaction of calcium ions and carbonate ions to form calcium carbonate (limestone):

$$Ca^{2+}(aq) + CO_3^{2-}(aq) \rightarrow CaCO_3(s) \quad \Delta H = 12.13 \text{ kJ/mol} \tag{22}$$

The overall reaction can be simplified as:

$$CaO(s) + CO_2(g) \rightarrow CaCO_3(s) \quad \Delta H = -178.39 \text{ kJ/mol} \tag{23}$$

While the solids are dissolving and hydrating, CO_2 in the vapor phase will also dissolve in water, based on its equilibrium solubility at the given pH and temperature (Pan et al., 2012). The metal ions frequently begin by leaching out quickly, then gradually slow down and increase until they reach their peak concentration in the pore solution (Wei et al., 2018). As the reactants and dissolved CO_2 create ionized species in the liquid phase, they reach a state of supersaturation. This state is often defined by the ratio of the ion activity product to the solubility product for a specific compound, such as calcite (Lothenbach & Zajac, 2019). Once this state is reached, precipitation happens, which lowers the level of supersaturation. Compounds in the fly ash that contain Ca^{2+} (mainly CaO and $Ca(OH)_2$) will continue to dissolve as long as the solution remains undersaturated with respect to these phases due to the precipitation of carbonates. The kinetics of precipitation reactions, as demonstrated in other studies on the carbonation of lime pastes, are significantly influenced by the initial chemical control at the exposed surface, which exhibits a high resistance to CO_2 diffusion (Cizer et al., 2012). This indicates that the process is subsequently succeeded by a shift to a phase where the reaction is governed by the diffusion of CO_2 through the layer of the carbonate product. This ensures the formation of Ca (and Mg) carbonates until the supply of these reactant compounds is depleted and the system achieves equilibrium. It is important to note that the pore solution is likely to maintain a high pH due to the plentiful alkaline compounds in the fly ash mixture (Wei et al., 2018). Certain previous investigations have examined the carbonation reaction mechanism in alkaline wastes and found that the rate of accelerated carbonation is primarily limited by the diffusion process within the ash layer (Chang et al., 2011; Lekakh et al., 2008; Pan et al., 2018).

A strategy employed to understand the kinetics and mechanisms of the reaction is the solid-state reaction approach, particularly relevant for the carbonation process. This

method proves to be particularly beneficial when the reaction involves solid reactants and products, such as the carbonation of CaO to produce $CaCO_3$.

Various kinetic functions correspond to distinct mechanisms for solid-state reactions, with a particular emphasis on the carbonation conversion of alkaline solid wastes (Miao et al., 2023). The functions f(α) and g(α) = kt are derived from the general kinetic equation dx/dt = k * f(x). The mechanisms are categorized based on the controlling step of the reaction, including nucleation, phase boundary reactions, and diffusion.

The kinetics of a typical solid-state reaction can be represented by the law of mass action, as depicted in Eq. (24), in conjunction with the Arrhenius theory. The equation is expressed as

$$dx/dt = k \cdot f(x) \tag{24}$$

In this equation, x signifies the proportion of reactants within the monolith that have transformed into carbonates, t stands for the reaction time (in seconds), k is the reaction rate constant, and f(X) is an algebraic function that is defined by the reaction mechanisms (Zhu et al., 2023).

Arrhenius equation is presented below.

$$k = Ae^{\frac{-E_a}{RT}} \tag{25}$$

where, k is rate constant, A is the pre-exponential (frequency) factor, e is Euler's number, E_a is the activation energy, T is absolute temperature, R is the gas constant.

Previous research has shown that two solid-state kinetic models that were integrated into Eq. (26) may sufficiently demonstrate the carbonation kinetics of industrial alkaline solid wastes. (Nam et al., 2012; Pan et al., 2018; Um & Ahn, 2017):

$$1 - (1 - \alpha)^{1/3})^n = kt \tag{26}$$

Using k as the rate constant, t representing the duration of the reaction, n as an adjustable index for the rate-controlling step, and α symbolizing the degree of conversion (with α = 1 indicating complete carbonation) as per Eq. (27).

$$\alpha = m_0 - m_t / m_0 - m_f \tag{27}$$

α represents the ratio of the difference between the initial weight (m_0) and the weight at time t (m_t) to the difference between the initial and final weight (m_f), as described by Eq. (27).

When adjusting the exponent n in Eq. (26), two distinct kinetic models emerge. For n = 1, Eq. (26) characterizes a strictly phase-boundary controlled reaction, pertinent to the early phases of carbonation. Here, the rate-determining factor is the chemical interaction at the phase boundary, such as the exterior of the untouched core. Conversely, for n = 2, Equation 26 is indicative of a diffusion-constrained reaction (as per the Jander equation). In this scenario, the rate is constrained by the diffusion through the accumulating layer of precipitated $CaCO_3$. The alignment between the experimental findings and the kinetic model is denoted by the correlation coefficients (R^2).

The activation energy can be deduced from the slope of the ensuing adjusted equation, given by:

$$\ln(k) = \ln(A) - E_a/RT \tag{28}$$

with the linear fitting of ln(k) and 1/T (See Paper II, Appendix). The activation energy (E_a) for OSA and WA have been determined to be 3.55 kJ/mol and 17.06 kJ/mol, respectively.

The calculated values in this work are consistent with the activation energy estimates for CaO and $Ca(OH)_2$ carbonation processes given in literature (Nikulshina et al., 2007).

The translated experimental data from the carbonation experiments are shown in figure 7 (reproduced from Paper II, figure 17). A relatively high R^2 value suggests that the model accurately captures the carbonation dynamics. For OSA (ln(t) < 2.5) and WA (ln(t) < 2.9) samples, values of Eq. (26) to the transformed data imply that the reaction is phase-boundary regulated during the initial stages of accelerated carbonation. Following the alteration in reaction rate, diffusion through the product layer now regulates carbonation. The change in slope for the plot of $\ln(1 - (1 -)^{1/3})^n$ vs. ln (t) serves as an example of the transition between the two kinetic models (t). For WA reaction circumstances, the shift in slope appears to be less pronounced and occurs later than for OSA, which is consistent with the CO_2 monitoring graphs and can be attributed to the higher SSA of WA delaying the onset of the diffusion phase (Paper II, figure 14–15). This supports the greater CO_2-uptake by showing that rate restrictions caused by diffusion through a developing layer of precipitated $CaCO_3$ are less significant when the solid is moving (exposing interior surfaces).

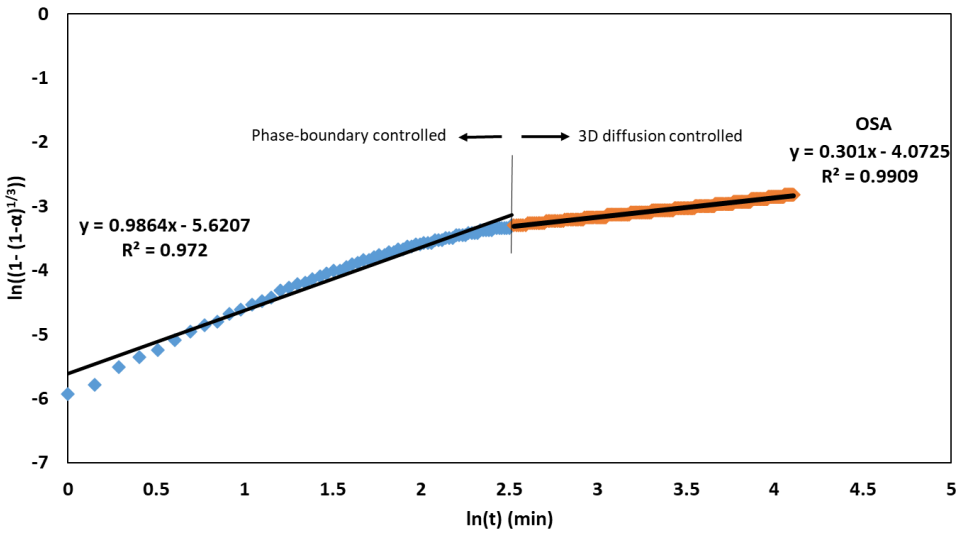

Figure 7. Assessment of the carbonation kinetics is presented through the relationship $\ln(1- (1 - \alpha)^{1/3})$ versus ln(t) for the carbonation of OSA monoliths, where R^2 denotes the correlation coefficient.

3.3.4 Microstructural and mineralogical changes

This section delves into the detailed investigations conducted to discern the nuanced changes at the microscopic level. Advanced analytical techniques, including XRD for mineralogical characterization, MIP for pore size distribution and porosity, SEM for detailed microstructural visualization, and EDS for elemental composition, were employed. The integration of these techniques provides a comprehensive understanding of the transformations that take place, bridging the knowledge gap between the macroscopic properties and the underlying microstructural causes.

Effect of carbonation on mineralogical properties

The mineralogical composition of the monoliths, as determined by XRD analysis, is explored for both OSA and WA samples. This investigation seeks to discern phase transformations resulting from carbonation as well as NS addition.

In uncarbonated OSA monoliths, the primary constituents are portlandite, calcite, and quartz, ettringite, anhydrite, orthoclase, and hematite also present in minor quantities (Paper III, figures 4–5). The XRD spectra of the hydrated specimens distinctly exhibited portlandite peaks, evident for both OSA and WA substrates (Paper II, Figure 18–19). Calcite predominantly emerges as the principal byproduct, whereas portlandite undergoes near-complete consumption. This suggests that the carbonation of portlandite is not strongly impeded by NS addition. The detection of the CSH phases in XRD analysis is challenging due to its amorphous nature and complex structure resulting weak diffraction patterns (Yang et al., 2018). Therefore, hydrated products (CH, CSH, CAH, CASH) are visible in small diffraction peaks and further existence of these phases are verified in SEM images with EDS analysis.

It is crucial to note that the development of strength cannot be simply attributed to the creation of calcite during carbonation; rather, the generation of hydrated compounds like CSH continues and plays a significant role in the increase in total strength (Zhan et al., 2016). This may explain why, in some cases, WA monoliths exhibit a stronger overall gain in strength than OSA monoliths after carbonation, despite absorbing less CO_2 (See Figure 12, Appendix 4).

The emergence of ettringite during the hydration/curing phase of monoliths is substantiated by the XRD pattern and the TGA of the uncarbonated OSA samples. Ettringite results from the reaction between calcium and alumina, elements typically found in cementitious matrices and supplementary cementitious materials, with sulphate (Wolf et al., 2019). The sulphates can either be naturally present in the cement paste or introduced externally.

Considering the NS added monoliths, it is known that calcium aluminates are often employed in ternary blend studies alongside other supplementary cementitious materials (Fernández-Carrasco & Vázquez, 2009). In this context, NS serves as a source of amorphous calcium aluminate.

In NS-added monoliths, peaks of CAH, CA(S)H and partial conversion of ettringite to amorphous phases are noted. When aluminosilicate materials are alkaline activated, NS introduces calcium aluminates as a source of aluminium that reacts, resulting in the formation of gels of binding CASH that hasten the development of strength (Zhang et al., 2021). Post-carbonation, partial ettringite decomposition is observed, see Eq. (29), potentially leading to the formation of calcium carbonate, gypsum, and alumina gel (Chen et al., 2020). Gypsum, being more soluble than anhydrite and ettringite, releases more sulphates into the leachate of the carbonated OSA monolith. While delayed ettringite formation can be detrimental to regular cement systems, in calcium aluminate cement systems, ettringite formed during hydration is typically the most significant hydrate. It largely contributes to these systems' unique properties, including rapid setting, hardening, drying, and shrinkage compensation (Amathieu & Touzo, 2007).

$$3CaO{\bullet}Al_2O_3{\bullet}3CaSO_4{\bullet}32H_2O + 3CO_2 \rightarrow 3CaCO_3 + 3(CaSO_4{\bullet}2H_2O) + Al_2O_3{\bullet}xH_2O + (26\text{-}x)\ H_2O \quad (29)$$

It is known that the phase and content of sulphates in fly ashes are important with the respect to problems occurring in fly ash blended PC concrete. The primary alkali sulphate-bearing phase in WA is arcanite with different chemical composition (K_2SO_4)

and different hydration reactivity (with C_3A) than gypsum or anhydrite. As a result of this, ettringite formation during the hydration/curing period is observed to be lower compared to OSA, which can be attributed to the lower Al content and lower hydration reactivity of K_2SO_4 in WA (Ma & Qian, 2022). In NS-added monoliths of WA, the intensity of arcanite peaks is lower compared to uncarbonated and carbonated monoliths, which could indicate the binding of sulphates in amorphous calcium aluminate phases observed by SEM-EDS analysis (Paper III, figure 8–9). Changes in the CAS phases are discussed in subsection 3.4.1, which are explained in greater detail with the aid of additional figures, in conjunction with the sulphate leaching process. However, it can be challenging to determine exact phases due to the amorphous nature and complex structure of the material. Hydroxyapatite, also observed in WA monoliths (Paper III, figure 5), could be partially responsible for high compressive strength values (Paper III, figure 2) (Wang et al., 2023; Tang et al., 2023). Figure 14 in Appendix 4 displays a schematic illustration of a representative segment "X" of a carbonated monolith produced under this research. One can see that the monolith in the figure is composed of tightly packed fly ash particles connected by a recently created carbonate network.

Effect of carbonation on microstructural properties

Another crucial factor that determines the physical strength of solidified formations is the porous structure and porosity. The precipitation of carbonate minerals, primarily calcite, which fills the porous spaces between the particles and fuses the various glassy fly ash particles together, contributes to the strength of the monoliths (Zajac et al., 2021; Monrose et al., 2020). MIP was utilized to calculate the pore size distribution of the OSA and WA monoliths in order to explore the effects of carbonation on the microstructure of the hardened monoliths. The MIP theory states that a non-wetting liquid (one with a contact angle greater than 90°) will only enter capillaries under pressure. The following is how Washburn (Diamond, 2000) discusses the connection between pressure and capillary diameter (Eq. (30)):

$$P = \frac{4\gamma cos\theta}{d} \tag{30}$$

where P = pressure, = liquid surface tension, = liquid contact angle (140° is chosen), and d = capillary diameter. The pore size distribution is computed using the volume intruded at each pressure increase. Total porosity is ascertained by dividing the cumulative volume of mercury intruded at the peak experimental pressure by the sample's bulk volume. Effective porosity is characterized by the volume of mercury extricated during the extrusion process. It should be noted that the MIP approach only determines the open porosity and does not measure pore size. Instead, it measures pore entry size. Big pores are overstated while small pores are underestimated as a result of the "ink-bottle effect". The water-to-solid ratio, mixing technique, and fineness of the particles are the key factors that determine how porous hydrated cementitious materials are.

After carbonation, OSA monoliths show a decrease in macropores with total porosity decreasing from 32% to 27% (see figure 8 reproduced from Paper III, figure 6), according to the MIP evaluation, which raises the corresponding compressive strength from 11.8 MPa to 41.5 MPa. With increasing calcite deposition and the filling impact of hydrated phases, total porosity decreases, and the drop becomes more pronounced. During carbonation, calcite is deposited on the inside of pores as well as at their entry, closing part of these pores and preventing mercury ingress. NS-added carbonated monoliths demonstrated fewer macropores than their carbonated OSA counterparts,

with a reduction in total porosity from 27% to 24%. Ettringite has a high molecular volume and low density, which might result in a partial reduction in it after carbonation leading to an overall increase in porosity (Justnes et al., 2020; Chen et al., 2022). This effect is lessened in the case of OSA by the later development of calcite polymorphs on the pore mouths. The space vacated by diminishing ettringite is in part reclaimed by the growth of denser calcite polymorphs, leading to fewer macropores in the NS-added carbonated monoliths. In the WA specimen, a discernible reduction in macroporosity from 20% to 15% underscores the pronounced influence of carbonation (See figure 9 reproduced from Paper III, figure 7). In the case of WA monoliths augmented with NS, there was a slight increase in macroporosity (from 20% to 21%) compared to the monoliths composed solely of WA. This observation can be attributed to the significant particle size disparity, with NS exhibiting coarser particles (Paper III, figure 1). Furthermore, the variance in macroporosity between monoliths derived from WA and those from OSA can be ascribed to the inherent compaction characteristics of the respective ashes. Specifically, WA tends to yield a denser structure upon compaction.

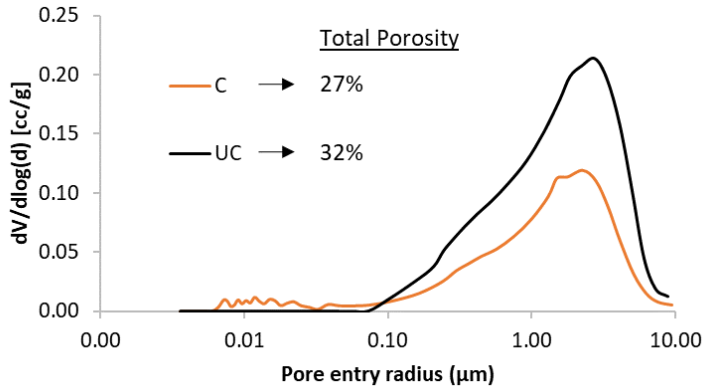

Figure 8. Differential pore volume distribution with total porosity values of uncarbonated (UC) and carbonated (C) OSA samples.

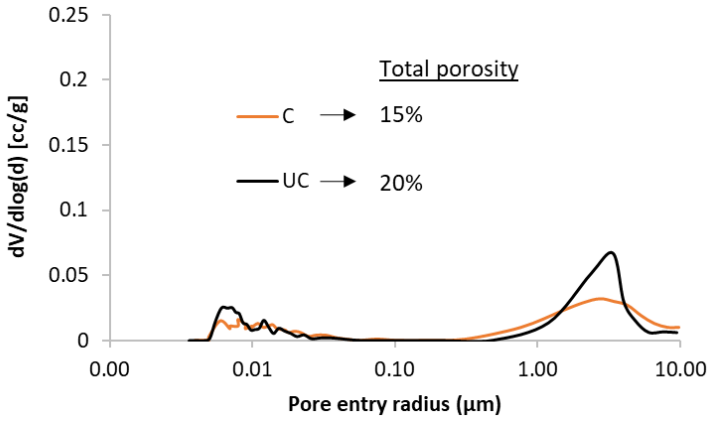

Figure 9. Differential pore volume distribution with total porosity values of uncarbonated (UC) and carbonated (C) WA samples.

SEM pictures (1000–5000 times magnified) and EDS examination of monoliths with uncarbonated, carbonated, and NS additions allowed for the identification of the morphological alterations and chemical composition. For the comparative microstructural analysis of hydrated and carbonated monoliths, samples are extracted proximal to the cylinder's surface (Paper II, figures 21–23; Paper III, figures 8–9). This selection criterion is based on the observation that the depth of the carbonation front progresses more slowly towards the inner sections of the monolith. This retardation is attributed to a reduced permeability of CO_2 stemming from the pore-clogging effects and the denser microstructure resulting from the precipitation of $CaCO_3$. Figure 10 (reproduced from Figure 8 in Paper III and figure 20-a in Paper II) depicts the OSA uncarbonated monolith with hexagonal lamellar portlandite crystals. The particles seem to merge, and the hydrated components appear intertwined, the hexagonal lamellae of portlandite seem enveloped by irregular, grainy products with approximate diameters around 1 m. The particles have a gritty look, along with some obvious large pores in hydrated samples and stubby laths. The elemental ratio for $Ca(OH)_2$ crystals is supported by the EDS of uncarbonated monoliths, which demonstrates that the end products are an amalgam of calcium and oxygen. Glassy fly ash particles that are spherical and surrounded by hydrated products can be seen in the uncarbonated WA image (Paper III, figure 9). In the carbonated OSA monolith, decalcified CSH or silica gel were combined with polymorphs of calcium carbonate that precipitated during carbonation into acicular and globular forms. The porous morphology of the hydrated monoliths undergoes a transformation, becoming denser upon carbonation. The non-presence of portlandite crystals within the carbonated samples aligns with the near-complete conversion anticipated from the XRD findings (Paper III, figures 18–19). While carbonated WA monoliths had calcite formations resembling those in OSA monoliths, they also had more of the smother gel-like surfaces with less porous structures (Paper III, figure 9). EDS has demonstrated that some of these locations include a combination of several elements in amorphous matrixes. The accelerated carbonation kinetics observed at elevated temperatures, as delineated in the section on the temperature's effect on carbonation, is manifested through the evolution of microcracks at these heightened temperatures. This phenomenon offers a plausible explanation for the diminished strength values recorded at the peak temperature of 75 °C, as depicted in Figure 21 of Paper II.

Along with calcite polymorphs, NS-added monoliths have shown needle-like CAS crystal growths (Paper III, figure 8–9). In general, WA monoliths were found to be denser and less porous than OSA monoliths, which is consistent with the findings of the MIP study (Paper III, figure 6–7).

Clusters of portlandite crystals are only found in the inner portion of the cylindrical specimens where carbonation front has not reached yet, according to SEM analyses along the sample depth. There are two plausible hypotheses that can coexist to account for this unsatisfactory conversion. The initial carbonated layer offers a macroscopic layer that prevents CO_2 gas from diffusing to the portlandite crystals, which is the first factor. This carbonated layer is expected to be less permeable because of the pore closure caused by the precipitation of larger $CaCO_3$ crystals (36.9 cm^3/mol) than $Ca(OH)_2$ crystals (33.6 cm^3/mol) on the pore throats. The second explanation might be that not enough water is present for the reaction to occur because of the increased carbonation reaction's exothermic nature and the hydrophilicity of $CaCO_3$ crystals is lower than that of $Ca(OH)_2$ crystals (Costa et al., 2021; Gluth et al., 2022).

Figure 10. SEM images and numbered positions for quantitative EDS analysis of OSA uncarbonated (top) and, carbonated (bottom) samples.

3.3.5 Leaching properties of monoliths

One of the most important aspects of waste disposal in landfills or reuse is the release of dangerous compounds into the environment. In accordance with the criteria and procedures for waste acceptance at landfills set forth in Council Directive 1999/31/EC of April 26, 1999, wastes transferred to landfills are divided into three categories: “inert”, “non-hazardous”, and “hazardous” based on their leachability and stability. Sulphate leaching limitations are 1000, 20000, and 50000 mg/kg of waste, respectively, for these landfills.

OSA and WA often contain elevated concentrations of heavy metals such as cadmium, lead, and arsenic, which are known to be toxic to both aquatic and terrestrial ecosystems. Additionally, the presence of sulphates in these ashes can lead to the formation of acid when they come into contact with water, potentially resulting in acid mine drainage-like conditions. When these ashes are disposed of in landfills without proper containment

measures, there is a risk of leachate generation, which can contaminate surrounding soil and groundwater. This contamination can disrupt local ecosystems, pose health risks to communities relying on affected water sources, and result in long-term environmental degradation. The complex mineralogy and potential reactivity of OSA and WA necessitate a comprehensive understanding of their environmental behaviour and the development of strategies to mitigate their impact.

The pH measurements of the successive leachates indicate a steady decrease from around 12.8 at the beginning stage to around 11.4 when $Ca(OH)_2$ is depleted in the monoliths of OSA (Paper III, Figure 10). The pH levels for WA also dropped from an initial value of 13.1 to approximately 11.8.

OSA and WA uncarbonated monoliths have pH levels between 12.3 and 12.7, which fall to 11.4 to 11.9 after carbonation. At the various pH ranges mentioned in the literature, the stability domain of sulphate ettringite typically ranges between 10.5 and 13.

According to sulphate leaching results, after carbonation, the sulphate content in 100% OSA increases from 2260 mg/kg to 6510 mg/kg (Paper III, Figure 11). Carbonation leads to the creation of carbonates in the pore water contending with anions such as hydroxides and sulphates for combining with positively charged ions [Schnabel, 2021]. Furthermore, in standard cement-based structures, sulphate formation occurs as a result of ettringite breaking down during carbonation (Paper III, Section 3.2). OSA monoliths that have been carbonated have more sulphates seeping out of them than monoliths that have not been carbonated. Due to the greater starting concentration in WA and the higher solubility of arcanite compared to anhydrite, WA showed significantly higher sulphate leaching levels than OSA. When compared to OSA monoliths, ettringite and other CAS production during the hydration period is seen to be significantly reduced in WA monoliths. The diminished ettringite crystallization observed in WA pre-carbonation, a principal determinant for augmented sulphate solubilization in OSA, provides a rationale for the differential sulphate leaching behaviour exhibited by WA upon carbonation. Compared to OSA, a modest decrease following carbonation is seen in WA monoliths. This could be because sulphates are physically encapsulated when calcite is formed.

The highly soluble minerals halite and sylvite contain chloride ions, according to the mineralogical study. Thus, as shown in Paper III, figure 14, the chloride leaching values from monoliths are below the non-hazardous waste landfill limitations. For both OSA and WA monoliths, carbonation has marginally reduced the concentrations of Cl^- leaching. The landfill limit for non-hazardous wastes, which is 15000 mg/kg of waste, is not reached for any Cl^- leaching levels.

According to leaching data, the levels of Cr, Cu, and Zn for OSA increased after carbonation curing, while the levels of Ba for WA barely increased (Paper III, Table 6). All the leaching values for heavy metals are below the permissible level for non-hazardous waste landfills. While Zn, Cu and Ba were below the inert limit for uncarbonated samples, Cr was the sole element that remained above the inert landfill limit. The leaching characteristics of several types of OSA as well as OSA-based mortars have been discussed by Irha et al. (2014) and Uibu et al. (2016). Their research demonstrates that during the curing process, the fraction of readily soluble inorganic components decreased while the mobility of potentially hazardous Cd and Zn did not change, despite the fact that the leachates under study were highly alkaline and saturated with various ions (the predominant ions were Ca^{2+}, K^+, Na^+, and SO_4^{2-}). Due to the carbonated layer

reducing the amount of free ions in the material, which are responsible for conducting electricity, EC values show a reduction with carbonation (Paper III, figure 15). The loss in porosity caused by the creation of the carbonated layer can further restrict ion mobility and help explain the decline in EC.

In general, carbonation significantly influences the leaching behaviours of OSA and WA monoliths, with OSA showing an increased sulphate content post-carbonation, while WA exhibited subdued sulphate leaching due to limited ettringite formation. Concurrently, heavy metal leaching, including elements like Cr, Cu, and Zn, varied after carbonation yet remained within acceptable limits for non-hazardous waste landfills.

Effect of NS addition on sulphate control and leaching properties

The noted reduction in pH after introducing NS, when contrasted with the uncarbonated NS-integrated monolith, offers evidence in favour of the carbonation reaction hypothesis. As the pH of the system decreases due to carbonation, the solubility of sulphate compounds can increase. Specifically, calcium sulphoaluminate phases, which are present in cementitious systems, can become more soluble in less alkaline conditions. When these phases dissolve, they release sulphate ions into the solution (Hou et al., 2022). Notably, in this context, the pH remains above 11, a stability threshold for ettringite formation (Paper III, figure 10).

In the context of OSA monoliths, both the uncarbonated and carbonated forms, after NS addition, exhibited no significant sulphate leaching. Following NS incorporation, a residual sulphate concentration below 2 mg SO_4^{2-}/kg of ash was discerned, which persisted post-carbonation. This demonstrates the efficacy of NS in mitigating the adverse consequences of carbonation-induced sulphate leaching in OSA matrices.

For WA samples, the introduction of NS substantially curtailed the sulphate leaching concentration prior to carbonation, with an additional reduction observed post-carbonation. Relative to a pure WA sample, the post-carbonation and NS addition led to a significant reduction, approximating 14,000 mg SO_4^{2-}/kg of ash.

Rapid hydration of calcium aluminates yields calcium ions, which can foster the carbonation of fly ash by providing carbon dioxide a reactive surface. Such a phenomenon potentially augments the carbonation propensity of fly ashes, thereby enhancing carbon dioxide sequestration within cementitious systems. This rapid hydration might also precipitate the formation of CAS phases, scavenging sulphate ions and consequently reducing their mobility — a pivotal consideration.

Considering sulphate leaching, SEM images of NS-added monoliths and associated mineralogical analyses have been scrutinized. The chemical composition of hydrated phases and the overarching mineralogical configuration undergo transformations upon niobium slag introduction, profoundly influencing bound sulphate (See figures 11–12 reproduced from Paper III, figures 12–13). Broadly, alterations in monolith microstructure induced by both chemical and physical processes, notably carbonation and NS introduction, modulate sulphate mobility in OSA and WA. This modulation mechanism is underpinned by complex mechanical, chemical, and microstructural dynamics. Predicated on clinker mineralogy, the hydrated phases manifest as CSH, AFt, and AFm. The SO_4^{2-} is stabilized by ettringite crystal formations and within C(A)SH gels, with matrix heavy metals additionally sequestered by AFm and CSH phases (Zajac et al., 2023; Keulen et al., 2018). Figure 11 delineates a SEM representation of the NS-added OSA monolith juxtaposed with XRD patterns highlighting recognized CAS peak locations. Notably, ettringite peaks remain robust post-carbonation, albeit with diminished intensity in NS-added monoliths. Concurrent with NS incorporation, the emergence of divergent CAS

phase peaks becomes pronounced. Within the OSA context, it's inferred that specific CAS phases, alongside a more stable anhydrite, are observable in NS-added monoliths. Xu et al. (2018) have mentioned that anhydrite's presence enhances ettringite's stability over alternative calcium sulphate sources. Analogously, for WA, a SEM portrayal of an NS-added monolith, depicting the enhanced precision of needle-like formations, was coupled with XRD patterns highlighting arcanite and CAS phases (figure 12). The intensity and distinction of sulphate-rich arcanite in NS-added WA monoliths appeared diminished.

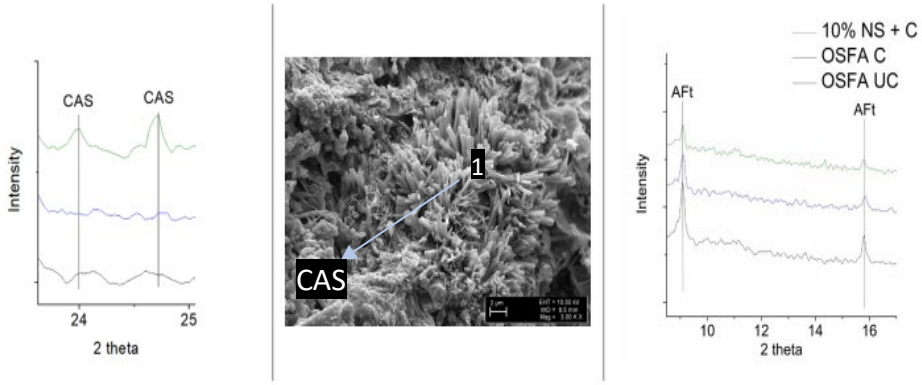

Figure 11. SEM imagery of carbonated OSA with added NS, accompanied by segmented XRD patterns highlighting the CAS peaks of uncarbonated (UC) and carbonated (C), and added NS.

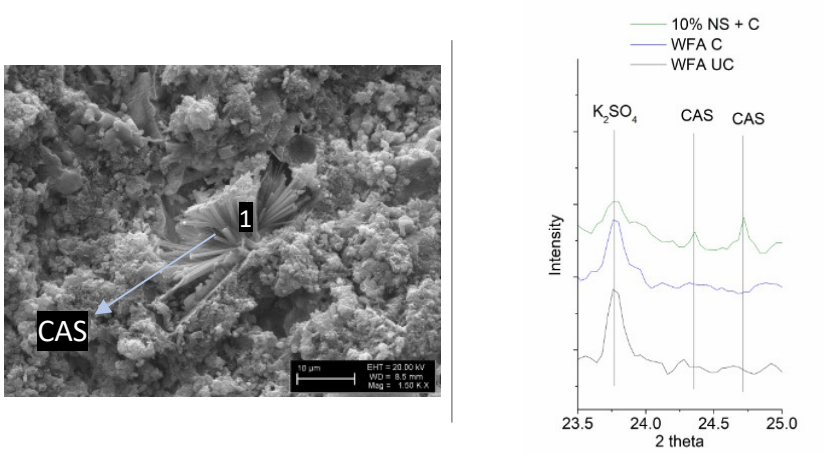

Figure 12. SEM imagery of WA with added NS, accompanied by segmented XRD patterns highlighting the K_2SO_4 and CAS peaks

The mobility of Cl^- in WA manifests a marked reduction with NS addition, with a subsequent decline post-carbonation. Post procedural NS addition and carbonation, a congruent trend in SO_4^{2-} and Cl^- mobility was observed in WA monoliths. Notably, either NS incorporation or the carbonation process exerted negligible influence on Cl^- leaching metrics within OSA. Conversely, NS integration consistently lowered heavy metal leaching readings. Both carbonation and NS addition led to pronounced reductions in Sr

and Rb mobility across WA and OSA monoliths. Barring Cr, Cu, and Zn, which remained below thresholds in NS-added monoliths, landfilling regulatory limits for inert waste pertaining to OSA were adhered to. Subsequent to chemical and structural modifications induced by carbonation and NS addition in fly ash monoliths, both ions and heavy metals are immobilized, thereby curtailing their availability for EC.

4 CONCLUSIONS

This study primarily investigates the accelerated carbonation process to repurpose fly ashes into compacted monoliths for potential use in construction sector, addressing the challenges of CO_2 emissions and ash accumulation in Estonia. Owing to the abundant presence of free lime (14–23 %) conducive to CO_2 uptake and the existence of active Ca-silicates that impart self-cementitious properties, the compaction and carbonation process is acknowledged as a sustainable approach for waste utilization, serving dual purposes: CO_2 sequestration and the possible application of cement-free construction materials.

Through the accelerated carbonation process, the monoliths demonstrated a compressive strength ranging from 10–45 MPa, contingent upon diverse curing parameters and the specific ash types utilized and an average of 10 to 15 wt.% of CO_2 uptake was achieved. The study further examined the leaching properties of carbonated monoliths to ensure compliance with environmental and safety standards. The results highlighted that the accelerated carbonation process, combined with the addition of calcium aluminate-enriched NS (10 wt.%), enhanced the compressive strength of high sulphur fly ash (4 to 8 wt.% S) -based monoliths, reduced heavy metal leaching, and effectively immobilized sulphates without compromising the monoliths' structural integrity.

The primary findings of this research can be summarized as:

- Based on TGA and XRD analyses, approximately 90% of the portlandite undergoes carbonation, resulting in the formation of calcite. MIP results indicate that this calcite fills the pores, while SEM and EDS analyses suggest that it acts as a bridging between gaps around the particles. Primarily accelerated carbonation process and together with hydraulic and limited pozzolanic reactions contribute to a strength development, amplifying it up to fourfold within short curing durations of 2–4 hours.
- The kinetics of the carbonation conversion reaction were assessed using various reaction-order models, leveraging real-time gas monitoring data at specific temperatures. In the initial phases of accelerated carbonation of the samples, the reaction predominantly aligns with phase-boundary control. Yet, as the reaction rate conversion degree evolves, carbonation becomes predominantly governed by diffusion through the product layer.
- Carbonation curing marginally reduces leachate pH, influenced by extended hydration reactions and the distinct chemical and mineralogical profiles of various fly ashes. As a result of this pH alteration is not solely attributed to portlandite consumption.
- Sulphate leaching is effectively curtailed through a bifurcated mechanism: the chemical association with calcium aluminate sulphate (CAS) phases and the physical encapsulation within the matrix of calcium aluminate hydrate (CAH).
- Sulphate leaching tests in case of OSA indicated that after carbonation curing concentrations escalated to roughly 2.88 times the initial concentration (from 2260 mg SO_4^{2-}/kg to 6510 mg SO_4^{2-}/kg) due to ettringite carbonation. However, with a 10% NS addition, sulphate leaching was reduced to below 2 mg SO_4^{2-}/kg of ash which is less than 0.1% of the initial concentration, indicating a substantial mitigation in sulphate presence.
- In WA, the similar increase in sulphate leaching was not observed upon carbonation, due to the absence of stable sulphate-bearing compounds (such as ettringite, monosulphoaluminate, thaumasite). Conversely, a slight decrease in leaching

was noted, attributable to the physical entrapment of sulphates by calcite formation and calcium aluminate hydrate.

- In WA, the incorporation of NS markedly reduces the sulphate leaching concentration prior to carbonation, with a subsequent decline observed after carbonation curing, culminating in a 30% reduction from the initial concentration of 48,000 mg SO_4^{2-}/kg.

The originality and the novelty of this research are three-fold relating to waste utilization, atmospheric carbon reduction and environmental safeguarding. Firstly, the study utilizes 100% waste to produce construction materials, underscoring a significant advancement in resource recovery. Secondly, the CO_2 sequestration in the repurposed waste contributes to environmental sustainability by reducing carbon emissions. Lastly, despite the deliberate choice of high sulphur ashes, a notable characteristic of the end product is its low-leaching behaviour concerning sulphur and heavy metals at the studied conditions. This attribute establishes the material's thermodynamic stability, mitigating the environmental impact of potentially hazardous wastes.

The methodology of accelerated carbonation of fly ashes presents potential applicability in the synthesis of structural building materials which may pave the way of new ash utilization and carbonation routes. Future research endeavours should emphasize enhancing the augmentation of both mechanical and surface attributes of targeted products. A thorough market assessment and cost-benefit analysis are recommended to ascertain the feasibility of targeted applications.

REFERENCES

Afroz, S., Zhang, Y., Nguyen, Q. D., Kim, T., & Castel, A. (2023). Shrinkage of blended cement concrete with fly ash or limestone calcined clay. *Materials and Structures*, 56(1), 15.

Aghaeipour, A., & Madhkhan, M. (2020). Mechanical properties and durability of roller compacted concrete pavement (RCCP)–a review. *Road Materials and Pavement Design*, 21(7), 1775-1798.

Alaloul, W. S., Al Salaheen, M., Malkawi, A. B., Alzubi, K., Al-Sabaeei, A. M., & Musarat, M. A. (2021). Utilizing of oil shale ash as a construction material: A systematic review. *Construction and Building Materials*, 299, 123844.

Alterary, S. S., & Marei, N. H. (2021). Fly ash properties, characterization, and applications: A review. *Journal of King Saud University-Science*, 33(6), 101536.

Amathieu, L., & Touzo, B. (2007). Ettringite binder for dense mortar, comprising calcium sulphates and a mineral compound of calcium aluminates. In: *Google Patents*.

American Coal Ash Association Coal Combustion Product (CCP) Production & Use Survey Report 2020 ; 2020; https://acaa-usa.org/wp-content/uploads/2021/12/2020-Production-and-Use-Survey-Results-FINAL.pdf.

Aresta, M., Karimi, I., & Kawi, S. (2019). *An economy based on carbon dioxide and water*. Springer International Publishing, Germany.

ASTM Committee C-09 on Concrete and Concrete Aggregates. (2013). *Standard specification for coal fly ash and raw or calcined natural pozzolan for use in concrete* (ASTM C618-12a). ASTM International.

Ates, F., Park, K. T., Kim, K. W., Woo, B. H., & Kim, H. G. (2023). Effects of treated biomass wood fly ash as a partial substitute for fly ash in a geopolymer mortar system. *Construction and Building Materials*, 376, 131063.

Azdarpour, A., Junin, R., Asadullah, M., Hamidi, H., Manan, M., & Mohamad Daud, A. R. (2015). Calcium carbonate production through direct mineral carbon dioxide sequestration. *Applied Mechanics and Materials*, 699, 1020-1025.

Baciocchi, R., & Costa, G. (2022). CO_2 Storage Utilization in Useful and Mineral Long-Term Products by Carbonation of Alkaline Feedstocks. In (Aresta, Dibenedetto, & Bocarsly, Eds) *Beyond Current Research Trends in CO_2 Utilization*.

Back, M., Kuehn, M., Stanjek, H., & Peiffer, S. (2008). Reactivity of alkaline lignite fly ashes towards CO_2 in water. *Environmental Science & Technology*, 42(12), 4520-4526.

Baena-Moreno, F. M., Leventaki, E., Riddell, A., Wojtasz-Mucha, J., & Bernin, D. (2023). Effluents and residues from industrial sites for carbon dioxide capture: a review. *Environmental Chemistry Letters*, 21(1), 319-337.

Balachandra, A. M., Abdol, N., Darsanasiri, A. G. N. D., Zhu, K., Soroushian, P., & Mason, H. E. (2021). Landfilled coal ash for carbon dioxide capture and its potential as a geopolymer binder for hazardous waste remediation. *Journal of Environmental Chemical Engineering*, 9(4), 105385.

Banaszkiewicz, K., Marcinkowski, T., & Pasiecznik, I. (2022). Fly Ash as an ingredient in the contaminated soil stabilization process. *Energies*, 15(2), 565.

Bauert, H., & Kattai, V. (1997). Kukersite oil shale. *Geology and mineral resources of Estonia*, 313-327.

Becerra-Duitama, J. A., & Rojas-Avellaneda, D. (2022). Pozzolans: A review. *Engineering and Applied Science Research*, 49(4), 495-504.

Berber, H. (2020). *Accelerated Carbonation Treatment of Industrial Wastes: Physicochemical, Environmental and Economic Aspects* (Doctoral Dissertation). Tallinn University of Technology.

Bernal, S. A., Rodríguez, E. D., Kirchheim, A. P., & Provis, J. L. (2016). Management and valorisation of wastes through use in producing alkali-activated cement materials. *Journal of Chemical Technology & Biotechnology*, 91(9), 2365-2388.

Berra, M., Ippolito, N. M., Mangialardi, T., Paolini, A. E., & Piga, L. (2019). Leaching test procedure for assessing the compliance of the chemical and environmental requirements of hardened woody biomass fly ash cement mixtures. *Waste Management,* 90, 10-16.

Bertos, M. F., Simons, S., Hills, C., & Carey, P. (2004). A review of accelerated carbonation technology in the treatment of cement-based materials and sequestration of CO_2. *Journal of Hazardous Materials*, 112(3), 193-205.

Bhagat, M., Singh, S., Suresh, S., Arisutha, S., Verma, S., & Kansal, S. K. (2023). Utilization of value-added products from fly ash: An industrial waste. In (Srivastava et.al Eds) *Advanced Materials from Recycled Waste*. Elsevier.

Board, O. S., & National Academies of Sciences, Engineering, and Medicine. (2019). *Negative emissions technologies and reliable sequestration: a research agenda.*

Bobicki, E. R., Liu, Q., Xu, Z., & Zeng, H. (2012). Carbon capture and storage using alkaline industrial wastes. *Progress in Energy and Combustion Science*, 38(2), 302-320.

Burger, M., & Gundlach, J. (2017). *Status of Climate Change Litigation, a Global Review*. Kenya: United Nations Environment Programme.

Carević, V., Ignjatović, I., & Dragaš, J. (2019). Model for practical carbonation depth prediction for high volume fly ash concrete and recycled aggregate concrete. *Construction and Building Materials*, 213, 194-208.

Carro-López, D., González-Fonteboa, B., Eiras-López, J., & Seara-Paz, S. (2019). Comparing circulating fluidised bed fly ash and limestone as additions for cement. *Magazine of Concrete Research*, 71(24), 1302-1311.

Chai, S. Y. W., Ngu, L. H., How, B. S., Chin, M. Y., Abdouka, K., Adini, M. J. B. A., & Kassim, A. M. (2022). Review of CO_2 capture in construction-related industry and their utilization. *International Journal of Greenhouse Gas Control*, 119, 103727.

Chaipanich, A., & Chindaprasirt, P. (2015). The properties and durability of autoclaved aerated concrete masonry blocks. In (Chindaprasirt et al., Eds) *Eco-Efficient Masonry Bricks and Blocks*. Woodhead Publishing.

Chang, E.-E., Chen, C.-H., Chen, Y.-H., Pan, S.-Y., & Chiang, P.-C. (2011). Performance evaluation for carbonation of steel-making slags in a slurry reactor. *Journal of Hazardous Materials*, 186(1), 558-564.

Chen, B., Horgnies, M., Huet, B., Morin, V., Johannes, K., & Kuznik, F. (2020). Comparative kinetics study on carbonation of ettringite and meta-ettringite based materials. *Cement and Concrete Research*, 137, 106209.

Chen, K., Wu, D., Zhang, Z., Pan, C., Shen, X., Xia, L., & Zang, J. (2022). Modeling and optimization of fly ash–slag-based geopolymer using response surface method and its application in soft soil stabilization. *Construction and Building Materials*, 315, 125723.

Chen, T. L., Chen, Y. H., Dai, M. Y., & Chiang, P. C. (2021). Stabilization-solidification-utilization of MSWI fly ash coupling CO_2 mineralization using a high-gravity rotating packed bed. *Waste Management*, *121*, 412-421.

Chen, X., Gao, J., Yan, Y., & Liu, Y. (2017). Investigation of expansion properties of cement paste with circulating fluidized bed fly ash. *Construction and Building Materials*, 157, 1154-1162.

Chen, X., Zhang, J., Lu, M., Chen, B., Gao, S., Bai, J., ... & Yang, Y. (2022). Study on the effect of calcium and sulphur content on the properties of fly ash based geopolymer. *Construction and Building Materials*, 314, 125650.

Cherian, C., & Siddiqua, S. (2019). Pulp and paper mill fly ash: A review. *Sustainability*, 11(16), 4394.

Chindaprasirt, P., Kasemsiri, P., Poomsrisa-Ard, S., & Posi, P. (2019). Fluidized bed coal-bark fly ash geopolymer with additives cured at ambient temperature. *Geomate Journal*, 16(54), 29-35.

Cizer, Ö., Van Balen, K., Elsen, J., & Van Gemert, D. (2012). Real-time investigation of reaction rate and mineral phase modifications of lime carbonation. *Construction and Building Materials*, 35, 741-751.

Colman, C., Bulteel, D., Elkarim, B. M., Rémond, S., & Courard, L. (2023). Expansion of concrete by secondary ettringite formation due to fine recycled aggregates contaminated with gypsum. *Advances in Cement Research*, 1-9.

Costa, A. R. D., & Gonçalves, J. P. (2021). Accelerated carbonation of ternary cements containing waste materials. *Construction and Building Materials*, 302, 124159.

Da Silva, S. R., & Andrade, J. J. D. O. (2022). A review on the effect of mechanical properties and durability of concrete with construction and demolition waste (CDW) and fly ash in the production of new cement concrete. *Sustainability*, 14(11), 6740.

Dai, X., Aydin, S., Yardimci, M. Y., Qiang, R. E. N., Lesage, K., & De Schutter, G. (2021). Rheology, early-age hydration and microstructure of alkali-activated GGBFS-Fly ash-limestone mixtures. *Cement and Concrete Composites*, 124, 104244.

Danraka, M. N., Aziz, F. N. A. A., Jaafar, M. S., Nasir, N. M., & Abdulrashid, S. (2019). Application of wood waste ash in concrete making: revisited. In GCEC 2017: *Proceedings of the 1st Global Civil Engineering Conference 1* (pp. 69-78). Springer Singapore.

Das, D., & Rout, P. K. (2023). A Review of Coal Fly Ash Utilization to Save the Environment. *Water, Air, & Soil Pollution*, 234(2), 128.

Dave, N., Misra, A. K., Srivastava, A., & Kaushik, S. K. (2016). Experimental analysis of strength and durability properties of quaternary cement binder and mortar. *Construction and Building Materials*, 107, 117-124.

De Maeijer, P. K., Craeye, B., Snellings, R., Kazemi-Kamyab, H., Loots, M., Janssens, K., & Nuyts, G. (2020). Effect of ultra-fine fly ash on concrete performance and durability. *Construction and Building Materials*, 263, 120493.

Deonarine, A., Schwartz, G. E., & Ruhl, L. S. (2023). Environmental Impacts of Coal Combustion Residuals: Current Understanding and Future Perspectives. *Environmental Science & Technology*, 57(5), 1855-1869.

Diamond, S. (2000). Mercury porosimetry: an inappropriate method for the measurement of pore size distributions in cement-based materials. *Cement and Concrete Research*, 30(10), 1517-1525.

Dindi, A., Quang, D. V., Vega, L. F., Nashef, E., & Abu-Zahra, M. R. (2019). Applications of fly ash for CO2 capture, utilization, and storage. *Journal of CO_2 Utilization*, 29, 82-102.

Dos Reis, G. S., Cazacliu, B. G., Cothenet, A., Poullain, P., Wilhelm, M., Sampaio, C. H., ... & Torrenti, J. M. (2020). Fabrication, microstructure, and properties of fired clay bricks using construction and demolition waste sludge as the main additive. *Journal of Cleaner Production*, 258, 120733.

du Toit, G., van der Merwe, E. M., Kruger, R. A., McDonald, J. M., & Kearsley, E. P. (2022). Characterisation of the hydration products of a chemically and mechanically activated high coal fly ash hybrid cement. *Minerals*, 12(2), 157.

Du, H., Steinacher, M., Borca, C., Huthwelker, T., Murello, A., Stellacci, F., & Amstad, E. (2018). Amorphous $CaCO_3$: Influence of the formation time on its degree of hydration and stability. *Journal of the American Chemical Society*, 140(43), 14289-14299.

Du, Y., Fu, C., Gong, B., Miao, E., Zheng, X., Xiong, Z., ... & Zhang, J. (2021). Real-time investigation of the CO_2 mineral carbonation reaction rate through direct aqueous route using semi-dry desulphurization slag. *Journal of CO_2 Utilization*, 51, 101614.

Duan, S., Liao, H., Cheng, F., & Tao, M. (2020). Effect of curing condition and carbonization enhancement on mechanical properties of fly ash-desulphurization gypsum-steel slag blocks. *Journal of CO_2 Utilization*, 38, 282-290.

Elahi, M. M. A., Shearer, C. R., Reza, A. N. R., Saha, A. K., Khan, M. N. N., Hossain, M. M., & Sarker, P. K. (2021). Improving the sulphate attack resistance of concrete by using supplementary cementitious materials (SCMs): A review. *Construction and Building Materials*, 281, 122628.

Ellis, P. R., Hayes, M. J., Macleod, N., Schuyten, S. J., Tway, C. L., & Zalitis, C. M. (2023). Carbon conversion: opportunities in chemical productions. In (Wang, Eds) *Surface Process, Transportation, and Storage*. Gulf Professional Publishing.

Environmental Protection Agency. (2015, April 17). *Hazardous and Solid Waste Management System; Disposal of Coal Combustion Residuals from Electric Utilities*. Federal Register. Retrieved from https://www.federalregister.gov/documents/2015/04/17/2015-00257/hazardous-and-solid-waste-management-system-disposal-of-coal-combustion-residuals-from-electric

ERIA (Economic Research Institute for ASEAN and East Asia). (2022). *Annual Report 2022*. Retrieved from https://www.eria.org/publications/annual-report-2022/.

European Committee for Standardization. (2012). *Fly ash for concrete - Definition, specifications and conformity criteria* (EN 450-1:2012). Brussels, Belgium: CEN

Fang, Y., & Chang, J. (2015). Microstructure changes of waste hydrated cement paste induced by accelerated carbonation. *Construction and Building Materials*, 76, 360-365.

Farhan, N. A., Sheikh, M. N., & Hadi, M. N. (2019). Investigation of engineering properties of normal and high strength fly ash based geopolymer and alkali-activated slag concrete compared to ordinary Portland cement concrete. *Construction and Building Materials*, 196, 26-42.

Fernández-Carrasco, L., & Vázquez, E. (2009). Reactions of fly ash with calcium aluminate cement and calcium sulphate. *Fuel*, 88(9), 1533-1538.

Fořt, J., Šál, J., Žák, J., & Černý, R. (2020). Assessment of wood-based fly ash as alternative cement replacement. *Sustainability*, 12(22), 9580.

Freidin, C. (1998). Hydration and strength development of binder based on high-calcium oil shale fly ash. *Cement and Concrete Research*, 28(6), 829-839.

Gartner, E., & Sui, T. (2018). Alternative cement clinkers. *Cement and Concrete Research*, 114, 27-39.

Gerdemann, S. J., O'Connor, W. K., Dahlin, D. C., Penner, L. R., & Rush, H. (2007). Ex situ aqueous mineral carbonation. *Environmental Science & Technology*, 41(7), 2587-2593.

Ghacham, A. B., Pasquier, L. C., Cecchi, E., Blais, J. F., & Mercier, G. (2017). Valorization of waste concrete through CO_2 mineral carbonation: Optimizing parameters and improving reactivity using concrete separation. *Journal of Cleaner Production*, 166, 869-878.

Glinicki, M. A., Jóźwiak-Niedźwiedzka, D., & Dąbrowski, M. (2019). The influence of fluidized bed combustion fly ash on the phase composition and microstructure of cement paste. *Materials*, 12(17), 2838.

Gluth, G. J., Ke, X., Vollpracht, A., Weiler, L., Bernal, S. A., Cyr, M., ... & Walkley, B. (2022). Carbonation rate of alkali-activated concretes and high-volume SCM concretes: a literature data analysis by RILEM TC 281-CCC. *Materials and structures*, 55(8), 225.

Gorkunov, V., & Munter, R. (2007, September). Calcium-aluminothermal production of niobium and mineral composition of the slag. *In Proceedings of the Estonian Academy of Sciences, Chemistry*, 56(3), 142–156.

Gökçe, H. S., M. Tuyan, K. Ramyar, and M. L. Nehdi. (2020). Development of eco-efficient fly ash–based alkali-activated and geopolymer composites with reduced alkaline activator dosage. *Journal of Materials in Civil Engineering,* 32(2), 04019350.

Grünhäuser Soares, E., Castro-Gomes, J., Sitarz, M., Zdeb, T., & Hager, I. (2021). The immobilisation of heavy metals from sewage sludge ash in CO_2-cured mortars. *Sustainability*, *13*(22), 12893.

Gu, Q., Wang, T., Wu, W., Wang, D., & Jin, B. (2021). Influence of pretreatments on accelerated dry carbonation of MSWI fly ash under medium temperatures. *Chemical Engineering Journal*, 414, 128756.

Gunning, P. J., Hills, C. D., & Carey, P. J. (2010). Accelerated carbonation treatment of industrial wastes. *Waste Management*, 30(6), 1081-1090.

Han, Q., Zhang, P., Wu, J., Jing, Y., Zhang, D., & Zhang, T. (2022). Comprehensive review of the properties of fly ash-based geopolymer with additive of nano-SiO_2. *Nanotechnology Reviews*, 11(1), 1478-1498.

Hanisková, D., Bartoníčková, E., Koplík, J., & Opravil, T. (2016). The ash from fluidized bed combustion as a donor of sulphates to the Portland clinker. *Procedia Engineering*, 151, 394-401.

Hao, Y., Yang, G., & Liang, K. (2022). Development of fly ash and slag based high-strength alkali-activated foam concrete. *Cement and Concrete Composites*, 128, 104447.

Hassan, A., Ilyas, S. Z., Jalil, A., & Ullah, Z. (2021). Monetization of the environmental damage caused by fossil fuels. *Environmental Science and Pollution Research*, 28, 21204-21211.

He, J., Long, G., Ma, K., & Xie, Y. (2021). Influence of fly ash or slag on nucleation and growth of early hydration of cement. *Thermochimica Acta*, 701, 178964.

Herath, C., Gunasekara, C., Law, D. W., & Setunge, S. (2020). Performance of high volume fly ash concrete incorporating additives: A systematic literature review. *Construction and Building Materials*, 258, 120606.

Hewlett, P., & Liska, M. (Eds.). (2019). *Lea's chemistry of cement and concrete*. Butterworth-Heinemann.

Hills, C. D., & Pollard, S. J. (1997). The influence of interference effects on the mechanical, microstructural and fixation characteristics of cement-solidified hazardous waste forms. *Journal of Hazardous Materials*, 52(2-3), 171-191.

Hills, C. D., Tripathi, N., & Carey, P. J. (2020). Mineralization technology for carbon capture, utilization, and storage. *Frontiers in Energy Research*, 8, 142.

Hosan, A., & Shaikh, F. U. A. (2022). Chloride-Induced Corrosion Resistance of High-Volume Slag and High-Volume Slag–Fly Ash Blended Concretes Containing Nanomaterials. *Journal of Materials in Civil Engineering*, 34(5), 04022041.

Hošková, Š. Á. R. K. A., Tichá, P. E. T. R. A., & Demo, P. (2009). Determination of Ca2+ ions at early stage of hydrating cement paste. *Ceram.-Silik*, 53, 76-80.

Hou, W., Liu, J., Liu, Z., He, F., Zhu, J., Cui, Y., & Jinyang, W. (2022). Calcium transfer process of cement paste for ettringite formation under different sulphate concentrations. *Construction and Building Materials*, 348, 128706.

Huijgen, W. J. J., & Comans, R. N. J. (2005). Mineral CO_2 sequestration by carbonation of industrial residues. *Energy Research Centre of the Netherlands (ECN). Petten, The Netherlands.*

Hui-Teng, N., Cheng-Yong, H., Yun-Ming, L., Abdullah, M. M. A. B., Hun, K. E., Razi, H. M., & Yong-Sing, N. (2021). Formulation, mechanical properties and phase analysis of fly ash geopolymer with ladle furnace slag replacement. *Journal of Materials Research and Technology*, 12, 1212-1226.

Humbert, P. S., & Castro-Gomes, J. (2019). CO_2 activated steel slag-based materials: A review. *Journal of Cleaner Production*, 208, 448-457.

Humbert, P. S., Castro-Gomes, J. P., & Savastano Jr, H. (2019). Clinker-free CO_2 cured steel slag based binder: Optimal conditions and potential applications. *Construction and Building Materials*, 210, 413-421.

Huntzinger, D. N., Gierke, J. S., Kawatra, S. K., Eisele, T. C., & Sutter, L. L. (2009). Carbon dioxide sequestration in cement kiln dust through mineral carbonation. *Environmental Science & Technology*, 43(6), 1986-1992.

Hussain, S. E. (1994). Corrosion resistance performance of fly ash blended cement concrete. *Materials Journal*, 91(3), 264-272.

Ihli, J., Wong, W. C., Noel, E. H., Kim, Y.-Y., Kulak, A. N., Christenson, H. K., Duer, M. J., & Meldrum, F. C. (2014). Dehydration and crystallization of amorphous calcium carbonate in solution and in air. *Nature Communications*, 5(1), 3169.

Illikainen, M., Tanskanen, P., Kinnunen, P., Körkkö, M., Peltosaari, O., Wigren, V., ... & Niinimäki, J. (2014). Reactivity and self-hardening of fly ash from the fluidized bed combustion of wood and peat. *Fuel*, 135, 69-75.

International Energy Agency. (2021). *Supply – Key World Energy Statistics 2021 – Analysis*. Retrieved from https://www.iea.org/reports/key-world-energy-statistics-2021/supply.

International Energy Agency. (2022). *Executive summary – Coal 2022 – Analysis*. Retrieved from https://www.iea.org/reports/coal-2022/executive-summary.

IPCC. (2021). Climate Change 2021: The Physical Science Basis. *Contribution of Working Group I to the Sixth Assessment Report of the Intergovernmental Panel on Climate Change*. V. Masson-Delmotte, P. Zhai, A. Pirani, S.L. Connors, C. Péan, S. Berger, N. Caud, Y. Chen, L. Goldfarb, M.I. Gomis, M. Huang, K. Leitzell, E. Lonnoy, J.B.R. Matthews, T.K. Maycock, T. Waterfield, O. Yelekçi, R. Yu, & B. Zhou (Eds.). Cambridge University Press.

Irha, N., Uibu, M., Jefimova, J., Raado, L.-M., Hain, T., & Kuusik, R. (2014). Leaching behaviour of Estonian oil shale ash-based construction mortars. *Oil Shale*, 31(4), 394.

Jamil, S., Shi, J., & Idrees, M. (2023). Effect of various parameters on carbonation treatment of recycled concrete aggregate using the design of experiment method. *Construction and Building Materials*, 382, 131339.

Jianming, Y., Luming, W., & Jie, Z. (2019). Experimental study on the deformation characteristics of magnesium potassium phosphate cement paste at early hydration ages. *Cement and Concrete Composites*, 103, 175-182.

Juenger, M. C., Snellings, R., & Bernal, S. A. (2019). Supplementary cementitious materials: New sources, characterization, and performance insights. *Cement and Concrete Research*, 122, 257-273.

Justnes, H., Skocek, J., Østnor, T. A., Engelsen, C. J., & Skjølsvold, O. (2020). Microstructural changes of hydrated cement blended with fly ash upon carbonation. *Cement and Concrete Research*, 137, 106192.

Kaja, A. M., Delsing, A., Van Der Laan, S. R., Brouwers, H. J. H., & Yu, Q. (2021). Effects of carbonation on the retention of heavy metals in chemically activated BOF slag pastes. *Cement and Concrete Research*, *148*, 106534.

Kaliyavaradhan, S. K., Li, L., & Ling, T. C. (2022). Response surface methodology for the optimization of CO_2 uptake using waste concrete powder. *Construction and Building Materials*, 340, 127758.

Kaljuvee, T., Štubňa, I., Húlan, T., Uibu, M., Einard, M., Traksmaa, R., ... & Trikkel, A. (2021). Thermal behavior of ceramic bodies based on Estonian clay from the arumetsa deposit with oil shale ash and clinker dust additives. *Processes*, 10(1), 46.

Kalpokaitė-Dičkuvienė, R., Pitak, I., Baltušnikas, A., Čėsnienė, J., Kriūkienė, R., & Lukošiūtė, S. I. (2023). Functional and microstructural alterations in hydrated and freeze–thawed cement-oil shale ash composites. *Case Studies in Construction Materials*, 19, e02302.

Kanger, L., & Sovacool, B. K. (2022). Towards a multi-scalar and multi-horizon framework of energy injustice: A whole systems analysis of Estonian energy transition. *Political Geography*, 93, 102544.

Kanhar, A. H., Chen, S., & Wang, F. (2020). Incineration fly ash and its treatment to possible utilization: A review. *Energies*, 13(24), 6681.

Karunadasa, K. S., Manoratne, C., Pitawala, H., & Rajapakse, R. (2019). Thermal decomposition of calcium carbonate (calcite polymorph) as examined by in-situ high-temperature X-ray powder diffraction. *Journal of Physics and Chemistry of Solids*, 134, 21-28.

Kelechi, S. E., Adamu, M., Uche, O. A. U., Okokpujie, I. P., Ibrahim, Y. E., & Obianyo, I. I. (2022). A comprehensive review on coal fly ash and its application in the construction industry. *Cogent Engineering*, 9(1), 2114201.

Kelland, M., Rau, G., Battochio, B., Vallis, J., Gladkovas, M., Thomas, S., ... & Mezei, A. (2023, January). Integrating Carbon Capture in Mining Through Metallurgy. Part 1: Leaching and Reclamation of Asbestos Tailings: Thetford Mines Carbon Capture and Remediation Project. In *Proceedings of the 61st Conference of Metallurgists, COM 2022* (pp. 515-527). Cham: Springer International Publishing.

Keulen, A., Van Zomeren, A., & Dijkstra, J. J. (2018). Leaching of monolithic and granular alkali activated slag-fly ash materials, as a function of the mixture design. *Waste Management*, 78, 497-508.

Khan, S., Wani, O. B., Shoaib, M., Forster, J., Sodhi, R. N., Boucher, D., & Bobicki, E. R. (2021). Mineral carbonation for serpentine mitigation in nickel processing: a step towards industrial carbon capture and storage. *Faraday Discussions*, 230, 172-186.

Khawam, A., & Flanagan, D. R. (2006). Solid-state kinetic models: basics and mathematical fundamentals. *The Journal of Physical Chemistry B*, 110(35), 17315-17328.

Kim, H. J., Tafesse, M., Lee, H. K., & Kim, H. K. (2019). Incorporation of CFBC ash in sodium silicate-activated slag system: Modification of microstructures and its effect on shrinkage. *Cement and Concrete Research*, 123, 105771.

Kledyński, Z., Machowska, A., Pacewska, B., & Wilińska, I. (2017). Investigation of hydration products of fly ash–slag pastes. *Journal of Thermal Analysis and Calorimetry*, 130(1), 351–363.

Knaus, E., Killen, J., Biglarbigi, K., & Crawford, P. (2010). An overview of oil shale resources. In (Hartstein, et.al., Eds.) *Oil Shale: A Solution to the Liquid Fuel Dilemma*, American Chemical Society.

Koley, S., Ghosh, A., Sahu, A. K., Tewari, R., & Suri, A. K. (2011). Correlation of compaction pressure, green density, pore size distribution and sintering temperature of a nano-crystalline 2Y-TZP-Al_2O_3 composite. *Ceramics International*, 37(3), 731-739.

Konist, A., Neshumayev, D., Baird, Z. S., Anthony, E. J., Maasikmets, M., & Järvik, O. (2020). Mineral and heavy metal composition of oil shale ash from oxyfuel combustion. *ACS Omega*, 5(50), 32498-32506.

Kothari, C., & Takahashi, Y. (2022). The effect of heat treatment on the kinetics of the delayed ettringite formation–An improved chemo-thermal-hygral model. *Construction and Building Materials*, 331, 127358.

Kumar, M. A., Prasanna, K., Raj, C. C., Parthiban, V., Kulanthaivel, P., Narasimman, S., & Naveen, V. (2022). Bond strength of autoclaved aerated concrete manufactured using partial replacement of flyash with fibers–A review. *Materials Today: Proceedings*, 65, 581-589.

Kurdowski, W. (2014). *Cement and Concrete Chemistry*. Springer Dordrecht.

Kusin, F. M., Hasan, S. N. M. S., Molahid, V. L. M., Yusuff, F. M., & Jusop, S. (2023). Carbon dioxide sequestration of iron ore mining waste under low-reaction condition of a direct mineral carbonation process. *Environmental Science and Pollution Research*, 30(9), 22188-22210.

Kuusik, R., Uibu, M., Kirsimäe, K., Motlep, R., & Meriste, T. (2012). Open-Air Deposition of Estonian Oil Shale Ash: Formation, State Of Art, Problems And Prospects For The Abatement Of Environmental Impact. *Oil Shale*, 29(4).

LaRosa, P. J., Karnavas, J. A., Pelczarski, E. A. (1971). *Carbonate Bonding of Coal Refuse*. United States: U.S. Government Printing Office.

Leben, K., Motlep, R., Konist, A., Pihu, T., & Kirsimäe, K. (2021). Carbon dioxide sequestration in power plant Ca-rich ash waste deposits. *Oil Shale*, 38(1).

Leben, K., Mõtlep, R., Paaver, P., Konist, A., Pihu, T., Paiste, P., Heinmaa, I., Nurk, G., Anthony, E. J., & Kirsimäe, K. (2019). Long-term mineral transformation of Ca-rich oil shale ash waste. *Science of the Total Environment*, 658, 1404-1415.

Lees, H., Järvik, O., Konist, A., Siirde, A., & Maaten, B. (2022). Comparison of the ecotoxic properties of oil shale industry by-products to those of coal ash. *Oil Shale*, 39(1), 1-19.

Lekakh, S. N., Rawlins, C. H., Robertson, D. G., Richards, V. L., & Peaslee, K. D. (2008). Kinetics of aqueous leaching and carbonization of steelmaking slag. *Metallurgical and Materials Transactions B*, 39, 125-134.

Bílek, J. V., Paøízek, L. & Kalina, L. (2015). Effect of the by-pass cement-kiln dust and fluidized-bed-combustion fly ash on the properties of fine-grained alkali-activated slag-based composites. *Materiali in tehnologije*, 49(4), 549-552.

Li, N., Mo, L., & Unluer, C. (2022). Emerging CO_2 utilization technologies for construction materials: A review. *Journal of CO_2 Utilization*, 65, 102237.

Li, P., Li, W., Yu, T., Qu, F., & Tam, V. W. (2020). Investigation on early-age hydration, mechanical properties and microstructure of seawater sea sand cement mortar. *Construction and Building Materials*, 249, 118776.

Li, X. (2022). *Mechanisms Governing Ash Aerosol Formation and Deposition during Solid Fuel Combustion* (Doctoral dissertation). The University of Utah.

Li, X. G., Chen, Q. B., Huang, K. Z., Ma, B. G., & Wu, B. (2012). Cementitious properties and hydration mechanism of circulating fluidized bed combustion (CFBC) desulphurization ashes. *Construction and Building Materials*, 36, 182-187.

Li, Z., & Shi, X. (2020). Graphene oxide modified, clinker-free cementitious paste with principally alkali-activated fly ash. *Fuel*, 269, 117418.

Librandi, P., Nielsen, P., Costa, G., Snellings, R., Quaghebeur, M., & Baciocchi, R. (2019). Mechanical and environmental properties of carbonated steel slag compacts as a function of mineralogy and CO_2 uptake. *Journal of CO_2 Utilization*, *33*, 201-214.

Librandi, P., Costa, G., de Souza, A. C. B., Stendardo, S., Luna, A. S., & Baciocchi, R. (2017). Carbonation of steel slag: testing of the wet route in a pilot-scale reactor. *Energy Procedia*, *114*, 5381-5392.

Liendo, F., Arduino, M., Deorsola, F. A., & Bensaid, S. (2022). Factors controlling and influencing polymorphism, morphology and size of calcium carbonate synthesized through the carbonation route: A review. *Powder Technology*, 398, 117050.

Liira, M., Kirsimäe, K., Kuusik, R., & Mõtlep, R. (2009). Transformation of calcareous oil-shale circulating fluidized-bed combustion boiler ashes under wet conditions. *Fuel*, 88(4), 712-718.

Lin, K. L., Cheng, T. W., Ho, C. H., Chang, Y. M., & Lo, K. W. (2017). Utilization of circulating fluidized bed fly ash as pozzolanic material. *The Open Civil Engineering Journal*, 11(1).

Liu, B., Yang, L., Shi, J., Zhang, S., Yalçınkaya, Ç., & Alshalif, A. F. (2023). Effect of curing regime on the immobilization of municipal solid waste incineration fly ash in sustainable cement mortar. *Environmental Pollution*, *317*, 120839.

Liu, B., Qin, J., Shi, J., Jiang, J., Wu, X., & He, Z. (2021). New perspectives on utilization of CO2 sequestration technologies in cement-based materials. *Construction and Building Materials*, 272, 121660.

Liu, C., & Zhang, M. (2021). Effect of curing temperature on hydration, microstructure and ionic diffusivity of fly ash blended cement paste: A modelling study. *Construction and Building Materials*, 297, 123834.

Liu, Q., Liu, J., & Qi, L. (2016). Effects of temperature and carbonation curing on the mechanical properties of steel slag-cement binding materials. *Construction and Building Materials*, 124, 999-1006.

Liu, W., Du, R., Zhang, R., Zhao, Z., Zhang, L., & Li, H. (2023). Optimal design and performance of eco-friendly materials stabilized with inorganic binder based on fluidized bed coal combustion fly ash and regenerated brick powder. *Journal of Building Engineering*, 65, 105800.

Liu, X., Feng, P., Cai, Y., Yu, X., Yu, C., & Ran, Q. (2022). Carbonation behavior of calcium silicate hydrate (CSH): Its potential for CO2 capture. *Chemical Engineering Journal*, 431, 134243.

Lodeiro, I. G., Fernández-Jiménez, A., Palomo, A., & Macphee, D. E. (2010). Effect on fresh CSH gels of the simultaneous addition of alkali and aluminium. *Cement and Concrete Research*, 40(1), 27-32.

Lothenbach, B., & Zajac, M. (2019). Application of thermodynamic modelling to hydrated cements. *Cement and Concrete Research*, 123, 105779.

Lu, Z., Tan, Q., Lin, J., & Wang, D. (2022). Properties investigation of recycled aggregates and concrete modified by accelerated carbonation through increased temperature*. Construction and Building Materials*, 341, 127813.

Luo, Y., Wu, Y., Ma, S., Zheng, S., Zhang, Y., & Chu, P. K. (2021). Utilization of coal fly ash in China: a mini-review on challenges and future directions. *Environmental Science and Pollution Research*, 28, 18727-18740.

Luo, Z., Wang, Y., Yang, G., Ye, J., Zhang, W., Liu, Z., & Mu, Y. (2021). Effect of curing temperature on carbonation behavior of steel slag compacts. *Construction and Building Materials*, 291, 123369.

Maddalena, R., Roberts, J. J., & Hamilton, A. (2018). Can Portland cement be replaced by low-carbon alternative materials? A study on the thermal properties and carbon emissions of innovative cements. *Journal of Cleaner Production*, 186, 933-942.

Majhi, R. K., Padhy, A., & Nayak, A. N. (2021). Performance of structural lightweight concrete produced by utilizing high volume of fly ash cenosphere and sintered fly ash aggregate with silica fume. *Cleaner Engineering and Technology*, 3, 100121.

Martínez-García, R., Jagadesh, P., Zaid, O., Șerbănoiu, A. A., Fraile-Fernández, F. J., de Prado-Gil, J., ... & Grădinaru, C. M. (2022). The present state of the use of waste wood ash as an eco-efficient construction material: A review. *Materials*, 15(15), 5349.

Mathapati, M., Amate, K., Prasad, C. D., Jayavardhana, M. L., & Raju, T. H. (2022). A review on fly ash utilization. *Materials Today: Proceedings*, 50, 1535-1540.

Matschei, T., Lothenbach, B., & Glasser, F. P. (2007). The AFm phase in Portland cement. *Cement and Concrete Research*, 37(2), 118-130.

Mazzella, A., Errico, M., & Spiga, D. (2016). CO2 uptake capacity of coal fly ash: Influence of pressure and temperature on direct gas-solid carbonation. *Journal of Environmental Chemical Engineering,* 4(4), 4120-4128.

Mehta, A., & Siddique, R. (2016). An overview of geopolymers derived from industrial by-products. *Construction and Building Materials*, 127, 183-198.

Miao, E., Du, Y., Zheng, X., Zhang, X., Xiong, Z., Zhao, Y., & Zhang, J. (2023). CO2 sequestration by direct mineral carbonation of municipal solid waste incinerator fly ash in ammonium salt solution: Performance evaluation and reaction kinetics. *Separation and Purification Technology*, 309, 123103.

Mishra, J., Nanda, B., Patro, S. K., Das, S. K., & Mustakim, S. M. (2022). Influence of ferrochrome ash on mechanical and microstructure properties of ambient cured fly ash-based geopolymer concrete. *Journal of Material Cycles and Waste Management*, 24(3), 1095-1108.

Monkman, S., & Shao, Y. (2006). Assessing the carbonation behavior of cementitious materials. *Journal of Materials in Civil Engineering*, 18(6), 768-776.

Monrose, J., Tota-Maharaj, K., Mwasha, A., & Hills, C. (2020). Effect of carbon-negative aggregates on the strength properties of concrete for permeable pavements. *International Journal of Pavement Engineering*, 21(14), 1823-1831.

Moon, E. J., & Choi, Y. C. (2019). Carbon dioxide fixation via accelerated carbonation of cement-based materials: Potential for construction materials applications. *Construction and Building Materials*, 199, 676-687.

Mudasir, M., Roto, R., Kuboki, Y., & Begum, P. (2022). Coal Fly/Bottom Ash, Hydroxylapatite, and Hydrotalcite. In (Tanaka et.al, Eds) *Design of Materials and Technologies for Environmental Remediation.* Springer Singapore.

Nadesan, M. S., & Dinakar, P. (2017). Mix design and properties of fly ash waste lightweight aggregates in structural lightweight concrete. *Case Studies in Construction Materials*, 7, 336-347.

Nam, S.-Y., Seo, J., Thriveni, T., & Ahn, J.-W. (2012). Accelerated carbonation of municipal solid waste incineration bottom ash for CO_2 sequestration. *Geosystem Engineering*, 15(4), 305-311.

Nath, S. K. (2020). Fly ash and zinc slag blended geopolymer: Immobilization of hazardous materials and development of paving blocks. *Journal of Hazardous Materials*, 387, 121673.

Nayak, D. K., Abhilash, P. P., Singh, R., Kumar, R., & Kumar, V. (2022). Fly Ash for sustainable construction: A review of fly ash concrete and its beneficial use case studies. *Cleaner Materials*, 100143.

Nedunuri, A. S. S. S., yar Mohammed, A., & Muhammad, S. (2021). Carbonation potential of concrete debris fines and its valorisation through mineral carbonation. *Construction and Building Materials*, 310, 125162.

Nielsen, P., Baciocchi, R., Costa, G., Quaghebeur, M., & Snellings, R. (2017). Carbonate-bonded construction materials from alkaline residues. *RILEM Technical Letters*, 2, 53-58.

Nielsen, P., Boone, M. A., Horckmans, L., Snellings, R., & Quaghebeur, M. (2020). Accelerated carbonation of steel slag monoliths at low CO_2 pressure–microstructure and strength development. *Journal of CO_2 Utilization*, 36, 124-134.

Nikulshina, V., Gálvez, M., & Steinfeld, A. (2007). Kinetic analysis of the carbonation reactions for the capture of CO_2 from air via the Ca $(OH)_2$–$CaCO_3$–CaO solar thermochemical cycle. *Chemical Engineering Journal*, 129(1-3), 75-83.

NOAA National Centers for Environmental Information, *Monthly Global Climate Report for December 2022,* (January 2023). https://www.ncei.noaa.gov/access/monitoring/monthly-report/global/202300.

Ohenoja, K., Pesonen, J., Yliniemi, J., & Illikainen, M. (2020). Utilization of fly ashes from fluidized bed combustion: A review. *Sustainability*, 12(7), 2988.

Ohenoja, K., Tanskanen, P., Peltosaari, O., Wigren, V., Österbacka, J., & Illikainen, M. (2016-b). Effect of particle size distribution on the self-hardening property of biomass-peat fly ash from a bubbling fluidized bed combustion. *Fuel Processing Technology*, 148, 60-66.

Ohenoja, K., Tanskanen, P., Wigren, V., Kinnunen, P., Körkkö, M., Peltosaari, O., ... & Illikainen, M. (2016-a). Self-hardening of fly ashes from a bubbling fluidized bed combustion of peat, forest industry residuals, and wastes. *Fuel*, 165, 440-446.

Ojha, P. N., Singh, B., Kaura, P., & Satyakam, R. (2022). Ash Utilization Strategy in India—A Way Forward. In (Reddy et al., Eds.) *Advances in Sustainable Materials and Resilient Infrastructure*. Singapore: Springer Singapore.

Ojha, P. N., Singh, B., Singh, P., Singh, A., & Mandre, M. K. (2022). Study on effect of fly ash and limestone powder on compressive strength of roller compacted concrete for dam construction. *Journal of Asian Concrete Federation*, 8(1), 37-50.

Özen, S., Altun, M. G., Mardani-Aghabaglou, A., & Ramyar, K. (2022). Multi-effect of superplasticisers main and side-chain length on cementitious systems with fly ash. *Magazine of Concrete Research*, 74(14), 727-739.

Paaver, P., Järvik, O., & Kirsimäe, K. (2021). Design of High Volume CFBC Fly Ash Based Calcium Sulphoaluminate Type Binder in Mixtures with Ordinary Portland Cement. *Materials*, 14(19), 5798.

Paaver, P., Paiste, P., Liira, M., & Kirsimäe, K. (2019). Alkali activation of Estonian ca-rich oil shale ashes: A synthesis. *Oil Shale*, 36(2S), 214-225.

Pacewska, B., & Wilińska, I. (2013). Hydration of cement composites containing large amount of waste materials. *Procedia Engineering*, 57, 53-62.

Paiste, P., Külaviir, M., Paaver, P., Heinmaa, I., Vahur, S., & Kirsimäe, K. (2019). Beneficiation of oil shale processing waste: secondary binder phases in alkali activated composites. *Waste and Biomass Valorization*, 10, 1407-1417.

Pan, S.-Y., Chang, E., & Chiang, P.-C. (2012). CO_2 capture by accelerated carbonation of alkaline wastes: a review on its principles and applications. *Aerosol and Air Quality Research*, 12(5), 770-791.

Pan, S.-Y., Ling, T.-C., Park, A.-H. A., & Chiang, P.-C. (2018). An overview: Reaction mechanisms and modelling of CO_2 utilization via mineralization. *Aerosol and Air Quality Research*, 18(4), 829-848.

Panda, L., & Dash, S. (2020). Characterization and utilization of coal fly ash: a review. *Emerging Materials Research*, 9(3), 921-934.

Panesar, D. K. (2019). Supplementary cementing materials. In (Mindess, Eds.) *Developments in the Formulation and Reinforcement of Concrete*. Elsevier.

Park, H., Wang, L., & Yun, J. H. (2021). Coal beneficiation technology to reduce hazardous heavy metals in fly ash. *Journal of Hazardous Materials*, 416, 125853.

Patil, L., Nayak, C. B., & Jagadale, U. T. (2022). Effect of copper slag and fly ash and Nano Material to strengthen the properties of concrete. *J Emergin Technol Innovative Res (JETIR)*, 9(6), 831-838.

Pedraza, J., Zimmermann, A., Tobon, J., Schomäcker, R., & Rojas, N. (2021). On the road to net zero-emission cement: Integrated assessment of mineral carbonation of cement kiln dust. *Chemical Engineering Journal*, 408, 127346.

Pihu, T., Arro, H., Prikk, A., Rootamm, R., Konist, A., Kirsimäe, K., Liira, M., & Mõtlep, R. (2012). Oil shale CFBC ash cementation properties in ash fields. *Fuel*, 93, 172-180.

Pihu, T., Konist, A., Puura, E., Liira, M., & Kirsimae, K. (2019). Properties and Environmental Impact of Oil Shale Ash Landfills. *Oil Shale*, 36(2), 257-271.

Popova, M., Boycheva, S., Lazarova, H., Zgureva, D., Lázár, K., & Szegedi, Á. (2020). VOC oxidation and CO_2 adsorption on dual adsorption/catalytic system based on fly ash zeolites. *Catalysis Today*, 357, 518-525.

Pour, A. K., Shirkhani, A., Kirgiz, M. S., Nehdi, M., Syarif, M., Irfan-Ul-Hassan, M., ... & de Sousa Galdino, A. G. (2022). Alkali-activated fly ash concrete with untreated coal aggregate: Fresh-and hardened state properties. *Case Studies in Construction Materials*, 17, e01141.

Pozniak, O., Melnyk, V., Margal, I., & Novosad, P. (2021). Production of fly ash aerated concrete and efficiency of its application. In (Blikharskyy, Eds.) *Proceedings of EcoComfort 2020.* Springer International Publishing.

Pu, Y., Li, L., Shi, X., Wang, Q., & Abomohra, A. (2023). Recent advances in accelerated carbonation for improving cement-based materials and CO_2 mitigation from a life cycle perspective. *Construction and Building Materials*, *388*, 131695.

Qian, X., Wang, J., Fang, Y., & Wang, L. (2018). Carbon dioxide as an admixture for better performance of OPC-based concrete. *Journal of CO_2 Utilization*, 25, 31-38.

Qu, X., Yang, X., Li, S., Tian, C., Li, Z., & Zhao, Z. (2022). Preparation and Properties of Eco-Friendly Aerated Concrete Utilizing High-Volume Fly Ash with MgO and CaO Activators. *Journal of Renewable Materials*, 10(12), 3335.

Raado, L. M., Kuusik, R., Hain, T., Uibu, M., & Somelar, P. (2014). Oil Shale Ash Based Stone Formation - Hydration, Hardening Dynamics and Phase Transformations. *Oil Shale,* 31(1), 91-101.

Raado, L., Tuisk, T., Rosenberg, M., & Hain, T. (2011). Durability behavior of Portland burnt oil shale cement concrete. *Oil Shale*, 28(4), 507.

Rafieizonooz, M., Khankhaje, E., & Rezania, S. (2022). Assessment of environmental and chemical properties of coal ashes including fly ash and bottom ash, and coal ash concrete. *Journal of Building Engineering*, 49, 104040.

Rahmanihanzaki, M., & Hemmati, A. (2022). A review of mineral carbonation by alkaline solidwaste. *International Journal of Greenhouse Gas Control*, 121, 103798.

Rausis, K., Ćwik, A., Casanova, I., & Zarębska, K. (2021). Carbonation of high-Ca fly ashes under flue gas conditions: implications for their valorization in the construction industry. *Crystals*, 11(11), 1314.

Reispere, H. J. (1966). Determination of free CaO content in oil shale ash. Transact. *Tallinn Polytechnical Institute, series A*, 245, 73-76.

ResearchAndMarkets. (2022). Fly Ash Market - Forecasts from 2022 to 2027. Retrieved from https://www.researchandmarkets.com/reports/5576398/fly-ash-market-forecasts-from-2022-to-2027.

Rissanen, J., Giosué, C., Ohenoja, K., Kinnunen, P., Marcellini, M., Ruello, M. L., ... & Illikainen, M. (2019). The effect of peat and wood fly ash on the porosity of mortar. *Construction and Building Materials*, 223, 421-430.

Rissanen, J., Ohenoja, K., Kinnunen, P., & Illikainen, M. (2017). Partial replacement of portland-composite cement by fluidized bed combustion fly ash. *Journal of Materials in Civil Engineering*, 29(8), 04017061.

Rodriguez-Navarro, C., Ilić, T., Ruiz-Agudo, E., & Elert, K. (2023). Carbonation mechanisms and kinetics of lime-based binders: An overview. *Cement and Concrete Research*, 173, 107301.

Rose, J., Benard, A., El Mrabet, S., Masion, A., Moulin, I., Briois, V., ... & Bottero, J. Y. (2006). Evolution of iron speciation during hydration of C4AF. *Waste Management*, 26(7), 720-724.

Rusanowska, P., Zieliński, M., & Dębowski, M. (2023). Removal of CO2 from Biogas during Mineral Carbonation with Waste Materials. *International Journal of Environmental Research and Public Health*, 20(9), 5687.

Samadi, M., Hussin, M. W., Lee, H. S., Sam, A. R. M., Ismail, M., Lim, N. H. A. S., ... & Khalid, N. H. A. (2015). Properties of mortar containing ceramic powder waste as cement replacement. *J. Teknol*, *77*(12), 93-97.

Sanna, A., Gaubert, J., & Maroto-Valer, M. M. (2016). Alternative regeneration of chemicals employed in mineral carbonation towards technology cost reduction. *Chemical Engineering Journal*, 306, 1049-1057.

Saran, R. K., Arora, V., & Yadav, S. (2018). CO2 sequestration by mineral carbonation: a review. *Global NEST Journal*, 20(3), 497-503.

Schnabel, K., Brück, F., Pohl, S., Mansfeldt, T., & Weigand, H. (2021). Technically exploitable mineral carbonation potential of four alkaline waste materials and effects on contaminant mobility. *Greenhouse Gases: Science and Technology*, 11(3), 506-519.

Scrivener, K., Snellings, R., & Lothenbach, B. (2018). *A Practical Guide to Microstructural Analysis of Cementitious Materials*. CRC Press.

Šebestová, P., Ćerny, V., & Drochytka, R. (2020). Experimental study of autoclaved aerated concrete using circulating fluidized-bed combustion fly ash. *Mater. Techno*l, 54, 157-161.

Senadeera, K. R., Jayasinghe, T. K., Jayasundara, P. M., Nanayakkara, G., & Rathnayake, M. (2020, July). Investigation of CO_2 sequestration possibility via indirect mineral carbonation using waste coal fly ash. In *2020 Moratuwa Engineering Research Conference* (MERCon) (pp. 119-123). IEEE.

Shaikh, F. U., & Supit, S. W. (2014). Mechanical and durability properties of high volume fly ash (HVFA) concrete containing calcium carbonate ($CaCO_3$) nanoparticles. *Construction and Building Materials,* 70, 309-321.

Shee-Ween, O., Cheng-Yong, H., Yun-Ming, L., Abdullah, M. M. A. B., Ngee, H. L., Chan, L. W. L., Wan-En, O., Jaya, N. A., & Yong-Sing, N. (2021). Cold-pressed fly ash geopolymers: Effect of formulation on mechanical and morphological characteristics. *Journal of Materials Research and Technology*, 15, 3028-3046.

Shen, Y., Qian, J., & Zhang, Z. (2013). Investigations of anhydrite in CFBC fly ash as cement retarders. *Construction and Building Materials*, 40, 672-678.

Shi, Y., Li, Y., Tang, Y., Yuan, X., Wang, Q., Hong, J., & Zuo, J. (2019). Life cycle assessment of autoclaved aerated fly ash and concrete block production: a case study in China. *Environmental Science and Pollution Research*, 26, 25432-25444.

Siddique, S., Naqi, A., & Jang, J. G. (2020). Influence of water to cement ratio on CO2 uptake capacity of belite-rich cement upon exposure to carbonation curing. *Cement and Concrete Composites*, 111, 103616.

Sigvardsen, N. M., Geiker, M. R., & Ottosen, L. M. (2021). Phase development and mechanical response of low-level cement replacements with wood ash and washed wood ash. *Construction and Building Materials*, 269, 121234.

Singh, A., Singh, J., Sinha, M. K., Kumar, R., & Verma, V. (2021). Compaction and densification characteristics of iron powder/coal fly ash mixtures processed by powder metallurgy technique. *Journal of Materials Engineering and Performance*, 30, 1207-1220.

Snellings, R. (2016). Assessing, understanding, and unlocking supplementary cementitious materials. *RILEM Technical Letters*, 1, 50-55.

Song, X., Xiaoyu, C., Lin, Q., & Yanna, L. (2019, November). A review of mineral carbonation from industrial waste. In I*OP Conference Series: Earth and Environmental Science* (Vol. 401, No. 1, p. 012008). IOP Publishing.

Song, Y., Guo, C., Qian, J., & Ding, T. (2015). Effect of the Ca-to-Si ratio on the properties of autoclaved aerated concrete containing coal fly ash from circulating fluidized bed combustion boiler. *Construction and Building Materials*, 83, 136-142.

Steiner, S., Lothenbach, B., Proske, T., Borgschulte, A., & Winnefeld, F. (2020). Effect of relative humidity on the carbonation rate of portlandite, calcium silicate hydrates and ettringite. *Cement and Concrete Research*, 135, 106116.

Sudha, G., Stalin, B., Ravichandran, M., & Balasubramanian, M. (2020). Mechanical properties, characterization and wear behavior of powder metallurgy composites-a review. *Materials Today: Proceedings*, 22, 2582-2596.

Sultana, S., Ahsan, S., Tanvir, S., Haque, N., Alam, F., & Yellishetty, M. (2021). Coal fly ash utilisation and environmental impact. In (Parhi & Jyothi, Eds.) *Clean Coal Technologies: Beneficiation, Utilization, Transport Phenomena and Prospective*. Springer International Publishing.

Sun, Y., Zhao, Y., Wan, X., Qiu, J., Wu, P., & Sun, X. (2022). Stabilization/solidification of lead-and cadmium-containing tailings for cemented paste backfill by using clinker-free binders. *Construction and Building Materials*, 359, 129469.

Tamanna, K., Raman, S. N., Jamil, M., & Hamid, R. (2020). Utilization of wood waste ash in construction technology: A review. *Construction and Building Materials*, 237, 117654.

Tang, J., Xiao, S., Huang, J., Liu, K., Han, F., Gao, C., ... & Liu, J. (2023). Investigation on the reinforcing of cementitious materials by nano-hydroxyapatites. *Journal of Sustainable Cement-Based Materials*, 1-16.

Teir, S. (2008). Fixation of carbon dioxide by producing carbonates from minerals and steelmaking slags. *Teknillinen korkeakoulu.*

Teir, S., Eloneva, S., Fogelholm, C. J., & Zevenhoven, R. (2007). Dissolution of steelmaking slags in acetic acid for precipitated calcium carbonate production. *Energy*, 32(4), 528-539.

Telesca, A., Marroccoli, M., Montagnaro, F., Tomasulo, M., & Valenti, G. L. (2015). Enhancement of selectivity toward ettringite during hydrothermal processes on fluidized bed combustion wastes for the manufacture of preformed building components*. RSC advances*, 5(123), 101887-101893.

Thonemann, N., Zacharopoulos, L., Fromme, F., & Nühlen, J. (2022). Environmental impacts of carbon capture and utilization by mineral carbonation: A systematic literature review and meta life cycle assessment. *Journal of Cleaner Production,* 332, 130067.

Trikkel, A., Kuusik, R., Martins, A., Pihu, T., & Stencel, J. M. (2008). Utilization of Estonian oil shale semicoke. *Fuel processing technology*, 89(8), 756-763.

Turgut, P., & Demir, F. (2019). The influence of disposed fly ash on Ca2+ leaching and physico-mechanical properties of mortars. *Journal of Cleaner Production*, 226, 270-281.

Turkane, S. D., & Chouksey, S. K. (2022). Design of flexible pavement thickness using stabilized high plastic soil by means of fly ash-based geopolymer. *International Journal of Pavement Engineering*, 1-15.

Uibu, M. (2008). *Abatement of CO2 emissions in Estonian oil shale-based power production* (Doctoral Dissertation). Tallinn University of Technology.

Uibu, M., Somelar, P., Raado, L.-M., Irha, N., Hain, T., Koroljova, A., & Kuusik, R. (2016). Oil shale ash based on backfilling concrete–strength development, mineral transformations, and leachability. *Construction and Building Materials*, 102, 620-630.

Uibu, M., Tamm, K., Viires, R., Reinik, J., Somelar, P., Raado, L., ... & Trikkel, A. (2021). The composition and properties of ash in the context of the modernisation of oil shale industry. *Oil Shale*, 38(2).

Um, N., & Ahn, J.-W. (2017). Effects of two different accelerated carbonation processes on MSWI bottom ash. *Process Safety and Environmental Protection*, 111, 560-568.

Van Gerven, T., Moors, J., Dutre, V., & Vandecasteele, C. (2004). Effect of CO_2 on leaching from a cement stabilized MSWI fly ash. *Cement and Concrete Research*, 34(7), 1103-1109.

Vanoutrive, H., Minne, P., Van de Voorde, I., Cizer, Ö., & Gruyaert, E. (2022). Carbonation of cement paste with GGBFS: Effect of curing duration, replacement level and CO2 concentration on the reaction products and CO_2 buffer capacity. *Cement and Concrete Composites*, 129, 104449.

Vassilev, S. V., & Vassileva, C. G. (2007). A new approach for the classification of coal fly ashes based on their origin, composition, properties, and behaviour. *Fuel*, 86(10-11), 1490-1512.

Vig, N., Mor, S., & Ravindra, K. (2023). The multiple value characteristics of fly ash from Indian coal thermal power plants: a review. *Environmental Monitoring and Assessment*, 195(1), 33.

von Greve-Dierfeld, S., Lothenbach, B., Vollpracht, A., Wu, B., Huet, B., Andrade, C., ... & De Belie, N. (2020). Understanding the carbonation of concrete with supplementary cementitious materials: a critical review by RILEM TC 281-CCC. *Materials and structures*, 53(6), 136.

Wang, B., & Song, Y. (2013). Methods for the control of volume stability of sulphur rich CFBC ash cementitious systems. *Magazine of Concrete Research*, 65(19), 1168-1172.

Wang, F., Dreisinger, D. B., Jarvis, M., & Hitchins, T. (2018). The technology of CO2 sequestration by mineral carbonation: current status and future prospects. *Canadian Metallurgical Quarterly*, 57(1), 46-58.

Wang, N., Sun, X., Zhao, Q., Yang, Y., & Wang, P. (2020). Leachability and adverse effects of coal fly ash: A review. *Journal of Hazardous Materials*, 396, 122725.

Wang, X., Fu, P., Deng, W., Shi, J., & Xu, M. (2023). Study on Mechanism of MSWI Fly Ash Solidified by Multiple Solid Waste-Based Cementitious Material Using the Rietveld Method. *Processes*, 11(8), 2311.

Wang, Z., & Song, Y. (2016). Adsorption properties of CFBC ash–cement pastes as compared with PCC fly ash–cement pastes. *International Journal of Coal Science & Technology*, 3, 62-67.

Wei, Z., Wang, B., Falzone, G., La Plante, E. C., Okoronkwo, M. U., She, Z., Oey, T., Balonis, M., Neithalath, N., & Pilon, L. (2018). Clinkering-free cementation by fly ash carbonation. *Journal of CO_2 Utilization*, 23, 117-127.

Winnefeld, F., Leemann, A., German, A., & Lothenbach, B. (2022). CO2 storage in cement and concrete by mineral carbonation. *Current Opinion in Green and Sustainable Chemistry*, 100672.

Wolf, J. J., Jansen, D., Goetz-Neunhoeffer, F., & Neubauer, J. (2019). Mechanisms of early ettringite formation in ternary CSA–OPC–anhydrite systems. *Advances in Cement Research*, 31(4), 195-204.

Wongkeo, W., Thongsanitgarn, P., Ngamjarurojana, A., & Chaipanich, A. (2014). Compressive strength and chloride resistance of self-compacting concrete containing high level fly ash and silica fume. *Materials & Design*, 64, 261-269.

Woodall, C. M., McQueen, N., Pilorgé, H., & Wilcox, J. (2019). Utilization of mineral carbonation products: current state and potential. *Greenhouse Gases: Science and Technology*, 9(6), 1096-1113.

World Steel Association. (2022). *World steel in figures 2022*. Retrieved from https://worldsteel.org/steel-topics/statistics/world-steel-in-figures-2022/

Wu, C. R., Zhan, B. J., Hong, Z. Q., Cui, S. C., Cui, P., & Kou, S. C. (2022). Hydration behavior of circulating fluidized bed fly ash (CFBFA) as a cementitious binder. *Construction and Building Materials*, 314, 125625.

Wu, R., Dai, S., Jian, S., Huang, J., Lv, Y., Li, B., & Azizbek, N. (2020). Utilization of the circulating fluidized bed combustion ash in autoclaved aerated concrete: Effect of superplasticizer. *Construction and Building Materials*, 237, 117644.

Wu, Y. H., Huang, R., Tsai, C. J., & Lin, W. T. (2015). Utilizing residues of CFB co-combustion of coal, sludge and TDF as an alkali activator in eco-binder. *Construction and Building Materials*, 80, 69-75.

Wu, Y., Mehdizadeh, H., Mo, K. H., & Ling, T.-C. (2022). High-temperature CO2 for accelerating the carbonation of recycled concrete fines. *Journal of Building Engineering*, 52, 104526.

Xu, L., Li, N., Wang, R., & Wang, P. (2018). A comprehensive study on the relationship between mechanical properties and microstructural development of calcium sulfoaluminate cement based self-leveling underlayments. *Construction and Building Materials*, 163, 225-234.

Xun, X., Xiaoling, F., & Chenglin, Y. (2020). Investigation on physical properties, strength and phase evolution of binary cementitious materials made of CFBC ash and lime. *Construction and Building Materials*, 265, 120302.

Yadav, S., & Mehra, A. (2021). A review on ex situ mineral carbonation. *Environmental Science and Pollution Research*, 28, 12202-12231.

Yadav, V. K., Gacem, A., Choudhary, N., Rai, A., Kumar, P., Yadav, K. K., ... & Islam, S. (2022). Status of Coal-Based Thermal Power Plants, Coal Fly Ash Production, Utilization in India and Their Emerging Applications. *Minerals,* 12(12), 1503.

Yadav, V. K., Gnanamoorthy, G., Cabral-Pinto, M. M., Alam, J., Ahamed, M., Gupta, N., ... & Yadav, K. K. (2021). Variations and similarities in structural, chemical, and elemental properties on the ashes derived from the coal due to their combustion in open and controlled manner. *Environmental Science and Pollution Research*, 28, 32609-32625.

Yang, H., Che, Y., & Leng, F. (2018). High volume fly ash mortar containing nano-calcium carbonate as a sustainable cementitious material: microstructure and strength development. *Scientific Reports*, 8(1), 16439.

Yang, Q., Yang, Q., Man, Y., Zhang, D., & Zhou, H. (2020). Technoeconomic and environmental evaluation of oil shale to liquid fuels process in comparison with conventional oil refining process. *Journal of Cleaner Production*, 255, 120198.

Yao, Z. T., Ji, X. S., Sarker, P. K., Tang, J. H., Ge, L. Q., Xia, M. S., & Xi, Y. Q. (2015). A comprehensive review on the applications of coal fly ash. *Earth-Science Reviews*, 141, 105-121.

Yousuf, A., Manzoor, S. O., Youssouf, M., Malik, Z. A., & Khawaja, K. S. (2020). Fly ash: production and utilization in India-an overview. *J Mater Environ Sci*, 11(6), 911-921.

Zahedi, M., & Rajabipour, F. (2019). Fluidized Bed Combustion (FBC) fly ash and its performance in concrete. *ACI Materials Journal*, 116(4), 163-172.

Zajac, M., Skocek, J., Gołek, Ł., & Deja, J. (2023). Supplementary cementitious materials based on recycled concrete paste. *Journal of Cleaner Production*, 387, 135743.

Zajac, M., Skocek, J., Skibsted, J., & Haha, M. B. (2021). CO_2 mineralization of demolished concrete wastes into a supplementary cementitious material–a new CCU approach for the cement industry. *RILEM Technical Letters*, 6, 53-60.

Zdeb, J., Howaniec, N., & Smoliński, A. (2023). Experimental study on combined valorization of bituminous coal derived fluidized bed fly ash and carbon dioxide from energy sector. *Energy*, 265, 126367.

Zhan, B. J., Xuan, D. X., Poon, C. S., & Shi, C. J. (2016). Effect of curing parameters on CO2 curing of concrete blocks containing recycled aggregates. *Cement and Concrete Composites*, 71, 122-130.

Zhang, J., Shi, C., Zhang, Z., & Hu, X. (2022). Reaction mechanism of sulphate attack on alkali-activated slag/fly ash cements. *Construction and Building Materials*, 318, 126052.

Zhang, N., Zhang, D., Zuo, J., Miller, T. R., Duan, H., & Schiller, G. (2022). Potential for CO2 mitigation and economic benefits from accelerated carbonation of construction and demolition waste. *Renewable and Sustainable Energy Reviews*, 169, 112920.

Zhang, W., Liu, X., Zhang, Z., Li, Y., Gu, J., Wang, Y., & Xue, Y. (2022). Circulating fluidized bed fly ash-blast furnace slag based cementitious materials: Hydration behaviors and performance. *Construction and Building Materials*, 342, 128006.

Zhang, Y., Zhang, H., & Zhang, X. (2021). Influence of calcined flue gas desulphurization gypsum and calcium aluminate on the strength and AFt evolution of fly ash blended concrete under steam curing. *Materials,* 14(23), 7171.

Zhao, J., Li, D., Liao, S., Wang, D., Wang, H., & Yan, P. (2018). Influence of mechanical grinding on pozzolanic characteristics of circulating fluidized bed fly ash (CFA) and resulting consequences on hydration and hardening properties of blended cement. *Journal of Thermal Analysis and Calorimetry*, 132, 1459-1470.

Zhao, Y., Qiu, J., Wu, P., Guo, Z., Zhang, S., & Sun, X. (2022). Preparing a binder for cemented paste backfill using low-aluminum slag and hazardous oil shale residue and the heavy metals immobilization effects. *Powder Technology*, 399, 117167.

Zhong, X., Li, L., Jiang, Y., & Ling, T.-C. (2021). Elucidating the dominant and interaction effects of temperature, CO2 pressure and carbonation time in carbonating steel slag blocks. *Construction and Building Materials*, 302, 124158.

Zhu, X., Guo, W., Luo, Z., Zhu, X., Cai, W., & Zhu, X. (2023). Combined with co-hydrothermal carbonation of wood waste and food waste digestate for enhanced gasification of wood waste. *Fuel*, 331, 125789.

Zhuang, X. Y., Chen, L., Komarneni, S., Zhou, C. H., Tong, D. S., Yang, H. M., ... & Wang, H. (2016). Fly ash-based geopolymer: clean production, properties, and applications. *Journal of Cleaner Production*, 125, 253-267.

ABSTRACT

Accelerated carbonation of Ca-rich fly ashes in non-cement applications

The prolific utilization of low-grade solid fuels in global heat and power production gives rise to salient challenges, notably the emissions of CO_2 and the meticulous handling or valorisation of solid waste by-products. Accelerated carbonation can be employed as a method to stabilize potentially harmful waste streams, transforming them into viable alternative building materials.

In Estonia, the energy sector is principally anchored to indigenous oil shale extraction, supplemented by biofuels – predominantly wood chips and forestry derivatives – and stands as a paramount CO_2 emitter, concurrently generating substantial quantities of waste ash. The presence of free Ca-Mg oxides, constituting nearly a quarter of the ash composition coupled with the intrinsic cementitious attributes derived from portlandite, active calcium silicates, and aluminates, positions it as a prime candidate for upcycling into a building material, augmented by carbonation curing.

The objective of this research is to explore potential construction applications that can effectively utilize alkaline solid wastes in tandem with CO_2 emissions. In pursuit of this goal, various waste streams from Estonia, including oil shale fly ash (OSA), wood fly ash (WA), and landfilled ash (LFA), were evaluated for their capacity as CO_2 binders and assessed for cementitious properties.

The finding suggests that the self-cementing ability of OSA is of ashes comprising 15–22% of the material, calcium, magnesium silicates, and aluminates, in conjunction with lime and portlandite (14–23%), partake in pozzolanic processes. This results in an average of 10 MPa compressive strength and swift setting durations (0.3–1 h), suggesting a constrained scope for self-cementing uses. Additionally, using fly ash in clay brick production boosts thermal properties, offering about 50% better insulation and reduced shrinkage. However, fly ash components introduce additional chemical reactions during firing, which release gases that can reduce brick density by 21% and strength by 33%. Without careful management, this can lead to warping or cracking.

The data underscores that both OSA and WA effectively act as sorbents for CO_2 mineralization when used in compacted, cement-free monoliths. Experiments highlighted that free CaO predominantly serves as the principal CO_2-sequestering constituent in the ash. Under alkaline conditions, Ca-Mg silicates exhibit diminished reactivity. Given that the observed pH values approximate 11–12, the involvement of Ca-Mg silicates in the carbonation reaction is negligible. In the initial phase of processing, compaction serves as a pivotal parameter, predominantly modulating the compressive strength through pore minimization. An increase in compaction intensity bolsters strength, yet concurrently impedes the diffusion of CO_2, culminating in diminished CO_2 sequestration. Modifications in curing parameters, such as elevated temperature, gas pressure, and concentration, generally enhance the carbonation reaction rate. However, while an increase in curing temperatures might intensify carbonation, it doesn't correspondingly boost compressive strength. This discrepancy could arise from the formation of micro-cracks and alterations in the micro-mechanical properties of CSH. At higher temperatures, the diminished availability of liquid water in monoliths can lead to rapid and uneven particulate deposition on $Ca(OH)_2$ surfaces.

The carbonation reaction in OSA and WA monoliths is initially rapid due to the open porous surfaces and the presence of physically bound water in the pore structures. However, as carbonation progresses from the outer surface inwards, the rate slows due to diffusion limitations through the product layer. The initial exothermic reaction can elevate particle temperatures, potentially accelerating water evaporation and thus hindering CO_2 diffusion and carbonic acid formation. While the early stages of carbonation show no distinct temperature dependency, increasing temperatures positively influence CO_2 uptake, especially during the diffusion-controlled stage in OSA. In contrast, WA displays a more pronounced temperature effect, suggesting a more kinetically controlled reaction from the outset. Thermal analysis corroborates the CO_2 uptake values obtained from gas monitoring.

The results suggest that, following niobium slag (NS) addition and carbonation, sulphate leaching is proficiently curtailed through a synergistic mechanism: chemical interactions with calcium aluminate sulphate (CAS) phases and physical encapsulation by calcium aluminate hydrate (CAH) gels. In monoliths enriched with NS, heavy-metal concentrations diminish due to the ion-stabilizing attributes of the CAH gel.

The notion of CO_2 mineral sequestration in cement-free ash monoliths, derived from ash produced by Estonian power and heat generation, has been advanced as a strategy to counteract the atmospheric accumulation of CO_2 emanating from the combustion of the fossil fuel, oil shale. CO_2 emissions from Estonian power generation, which predominantly relies on oil shale, could be substantially mitigated by utilizing waste ash as a CO_2 sorbent and subsequently valorising the resultant product for building material applications. Through the carbonation curing process, the sequestration of CO_2 averaged between 10–15% by weight, and the monoliths exhibited a compressive strength reaching up to 47 MPa.

LÜHIKOKKUVÕTE

Kaltsiumirikka lendtuha kiirendatud karboniseerimine tsemendivabades rakendustes

Madalakvaliteediliste tahkekütuste ulatuslik kasutamine soojuse ja elektri tootmiseks on globaalseks väljakutseks, seda nii CO_2 heitkoguste kui ka tahkete jäätmete vastutustundliku käitlemise ning väärindamise osas. Kiirendatud karboniseerimine on meetod potentsiaalselt kahjulike jäätmevoogude stabiliseerimiseks, muutes need ühtlasi alternatiivsete ehitusmaterjalidena kasutatavaks.

Eesti põlevkivil baseeruvat energiasektorit täiendavad järjest enam biokütused, valdavalt hakkpuit ja teised metsandussaadused, mis on oluliseks CO_2 emissioonide ja tahkjäätmete allikaks. Tuha koostisest (vabade Ca-Mg-oksiidide olemasolu koos portlandiidist tulenevate sideaineliste omadustega ning aktiivsed kaltsiumsilikaadid ja aluminaadid) tingitud väärindamispotentsiaali ehitusmaterjalina saaks võimendada läbi karboniseerimispõhise kõvenemise.

Antud uuringu eesmärgiks oli leeliseliste tahkete jäätmete ja CO_2 heitmete põhiste meetodite arendamine kasutamaks neid sobivates ehitusrakendustes. Lähtuvalt nii karboniseeritavusest kui ka tsemendiomadustest uuriti Eestis tekkivaid jäätmevooge, nagu põlevkivituhk (OSA), puidutuhk (WA) ja ladestatud põlevkivituhk (LFA), kui potentsiaalseid sideaineid.

Katsetulemuste kohaselt on OSA isetsementeeruvate tuhkade hulgas, mis koosnevad 15–22% ulatuses Ca-Mg-silikaatidest ja aluminaatidest, mis koos lubja ja portlandiidiga (14–23%) osalevad putsolaansetes protsessides. Selle tulemusena saavutatakse katsekehadel keskmiselt 10 MPa-ne survetugevus ja lühike tardumisaeg (0,3–1 h), mis viitavad piiratud võimalustele isetsementeeruvates rakendustes. Lendtuha kasutamine savitelliste tootmises parandab nende termilisi omadusi, andes umbes 50% parema soojusisolatsiooni ja vähendab kokku tõmbumist. Siiski toovad lendtuhakomponendid põletamise ajal sisse täiendavaid keemilisi reaktsioone, mille käigus vabanevad gaasid võivad vähendada tellise tihedust ja tugevust, vastavalt 21% ja 33%. Paagutusprotsessi hoolika juhtimiseta võib see põhjustada väändumist või pragunemist.

Teisalt aga saab nii põlevkivituhka kui ka puidutuhka kasutada tihendatud tsemendivabades monoliitides, kus nad toimivad CO_2 sorbentidena. Vaba CaO toimib tuhas peamise CO_2 siduva komponendina, samas kui Ca-Mg silikaadid näitavad leeliselistes tingimustes vähenenud reaktiivsust. Kuna täheldatud pH väärtused on ligikaudu 11–12, on Ca-Mg silikaatide osalemine karboniseerimisreaktsioonis marginaalne. Töötlemise algfaasis on tihendamine oluline parameeter, mis mõjutab survetugevust peamiselt pooride vähendamise kaudu. Tihendusintensiivsuse tõstmine annab katsekehale suurema tugevuse, kuid samas takistab CO_2 difusiooni, mis omakorda vähendab CO_2 sidumist. Karboniseerimisprotsessi parameetrite, näiteks temperatuuri, gaasirõhu ja kontsentratsiooni tõstmine, suurendab üldiselt ka karboniseerimisreaktsiooni kiirust. Samas ei pruugi intensiivsem karboniseerimisprotsess tagada vastavalt suuremat survetugevust, seda peamiselt mikropragude tekkimise ja CSH mikromehaaniliste omaduste muutumise tõttu. Kõrgematel temperatuuridel võib katsekehade vedelfaasis oleva vee kättesaadavuse vähenemine põhjustada kiiret ja ebaühtlast osakeste ladestumist $Ca(OH)_2$ pinnale.

OSA ja WA põhistes katsekehades on karboniseerimisreaktsioon avatud poorsete pindade ja poorstruktuurides oleva füüsiliselt seotud vee olemasolu tõttu alguses kiire.

Kuna aga karboniseerimine edeneb välispinnalt sissepoole, siis aeglustub protsess materjalikihi difusioonipiirangute tõttu. Algse eksotermilise reaktsiooni korral võivad osakeste temperatuurid tõusta, kiirendades potentsiaalselt vee aurustumist ja takistades seeläbi CO_2 difusiooni ja süsihappe teket. Kuigi karboniseerimise varajased etapid ei viita erilisele temperatuursõltuvusele, mõjutab temperatuuri tõstmine positiivselt CO_2 omastamist, OSA puhul just difusioonkontrollitud faasis. WA puhul, vastupidi, on temperatuuriefekt selgemalt väljendunud, viidates pigem kineetiliselt kontrollitud reaktsioonile algusest peale. Termiline analüüs kinnitab gaasianalüüsi abil saadud CO_2 sidumise väärtusi.

Niobiumi räbu (NS) lisamine koos karboniseerimisega vähendavad sulfaatioonide leostumist keemiliste interaktsioonide ja kaltsium-aluminaat-sulfaadi (CAS) faaside ning kaltsium-aluminaat-hüdraadi (CAH) geelide tekkest tingitud füüsilise kapseldamise kaudu. Samuti vähenevad NS-iga rikastatud monoliitide puhul raskmetallide kontsentratsioonid moodustuva CAH geeli ioone stabiliseerivate omaduste tõttu.

Käesolevaga näidati CO_2 mineraalse sidumise kontseptsiooni rakendatavust tsemendivabades elektri- ja soojusenergia tootmisjäätmetel põhinevates tuhamonoliitides, mida saaks arendada strateegiana CO_2 emissioonide vähendamiseks. Eesti põlevkivipõhise elektrienergia tootmise ökoloogilist jalajälge saaks oluliselt väheneda kasutades jäätmetuhka CO_2 sorbendina ja väärindades seejärel saadud toodet ehitusmaterjalina. Karboniseerimispõhise kõvenemisprotsessi rakendamisel ulatus CO_2 sidumine keskmiselt 10–15%-ni kaalust ja tuhamonoliitide survetugevus kuni 47 MPa.

Appendix 1

Publication I

Usta, M. C., Yörük, C. R., Hain, T., Paaver, P., Snellings, R., Rozov, E., ... & Uibu, M. (2020). Evaluation of new applications of oil shale ashes in building materials. *Minerals*, *10*(9), 765. https://doi.org/10.3390/min10090765

minerals

MDPI

Article

Evaluation of New Applications of Oil Shale Ashes in Building Materials

Mustafa Cem Usta [1,*], Can Rüstü Yörük [1], Tiina Hain [2], Peeter Paaver [3], Ruben Snellings [4], Eduard Rozov [5], Andre Gregor [1], Rein Kuusik [1], Andres Trikkel [1] and Mai Uibu [1]

1 Department of Materials and Environmental Technology, Tallinn University of Technology, 19086 Tallinn, Estonia; can.yoruk@taltech.ee (C.R.Y.); andre.gregor@taltech.ee (A.G.); rein.kuusik@taltech.ee (R.K.); andres.trikkel@taltech.ee (A.T.); mai.uibu@taltech.ee (M.U.)
2 Department of Civil Engineering and Architecture, Tallinn University of Technology, 19086 Tallinn, Estonia; tiina.hain@taltech.ee
3 Department of Geology, University of Tartu, 50411 Tartu, Estonia; peeter.paaver@gmail.com
4 Sustainable Materials, VITO, 2400 Mol, Belgium; ruben.snellings@vito.be
5 Wienerberger, 43401 Aseri, Lääne-Virumaa, Estonia; eerozedu@gmail.com
* Correspondence: mustafa.usta@taltech.ee

Received: 3 July 2020; Accepted: 27 August 2020; Published: 29 August 2020

Abstract: Achieving sustainable zero-waste and carbon neutral solutions that contribute to a circular economy is critically important for the long-term prosperity and continuity of traditional carbon-based energy industries. The Estonian oil shale (OS) sector is an example where such solutions are more than welcome. The combustion of OS generates a continuous flow of ashes destined to landfills. In this study, the technical feasibility of producing monolith building materials incorporating different OS ashes from Estonia was evaluated. Three binder systems were studied: self-cementation of the ashes, ceramic sintering in clay brick production and accelerated carbonation of OS ash (OSA) compacts. Results showed that most of the OSAs studied have low self-cementitious properties and these properties were affected by ash fineness and mineralogical composition. In case of clay bricks, OSA addition resulted in a higher porosity and improved insulation properties. The carbonated OSA compacts showed promising compressive strength. Accelerated carbonation of compacted samples was found to be the most promising way for the future utilization of OSAs as sustainable zero-waste and carbon neutral solution.

Keywords: oil shale ash; waste utilization; concrete; bricks; carbonation curing

1. Introduction

New initiatives by the European Commission not only aim at reducing air and water emissions but also extensively encourage innovation in waste or residue recovery using "Best-Available Technologies" (BAT) that promote transitions towards green energy production under the principles of circular economy [1]. In this context, the Estonian oil shale (OS) sector is a good example where the management and utilization of waste is vital to ensure long term sustainability.

Estonia is still mostly utilizing low calorific fuel—OS as a primary source of energy including electricity, heat and oil production across the country. This heavy fossil fuel reliance produces abundant amounts of uncommon calcareous ash which has been deposited in landfills and waste piles over the years, since the ash lacks industrial applications [2,3]. Historically landfilled ashes as well as the currently generated ashes carry important risks to the biosphere such as emissions of hazardous trace elements (Sr, Zr, As, Cd, Cu, Cr, Zn, Pb) as well as alkalinity to groundwater and air [4–6].

In recent decades the implementation of circulating fluidized bed (CFB) boilers for combustion and advanced retorting technologies for oil production have greatly increased extraction efficiencies

and reduced GHG emissions. However, these changes in the process are not without pitfalls as the physical and chemical characteristics of the OSA were negatively affected. For instance, lowering the temperatures from 1300–1400 °C (previously used in pulverized firing (PF) boilers) to 700–800 °C (used in current CFB boilers) changed the phase composition of the ashes, altered the content of unburnt materials and increased calcium sulfate contents. The phase composition shifted away from high-temperature Ca-silicates towards free lime and quartz. This complicates the utilization of OSA by inducing volumetric expansion and poses environmental issues by increasing the pH of OSAs [7].

The utilization of OSA in the production of new valuable products could be a partial solution for the Estonian OS sector by integrating core concepts from circular economy. In this respect, OSA as any other industrial alkaline solid waste (such as lignite, coal, wood bottom and fly ashes (FAs), steel slags, cement production wastes and waste concrete), can be considered as a valuable raw material in the conventional production processes of cement, concrete and ceramics [8–10]. Evidence of this utilization has existed previously in the Estonian context, where OSA, collected from electrostatic precipitators (EP) of PF units, was used as a raw material for the production of Portland clinker. Additionally, coarse fractions were used as aggregates in the production of cellular concrete blocks and in the applications of road-base stabilization [2,7]. However, due to the above-mentioned changes in the OS incineration process such applications have been phased out. Therefore, there is an urgent need to investigate alternative application routes for OSAs.

The current study includes three sub-studies of oil shale ash utilization in building materials; first sub-study is testing of self-cementing properties of all the currently generated OSAs, second sub-study is the clay brick production with oil shale ash to test its performance as opening agent and the last sub-study is on the properties of OSA monoliths obtained by accelerated carbonation, which draws on the recent developments in research of carbonate bonded construction materials [11–13].

2. Materials and Methods

2.1. Self-Cementing Performance

2.1.1. Materials

A range of OSAs were included in the present study. The selected ashes were mainly FAs regularly collected in the period of 2018 and 2019 including electrostatic precipitator ash (EPA), cyclone ash (CA), total ash (Mixture of all flow of ashes from PP, except EPAs) (TA) and mixtures of different FAs from the Auvere (A) and Eesti (E) power plants (PP). Additionally, CA and TA from the Enefit 280 oil production plant were included. In total, 6 different ash streams (EPP-EPA, EPP-TA, APP-EPA, APP-TA, EN280-CA, EN280-TA) were considered.

2.1.2. Material Characterization

The physical, chemical and mineralogical characterization of the selected waste streams included determination of total carbon (TC) and total inorganic carbon (TIC) with an Eltra CS 580 (Haan, North Rhine-Westphalia, Germany) Carbon Sulphur Determinator and free CaO content (based on ethylene glycol method), X-ray fluorescence (XRF) and X-ray diffraction (XRD) analyses with Bruker S4 Pioneer (Karlsruhe, Baden-Württemberg, Germany) and Bruker D8 (Karlsruhe, Baden-Württemberg, Germany) diffractometers, respectively. For XRD analysis, randomly oriented preparations were made and scanned on a Bruker D8 Advance diffractometer using Cu Kα radiation with a Göbel mirror monochromator and LynxEye positive sensitive detector over a 2°–70° 2Θ range. The quantitative phase composition was analysed and modelled using the Rietveld algorithm-based program Topas (Karlsruhe, Baden-Württemberg, Germany). The relative error of quantification is better than 10% for major phases (>5 wt. %) and better than 20% for minor phases (<5 wt. %). The BET-N_2 sorption method was used to measure the specific surface area (SSA) with Kelvin 1042 sorptiometer.

The particle size distribution (PSD) was measured by laser diffraction using a Horiba (Kyoto, Japan) Laser Scattering instrument, LA-950 (with ethanol suspension).

2.1.3. Sample Preparation

In order to test the self-cementing properties of the OSAs, ash and sand pastes were prepared for all waste streams. 0.7 was found to be optimum ratio of water to ash [14] and ash to sand (cf. EN 196-1:2016) ratio was 0.33. Pastes were cast in 40 × 40 × 160 mm^3 prisms and compacted using a vibration table. The compacted pastes were first kept 48 h in molds, then five days at 60% RH and 20 ± 2 °C, and further curing continued for 28 days at >95% RH and 20 ± 2 °C. After 28 days, the failure strength (flexural and compressive strength) was tested following EN 196-1:2016 [15].

The aim of the work regarding self-cementing properties of oil shale ashes was to find possibilities for utilization of oil shale ashes. These types of studies are based on our own experience with oil shale throughout the years. The methods described therein might vary from those utilized in the applications of Portland cements due to the distinct influence of OSA types and properties of pastes and mortars.

2.1.4. Tests and Measurements

Flexural strength test determined the maximum bending stress of prisms before failure. This test was conducted on a Toni TechnikD-13355 (Berlin, Brandenburg, Germany) which works in accordance with EN ISO 7500-1 (2018) [16]. The compressive strength test was also performed using the same apparatus which applies a progressing load rate of 2400 N/S in accordance with EN 196-1:2016 and ISO 679 [17]. The split mortar bar halves from flexural strength test were used for the compressive strength measurements.

2.2. Clay Bricks with Sand to OSA Replacement

2.2.1. Materials

The clay (Cambrian blue clay) and clay/sand mixtures used in the green shaped bodies were obtained from Wienerberger Company—located in Aseri, Estonia. Similar physical and chemical characterization methods, as defined above for concrete application, have been used for the material characterization of the clay.

The studied OSA sample for clay bricks is EPP-EPA obtained in August 2018 which was separated into different size fractions by size classification. The coarse fraction was used as sand or opening agent replacement in the formulation of clay bricks. Material characterization considered both the initial EPP-EPA and coarse fraction of EPP-EPA in terms of PSD, SSA, XRF and XRD analyses.

2.2.2. Sample Preparation

In a first trial stage 3 brick formulations were tested. A reference brick was prepared with a mixture ratio of 80% clay/20% sand. A constant brick formulation of 80% clay/10% sand/10% EPP-EPA was used for both the initial and coarse ash. Bricks were prepared in triplicate by hand.

The obtained fresh clay was first dried in a ventilated oven at 105 °C for 4 h. Dried agglomerates were comminuted using a ball mill for 20 min. Subsequently, the clay was ground to fine powder using a four-ball planetary mill (clockwise rotation for 10 min at 350 rpm, anti-clockwise rotation for 5 min at 350 rpm) and dried again at 105 °C for 4 h. The dried raw materials were mixed in the specified ratios and water was added to obtain similar plasticity (sight/feeling) of the mixtures. An infrared moisture analyzer was used to measure the water content of the mixtures. For EPP-EPA added bricks 20 wt. % water was used while 15 wt. % water was required for the reference bricks. The pastes were placed into 40 × 40 × 160 mm^3 prisms and a hydraulic press applied a pressure of 75 kg/cm^2 for 10 s. After demolding, the prepared green bodies were left to dry; first at room temperature (12 h) then in a drying chamber (with slow temperature ramp (~15 °C/h) up to 105 °C) until water evaporation related mass change stops before transferring them to the sintering stage. This process was carried

out to avoid possible swelling or cracking of the samples in the furnace, caused by the expansion of entrapped water. Finally, the samples were sintered at 1020 °C which took approximately 48 h (including slow heating and cooling cycle) in an industrial tunnel furnace under oxidizing conditions.

2.2.3. Tests and Measurements

After press molding, the samples were weighed, and dimensions were measured to calculate the wet density. The same process was repeated after drying and sintering to obtain both dry density and end product density values. A water absorption test was carried out according to EN 771-1:2011 + A1:2015 [18]. The flexural and compressive strength tests were performed with Toni TechnikD-13355 (Berlin, Brandenburg, Germany). The thermal conductivity test was carried out with a HOT DISK TPS 2200 (Gothenburg, Västra Götaland County, Sweden) instrument which meets the ISO 22007-2 standard [19]. The intact samples were used for this analysis. The hot disk Teflon sensor was placed on opposite intact sides of the bricks and the thermal conductivity was measured at a rate of 10 K/s. The experiment is repeated on different sides of the same bricks and the mean value was recorded for further calculation. Porosity measurements were carried out with a POREMASTER PV007130 (Graz, Styria, Austria) which uses three automatic mercury intrusion cycles for pore size analysis. Measurements focused on intraparticle porosity which is the porosity within individual grains or particles. Total porosity was also measured to gain insight in all void spaces regardless of interconnectivity. In order to investigate the microstructure of the sintered bricks SEM images were obtained from the polished samples using a ZEISS Evo MA 15 (Oberkochen, Baden-Württemberg, Germany). The mineralogical composition was determined using XRD analysis.

2.3. Accelerated Carbonation of Compacted Samples

APP-EPA (October 2018) was chosen as starting material for the preliminary tests of compacted cylinders (Figure 1) as APP-EPA is enriched in free lime, therefore more suitable for carbonation purposes. A representative sample was taken and divided into two size fractions (fine (0–100 μm) and coarse (100–300 μm)) by sieving in order to investigate the effect of particle size on compaction behavior of ashes and extent of carbonation.

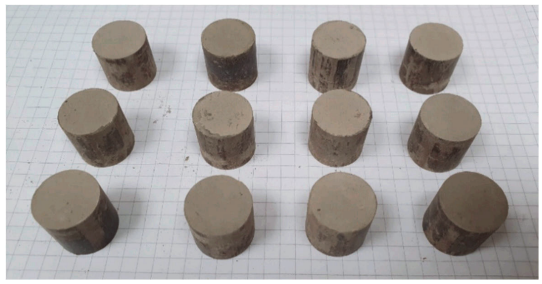

Figure 1. 100% APP-EPA compacted cylinders.

2.3.1. Sample Preparation

The accelerated carbonation process consisted of three main steps; the first step was proportioning of selected APP-EPA and prehydrating the sample to slake the free lime, the second step was the compaction of the sample using a hydraulic press and the third step was the carbonation of the product in an autoclave. In the first step the samples were mixed with water at a liquid to solid mass ratio of 0.25 in a semi-batch Eirich EL1 (Hardheim, Baden-Württemberg, Germany) type intensive mixer. The samples were homogeneously blended with water at a rotation speed of 600 rpm for 30 min. The samples were left to hydrate/cure in closed plastic bags overnight at room temperature and compacted on the following day using a hydraulic press into cylinders with diameter 20 mm and height 20 mm at a compaction pressure of 300 kg/cm^2. Carbonation experiments were performed in automated

carbonation units consisting of a temperature controlled stainless-steel autoclave. The autoclave was operated at two different pressure levels while temperature stayed at ambient levels; the compacted specimens were placed in the autoclave and cured by applying 100% CO_2 gas pressure of 5 and 10 bar for 4 h.

2.3.2. Tests and Measurements

The obtained results from compressive strength measurements were used as main parameter to evaluate the performance of the carbonated monoliths. The CO_2 uptake during carbonation was determined by thermogravimetric analysis (TGA). Additionally, XRD measurements were made to follow the formation of new phases during the carbonation process.

3. Results and Discussions

3.1. Oil Shale Ash Material Characterization

The BET specific surface area (SSA) and the mean particle size of the OSAs considered in this paper are summarized for APP (EPA, TA) in Figure 2, and for EPP (EPA, TA) and EN280 (TA, CA) in Figure 3. The variation of the physical properties is shown for different sampling dates. In case of APP OSA, EPA shows consistently finer particle sizes than TA, even though BET SSA fall within the same range. The EPP EPA and TA do not show this difference in particle size and are somewhat coarser (Appendix A: Tables A1 and A2). The particle size of EN280-TA is coarser than EN280-CA and showed a correspondingly lower SSA.

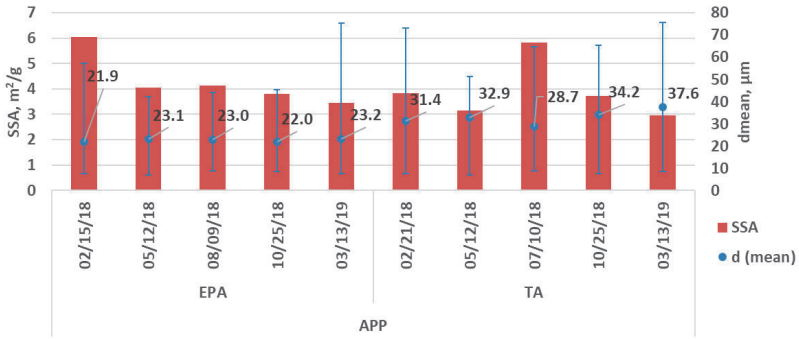

Figure 2. Particle size and BET SSA for APP (EPA, TA).

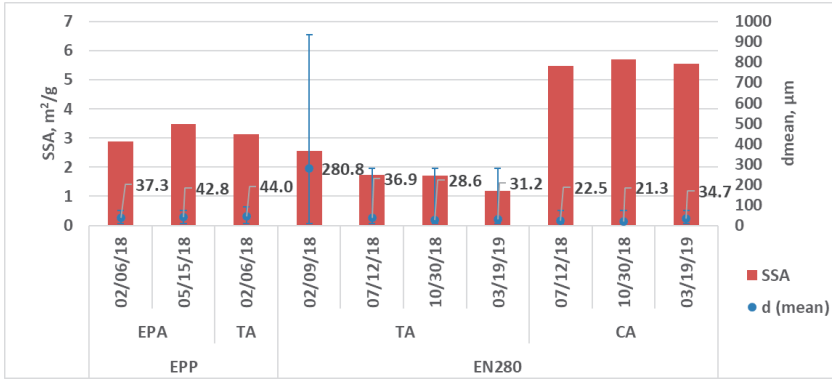

Figure 3. Particle size and BET SSA for EPP (EPA, TA) and EN280 (TA, CA).

All OSAs studied mainly consist of SiO_2, CaO and Al_2O_3, however in variable proportions (Figure 4). The main reason of such differences could be explained with several factors including characteristics of raw OS, OS processing conditions, thermochemical conversions, gaseous treatments for cleaning, boiler specifications, etc.

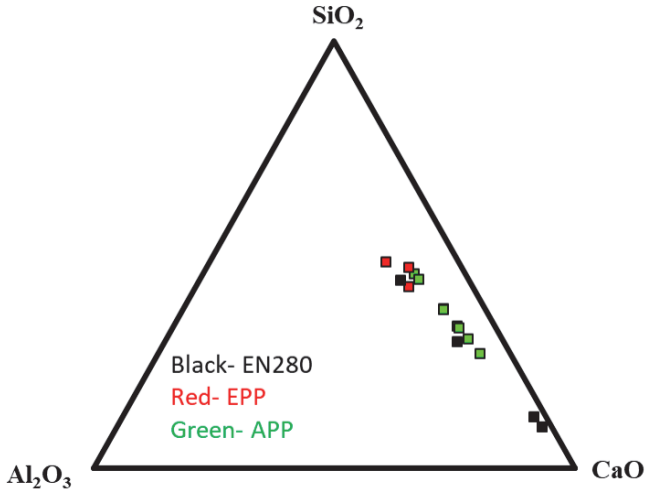

Figure 4. Ternary diagram of three major oxides in all OSAs.

In general, the high content of CaO can be explained by the decomposition of $CaCO_3$ which originally exists in the mineral part of OS and partially decomposes during the thermal processes. The presence of SiO_2 can be attributed to the inorganic part of the OS and mainly is representing finer particles as the content of silica is higher and lime content is lower in smallest size fractionated ashes. The chemical composition of OSAs differs and each type appears to show a distinct composition (Appendix B: Table A3). For instance, the high LOI of the EN280 residues is related to the lower temperature processing during retorting compared to combustion of OS causing delay in decomposition of carbonates and oxidation of unburnt carbon. Specifically, in case of EN280 TA, the high LOI of the residue correlates with a low SSA and coarse PSD which are all negative factors in terms of self-cementing behavior of these types of ashes especially when it is considered that fly ashes with high LOI can negatively affect the strength of the concrete (more water absorption, air-entraining, etc.) and increase setting times [20,21].

The variations in chemical composition are reflected in the phase composition as well as shown in Tables 1–3. Some fluctuations in phase composition of the ashes were observed throughout the year in the EPA fractions. The amount of free CaO is higher than 10% for EPP and APP ashes (EPA, TA) and mineral CO_2 content does not reach above 11%. Calcite and dolomite contents of EN280-CA and TAs are quite high, and the content of Ca/Mg silicates (C_2S, akermanite, mervinite) and aluminates are quite low compared to all other studied samples due to the low temperature processing during retorting.

Table 1. Phase composition of APP (EPA, TA).

Phase	APP EPA 25.10.2018	APP TA 25.10.2018	APP TA 21.02.2018	APP EPA 15.02.2018	APP EPA 9.08.2018	APP TA 10.07.2018
Quartz	12.6	9.9	12.2	15.5	13.1	12.2
K-feldspar	16.4	11.5	10.9	15.3	12.6	13.9
Mica	4.2	2.3	4.6	7.1	1.7	5.5
Calcite	13.5	20.7	23.1	17.0	12.7	15.6
Dolomite	tr *	0.6	-	-	tr	1.7
Hematite	1.5	1.2	1.5	1.7	1.2	1.2
Lime	19.3	15.1	18.5	13.5	18.4	9.0
Portlandite	3.4	6.4	0.7	-	4.4	11.0
Periclase	3.0	4.3	2.7	2.8	2.8	2.8
Anhydrite	5.9	7.0	6.2	8.9	8.3	9.8
C_2S	8	9	7.8	7.6	10.3	5.1
C_4AF	3.1	3.6	3.3	3.4	4.5	1.9
Akermanite	1.9	1.8	3.5	2.6	2.3	2.3
Merwinite	4.1	4.1	4.0	3.2	2.6	5.4
Diopside	1.7	1.2	-	-	2.8	-
Sylvite	0.6	0.6	-	0.5	0.5	0.5
Wollastonite	tr	0.7	-	-	1.1	-

* tr—Trace amount.

Table 2. Phase composition of EN280 (TA, CA).

Phase	EN280 CA 30.10.2018	EN280 TA 30.10.2018	EN280 CA 19.03.2019	EN280 TA 19.03.2019	EN280 CA 12.07.2018	EN280 TA 12.07.2018	EN280 TA 09.02.2018
Quartz	14.8	3.0	15.5	3.3	16.8	4.3	6.8
K-feldspar	17.7	2.8	15.1	1.2	17.8	2.1	8.1
Mica	5.8	1.8	10.9	-	7.3	1.4	1.2
Calcite	28.6	60.0	30.5	73.8	31.4	69.2	63.6
Dolomite	2.4	16.6	3.6	5.1	3.2	7.0	3.0
Hematite	2.3	1.1	2.1	1.0	2.8	1.1	0.9
Lime	0.2	-	-	-	-	-	-
Portlandite	tr	tr	-	-	-	-	-
Periclase	2.8	2.8	2.8	2.8	2.5	2.2	1.5
Anhydrite	9.1	2.7	8.2	6.0	8.8	5.5	6.3
C_2S	6.3	4.1	4.9	3.2	5.1	2.9	4.2
C_4AF	3.5	1.9	2.3	2.3	2.1	1.0	2.1
Akermanite	1.4	1.4	0.8	1.1	1.0	1.8	0.8
Merwinite	1.4	1.0	1.0	tr	1.1	1.3	0.4
Diopside	2.5	0.7	1.6	-	-	-	-
Wollastonite	tr	0.8	0.8	1.0	-	-	-

The samples that were used in last two sub-studies do not include ashes from oil shale retorting and these sub-studies only focus on the ashes produced from the combustion of oil shale. Both ashes used in the sub-studies are fly ashes (70% of the total ash produced) collected from electrostatic precipitators where most of the ash is accumulated during the combustion of oil shale. By studying these ashes throughout the year, we noticed that the minerology, chemical and physical properties do not change drastically. Another important factor for selecting the ashes in the last two sub-studies, is the content of free CaO.

Table 3. Phase composition of EPP (EPA, TA).

Phase	EPP EPA 15.5.2018	EPP EPA 06.02.2018	EPP TA 06.02.2018
Quartz	18.1	19.9	17.0
K-feldspar	13.9	15.5	12.7
Mica	5.4	4.7	4.5
Calcite	15.1	8.1	11.1
Dolomite	tr	-	-
Hematite	2.1	2.4	2.0
Lime	7.0	12.7	14.0
Portlandite	2.2	-	1.5
Periclase	4.8	4.1	5.0
Anhydrite	9.7	11.4	11.0
C_2S	9.2	4.9	5.6
C_4AF	4.1	2.4	2.7
Akermanite	4.5	8.6	8.2
Merwinite	1.6	3.6	3.8
Sylvite	1.2	-	-
Wollastonite	-	1.3	1.1

3.2. *Self-Cementing Properties of Oil Shale Ash*

Self-cementing ability and setting times of the considered OSAs are shown in Figures 5 and 6. The self-cementing ability is affected by the chemical composition and fineness of ashes, in particular the content of free CaO, portlandite, Ca/Mg silicates and SO_3 [22,23]. The self-cementing ability of ashes with coarse particle sizes and lowest temperature of treatment is generally lowest. This is demonstrated for EN280-CA and TAs.

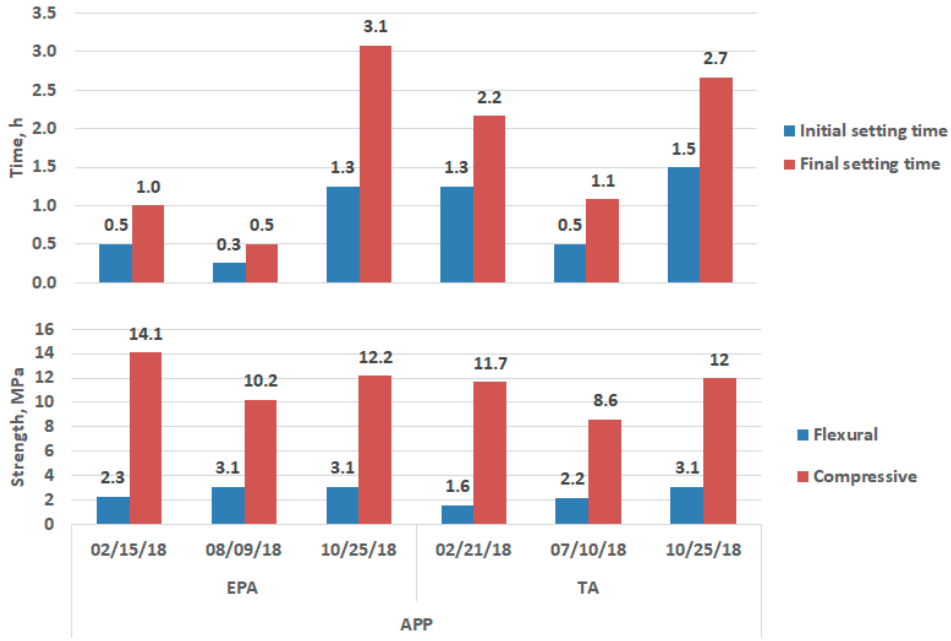

Figure 5. Setting times and Self-cementitious ability for APP-EPA and APP-TA.

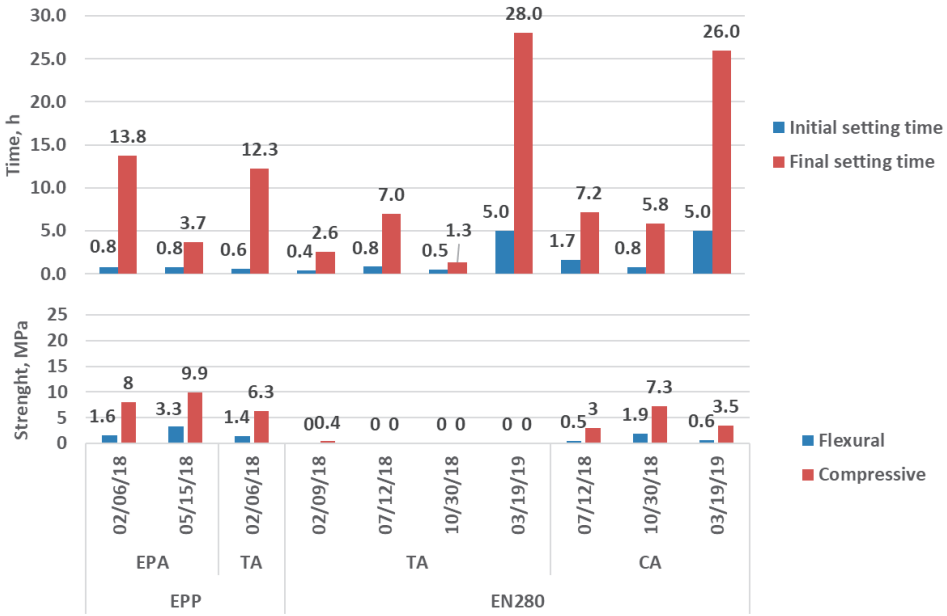

Figure 6. Setting times and self-cementitious ability for EPP (EPA, TA) and EN280 (TA, CA).

Comparing the self-cementing properties of all studied ashes, the performance of the APP-EPA and APP-TA was found to have better properties. Between these two samples of ashes, APP-EPA is shown to have optimal suitability. This is tentatively explained by a higher BET SSA and a considerable content of lime and portlandite (~14–23%), Ca-Mg silicates (C_2S) and C_4AF (~15–22%) that can participate in hydraulic or pozzolanic reactions. Therefore, APP-EPAs and EPP-EPAs have potential self-cementing properties.

Setting times were tested according to EN 196-3:2016 in order to evaluate how long the samples remain in a plastic state that enable placing or casting the mixes. However, most of the studied mixes demonstrated very short setting times. This is tentatively related to the quick hydration of free CaO [24].

Because of this reason, less reactive ashes (EN280) would require post-treatments like higher temperature treatment, grinding, sieving etc. in order to increase their performance. Due to insufficient amounts of reactive phases present the EN280 ash specimens fell apart during the curing of samples as cohesion is lost after evaporation of water in the 60% RH environment (Figure 7).

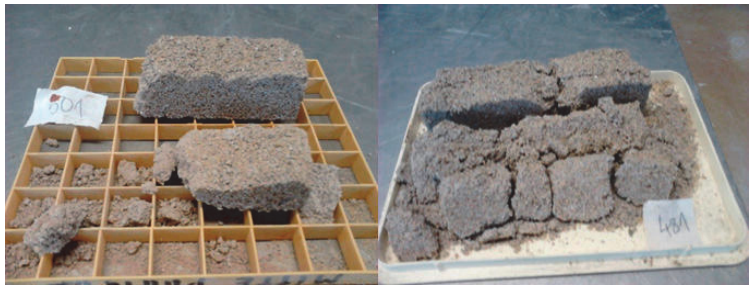

Figure 7. Spontaneous disintegration of EN280 specimens after 60% RH curing.

3.3. Clay Brick Production Using OSA

It can be seen from Table 4 that EPP-EPA has more complex and different chemical composition than the clay which mostly consists of SiO_2, Al_2O_3, Fe_2O_3 and K_2O. The main oxides in EPP-EPA are SiO_2—31.94%, CaO—35.25%, Al_2O_3, MgO and the content of SO_3 is relatively high as well. The LOI is 4.8% due to the release of combined water, crystalline water, combustion of organic carbon and oxidation of sulfur.

Table 4. Chemical composition of EPP-EPA and clay.

Oxides	EPP EPA (wt. %)	Clay (wt. %)
CaO total	35.25	0.4
MgO	5.85	2.3
SiO_2	31.94	61.4
Al_2O_3	7.46	17.8
Fe_2O_3	-	5.9
SO_3	7.12	1.6
K_2O	3.32	6.1
Na_2O	2.28	0.08
Mn_2O_3	0.06	-
TiO_2	0.38	-
P_2O_5	0.14	-
LOI *	4.82	4.8
TOC *	0.22	0.21

* LOI—Loss on ignition; TOC—Total organic carbon.

The mineralogy of the clay shows a heterogeneous mixture of minerals (Table 5) and can be subdivided into clay minerals (~60%) including kaolin, illite, illite-smectite, mica and chlorite, and non-clay minerals (~40%) including mainly quartz, orthoclase and minor constituents such as gypsum, pyrite and calcite. The clay used in this work is also characterized by a higher BET SSA—30.86 m^2/g and smaller mean particle size (15.1 μm).

Table 5. Phase composition of EPP-EPA and clay.

Phases	EPP EPA (wt. %)	Clay (wt. %)
Quartz	16.1	27.2
Free Lime	12.6	-
Anhydrite	9.1	-
Calcite	8	0.3
Kaolin	-	7.1
Periclase	3.8	-
Hematite	2.9	-
beta C_2S	2	-
gamma C_2S	4.4	-
C_4AF	2.1	-
Mullite	0	-
Pyrite	-	0.8
Ca-langbeinite	2.5	-
Gypsum	-	1.2
Chlorite	-	5.1
Orthoclase	4.5	5.2
Illite, Illite-smectite, Mica	3.6	52.2
Amorphous	28.3	-

Based on the observations made on prepared samples, as a first impression it can be mentioned that the color is one of the parameters to consider when producing bricks, as different type of ashes

would lead to significant changes in color when compared with the reference bricks. It can be observed in Figure 8, EPP-EPA does make the color of bricks lighter and give a new yellowish color.

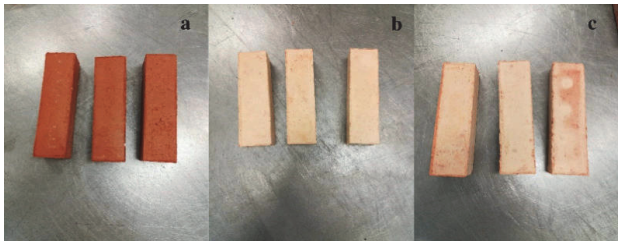

Figure 8. (**a**) Reference 4:1 clay:sand, (**b**) 8:1:1 clay:sand:EPP-EPA coarse and (**c**) 8:1:1 clay:sand:EPP-EPA.

The densities of bricks after molding, drying and sintering are presented in Table 6. Dry densities are lower than wet densities and values are proportional to the required initial water content for molding the bricks. The reaction between free CaO and water bonds water chemically which makes the dry density not exactly proportional to initial water added to the EPP-EPA added raw mixtures. It can also be seen that the values of reference bricks show a noteworthy increase in density after sintering while the density of EPP-EPA added bricks show only a slight increase. The shrinkage of bricks after sintering is given based on the volume changes and it can be noted that the reference bricks have the highest shrinkage. With the addition of EPP-EPA, a notable reduction of shrinkage can be explained due to the different phase composition of EPP-EPA compared to sand which is mainly inert and as a result accompanies different volume reduction. The presence of $Ca(OH)_2$, Ca and Mg carbonates, partially Ca- sulphate (the decomposition of sulphates can proceed well below 1000 °C in presence of CO [25]) in EPP-EPA strongly influences the brick microstructure by releasing H_2O, CO_2 and SO_2 due to the new decomposition reactions attributed to EPP-EPA (Equations (1)–(4)) in addition to clay mineral dehydroxylation, quartz inversion, crystallization and formation of vitreous phase reactions [26].

$$Ca(OH)_2 \rightarrow CaO + H_2O \quad (1)$$

$$CaCO_3 \rightarrow CaO + CO_2 \quad (2)$$

$$MgCO_3 \rightarrow MgO + CO_2 \quad (3)$$

$$CaSO_4 + CO \rightarrow CaO + SO_2 + CO_2 \quad (4)$$

Table 6. Physical properties of sintered bricks.

Physical Properties	Reference	EPP-EPA Initial	EPP-EPA Coarse
Wet Density (kg/m^3)	2138	1868	1818
Dry Density (kg/m^3)	1845	1779	1744
Sintered density (kg/m^3)	2185	1723	1766
Sintering shrinkage (%)	12	5	6

The physical and performance properties of the bricks are affected by the increased porosity of the EPP-EPA bricks. The compressive and flexural strength constitute the main parameters of brick performance. The obtained average value for the compressive strength EPP-EPA added bricks was ~20 MPa and for reference bricks ~30 MPa. These results correlate with the increased porosity of the EPP-EPA bricks as higher water absorption is usually associated with higher porosity as well. Water absorption values (Table 7) showed lowest water absorption for the reference bricks and EPP-EPA addition led to an increase in water absorption value (2.5 times).

Table 7. Mechanical and thermal properties of bricks.

Sample Name	Compressive Strength (MPa)	Flexural Strength (MPa)	Water Absorption (%)	Thermal Conductivity (W/mK)
Reference	30.6	8.9	5.2	1.22
EPP-EPA initial	21.5	4.2	13.9	0.67
EPP-EPA coarse	19.3	4.4	13.3	0.71

Thermal properties are important in terms of heat insulation and energy performance of buildings. The thermal conductivity of a composite material is determined by the properties of its constituents. In case of clay bricks the thermal conductivity varies depending on porosity and conductivity of the solid constituents and exhibits a decrease in trend with bulk density [27]. It can be seen from the measured thermal conductivity values of the fired bricks, given in Table 7, that EPP-EPA bricks have 50 % better insulation properties than the reference bricks.

An overall porosity reduction is expected when above 1000 °C the vitreous phase fills the pores and the ceramic body shrinks. From the porosity results shown in Figure 9, it can be understood that the EPP-EPA samples show a higher volume of pore features in the range of 0–4 µm compared to the reference.

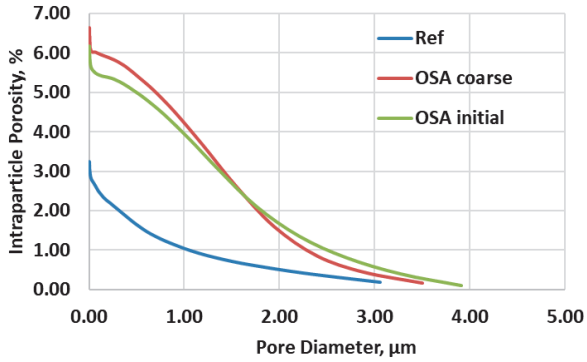

Figure 9. Intraparticle porosity as a function of pore diameter size.

Additionally, the SEM images of the brick samples are shown in Figure 10 and it is evident that a higher degree of particle interlocking, and more homogeneous texture can be observed for the reference brick microstructure.

The presence of carbonates strongly influences the brick microstructures and lowers the degree of shrinkage. This is partially due to the additional porosity generated during decomposition of the Ca carbonate into free lime and CO_2 gas (Equation (2)). The CaO further recombines with the clay minerals during crystallization reactions and results in changes of the brick phase composition. Similar findings were also mentioned in other studies (Junge [28], Sütcü and Akkurt [29]) where other waste additives with high $CaCO_3$ content (i.e., paper making sludge, limestone powder) were evaluated for brick production and these types of residues were identified as pore-forming additives.

The phase composition of the EPP-EPA and the reference bricks is compared in Table 8, the main difference is the presence of a significant fraction of plagioclase (Ca-feldspar) in the EPP-EPA bricks. In addition, small amounts of anhydrite and mullite were identified as well. Clearly CaO introduced by the EPP-EPA reacted with the aluminosilicates in the clay to form plagioclase feldspar. Anhydrite did not decompose fully during the sintering.

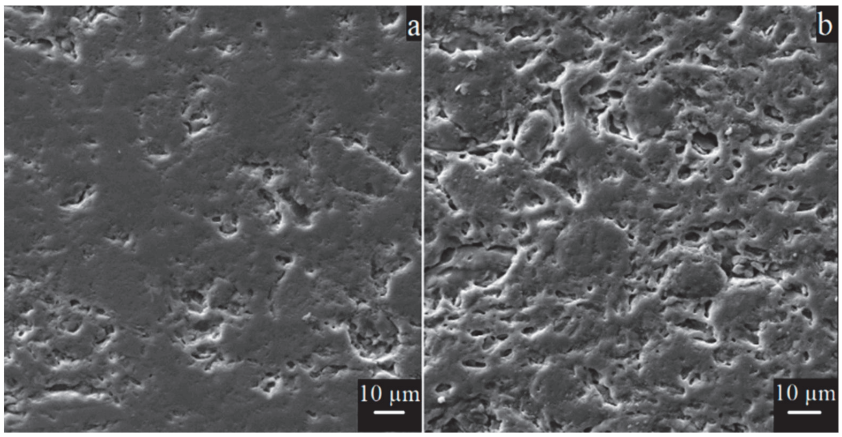

Figure 10. The SEM images of the brick samples, (**a**) Reference sample, (**b**) EPP-EPA (coarse).

Table 8. Phase composition of Reference and EPP-EPA added bricks (coarse).

Phase	Reference (wt. %)	EPP-EPA (wt. %)
Quartz	58.0	31.3
K-feldspar	12.6	20.8
Plagioclase	-	17.7
Mica	3.6	6.03
Hematite	3.8	4.5
Anhydrite	-	2.1
C_2S	-	1.3
C_4AF		0.5
Sanidine	9.7	-
Spinel	11.8	10.2
Mullite	-	3.7

3.4. Carbonate Bound Monolith Production from Oil Shale Ash

CaO/MgO and Ca/Mg-silicates in OSA are potential phases for CO_2 sequestration via carbonation. By carbonation of compacted samples, CO_2 can be permanently stored as Ca or Mg carbonates. The formation of carbonates is associated with an increase in solid volume and a decrease in porosity of the compacts. The carbonates act as cement by forming solid bridges between reacting particles and infilling of porosity.

The compressive strength test results of the compacted APP-EPAs are quite promising and compacts that are made of coarser fraction have greater compressive strength (up to 41.4 MPa) for both tested pressure levels (Table 9). Interestingly, the compacts carbonated at 5 bar show higher strength values compared to 10 bar. This may suggest that high pressures lead to fast reactions causing pore clogging near the surface of the compacts and zonation instead of homogeneous carbonation. In fact, previous studies have also shown that excess CO_2 pressure does not necessarily lead to a higher compressive strength as slower reaction would allow for dissipation of heat and reduce stresses on the product [30]. Further research into the microstructure of the carbonated compacts is needed to verify the mechanism controlling the carbonation reaction and to further optimize the performance of the carbonated products.

Table 9. Compressive strength, water absorption and density results for carbonated APP EPA compacts.

Particle Size (μm) and Pressure (bar)	Compressive Strength (MPa)	Density (kg/m^3)	Water Absorption (%)
0–100 μm 5 bar	24.9 ± 4.5	1992	11.2
0–100 μm 10 bar	8.6 ± 1.3	1807	12.3
100–300 μm 5 bar	38.1 ± 1.9	1882	9.8
100–300 μm 10 bar	20.1 ± 1.6	1675	10.4

Thermogravimetric analysis measurements of the compacts made from coarse fraction of APP EPA are presented in Figure 11. The mass loss due to the release of CO_2 that is related to decomposition of carbonates is indicated for the uncarbonated sample as well as it already includes $CaCO_3$ in the raw untreated ash which is measured as 6%. The samples cured at 5 and 10 bar show higher mass loss which is related to the mineral CO_2 bounded during carbonation, indicating that the CO_2 uptake during the carbonation treatment can be up to ~9% of the total mass of the sample.

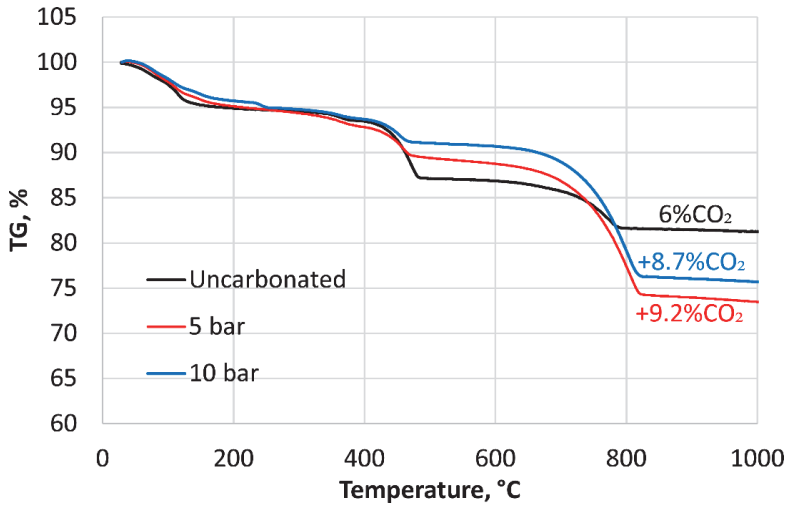

Figure 11. TGA curves for monoliths made from coarse fraction of APP EPA.

The phase composition of the uncarbonated and carbonated compacts are given in Table 10. Portlandite $Ca(OH)_2$ and ettringite are major phases present in the uncarbonated sample. In the carbonated samples a strong increase in the calcite ($CaCO_3$) fraction is notable. Calcite appears to form mainly at the expense of portlandite and ettringite. Additional to calcite, some gypsum has formed by carbonation of ettringite. Also, C_2S and merwinite appear to have partially carbonated. As noticed as well in the TGA, portlandite is not fully consumed indicating that further improvement of the process is possible. The fine ash fraction of 0–100 μm shows differences in its initial phase composition being higher in quartz, K-feldspar and mica and lower in anhydrite phases. This is reflected in the phase composition of the carbonated material.

Table 10. Phase composition of monoliths.

Phase	100–300 μm Uncarbonated	0–100 μm 5 bar	100–300 μm 5 bar	100–300 μm 10 bar
Quartz	5.4	12.7	4.6	5
K-feldspar	1.5	14.4	1.7	1.4
Mica	-	3.1	-	-
Calcite	10.2	43.5	35.1	38.4
Dolomite	1.9	3.1	2.7	3.6
Anhydrite	16.1	5.9	16.9	16.2
Periclase	2.4	2.6	3.6	3.9
Portlandite	36.1	trace	17.2	15.4
Vaterite	-	0.5	-	-
Akermanite	1.8	4	2.2	1.6
Merwinite	3	0.5	1.5	1.5
C_2S	4.7	0.8	1.6	1.3
Hematite	1.1	2.2	1	0.8
Ettringite	10.1	1.9	5.7	4.5
Gypsum	0.7	4.1	2.9	3.9
Brucite	4.7	trace	3	2.5

4. Conclusions and Perspectives

Estonian oil shale ash (OSA) characterization results showed that the new types of OSA from Enefit280 units contain significantly less free lime and more undecomposed carbonates compared to other combustion technologies. Additionally, chemical and physical composition of this type of ash is quite variable throughout the testing period of this study. In contrast, both the chemical and physical composition of APP and EPP ashes stay practically unchanged providing easier implementation of storage or recycling treatments.

APP-EPA is the only type of ash which can be considered as an independent potential binder. The rest of the tested ashes would require additional physical or thermal pre-treatments to make them fit for use in cement and concrete applications. These types of wastes for instance could be re-evaluated as a composite raw material for mixed binders including other constituents.

The effect of EPP-EPA addition was investigated in terms of physical, mechanical and thermal properties of clay bricks. From a broad perspective it can be concluded that the physical, mechanical and thermal properties (i.e., workability of raw mixtures, water absorption, color, texture, density, porosity, strength, and thermal conductivity) of the produced bricks are affected by the composition of the OSA. There is a continuous effect of the exothermic $CaO–H_2O$ reaction (forming $Ca(OH)_2$) being active as soon as raw materials are in contact with water and prolonged even after press molding which may cause slight expansion and higher porosity already before the firing stage. Further, release of bound water due to the decomposition of hydrates and decomposition of $Ca(OH)_2$, $CaCO_3$ and partially $CaSO_4$ lead to the creation of additional porosity during the firing process. In this respect, EPP-EPA and similar OSAs or carbonate rich wastes with high reactive free lime content can be considered as pore forming agent for clay bricks and applications require specific care to control the product performances.

From a technical point of view, the results obtained from accelerated carbonation of compacted APP-EPAs demonstrate that this type of compaction and carbonation process can be a promising way of waste utilization as it provides a way to produce valuable construction materials with high material strength while also binding CO_2. In this context, efforts and studies should proceed to further develop and optimize this process for OSA in order to improve the extent of the carbonation and produce specific building materials, for instance with good thermal and sound insulation characteristics.

To conclude, the results presented in this study indicate potentially interesting pathways for OSA utilization and all observations provide a basis of the future optimization of OS combustion and treatment processes in view of utilization of the generated ashes.

Author Contributions: Conceptualization, M.C.U., C.R.Y. and R.S.; data curation, P.P.; formal analysis, M.U.; investigation, T.H.; methodology, A.G.; resources, E.R.; validation, R.K. and A.T. All authors have read and agreed to the published version of the manuscript.

Funding: This work is partly supported by the CLEANKER project which has received funding from the European Union's Horizon 2020 Framework Program under Grant Agreement No. 764816 and from the China Government (National Natural Science Foundation of China) under contract No. 91434124 and No. 51376105. This study is also supported by the Estonian Ministry of Education and Research (IUT33-19), the European Regional Development Fund (RITA1/01-01-07), and Eesti Energia AS. Additionally, the activities related to clay bricks have received funding from EIT Raw Materials a body of the EU under Horizon 2020, under the grant name Flame: Fly ash to valuable minerals.

Conflicts of Interest: The authors declare no conflict of interest.

Abbreviations

OSA	Oil Shale Ash
CFB	Circulating fluidized bed
PF	Pulverized firing
EPA	Electrostatic precipitator ash
CA	Cyclone ash
TA	Total ash
FA	Fly ash
EPP	Estonian power plant
APP	Auvere power plant
EN280	Enefit 280 shale oil plant
PSD	Particle size distribution
SSA	Specific surface area
XRF	X-ray fluorescence
XRD	X-ray diffraction
TGA	Thermogravimetric analysis

Appendix A

Table A1. Particle size distribution of EPP and EN280 ashes (*d*50, *d*90, *d*10).

Name	Type	Date	*d*50	*d*90	*d*10
EPP	EPA	02.06.2018	37.3	74.2	10.1
EPP	EPA	05.15.2018	42.8	74.2	10.1
EPP	TA	02.06.2018	44.0	89.5	10.6
EN280	TA	02.09.2018	280.8	934.5	8.1
EN280	TA	07.12.2018	36.9	279.4	8.1
EN280	TA	10.30.2018	28.6	279.4	8.1
EN280	TA	03.19.2019	31.2	279.4	8.1
EN280	CA	07.12.2018	22.5	74.2	10.1
EN280	CA	10.30.2018	21.3	74.2	10.1
EN280	CA	03.19.2019	34.7	74.2	10.1

Table A2. Particle size distribution of APP ashes (*d*50, *d*90, *d*10).

Name	Type	Date	*d*50	*d*90	*d*10
APP	EPA	02.15.2018	21.9	57.1	7.7
APP	EPA	05.12.2018	23.1	42.3	7.1
APP	EPA	08.09.2018	23.0	44.2	8.9
APP	EPA	10.25.2018	22.0	45.3	8.4
APP	EPA	03.13.2019	23.2	75.3	7.7
APP	TA	02.21.2018	31.4	73.1	7.7
APP	TA	05.12.2018	32.9	51.2	7.1
APP	TA	07.10.2018	28.7	64.7	8.9
APP	TA	10.25.2018	34.2	65.2	7.7
APP	TA	03.13.2019	37.6	75.7	8.4

Appendix B

Table A3. Chemical composition of all oil shale ashes.

Component	SiO_2	Al_2O_3	TiO_2	Fe_2O_3	MnO	CaO	MgO	Na_2O	K_2O	P_2O_5	SO_3	LOI
Unit	mass%	mass%	mass%	mass%	mass%	mass%	mass%	mass%	mass%	mass%	mass%	mass%
APP TA 25.10.2018	20.5	4.8	0.2	2.9	0.1	42.4	3.8	0.1	2.5	0.2	5.2	15.0
APP EPA 25.10.2018	27.1	6.3	0.3	3.1	0.0	39.3	2.9	0.4	3.1	0.1	3.8	12.5
APP EPA 13.03.2018	22.0	5.2	0.2	3.6	0.1	39.1	7.2	0.3	2.2	0.1	6.7	11.2
APP TA 13.03.2018	22.3	5.2	0.2	3.2	0.1	40.3	5.5	0.1	2.5	0.1	6.5	12.2
APP EPA 09.08.2018	26.6	6.3	0.3	3.2	0.0	38.9	2.8	0.2	3.0	0.1	4.3	12.6
APP TA 12.05.2018	17.3	4.0	0.2	2.7	0.1	43.1	5.1	0.1	2.1	0.2	5.0	17.8
EPP EPA 06.02.2018	35.8	11.3	0.7	5.5	0.1	27.3	4.4	0.1	4.5	0.1	5.6	4.0
EPP TA 06.02.2018	30.8	9.6	0.6	5.2	0.1	32.2	4.9	0.1	3.7	0.1	5.6	6.5
EPP EPA 15.05.2018	33.2	7.8	0.4	4.0	0.1	30.0	4.9	0.2	3.5	0.1	4.8	8.3
EN280 TA 19.03.2019	6.7	1.4	0.1	1.8	0.0	48.1	3.2	0.1	0.6	0.1	4.1	34.5
EN280 CA 19.03.2019	29.9	7.0	0.3	3.7	0.0	29.0	3.4	0.1	3.5	0.1	4.5	17.3
EN280 TA 30.10.2018	5.2	1.2	0.1	1.4	0.1	49.0	3.3	0.1	0.4	0.1	2.3	37.7
EN280 CA 30.10.2018	28.3	6.7	0.3	3.6	0.1	29.2	3.6	0.2	3.3	0.1	4.7	18.0

References

1. Publications Office of the European Union. Best Available Techniques (Bat) Reference Document for Waste Treatment Industrial Emissions Directive 2010/75/Eu (Integrated Pollution Prevention and Control). Available online: https://op.europa.eu/en/publication-detail/-/publication/782f0042-d66f-11e8-9424-01aa75ed71a1/language-en (accessed on 10 May 2020).
2. National Development Plan of Estonia 2016–2030. Available online: https://www.envir.ee/sites/default/files/2016_2030ak_ingl.pdf (accessed on 10 May 2020).
3. Estonian Oil Shale Industry Yearbook 2018. Available online: https://www.ttu.ee/public/p/polevkivi-kompetentsikeskus/aastaraamat/Polevkivi_aastaraamat_2019_ENG_veeb.pdf (accessed on 11 May 2020).
4. Kuusik, R.; Uibu, M.; Kirsimäe, K. Characterization of oil shale ashes formed at industrial-scale boilers. *Oil Shale* **2005**, *22*, 407–420.
5. Blinova, I.; Bityukova, L.; Kasemets, K.; Ivask, A.; Kakinen, A.; Kurvet, I.; Bondarenko, O.; Kanarbik, L.; Sihtmäe, M.; Aruoja, V.; et al. Environmental Hazard of Oil Shale Combustion Fly Ash. *J. Hazard. Mat.* **2012**, *229–230*, 192–200. [CrossRef] [PubMed]
6. Kahru, A.; Polluma, L. Environmental Hazard of the Waste Streams of Estonian Oil Shale Industry: An Ecotoxicological Review. *Oil Shale* **2006**, *23*, 53–93.
7. Kuusik, R.; Uibu, M.; Kirsimäe, K.; Mõtlep, R.; Meriste, T. Open-air Deposition of Estonian Oil Shale Ash: Formation, State of Art, Problems and Prospects for the Abatement of Environmental Impact. *Oil Shale* **2012**, *29*, 376–403. [CrossRef]
8. Mohammad, M.S.; Rami, H.H. The Use of Oil Shale Ash in Portland Cement Concrete. *Cem. Concr. Compos.* **2003**, *25*, 43–50.
9. Gomes, H.I.; Mayes, W.M.; Rogerson, M.; Stewart, D.I.; Burke, I.T. Alkaline Residues and the Environment: A Review of Impacts, Management Practices and Opportunities. *J. Clean. Prod.* **2016**, *112*, 3571–3582. [CrossRef]
10. Hadi, N.A.R.A.; Abdelhadi, M. Characterization and Utilization of Oil Shale Ash Mixed with Granitic and Marble Wastes to Produce Lightweight Bricks. *Oil Shale* **2018**, *35*, 56–69. [CrossRef]
11. Gunning, P.J.; Hills, C.D.; Carey, P.J. Production of Lightweight Aggregate from Industrial Waste and Carbon Dioxide. *Waste Manag.* **2009**, *29*, 2722–2728. [CrossRef]
12. Quaghebeur, M.; Nielsen, P.; Horckmans, L.; Van Mechelen, D. Accelerated Carbonation of Steel Slag Compacts: Development of High-Strength Construction Materials. *Front. Energy Res.* **2015**, *3*, 52. [CrossRef]
13. Nielsen, P.; Boone, M.A.; Horckmans, L.; Snellings, R.; Quaghebeur, M. Accelerated Carbonation of Steel Slag Monoliths at Low CO_2 Pressure–Microstructure and Strength Development. *J. CO2 Utiliz.* **2020**, *36*, 124–134. [CrossRef]
14. Raado, L.; Kuusik, R.; Hain, T.; Uibu, M.; Somelar, P. Oil Shale Ash Based Stone Formation—Hydration, Hardening Dynamics And Phase Transformations. *Oil Shale* **2014**, *31*, 91. [CrossRef]
15. EESTI Standard. Methods of Testing Cement—Part 1: Determination of Strength. Available online: https://www.evs.ee/preview/evs-en-196-1-2016-en.pdf (accessed on 12 May 2020).
16. EESTI Standard. Metallic Materials—Calibration and Verification of Static Uniaxial Testing Machines—Part 1:Tension/Compression Testing Machines—Calibration and Verification of the Force-Measuring System. Available online: https://www.evs.ee/tooted/evs-en-iso-7500-1-2018 (accessed on 12 May 2020).
17. ISO 679:2009. Cement-Test Methods-Determination of Strength. Available online: https://www.iso.org/standard/45568.html (accessed on 12 May 2020).
18. EESTI Standard. Specification for Masonry Units—Part 1: Clay Masonry Units. Available online: https://www.evs.ee/en/evs-en-771-1-2011%2Ba1-2015 (accessed on 12 May 2020).
19. International Standard. Transient Plane Heat Source (Hot Disc) Method. Available online: https://www.evs.ee/products/iso-22007-2-2015 (accessed on 12 May 2020).
20. Dhir, R.K.; Munday, J.G.L.; Ong, L.T. Strength variability of OPC/PFA concrete. *Concrete* **1981**, *15*, 33–37.
21. Das, S.K.; Yudhbir. A Simplified Model for Prediction of Pozzolanic Characteristics of Fly Ash, Based on Chemical Composition. *Cement Concr. Res.* **2006**, *36*, 1827–1832. [CrossRef]
22. Pihu, T.; Konist, A.; Puura, E.; Liira, M.; Kirsimäe, K. Properties and Environmental Impact of Oil Shale Ash Landfills. *Oil Shale* **2019**, *36*, 257. [CrossRef]

23. Pihu, T.; Arro, H.; Prikk, A.; Rootamm, R.; Konist, A.; Kirsimäe, K.; Mõtlep, R. Oil shale CFBC ash cementation properties in ash fields. *Fuel* **2012**, *93*, 172–180. [CrossRef]
24. Raado, L.; Hain, T.; Liisma, E.; Kuusik, R. Composition and Properties of Oil Shale Ash Concrete. *Oil Shale* **2014**, *31*, 147. [CrossRef]
25. Yörük, C.R.; Meriste, T.; Trikkel, A.; Kuusik, R. Thermo-Oxidation Characteristics of Oil Shale and Oil Shale Char Under Oxy-Fuel Combustion Conditions. *J. Therm. Anal. Calorim.* **2015**, *121*, 509–516. [CrossRef]
26. Ferrer, S.; Mezquita, A.; Gomez-Tena, M.P.; Machi, C.; Monfort, E. Estimation of The Heat of Reaction In Traditional Ceramic Compositions. *Appl. Clay Sci.* **2015**, *108*, 28–39. [CrossRef]
27. Kubiś, M.; Pietrak, K.; Cieślikiewicz, L.; Furmański, P.; Wasik, M.; Seredyński, M.; Wiśniewski, T.S.; Łapka, P. On the Anisotropy of Thermal Conductivity in Ceramic Bricks. *J. Build. Eng.* **2020**, *31*, 101418. [CrossRef]
28. Junge, K. Additives in the Brick and Tile Industry. *Ziegelind. Int.* **2000**, *53*, 25–39.
29. Sütcü, M.; Akkurt, S. The Use of Recycled Paper Processing Residues in Making Porous Brick with Reduced Thermal Conductivity. *Ceram. Int.* **2009**, *35*, 2625–2631. [CrossRef]
30. Fernandezbertos, M.; Simons, S.; Hills, C.; Carey, P. A Review of Accelerated Carbonation Technology in the Treatment of Cement-Based Materials and Sequestration of CO_2. *J. Hazard. Mat.* **2004**, *112*, 193–205. [CrossRef] [PubMed]

Appendix 2

Publication II

Usta, M. C., Yörük, C. R., Uibu, M., Hain, T., Gregor, A., & Trikkel, A. (2022). CO2 Curing of Ca-Rich Fly Ashes to Produce Cement-Free Building Materials. *Minerals*, *12*(5), 513. https://doi.org/10.3390/min12050513

minerals

MDPI

Article

CO_2 Curing of Ca-Rich Fly Ashes to Produce Cement-Free Building Materials

Mustafa Cem Usta [1,*], Can Rüstü Yörük [1], Mai Uibu [1], Tiina Hain [2], Andre Gregor [1] and Andres Trikkel [1]

[1] Department of Materials and Environmental Technology, Tallinn University of Technology, 19086 Tallinn, Estonia; can.yoruk@taltech.ee (C.R.Y.); mai.uibu@taltech.ee (M.U.); andre.gregor@ttu.ee (A.G.); andres.trikkel@taltech.ee (A.T.)

[2] Department of Civil Engineering and Architecture, Tallinn University of Technology, 19086 Tallinn, Estonia; tiina.hain@ttu.ee

* Correspondence: mustafa.usta@taltech.ee

Abstract: In this study, fly ash (FA) compacts were prepared by accelerated carbonation as a potential sustainable building material application with the locally available ashes (oil shale ash (OSA), wood ash (WA) and land filled oil shale ash (LFA)) of Estonia. The carbonation behaviour of FAs and the performance of 100% FA based compacts were evaluated based on the obtained values of CO_2 uptake and compressive strength. The influence of different variables (compaction pressure, curing temperature, CO_2 concentration, and pressure) on the CO_2 uptake and strength development of FA compacts were investigated and the reaction kinetics of the carbonation process were tested by different reaction-order models. A reasonable relation was noted between the CO_2 uptake and compressive strength of the compacts. The porous surface structure of the hydrated OSA and WA compacts was changed after carbonation due to the calcite formations (being the primary carbonation product), especially on portlandite crystals. The increase of temperature, gas pressure, and CO_2 concentration improved the CO_2 uptake levels of compacts. However, the positive effect of increasing compaction pressure was more apparent on the final strength of the compacts. The obtained compressive strength and CO_2 uptake values of FA compacts were between 10 and 36 MPa and 11 and 13 wt%, respectively, under various operation conditions. Moreover, compacts with mixed design (OSA/LFA and WA/LFA) resulted in low-strength and density compared to the single behaviour of OSA and WA compacts, yet a higher CO_2 uptake was achieved (approximately 15% mass) with mixed design. The conformity of Jander equation (3D-diffusion-limited reaction model) was higher compared to other tested reaction order models for the representation of the carbonation reaction mechanism of OSA and WA. The activation energy for OSA compact was calculated as 3.55 kJ/mol and for WA as 17.06 kJ/mol.

Keywords: fly ash utilization; accelerated carbonation; building materials

Citation: Usta, M.C.; Yörük, C.R.; Uibu, M.; Hain, T.; Gregor, A.; Trikkel, A. CO_2 Curing of Ca-Rich Fly Ashes to Produce Cement-Free Building Materials. *Minerals* **2022**, *12*, 513. https://doi.org/10.3390/min12050513

Academic Editors: Carlos Hoffmann Sampaio, Weslei Monteiro Ambros and Bogdan Grigore Cazacliu

Received: 22 March 2022
Accepted: 18 April 2022
Published: 21 April 2022

1. Introduction

Since the manufacture of cement, CO_2 emissions of the cement industry have been on a large scale and the direct CO_2 intensity of cement production increased 1.8% annually during 2015–2020 [1,2]. Cement production is estimated to increase even more, and thus reducing CO_2 emissions while producing enough cement to meet demand will be challenging until 2030 due to EU restrictions [1,2]. Carbon capture and storage at cement production plants could be a solution to this problem, yet there is no commercially available full-scale application until today [3,4]. Researchers throughout the world have been searching for alternatives to cement among waste materials to cut cement dependency and lower the related CO_2 emissions [3,5]. Primarily, fly ash (FA), which is generally disposed of in landfills, has always been an alternative to cement, as it is considered a supplementary cementitious material which provides one of the most feasible routes for concrete production with reduced CO_2 emissions [6].

The suitability of FA depends on the chemical and mineralogical composition such as the content of siliceous or siliceous-and-aluminous material, lime, portlandite, and its physical properties [7]. Although FA has several advantages on concrete properties, there are still several drawbacks that limit the applications on a big scale due to the reduction of mechanical properties of the concrete and its durability. As FA amounts increase in concrete, the mechanical properties of the concrete decrease, which means that remarkable replacement ratios are infeasible in today's construction applications [6–8].

With the increase of environmental consciousness, the building sector is evolving with the integration of circular economy concepts for better waste utilization and zero carbon emissions. Mineral carbonation is at the forefront due to recent progress when it comes to the utilization of both industrial alkaline waste materials and CO_2 gas without using traditional binders towards sustainable construction materials [9–13]. Considering the vast amount of ashes generated from both fossil and renewable fuels, and for the applications of non-traditional construction materials, the usage of FAs via carbonation activation could be a promising alternative for producing cement-free building materials.

Calcium (Ca) and magnesium (Mg) are considered as two of the most dominant and reactive (with respect to CO_2) alkaline earth metals found in industrial residues [14–16]. Based on the chemical composition of the ashes, Ca and Mg-rich FAs are found to be potential candidate materials for CO_2 mineralization due to their high alkalinity. The average CO_2 uptake level of most of the alkaline solid wastes including ashes can also be directly connected to the contents of Ca and Mg [12,15,17].

In Estonia, Ca-rich ashes; oil shale ash (OSA), and wood ash (WA) are widely produced, constituting more than 70% of the total residues generated by power plants. As a result of the past industrial processes involving oil shale (OS) combustion and retorting (approximately 100 years) and due to the limited ash utilization applications, there are more than 300 million tonnes of land filled OS ash (LFA) in plateau-like waste depositories [18,19]. The ash problem and CO_2 emissions, which are elevated by high carbonate content in OS, are key issues undermining the long-term sustainability of the energy sector of Estonia. Therefore, valorisation of the ashes in environmentally sound applications is of clear strategic interest to the country. The utilization of local alkaline waste streams together with CO_2 via mineral carbonation can contribute to the circular economy and sustainable development.

In an early investigation on typical residues from the OS industry of Estonia, a mineral carbonation approach was studied for the first-time to evaluate the suitability and reactivity of available OSAs. The preliminary findings on CO_2 uptake (up to 9%) were promising, reflecting on the improved strength (20–40 MPa) as a result of mainly the carbonation of $Ca(OH)_2$ forming $CaCO_3$ crystals [20]. With respect to this positive outcome, principally OSA, WA, and LFA could be useful waste materials for both capture and permanent sequestration of CO_2 through the formation of $CaCO_3$, as these waste streams contain high amounts of calcium mainly due to the presence of free lime and portlandite.

It is also known that the formation of the $CaCO_3$ phase has a positive effect on construction materials because of the increased density through a filling effect, which improves the microstructure, lowers the permeability, and improves strength [21,22]. This behaviour of strength development has been studied with different waste materials including steel slag, blast furnace slag, construction demolition waste, municipal solid waste, coal combustion FA, and ashes from wood and peat combustion under controlled process conditions [21–26]. In most of these studies, carbonation tests of compacted or granulated pellets, blocks, etc., were carried out both in a CO_2 rich and lean atmosphere for modelling flue gas (FG) curing as well. It has been shown that there is a direct relation with the CO_2 uptake level and the strength gain in compacts. Since carbonation is a dynamic process involving transport of CO_2 through a compact body and dissolution of Ca, studies have shown that the extent of carbonation reactions are influenced by various parameters (reaction time, curing temperature and pressure, relative humidity (RH), CO_2 concentration, physical properties of residues etc.) [12,16,22]. However, both an excess and a scarcity of the above-mentioned

parameters can result in negative effects for the entire process relating to CO_2 uptake and strengthening of the compacts.

Additionally, the achievement of the most effective CO_2 curing process and improvement in mechanical properties of compacts are highly dependent on the chemical composition and mineralogy of industrial residues [17]. It is important to bear in mind that these operation parameters must be optimized for each waste, as well as the relevant process stages for homogeneous carbonation and to lower the operational energy costs. Therefore, there is a necessity to address a research study focusing on the utilization of Ca-rich FAs in an Estonian context (OSA, WA, LFA) to gain in-depth understanding of the impacts of operation conditions during CO_2 curing to produce cement-free building materials.

The main aim of the study is to evaluate and characterize the carbonation behaviour of selected ashes based on the obtained values of CO_2 uptake and compressive strength while providing a comparative crosscheck on the rate of carbonation and mechanical performance of compacts. This study undertakes parametric investigations to understand the effects of compaction pressure, curing temperature, CO_2 concentration, and pressure on the carbonation extent and related strength development of the compacts. The reaction kinetics of the carbonation process were also tested by different reaction-order models in order to identify the carbonation reaction behaviour of Ca-rich FAs. Furthermore, the preliminary tests with LFA and impacts of mixing LFA with OSA and WA are presented for future perspectives of potential sustainable building material applications with local available ashes.

2. Materials and Methods

2.1. Materials

Three different types of ash samples were selected from Estonia (OSA, WA, and LFA). OSA was obtained from *Auvere Power Plant* [27], which is operated by the direct combustion of OS in CFB boiler for power production, and ash was collected from the electrostatic precipitators. WA was obtained from *Utilitas District Heating Plant* [28] which is operated by forestry wood (a mix of pine chips and bark residues) and ash was collected from bag filters located in the post-combustion zones of the grate combustor. The LFA samples were taken from a drill core made on the rim of the ash disposal site at *Eesti Power Plant* [29], north-eastern Estonia (Figure 1). The selected LFA is the ash taken from the depths of 32.4–32.6 m, where mainly burnt OS FA residues exist from electricity production without including shale oil processing residues.

Figure 1. Drill core from ash disposal site at the Eesti Power Plant, north-eastern Estonia.

2.2. Characterization of Materials (Initial and Compacts)

All samples were obtained in fine fractions, which did not require pre-treatment (drying, milling, or grinding etc.) except the LFA samples, which were milled by Tartu University. Mean samples were taken from each collected ashes, and a size fraction below 200 µm (by sieving) was used for material characterization and further sample preparation. The physical characterization of the selected waste streams included particle size distribution (PSD) measurements. Horiba Laser Scattering instrument (LA-950) (Kyoto,

Japan) was used for PSD measurement (with ethanol suspension). The BET-N_2 sorption method was used to measure the specific surface area (SSA) with Kelvin 1042 sorptiometer (Tallinn, Estonia). The chemical and mineralogical characterization of the selected waste streams included X-ray fluorescence (XRF) and X-ray diffraction (XRD) analyses with Bruker S4 Pioneer (Karlsruhe, Baden-Württemberg, Germany) and Bruker D8 (Karlsruhe, Baden-Württemberg, Germany) diffractometers, respectively, using Cu Kα radiation with a Göbel mirror monochromator and LynxEye positive sensitive detector over a 2°–70° 2θ range. The thermogravimetric (TGA) and mass spectrometric (MS) analysis were also carried out to obtain thermal characterization of both carbonated and un-carbonated compacted samples (mainly for the calculation of CO_2 uptake) by using the Setaram Labsys 2000 thermoanalyzer (Geneva, Switzerland) (10 K/min, sample mass: 20 ± 1 mg, 21% O_2/79% Ar) with alumina (Al_2O_3) crucible. The SEM images of carbonated compacts were obtained from the polished samples using a ZEISS Evo MA 15 (Oberkochen, Baden-Württemberg, Germany) for the investigation of the microstructure. The mineralogical composition was determined using XRD analysis to compare mineralogical changes after carbonation curing. The compressive strength measurements were performed with Toni TechnikD-13355 (Berlin, Brandenburg, Germany). The measurements of pH were conducted according to EN 12457-2 on compacts. Tube test duration was 24 h with distilled water, 1/10 solid/liquid ratio, 32 rpm rotation speed, and 0–4 mm grain size particles were used. SevenGo Duo pH/Cond meter SG23 (Greifensee, Switzerland) was used for the pH measurements.

2.2.1. Physical Characterization

OSA, WA, and LFA samples have BET SSA of 5.8 m^2/g, 11.9 m^2/g, and 20.6 m^2/g respectively, which can indicate higher carbonation ability for LFA compared to other ashes, since the carbonation reaction is promoted by the presence of a higher number of sites available in the initial material [30] (see Figure 2). Although the SSA of LFA and WA was higher than OSA, due to the phases formed during natural hydration and biomaterial nature of WA respectively, it was revealed that the median particle diameter is 79.2 μm for LFA, 54.6 μm for WA, and 23.4 μm for OSA.

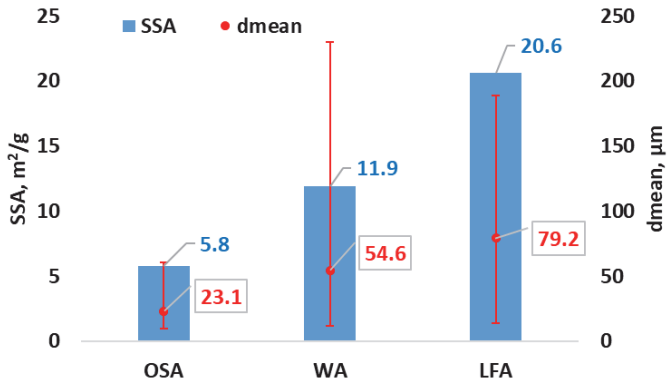

Figure 2. Average particle diameter (d_{mean}) and specific surface areas (SSA) of OSA, WA, and LFA samples.

2.2.2. Chemical Characterization

According to XRF analysis, all three types of samples were composed of mainly Ca and Si, adding up to 59–64% (see Table 1). The XRD analysis showed that OSA and WA contain a considerable amount of free lime (17–20%) with a small amount of portlandite (1.4–3%), which are supposed to be the main phases to react with CO_2 (see Table 2). Dicalcium silicate, 'C_2S', which is an important well-known component of clinker in cement industry, constitutes 13.9% of OSA and 4.1% of WA. Differently in LFA, hydration of CaO under

natural water produced $Ca(OH)_2$, which constitutes 18% of the phases. Similarly, dicalcium silicates in LFA are also hydrated and formed CSH (Calcium silicate hydrate), which is composed of 45% of the phase composition due to atmospheric water reacting with the constituents of the ash in the disposal area.

Table 1. Chemical composition of OSA, WA, and LFA.

Component	OSA1	WA	LFA
SiO_2	29.38	18.08	17.38
Al_2O_3	9.58	2.73	4.13
TiO_2	0.578	0.19	0.21
Fe_2O_3	5.12	1.17	2.43
MnO	0.067	0.32	0.03
CaO	34.67	44.44	42.21
MgO	3.12	2.82	3.75
Na_2O	0.12	0.52	0.10
K_2O	3.91	7.69	0.81
P_2O_5	0.128	4.14	0.13
SO_3	4.96	4.35	4.97
L.O.I.	7.73	12.79	22.90

Table 2. Phase composition of OSA, WA, and LFA.

Component	OSA (%)	WA (%)	LFA (%)
Quartz	15	7.5	5
K-feldspar	14.2	3.2	3
Plagioclase	0.7	0	0
Mica	3.6	0	0
Calcite	9.8	27.7	3
Lime	17	20.3	0
Portlandite	1.4	3	18
Periclase	4.2	2.9	2
Anhydrite	9.3	0	0
C_2S	13.9	4.1	3
Merwinite	3.2	4.3	2
Akermanite	4.5	3.8	5
Sylvite	0	1.7	0
Arcanite	0	8.6	0
Hematite	2.3	0	0
Apatite	0	12.6	0
CSH (tobermerite)	0	0	45
Gypsum	0	0	2
Ettringite	0	0	2

Cement powders require the presence of C_2S in the clinkers for strength development in concrete. These materials react vigorously with water to produce the cement paste formed in the final product. Within the building industry, the term "pozzolan" covers all the materials that react with lime and water, producing calcium silicate and aluminate hydrates. All pozzolans must be rich in reactive silica or alumina plus silica [31]. SiO_2, Al_2O_3, and Fe_2O_3 constitute 22–45% of the samples of which are described as main constituents of pozzolans. An internal sulphate attack is a deterioration mechanism of concrete. High percentages of SO_3 in the cement increase the risk of delayed ettringite formation, which can lead to significant deterioration of the concrete structure [32]. ASTM C618 (Standard specification for coal FA use in concrete) limits the sulphate content of fly ash to 5% SO_3 when the material is to be used in concrete [33].

2.3. Sample Preparation and Carbonation Apparatus

OSA and WA were selected as the two main samples for planned experiments within this study. LFA was included only for preliminary evaluation and for its capabilities as a potential mix design with OSA and WA at a ratio of 50/50.

In the first step, the hydrated OSA and WA samples have been prepared with a liquid to solid ratio of 0.25 w/v and LFA has been prepared with the liquid to solid ratio of 0.15 w/v (to ensure $10 \pm 1\%$ moisture content for all samples before curing). The moisture content has been measured using MB23 moisture analyser. The semi-batch Eirich EL1 type intensive mixer was used for mixing. The samples were homogeneously mixed with water at the fixed rotation speed (600 rpm) and time (20 min). Later, the samples were left to hydrate/cure in sealed and vacuumed containers at room temperature and were compacted on the following day using a hydraulic press into cylinders with diameter 20 ± 1 mm and height 20 ± 1 mm (Figure 3). Each batch of samples included minimum four cylindrical compacts and their average strength values are given in the results for each tested parameter.

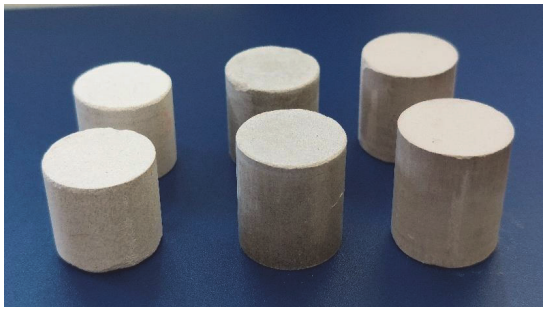

Figure 3. Prepared cylindrical compacts of LFA (**left**), WA (**middle**), and OSA (**right**).

The physically bound water (moisture content) after overnight hydration (24 h) was measured to be $10 \pm 1\%$ for all samples before compaction, which was found to be a critical parameter for optimum compaction (without having any cracks due to dryness or erosion on the surfaces due to excessive water) based on previous experiences [20]. As press moulding of compacts was carried out with manual hand operated hydraulic press, serious attention has been given to the uniform preparation of samples. Two different compaction pressures (150 ± 10 and 300 ± 10 kgf/cm^2) were applied to investigate the effect of compaction pressure. Carbonation experiments were performed in an automated carbonation unit (Figure 4) (stainless-steel 400 mL jacketed pressure vessel), consisting of apparatus controlling temperature (Circulator C-400) and monitoring CO_2 gas consumption (Buchi pressflow gas controller (bpc)).

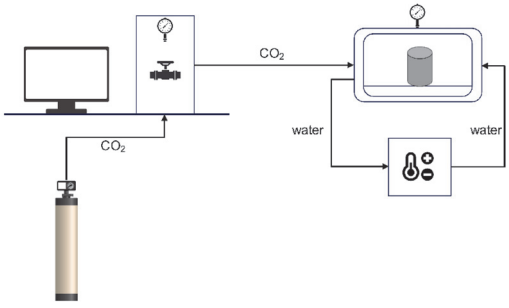

Figure 4. Scheme of the carbonation unit (including CO_2 gas cylinder, computer, pressure vessel).

Different sets of experimental conditions were applied, and parallel comparative tests were carried out to investigate the effects of different curing temperatures (25, 50, 75 °C), curing with typical flue gas CO_2 concentration (15% CO_2/6% O_2/N_2) compared to 100% CO_2, and different gas pressures (5, 10, and 15 bar) (see Table 3). To maintain stable CO_2 concentration during FG curing, the flushing and refilling steps were followed every 20 min. Furthermore, all tests were performed with the strategy of controlling the humidity using the potassium iodide saturated solution, which inhibits excessive humid conditions and maintains a RH between (61–68%) at different curing temperatures [34]. Density measurements were done with solid compacted cylinders.

Table 3. Experimental parameters to produce carbonated compacts.

Test Parameters		Curing CO_2%	Curing Gas Pressure	Curing Temperature	Compaction Pressure	Curing RH	Curing Time
Compaction pressure	150 kgf/cm^2 300 kgf/cm^2	100% CO_2	10 bar	25 °C	- -	61–68%	2 h
Gas Pressure	5 bar 10 bar 15 bar	100% CO_2	-	25 °C	150 kgf/cm^2		
CO_2%	100% CO_2 16% CO_2	-	10 bar	25 °C	150 kgf/cm^2		
Temperature	25 °C 50 °C 75 °C	100% CO_2	10 bar	-	150 kgf/cm^2		

3. Results

3.1. Variables Affecting CO_2 Uptake and Compressive Strength

3.1.1. Compaction Pressure and Mix Design

The forming compaction pressure of the FA in powder form prior to carbonation influences the physical properties of the compacted bodies and the mechanical properties of the resultant compacts. The porosity and permeability of the solid decrease when the compaction pressure is increased [35], which leads to a stronger structure and greater strength due to eliminated internal surface areas. Conversely, the lower gas permeability inhibits the penetration of the CO_2 passing through the inner surfaces of the compacted bodies. Thus, the efficiency of the accelerated carbonation process can be affected negatively due to the physical limitations of CO_2 permeability, diffusivity, and solubility, resulting in a lower amount of crystallized $CaCO_3$ formations and lower strength development. According to the obtained strength values of OSA, WA, and LFA there is a somewhat similar phenomenon as mentioned above. The results of compressive strength and CO_2 uptake of OSA, WA, and LFA together with mixed design compacts are presented in Figures 5 and 6.

The potential negative impact of increased compaction pressure on the CO_2 uptake of OSA compacts is negligible at the applied compaction pressure ranges. However, there are slight decreases on the CO_2 uptake level of WA and LFA compacts (Figure 5). The CO_2 uptake level of LFA with compaction pressure of 150 kg/cm^2 is 14.7% while samples with 300 kg/cm^2 compaction pressure is 11.9%, being the highest compared to the other ashes.

It is observed that a higher pressure of compaction (from 150 kg/cm^2 to 300 kg/cm^2) leads to higher compressive strength in all prepared samples. The increase in compaction pressure results in an average compressive strength increase of 63% in OSA compacts, 71% in WA compacts, and 25% in LFA compacts (Figure 6). Compressive strength values of LFA compacts are 7.8 and 10.8 MPa for a compaction pressure of 150 and 300 kg/cm^2 showing the lowest values compared to other ashes. This is mainly due to LFA being composed of already formed CSH before compaction, which can reduce the compressive strength development.

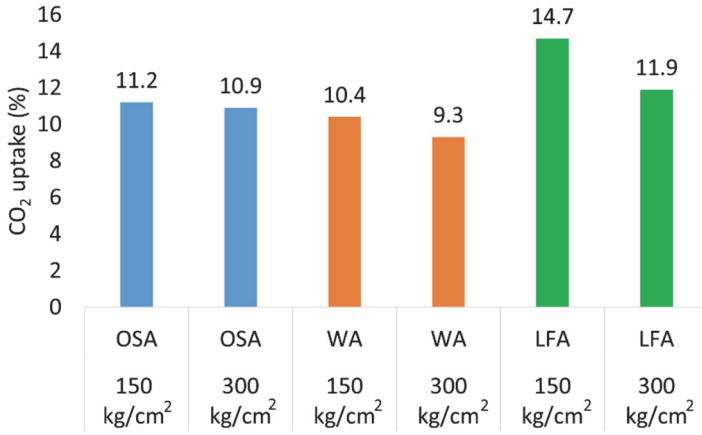

Figure 5. CO_2 uptake values at different compaction pressures for OSA, WA, and LFA (10 bar, 100% CO_2, 25 °C) (Average values obtained from min. 4 samples (std. deviation < 3%)).

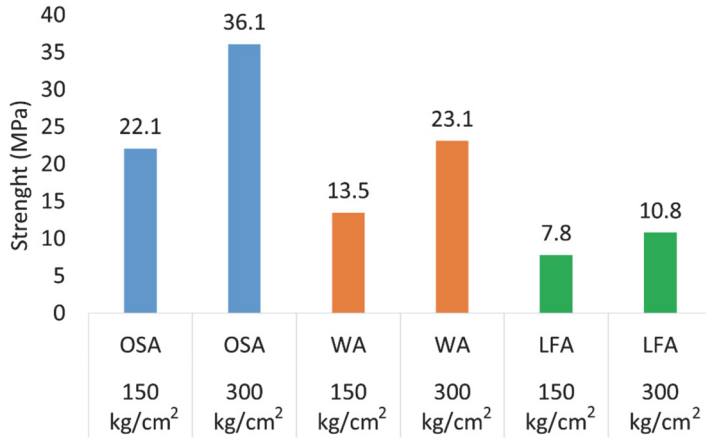

Figure 6. Compressive strength values at different compaction pressures for OSA, WA and LFA (10 bar, 100% CO_2, 25 °C) (Average values obtained from min. 4 samples (std. deviation < 2%)).

Two different types of mixed compacts were also designed; one containing 50% OSA/50% LFA (denoted by M1) and the other containing 50% WA/50% LFA (denoted by M2) (Figure 7). M1 compacts have an average compressive strength of 9.2 MPa while having a CO_2 uptake level of 13.1%. This indicates that LFA is slightly increasing the CO_2 uptake while reducing the compressive strength of the samples compared to 100% OSA compacts. M2 compacts have an average compressive strength of 10.4 MPa and CO_2 uptake level of 12.3%. A similar trend is observed with the strength and CO_2 uptake values of M2 compacts compared to 100% WA compacts. Both types of mixed designs exhibit more or less similar compressive strength and CO_2 uptake levels. LFA compacts exhibited overall lower density (1340 kg/m^3) compared to OSA (1595 kg/m^3) and WA (1830 kg/m^3) compacts. Higher compaction pressure of 300 kg/cm^2 increased the density to 1470 kg/m^3, which may show the potential usage of LFA for low density building material applications. Mixed designs demonstrate a median density based on the constituents. The M1 have an average density of 1380 kg/m^3 and the M2 compacts have and average density of 1420 kg/m^3 (see Table 4).

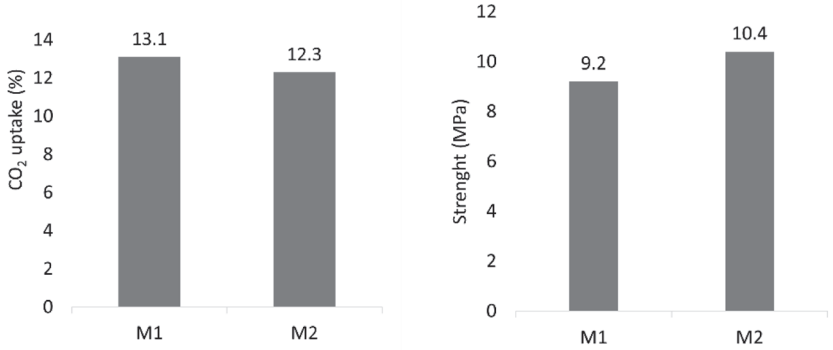

Figure 7. CO_2 uptake and compressive strength values of mixed design compacts (150 kgf/cm^2, 10 bar, 100% CO_2, 25 °C) (Average values obtained from min. 4 samples (std. deviation < 4%)).

Table 4. Density results of compacts (kg/m^3).

	OSA	WA	LFA	M1	M2
150 kg/cm^2	1595	1830	1340	1380	1420
300 kg/cm^2	1720	1970	1470	1560	1690

3.1.2. Gas Pressure and CO_2 Concentration

CO_2 partial pressure and CO_2 concentration are factors affecting the rate of CO_2 uptake due to their effect on physisorption process at the interface between the solid and the gas reactant where the formation and growth of a solid product layer of $CaCO_3$ occurs [36]. The influence of the CO_2 gas pressure and CO_2 concentration was examined by evaluating CO_2 uptake levels and compressive strength of OSA and WA compacts. With the increase of gas pressures from 5 to 15 bar, the final CO_2 uptake levels as well as compressive strength increases in both the OSA and WA compacts. This could be explained with the improved gas penetration of CO_2 into the compact under high pressures, which favours the extent of carbonation reaction. At 5 bar, the CO_2 uptake percentage for OSA is 10.7% and for WA it is 8.2%. At 15 bar, the CO_2 uptake values are improved to 12.2% for OSA and 10.2% for WA (Figure 8). At 5 bar, the compressive strength value for OSA is 21.5 MPa and for WA it is 10.1 MPa. At 15 bar, the compressive strength values are increased to 34.5 MPa for OSA and 16.7 MPa for WA (Figure 9). For both samples, linear increasing dependency is observed at similar rates for CO_2 uptake and compressive strength measurements under increasing curing pressures (cured for 2 h).

It is also known that the CO_2 gas penetration into cementitious materials under high and low CO_2 concentration levels would be different, which affects the total CO_2 uptake levels. [37]. The CO_2 uptake value for OSA is 10.8% and for WA it is 9.4% at the curing with 100% CO_2 concentration. The CO_2 uptake values are decreased to 7.6% for OSA and 7.9% for WA (Figure 10) at the curing with FG (16% CO_2). The compressive strength of samples cured in 100% CO_2 are higher than the samples cured in FG, which is in line with less CO_2 uptakes. Due to the higher content of Ca-Mg silicates, which participate in hydraulic or pozzolanic reactions in OSA compacts, the compressive strength values were higher than WA compacts. At longer curing periods, CO_2 uptake values of FG curing can reach the same level as 100% CO_2 curing.

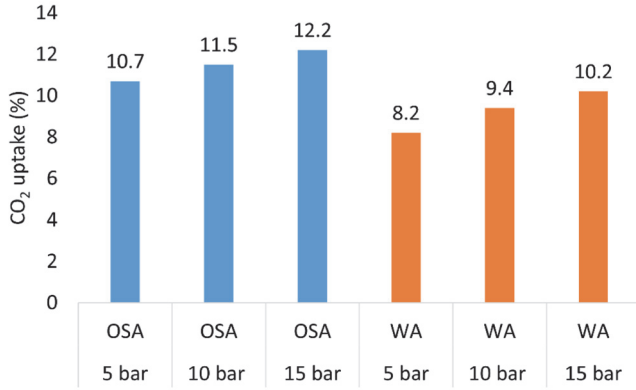

Figure 8. CO_2 uptake values at different curing pressures (100% CO_2, 25 °C, 150 kg/cm^2) (Average values obtained from min. 4 samples (std. deviation < 3%)).

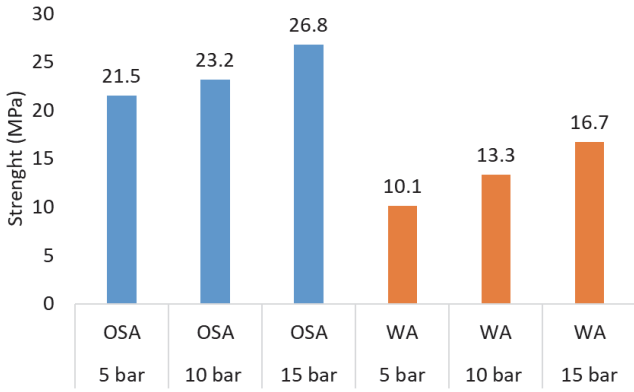

Figure 9. Compressive strength values at different curing pressures (100% CO_2, 25 °C, 150 kg/cm^2) (Average values obtained from min. 4 samples (std. deviation < 3%)).

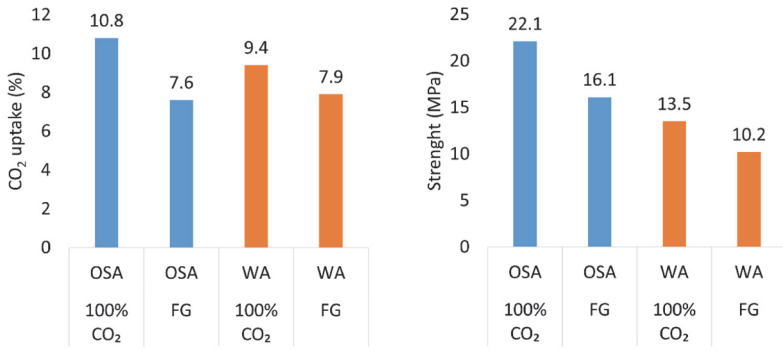

Figure 10. CO_2 uptake (**left**) and compressive strength (**right**) values at different CO_2 concentrations (10 bar, 25 °C, 150 kgf/cm^2) (Average values obtained from min. 4 samples (std. deviation < 3%)).

3.1.3. Temperature

It is noted in previous studies that the temperature during carbonation influences the dissolution rate of constituents, the solubility of CO_2 and the morphology and mineralogy of the carbonates [23]. An increase in process temperature simultaneously increases the

rates of all the chemical processes but reduces the CO_2-solubility in water and thus CO_2-availability [38]. The influence of temperature was examined by evaluating CO_2 uptake levels (Figure 11) and compressive strength (Figure 12). In both samples, the CO_2 uptake levels are elevated at higher temperatures; however, the same is not true for strength development. This indicates that a higher CO_2 uptake does not always validate higher strength development. A higher carbonation degree at high temperature can cause the double-chain silicate anion structure of CSH to decompose and consequently slow the compressive strength gain [39]. It is known that with increased carbonation, the micro-mechanical property of CSH is weakened [40]. For OSA, the highest compressive strength value (24.8 MPa) is attained at 50 °C. For WA, the highest compressive strength (14.7 MPa) is attained at 25 °C. For both samples, the lowest strength value is attained at the highest temperature. Reduction in compressive strength at higher temperatures in both samples can also be explained by the initial fast CO_2 uptake, causing weaker carbonate crystals in compacts. The temperature effect on the stability of carbonates is further discussed in the thermal analysis section.

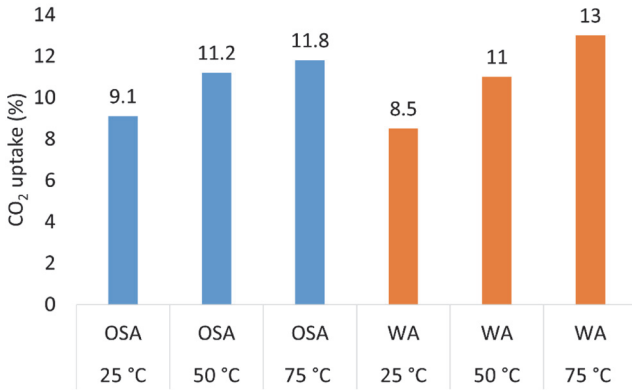

Figure 11. CO_2 uptake values at different temperatures (10 bar, 100% CO_2, 150 kgf/cm^2) (Average values obtained from min. 4 samples (std. deviation < 3%)).

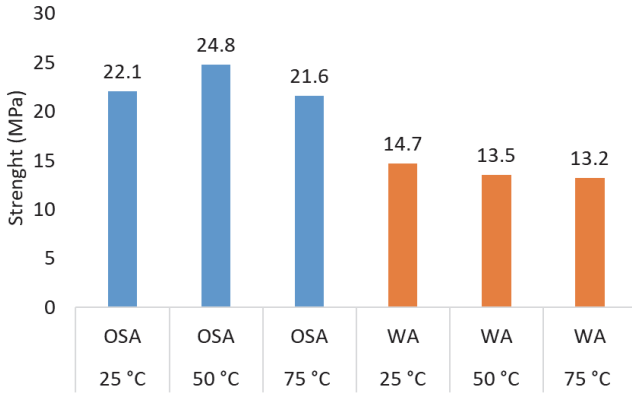

Figure 12. Compressive strength values at different temperatures (10 bar, 100% CO_2, 150 kgf/cm^2) (Average values obtained from min. 4 samples (std. deviation < 3%)).

3.2. Thermal Analysis

Based on the TGA/DTG curves of uncarbonated samples, there are three major mass loss steps which occur: First, related to water loss due to evaporation and later dehydration of crystalline and amorphous components i.e., ettringite (up to 200 °C); second, dehydration

of $Ca(OH)_2$ (up to 500 °C) (Equation (1)); and third, CO_2 loss due to decomposition of $CaCO_3$ (between 550–900 °C) (Equation (2)) (Figures 13 and 14).

$$Ca(OH)_2 \leftrightarrow CaO_{(s)} + H_2O_{(g)}\ \Delta H_{298K} = -104\ kJ/mol, \quad (1)$$

$$CaCO_{3(s)} \leftrightarrow CaO_{(s)} + CO_{2(g)}\ \Delta H_{298K} = +178\ kJ/mol. \quad (2)$$

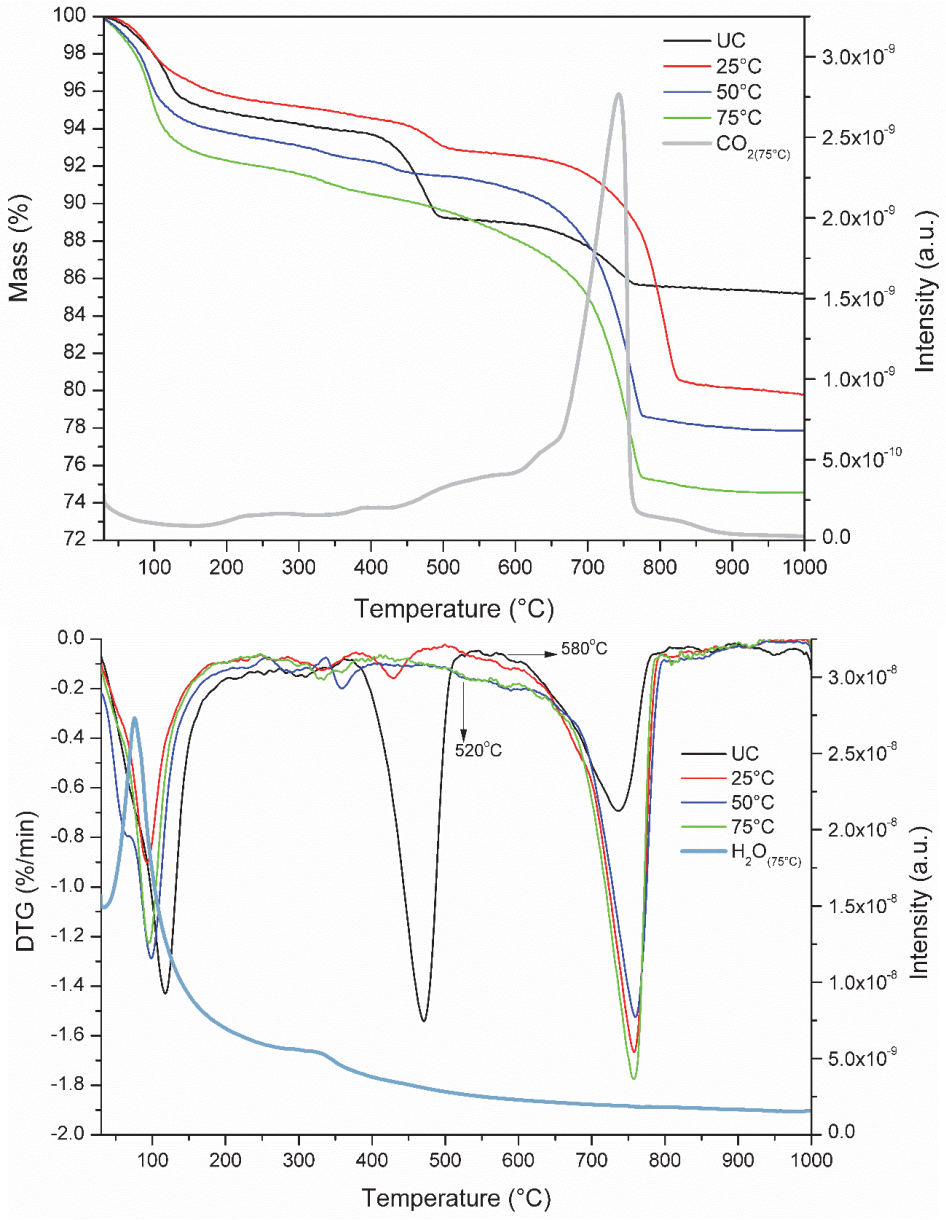

Figure 13. TGA and DTG with MS (75 °C) of OSA compacts that are uncarbonated (UC) and cured at 25 °C, 50 °C, and 75 °C.

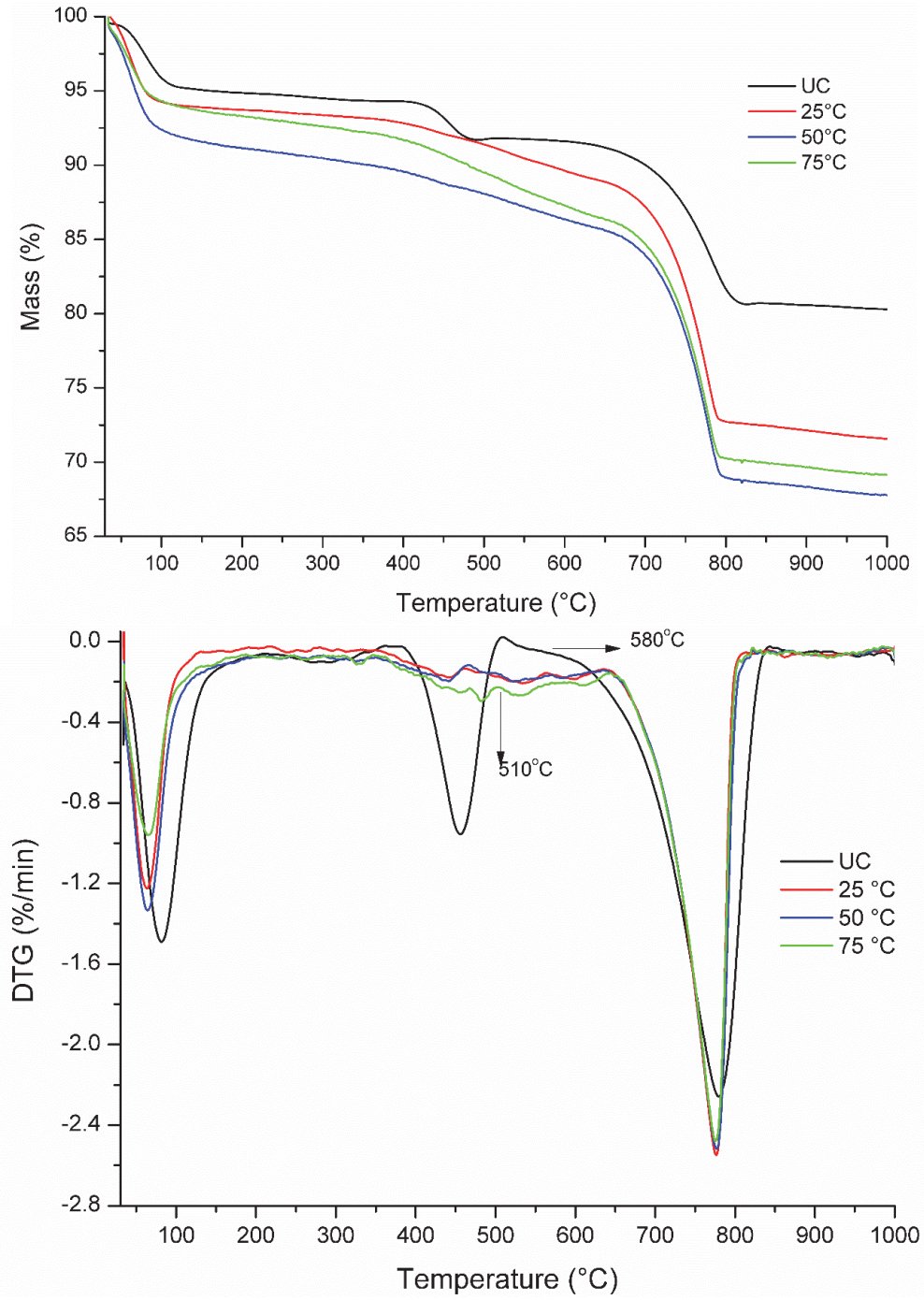

Figure 14. TGA and DTG of WA compacts that are uncarbonated (UC) and cured at 25 °C, 50 °C, and 75 °C.

There are mainly two mass loss step (water evaporation and CO_2 release from $CaCO_3$) for carbonated samples as the mass loss related to water from $Ca(OH)_2$ is not significant due to the carbonation of $Ca(OH)_2$ (Equation (3)), except for OSA carbonated at 25 °C. MS curves of OSA compacts cured at 75 °C are supporting the outcomes of the TGA curves (Figure 13).

$$Ca(OH)_{2(s)} + CO_{2(g)} \rightarrow CaCO_{3(s)} + H_2O_{(g)}\ \Delta H_{298K} = -113\ kJ/mol. \quad (3)$$

As can be seen from the third mass loss step of uncarbonated samples, both ashes already include $CaCO_3$ in their initial forms (before hydration and carbonation). Therefore, the net CO_2 uptake is calculated by subtracting the initial (uncarbonated) mineral CO_2 related mass loss from the total CO_2 related mass loss of carbonated samples. Samples cured at 25 °C had a CO_2 uptake of 9.1 and 8.5%, respectively, for OSA and WA.

In connection with previous section, the effect of curing temperature can also be followed by both TGA/DTG curves, showing that there is clear increase in CO_2 uptake values with increased curing temperatures of 25, 50, and 75 °C. Besides, the thermal stability of the newly formed $CaCO_3$ can also be characterized by looking at the TG/DTG curves. The onset temperatures (for OSA, 520 °C for curing temperatures of 25, 50 and 75 °C and 580 °C for initial sample. For WA, 510 °C for curing temperatures of 25, 50 and 75 °C and 580 °C for initial sample (Figure 14)) of the DTG curves representing the initial stage of decomposition $CaCO_3$ of carbonated samples are slightly lower than the detected onset temperatures of uncarbonated samples. Several authors have also presented similar findings of low thermal decomposition temperatures for $CaCO_3$ in case of occurrence in the not well crystalline form of calcite [41]. This may show different thermal stability of the formation of new $CaCO_3$ phases at above room temperatures within the applied curing conditions. This can also be attributed to poor transformation of amorphous $CaCO_3$ into calcite, which generally has more stable formations at room temperature [42]. However, it is also known that the thermal stability of amorphous calcium carbonate could eventually increase and spontaneously crystallize.

3.3. Kinetic Analysis

The experimental real time gas monitoring results of both OSA and WA compact carbonation are shown in Figures 15 and 16, where the CO_2 consumption kinetics are plotted at different temperatures. The carbonation reaction in OSA and WA compact are both fast at the initial stage, which can be explained by the available open porous surfaces and sufficient amount of physically bound water in the open pore structures of the specimens providing a fast start of carbonation. After this stage, a stage with a slower reaction rate takes place due to the diffusion limitation through the product layer, as carbonation proceeds from the outer surface into the internal spaces. Besides, initial fast exothermic carbonation reaction also influences the particle temperatures, which can accelerate the evaporation of the physically bound water. This would cause a restriction on the diffusion of CO_2 and carbonic acid formation. Although there is no clear temperature dependency at the initial stage of the carbonation reaction, there is a positive effect of increasing temperature on CO_2 uptake especially in the diffusion-controlled stage of OSA. The CO_2 consumption trend in terms of the carbonation rate is slightly different in WA compared to OSA and varies in different temperatures. The positive effect of increasing temperature on the rate growth of WA carbonation is more apparent, pointing out more kinetic controlled reaction phenomena, already at the early carbonation stage. The increase in temperature elongates the time of the fast carbonation period, provided that the WA reacts for a longer time, before the process reaches a more diffusion-controlled stage. The CO_2 uptake values obtained from the gas monitoring results support the total CO_2 uptake values detected in thermal analysis. The final conversion values after 2 h of curing are for OSA 0.57–0.63 and for WA 0.42–0.61. The extrapolation of graphs show that full conversion can be achieved in 12–14 h for OSA and 13–16 h for WA.

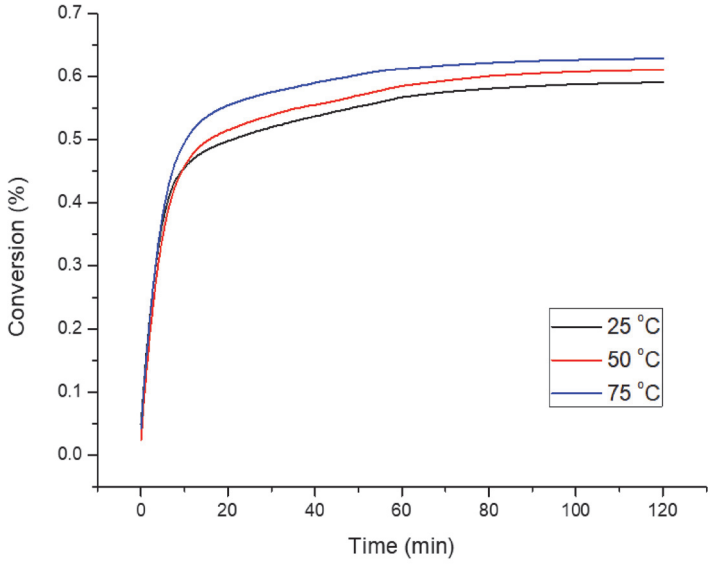

Figure 15. Gas consumption curves of OSA compacts cured at 25 °C, 50 °C, and 75 °C.

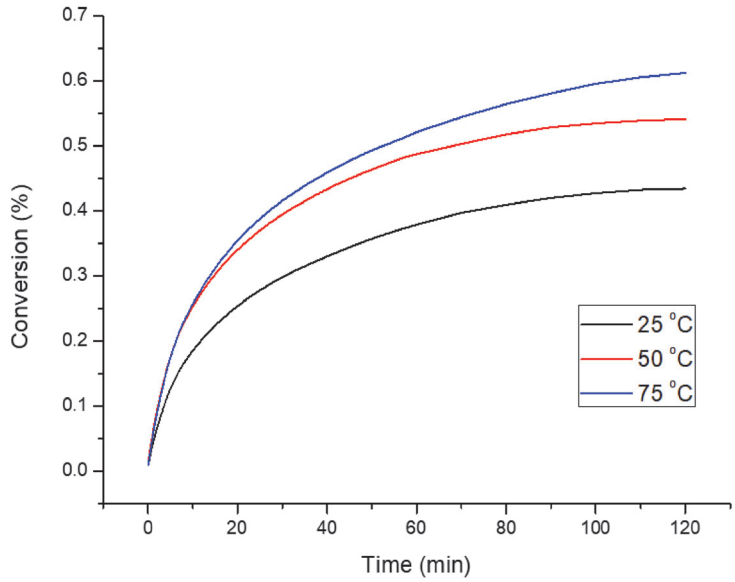

Figure 16. Gas consumption curves of WA compacts cured at 25 °C, 50 °C, and 75 °C.

By using real time gas monitoring results obtained at three different temperatures, the reaction kinetics of the carbonation conversion were tested by different diffusion-controlled reaction-order models [43]. It is known that carbonation of Ca-Mg silicates is less reactive at alkali conditions compared to $Ca(OH)_2$, where pH values should drop to 10 according to equilibrium calculations [6]. The obtained pH values could be considered to understand whether all Ca and Mg bearing phases are participating into carbonation reactions (see Appendix A). As the obtained pH values are around 11.5, the participation of Ca-Mg silicates into carbonation reaction should be negligible. Therefore, the amount of total CO_2 that can bound during carbonation is calculated according to most reactive available

phases of the ashes, which are CaO and $Ca(OH)_2$ without including Ca-Mg silicates. The quantitative XRD analysis (see Table 2) results of initial OSA and WA were used as the basis for the calculation with Equation (4) given below. In order to estimate and compare the CO_2 binding ability of different samples, CO_2max, the maximal possible CO_2 uptake capacity of the samples was calculated on the basis of the $Ca(OH)_2$ (taking into account its CaO as free CaO) and free CaO content of initial sample.

$$CO_{2max}(\%) = \frac{CaO(\%)}{\frac{MCaO}{MCO_2}} + \frac{Ca(OH)_2(\%)}{\frac{MCa(OH)_2}{MCO_2}}. \quad (4)$$

Previous studies have shown that carbonation kinetics of industrial alkaline solid wastes [44,45] can be sufficiently demonstrated by two solid-state kinetic models, which were combined into Equation (5) [46]:

$$1 - (1 - \alpha)1/3)^n = kt, \quad (5)$$

where k is the rate constant, t is the reaction time, n is a (parametrizable) index of the rate determining step, and α is the conversion degree (carbonation turnover, $\alpha = 1$ for full carbonation) according to Equation (6).

$$\alpha = m_0 - m_t/m_0 - m_{f,} \quad (6)$$

where, m_0 is the initial weight, m_t is the weight at time t, and m_f is the final weight.

By adapting the exponent n in Equation (5), two kinetic models can be defined. For $n = 1$, Equation (5) represents a purely phase-boundary controlled reaction that applies to the initial stages of carbonation. For $n = 2$, Equation (5) applies to a diffusion-limited reaction (Jander equation), where the rate-limiting step is diffusion through the growing layer of precipitated $CaCO_3$. The conformity between experimental data and the kinetic model was expressed by the correlation coefficients (R^2).

The Arrhenius equation is presented below.

$$k = Ae^{-(E_a/RT)}, \quad (7)$$

where k is the rate constant, A is the pre-exponential (frequency) factor, e is Euler's number, E_a is the activation energy, T is absolute temperature, and R is the gas constant. The activation energy can be determined from the slope of the transformed equation $\ln(k) = \ln(A) - E_a/RT$ (8) with the linear fitting of $\ln(k)$ and $1/T$ (See Appendix B). The activation energy (E_a) for OSA has been calculated as 3.55 kJ/mol and for WA as 17.06 kJ/mol. The activation energy values exhibited in literature for CaO and $Ca(OH)_2$ carbonation reactions are in line with the calculated values in this work [47].

Figure 17 shows the converted experimental data of the carbonation tests (i.e., $\ln(1 - (1 - \alpha)^{1/3})$ vs. ln(t). A relatively high R^2 value indicates that the model adequately represents the kinetics of carbonation. The values of Equation (5) to the converted data suggest that the reaction is phase-boundary controlled during the initial stages of accelerated carbonation for OSA ($\ln(t) < 2.5$) and WA ($\ln(t) < 2.9$) samples. After the change in reaction rate, carbonation becomes controlled by diffusion through the product-layer. The transition between the two kinetic models is illustrated by the change of the slope for the plot of $\ln(1 - (1 - \alpha)^{1/3})$ vs. ln(t). For WA reaction conditions, the change in slope seems to be less pronounced and later than OSA, which can be related to higher SSA of WA delaying the beginning of the diffusion phase, which is in line with the CO_2 monitoring graphs (Figures 14 and 15). This indicates that rate limitations by diffusion through a growing layer of precipitated $CaCO_3$ are less important when the solid is in motion (exposure of internal surfaces), corroborating the higher CO_2-uptake.

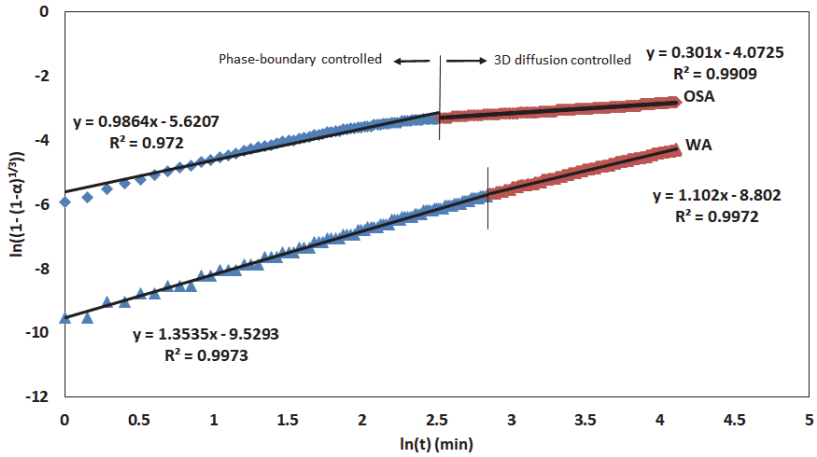

Figure 17. Evaluation of carbonation kinetics: $\ln(1-(1-\alpha)^{1/3})$ versus ln(t) for OSA and WA carbonation (R^2 = correlation coefficient).

3.4. Microstructural and Mineralogical Changes

3.4.1. XRD Analysis

XRD analysis was performed to confirm the products of carbonation and to identify what phases were consumed in the reaction. Evidence suggested that Portlandite was consumed almost completely, while calcite was the primary product. The XRD patterns of the hydrated samples in Figures 18 and 19 show evidence of some pre-existing carbonates present as calcite in the hydrated ashes, while the sample patterns included clear portlandite peaks for both OSA and WA. A good match was found in comparing the XRD pattern of the carbonated compacts to the XRD pattern of natural calcite, which confirmed that the major carbonation product was calcite. The carbonated samples showed new and more intense XRD peaks corresponding to calcite. The trace amount of Aragonite was detected with minimal intensities, which are not displayed here. Pre-existing Quartz peaks were identified in both OSA (higher intensity) and WA. CSH peaks were identified in both hydrated and carbonated samples, which indicates that CS were hydrated by the hydration process. Anhydrite and Ettringite were present in the OSA samples only.

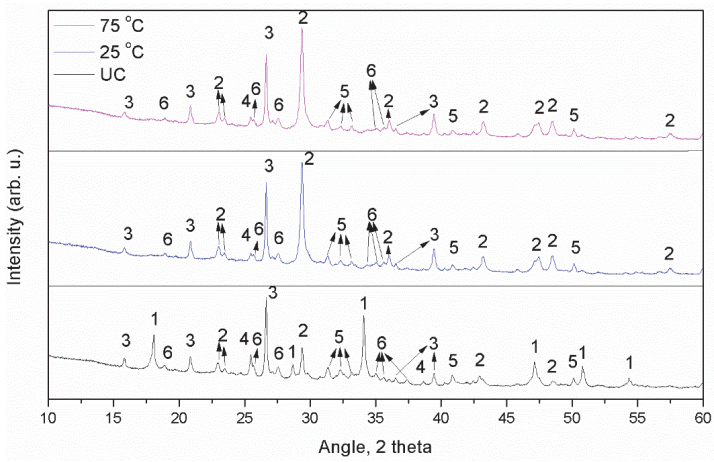

Figure 18. XRD patterns of OSA hydrated uncarbonated (UC), cured at 25 °C and 75 °C: 1—Portlandite; 2—Calcite; 3—Quartz; 4—Anhydrite; 5—CSH; 6—Ettringite.

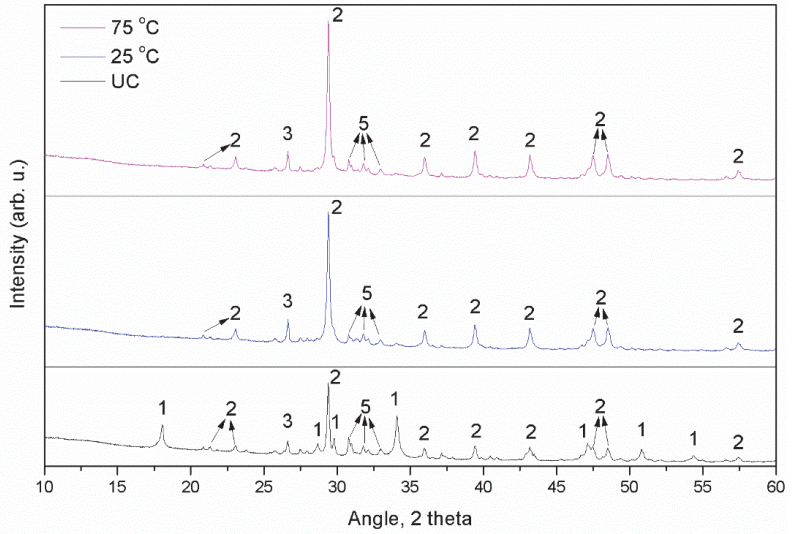

Figure 19. XRD patterns of WA hydrated uncarbonated (UC), cured at 25 °C and 75 °C: 1—Portlandite; 2—Calcite; 3—Quartz; 5—CSH.

3.4.2. SEM Analysis

Figure 20a shows the microstructure of an area near the surface of the hydrated OSA compact. Figure 20b shows the 5000× magnified surface of compact cured at 25 °C. Although the particles are not definitively separate and the hydrated products seem to be fused together, the hexagonal portlandite lamellar appears to be covered by irregular, flaky, and grainy products with dimensions in the order of 1 μm. The porous surface structure of the hydrated OSA compact changes after carbonation and becomes more compact. No visible portlandite crystals are identified in the carbonated compacts, which agrees with the near total conversion suggested by the XRD data. The carbonated products have fused into a coating that makes it difficult to discern the shape or location of the original OSA particles. It has been suggested [48] that the carbonation reaction products end up becoming intermixed into calcium silicate hydrate, such that it is unable to identify distinct carbonation product morphologies with SEM analyses. Nevertheless, the gel and the carbonation products have filled the spaces between the particles or even fused them together. The effect of fast carbonation in higher temperatures is observed as micro crack formations, which can explain the lower strength values attained at the highest temperature (75 °C) (Figure 21). Similarly, the microstructure of the hydrated WA specimen, as seen in Figure 22a, displays distinct morphological evidence of a more open structure near the surface of the hydrated WA compact. Figure 22b shows more compact structure of the WA compact cured at 25 °C, covered with globular formations. Some acicular or flaky products can be seen and were identified as calcium carbonates. Agglomeration of calcium silicate hydrate particles forming gel like structures surrounding the calcium carbonates can be observed. In carbonated compacts, no portlandite crystals are identified, which agrees with the near total conversion suggested by the XRD data.

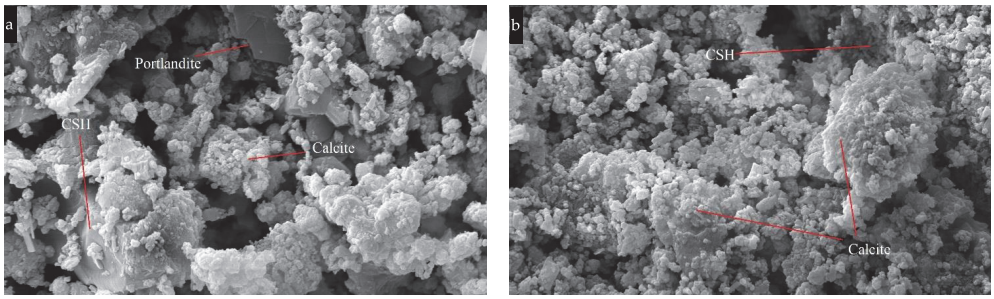

Figure 20. SEM images of OSA compacts 5000× magnified ((**a**) hydrated, (**b**) cured at 25 °C, 10 bar, 100% CO_2, 150 kgf/cm^2).

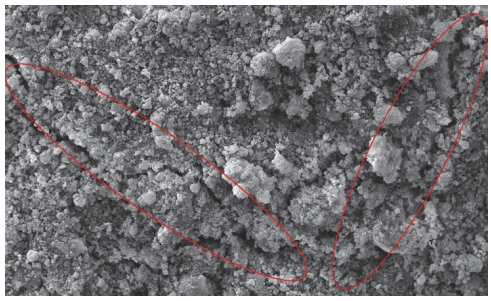

Figure 21. SEM image of OSA compact 2000× magnified exhibiting microcracks (cured at 75 °C, 10 bar, 100% CO_2, 150 kgf/cm^2).

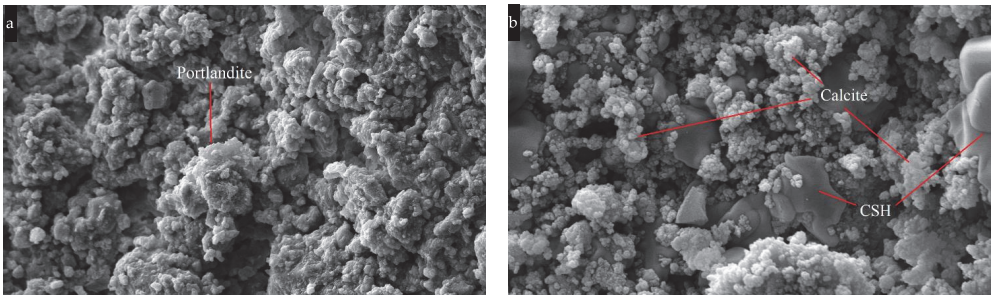

Figure 22. SEM images of WA compacts 5000× magnified ((**a**) hydrated, (**b**) cured at 25 °C, 10 bar, 100% CO_2, 150 kgf/cm^2).

3.5. Current Results in the Context of Sustainable Building Materials

The construction materials sector needs to become more diversified and sustainable, as well as safe and performant, in order to meet the stringent environmental and technical demands [49–51]. Furthermore, based on the type and availability of secondary raw materials from various industrial units, the manufacturing of new construction materials should be customized to local resources.

There are a variety of commercial technologies that combine CO_2 with solid waste streams due to the growing interest in waste mineralization as a feasible carbon capture and utilization technology. For instance, an accelerated carbonation technique was developed by Carbon8 Systems Ltd. (Gillingham, UK) for the remediation of industrial wastes and contaminated soils to produce construction products [52]. Additionally, Carbicrete (Montreal, Canada) uses a mineral carbonation method to create a concrete manufactured

from mainly steel slags and CO_2 (8% from flue gas) with a compressive strength 50% higher than ordinary concrete [53]. In addition, Carbstone Innovation (Genk, Belgium) uses CO_2 to cure slags from electric arc furnaces and basic oxygen furnaces for use as building material [54]. Similar to the commercialized technologies above, when the results of this study are considered for a specific target product, the process can be improved and optimized in line with the associated standards.

Compressive strength of 10–36 MPa and CO_2 uptake of 11–15% mass was achieved by mineral carbonation. These findings show that there is a room for improvement and potential for future applications such as kerbstone paver and paving blocks. The findings exhibited better performance of compressive strength compared to previous explorations of cementitious properties of similar FAs [20]. Telesca et al. [55,56] studied coal FA as a raw material to produce ettringite-based construction materials and discovered that it has the potential to be used in this method. They obtained a maximum compressive strength of around 6 MPa, which was achieved after 16 h of curing. Self-cementitious characteristics and pozzolanic reactivity of FA were examined by Li et al. [57]. They achieved a compressive strength of 11.4 MPa without chemical modifiers after 28 days, and 22.4 MPa with chemical modifiers and particle size distribution optimization. Ohenoja et al. [58] discovered that compressive strength was dependent on the selectively soluble calcium, aluminium, silicate, and sulphate content. Tests including different FAs have achieved a compressive strength of up to 6 MPa after 28 days.

4. Conclusions

This study analyses the performance of compacts produced from locally sourced distinct FAs such as OSA, WA, and LFA, in terms of CO_2 uptake and compressive strength under numerous process conditions (i.e., 25–75 °C, 5–15 bar, 15–100% CO_2, and compaction pressures of 150 and 300 kgf/cm^2).

Among the two main samples, OSA compacts exhibited 10–12 wt% CO_2 uptake with a compressive strength of 16–36 MPa, whereas WA compacts show a wider range of 8–13 wt% CO_2 uptake with a compressive strength of 10–16 MPa. Preliminary findings of LFA indicate that there is a future potential for applications of lightweight building materials by utilizing previously deposited combustion residues, binding ~15 wt% CO_2.

Changes in the curing conditions have a direct effect on the CO_2 uptake levels and related strength development;

- Increase in gas pressure and CO_2 concentration exhibited positive correlation with the CO_2 uptake and compressive strength values;
- Compaction pressure as a pre-processing parameter is mainly related to compressive strength. However, due to its physical effect on diffusivity, the compaction pressure increase showed an increase in strength while limiting CO_2 penetration in a small amount, causing less CO_2 uptake;
- Despite higher carbonation degrees at elevated curing temperatures, the compressive strength did not increase accordingly. High temperatures can increase the risks of micro cracks and change the micro-mechanical property of CSH, which in turn weakens the compressive strength;
- Additionally, at high temperatures, due to the reduction of liquid water in compacts, uneven and fast formation of particulates (amorphous formations of calcite polymorphs) on the surfaces of mainly $Ca(OH)_2$ can appear, yet such determination is rather complex for short curing times (2 h);
- SEM and XRD analysis further proved that Calcite was the dominant phase after carbonation and portlandite was almost completely consumed;
- Reaction mechanism corresponds to 3D-diffusion-controlled reaction order model for both OSA and WA. CO_2 diffusion through the product layer was estimated to be the rate-controlling step and surface passivation was clearer for OSA, except for WA, due to the short curing time. Calculated apparent activation energies are given for OSA as 3.55 kJ/mol and for WA as 17.06 kJ/mol.

The prospective result of this study enables greater insight into the CO_2 curing processes of ashes, which can be transferred to the industrial building material applications for tailoring of the locally available Estonian ash as well as similar ash elsewhere.

Author Contributions: Conceptualization, M.C.U.; methodology, M.C.U. and C.R.Y.; software, M.C.U.; validation, M.C.U., C.R.Y. and M.U.; formal analysis, M.C.U.; investigation, M.C.U.; resources, M.C.U. and A.G.; data curation, M.C.U.; writing—original draft preparation, M.C.U.; writing—review and editing, M.C.U., C.R.Y. and T.H.; visualization, M.C.U.; supervision, C.R.Y. and M.U.; project administration, A.T.; funding acquisition, A.T. All authors have read and agreed to the published version of the manuscript.

Funding: This research is funded by the CLEANKER project which has received funding from the European Union's Horizon 2020 Framework Program under Grant Agreement No. 764816 and the Government of China (National Natural Science Foundation of China) under contract No. 91434124 and No. 51376105. This work is also partially supported by ASTRA "TUT Institutional Development Program for 2016-2022" Graduate School of Functional Materials and Technologies and the Estonian ministry of Education and Research (IUT33-19).

Institutional Review Board Statement: Not applicable.

Informed Consent Statement: Not applicable.

Data Availability Statement: Not applicable.

Acknowledgments: This work was carried out as part of a Ph.D. project supported by the Estonian Ministry of Education and Research (IUT33-19). This work has been partially supported by ASTRA "TUT Institutional Development Program for 2016–2022" Graduate school of Functional Materials and Technologies. The help of Mart Viljus (SEM images) is gratefully acknowledged.

Conflicts of Interest: The authors declare no conflict of interest. The funders had no role in the design of the study; in the collection, analyses, or interpretation of data; in the writing of the manuscript, or in the decision to publish the results.

Appendix A

Table A1. pH measurements of compacts (UC: Uncarbonated, 25 °C: Carbonated at 25 °C, 75 °C: Carbonated at 75 °C).

	OSA			WA		
	UC	**25 °C**	**75 °C**	**UC**	**25 °C**	**75 °C**
pH	12.5	11.5	11.4	12.7	12.1	11.4

Appendix B

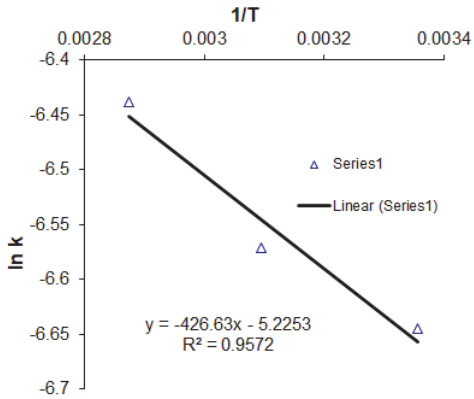

Figure A1. Arrhenius chart for OSA compacts.

Table A2. Reaction parameters for OSA compacts.

T, K	1/T	k	ln k
298	0.003355705	1.3×10^{-3}	−6.64539
323	0.003095975	1.4×10^{-3}	−6.57128
348	0.002873563	1.60×10^{-3}	−6.43775
Slope:	−426.63	Intercept:	−5.2253
E_A	**3.54700182**	kJ/mol	
A	**0.005378746**	min^{-1}	

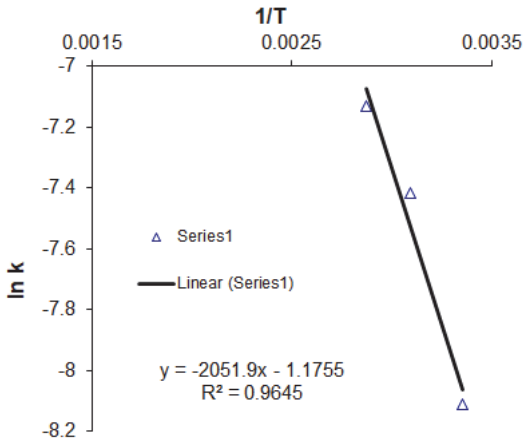

Figure A2. Arrhenius chart for WA compacts.

Table A3. * Reaction parameters for WA compacts.

T, K	1/T	k	ln k
298	0.003355705	3.0×10^{-4}	−8.11173
323	0.003095975	6.0×10^{-4}	−7.41858
348	0.002873563	8.00×10^{-4}	−7.1309
Slope:	−2051.9	Intercept:	−1.1755
E_A	**17.0594966**	kJ/mol	
A	**0.308664609**	min^{-1}	

* (T: Temperature (K), k: Rate constant, E_A: Activation Energy, A: Pre-exponential factor).

References

1. Torgal, F.P.; Shi, C.; Angel, S.P. Accelerated carbon dioxide sequestration. In *Carbon Dioxide Sequestration in Cementitious Construction Materials*; Woodhead Publishing: Sawston, UK, 2018; pp. 81–101.
2. IEA Cement Tracking Report, November 2021. Available online: https://www.iea.org/reports/cement (accessed on 4 December 2021).
3. Scrivener, K.L.; John, V.M.; Gartner, E.M. Eco-efficient cements: Potential economically viable solutions for a low-CO_2 cement-based Materials Industry. *Cem. Concr. Res.* **2018**, *114*, 2–26. [CrossRef]
4. HeidelbergCement AG. HeidelbergCement to Install the World's First Full-Scale CCS Facility in a Cement Plant. Available online: https://www.heidelbergcement.com/en/pr-15-12-2020 (accessed on 15 December 2020).
5. Yi, H.; Xu, G.; Cheng, H.; Wang, J.; Wan, Y.; Chen, H. An overview of utilization of steel slag. *Procedia Environ. Sci.* **2012**, *16*, 791–801. [CrossRef]
6. Von Greve-Dierfeld, S.; Lothenbach, B.; Vollpracht, A.; Wu, B.; Huet, B.; Andrade, C.; Medina, C.; Thiel, C.; Gruyaert, E.; Vanoutrive, H.; et al. Understanding the carbonation of concrete with supplementary cementitious materials: A critical review by RILEM TC 281-CCC. *Mater. Struct.* **2020**, *53*, 136. [CrossRef]

7. Hemalatha, T.; Ramaswamy, A. A review on fly ash characteristics—Towards promoting high volume utilization in developing sustainable concrete. *J. Clean. Prod.* **2017**, *147*, 546–559. [CrossRef]
8. Ramezanianpour, A.A. *Cement Replacement Materials*; Springer Geochemistry/Mineralogy: New York, NY, USA, 2014; pp. 70–74. ISBN 9783642367205.
9. Moon, E.J.; Choi, Y.C. Carbon dioxide fixation via accelerated carbonation of cement-based materials: Potential for construction materials applications. *Constr. Build. Mater.* **2019**, *199*, 676–687. [CrossRef]
10. Mo, L.; Zhang, F.; Deng, M.; Jin, F.; Al-Tabbaa, A.; Wang, A. Accelerated carbonation and performance of concrete made with steel slag as binding materials and aggregates. *Cem. Concr. Compos.* **2017**, *83*, 138–145. [CrossRef]
11. Guo, M.Z.; Tu, Z.; Poon, C.S.; Shi, C. Improvement of properties of architectural mortars prepared with 100% recycled glass by CO_2 curing. *Constr. Build. Mater.* **2018**, *179*, 138–150. [CrossRef]
12. Wei, Z.; Wang, B.; Falzone, G.; La Plante, E.C.; Okoronkwo, M.U.; She, Z.; Oey, T.; Balonis, M.; Neithalath, N.; Pilon, L.; et al. Clinkering-free cementation by fly ash carbonation. *J. CO2 Util.* **2018**, *23*, 117–127. [CrossRef]
13. Woodall, C.M.; McQueen, N.; Pilorgé, H.; Wilcox, J. Utilization of mineral carbonation products: Current state and potential. *Greenh. Gas. Sci. Technol.* **2019**, *9*, 1096–1113. [CrossRef]
14. Chang, R.; Kim, S.; Lee, S.; Choi, S.; Kim, M.; Park, Y. Calcium carbonate precipitation for CO_2 storage and utilization: A review of the carbonate crystallization and polymorphism. *Front. Energy Res.* **2017**, *5*, 17. [CrossRef]
15. Uibu, M.; Kuusik, R.; Andreas, L.; Kirsimäe, K. The CO_2 binding by Ca-Mg-silicates in direct aqueous carbonation of oil shale ash and steel slag. *Energy Procedia* **2011**, *4*, 925–932. [CrossRef]
16. Bobicki, E.R.; Liu, Q.; Xu, Z.; Zeng, H. Carbon capture and storage using alkaline industrial wastes. *Prog. Energy Combust. Sci.* **2012**, *38*, 302–320. [CrossRef]
17. Gunning, P.J.; Hills, C.D.; Carey, P.J. Accelerated carbonation treatment of industrial wastes. *Waste Manag.* **2010**, *30*, 1081–1090. [CrossRef]
18. Leben, K.; Motlep, R.; Konist, A.; Pihu, T.; Kirsimäe, K. Carbon dioxide sequestration in power plant Ca-rich ash waste deposits. *Oil Shale* **2021**, *38*, 65–88. [CrossRef]
19. Leben, K.; Mõtlep, R.; Paaver, P.; Konist, A.; Pihu, T.; Paiste, P.; Kirsimäe, K. Long-term mineral transformation of Ca-rich oil shale ash waste. *Sci. Total Environ.* **2019**, *658*, 1404–1415. [CrossRef]
20. Usta, M.C.; Yörük, C.R.; Hain, T.; Paaver, P.; Snellings, R.; Rozov, E.; Uibu, M. Evaluation of New Applications of Oil Shale Ashes in Building Materials. *Minerals* **2020**, *10*, 765. [CrossRef]
21. Gunning, P.J.; Hills, C.D.; Carey, P.J. Production of lightweight aggregate from industrial waste and carbon dioxide. *Waste Manag.* **2009**, *29*, 2722–2728. [CrossRef]
22. Quaghebeur, M.; Nielsen, P.; Horckmans, L.; Van Mechelen, D. Accelerated Carbonation of Steel Slag Compacts: Development of High-Strength Construction Materials. *Front. Energy Res.* **2015**, *3*, 52. [CrossRef]
23. Nielsen, P.; Boone, M.A.; Horckmans, L.; Snellings, R.; Quaghebeur, M. Accelerated Carbonation of Steel Slag Monoliths at Low CO_2 Pressure–Microstructure and Strength Development. *J. CO2 Util.* **2020**, *36*, 124–134. [CrossRef]
24. Sanjuán, M.Á.; Estévez, E.; Argiz, C. Carbon dioxide absorption by blast-furnace slag mortars in function of the curing intensity. *Energies* **2019**, *12*, 2346. [CrossRef]
25. Ohenoja, K.; Rissanen, J.; Kinnunen, P.; Illikainen, M. Direct carbonation of peat-wood fly ash for carbon capture and utilization in construction application. *J. CO2 Util.* **2020**, *40*, 101203. [CrossRef]
26. Liu, W.; Teng, L.; Rohani, S.; Qin, Z.; Zhao, B.; Xu, C.C.; Liang, B. CO_2 mineral carbonation using industrial solid wastes: A review of recent developments. *Chem. Eng. J.* **2021**, *416*, 129093. [CrossRef]
27. Affordable. Versatile. Sustainable. Available online: https://www.enefit.com/technology/power-production (accessed on 14 February 2022).
28. Okia. Utilitas Tallinn. *Utilitas*. Available online: https://www.utilitas.ee/en/company/as-utilitas-tallinn/ (accessed on 14 February 2022).
29. Electricity and Heat Production. Available online: https://www.energia.ee/en/ettevottest/tehnoloogia/elektri-ja-sooja-tootmine?tabgroup_1=auvere (accessed on 14 February 2022).
30. Arandigoyen, M.; Bicer-Simsir, B.; Alvarez, J.I.; Lange, D.A. Variation of microstructure with carbonation in lime and blended pastes. *Appl. Surf. Sci.* **2006**, *252*, 7562–7571. [CrossRef]
31. Barnes, P.; Bensted, J. *Structure and Performance of Cements*, 2nd ed.; CRC Press: Boca Raton, FL, USA, 2001. [CrossRef]
32. Horkoss, S.; Escadeillas, G.; Rizk, T.; Lteif, R. The effect of the source of cement SO_3 on the expansion of mortars. *Case Stud. Constr. Mater.* **2016**, *4*, 62–72. [CrossRef]
33. ASTM International. Standard Specification for Coal Fly Ash and Raw or Calcined Natural Pozzolan for Use in Concrete (ASTM C618-19). Available online: https://www.astm.org/ (accessed on 14 February 2022).
34. Humidity Fixed Points of Binary Saturated Aqueous Solutions: Semantic Scholar. Available online: https://www.semanticscholar.org/paper/Humidity-Fixed-Points-of-Binary-Saturated-Aqueous-Gree-span/9a90c8e8fb71c152ae3bacf9904e6c761cdf9de7 (accessed on 14 February 2022).
35. Fernandezbertos, M.; Simons, S.; Hills, C.; Carey, P. A review of accelerated carbonation technology in the treatment of cement-based materials and sequestration of CO_2. *J. Hazard. Mater.* **2004**, *112*, 193–205. [CrossRef]

36. Pizzol, V.D.; Mendes, L.M.; Savastano, H., Jr.; Frías, M.; Davila, F.J.; Cincotto, M.A.; Tonoli, G.H.D. Mineralogical and microstructural changes promoted by accelerated carbonation and ageing cycles of hybrid fiber–cement composites. *Constr. Build. Mater.* **2014**, *68*, 750–756. [CrossRef]
37. Cui, H.; Tang, W.; Liu, W.; Dong, Z.; Xing, F. Experimental study on effects of CO_2 concentrations on concrete carbonation and diffusion mechanisms. *Constr. Build. Mater.* **2015**, *93*, 522–527. [CrossRef]
38. Mohamed, M.F.; Nor, A.M.; Suhor, M.F.; Singer, M.; Choi, Y.S.; Nešic, S. Water Chemistry for Corrosion Prediction in High Pressure CO_2 Environments. *Corrosion* **2011**, NACE-11375.
39. Fang, Y.; Chang, J. Microstructure changes of waste hydrated cement paste induced by accelerated carbonation. *Constr. Build. Mater.* **2015**, *76*, 360–365. [CrossRef]
40. Liu, X.; Feng, P.; Cai, Y.; Yu, X.; Yu, C.; Ran, Q. Carbonation behavior of calcium silicate hydrate (CSH): Its potential for CO_2 capture. *Chem. Eng. J.* **2022**, *431*, 134243. [CrossRef]
41. Nejad, F.M.; Tolouei, M.; Nazari, H.; Naderan, A. Effects of calcium carbonate nanoparticles and fly ash on mechanical and permeability properties of concrete. Advances in Civil Engineering. *Materials* **2018**, *7*, 651–668. [CrossRef]
42. Usmany, Y.; Putranto, W.A.; Bayuseno, A.P.; Muryanto, S. Crystallization of calcium carbonate ($CaCO_3$) in a flowing system: Influence of Cu^{2+} additives on induction time and crystalline phase transformation. *AIP Conf. Proc.* **2016**, *1725*, 20093. [CrossRef]
43. Shih, Y. Thermal degradation and kinetic analysis of biodegradable PBS/multiwalled carbon nanotube nanocomposites. *J. Polym. Sci. Part B Polym. Phys.* **2009**, *47*, 1231–1239. [CrossRef]
44. Nam, S.-Y.; Seo, J.; Thriveni, T.; Ahn, J.-W. Accelerated carbonation of municipal solid waste incineration bottom ash for CO_2 sequestration. *Geosystem Eng.* **2012**, *15*, 305–311. [CrossRef]
45. Um, N.; Nam, S.-Y.; Ahn, J.-W. Effect of accelerated carbonation on the leaching behavior of Cr in municipal solid waste incinerator bottom ash and the carbonation kinetics. *Mater. Trans.* **2013**, *54*, 1510–1516. [CrossRef]
46. Khawam, A.; Flanagan, D.R. Solid-state kinetic models: Basics and mathematical fundamentals. *J. Phys. Chem. B.* **2006**, *110*, 17315–17328. [CrossRef] [PubMed]
47. Nikulshina, V.; Gálvez, M.; Steinfeld, A. Kinetic analysis of the carbonation reactions for the capture of CO_2 from air via the $Ca(OH)_2$–$CaCO_3$–CaO solar thermochemical cycle. *Chem. Eng. J.* **2007**, *129*, 75–83. [CrossRef]
48. Monkman, S.; Shao, Y. Assessing the carbonation behavior of cementitious materials. *J. Mater. Civ. Eng.* **2006**, *18*, 768–776. [CrossRef]
49. European Commission. Outcome of Proceedings. Circular Economy in the Construction Sector. Available online: https://data.consilium.europa.eu/doc/document/ST-14653-2019-INIT/en/pdf (accessed on 14 March 2022).
50. European Commission. European Green Deal: Commission Proposes to Boost Renovation and Decarbonisation of Buildings. Available online: https://ec.europa.eu/commission/presscorner/detail/en/IP_21_6683 (accessed on 14 March 2022).
51. European Commission. Construction Products Regulation Acquis. Internal Market, Industry, Entrepreneurship and SMEs. Available online: https://ec.europa.eu/growth/sectors/construction/construction-products-regulation-cpr/acquis_en (accessed on 14 March 2022).
52. Carbon8 Systems. Available online: http://www.c8s.co.uk/ (accessed on 12 April 2022).
53. Carbon-Negative Concrete. *CarbiCrete*. Available online: http://www.carbicrete.com/ (accessed on 12 April 2022).
54. Carbstone. *VITO*. Available online: https://vito.be/en/carbstone (accessed on 12 April 2022).
55. Telesca, A.; Marroccoli, M.; Montagnaro, F.; Tomasulo, M.; Valenti, G.L. Enhancement of selectivity toward ettringite during hydrothermal processes on fluidized bed combustion wastes for the manufacture of preformed building components. *RSC Adv.* **2015**, *5*, 101887–101893. [CrossRef]
56. Telesca, A.; Calabrese, D.; Marroccoli, M.; Valenti, G.L.; Montagnaro, F. Study of the hydrothermal treatments of residues from fluidized bed combustors for the manufacture of ettringite-based building elements. *Fuel Process. Technol.* **2014**, *126*, 188–191. [CrossRef]
57. Li, X.; Chen, Q.; Huang, K.; Ma, B.; Wu, B. Cementitious properties and hydration mechanism of circulating fluidized bed combustion (CFBC) desulfurization ashes. *Constr. Build. Mater.* **2012**, *36*, 182–187. [CrossRef]
58. Ohenoja, K.; Tanskanen, P.; Wigren, V.; Kinnunen, P.; Körkkö, M.; Peltosaari, O.; Österbacka, J.; Illikainen, M. Self-hardening of fly ashes from a bubbling fluidized bed combustion of peat, forest industry residuals, and wastes. *Fuel* **2016**, *165*, 440–446. [CrossRef]

Appendix 3

Publication III

Usta, M. C., Yörük, C. R., Uibu, M., Traksmaa, R., Hain, T., Gregor, A., & Trikkel, A. (2023). Carbonation and Leaching Behaviors of Cement-Free Monoliths Based on High-Sulfur Fly Ashes with the Incorporation of Amorphous Calcium Aluminate. *ACS omega*, *8*(32), 29543-29557. https://doi.org/10.1021/acsomega.3c03286

ACS OMEGA

http://pubs.acs.org/journal/acsodf

Article

Carbonation and Leaching Behaviors of Cement-Free Monoliths Based on High-Sulfur Fly Ashes with the Incorporation of Amorphous Calcium Aluminate

Mustafa Cem Usta,* Can Rüstü Yörük, Mai Uibu, Reiner Traksmaa, Tiina Hain, Andre Gregor, and Andres Trikkel

Cite This: *ACS Omega* 2023, 8, 29543−29557

Read Online

ACCESS | Metrics & More | Article Recommendations | Supporting Information

ABSTRACT: The high sulfate content in various alkaline wastes, including those from fossil fuel and biomass combustion, and other industrial processes, necessitates careful management when used in cementitious systems to prevent potential deterioration of construction materials and environmental safety concerns. This study explores the under-researched area of high-sulfur fly ash (HSFA) utilization in the production of cement-free monoliths through accelerated carbonation and further examines the effect of niobium slag (NS)—a calcium aluminate-containing slag—as an additive on the strength development and the mobility of SO_4^{2-}. The methodology involves mineralogical and microstructural analyses of monoliths before and after carbonation, accounting for the effects of accelerated carbonation treatment and NS addition. The findings suggest that accelerated carbonation significantly improves the initial compressive strength of the HSFA monoliths and generally immobilizes heavy metals, while the effect on sulfate immobilization can vary depending on the ash composition. Moreover, the addition of NS further enhances strength without substantially hindering CO_2 uptake, while reducing the leaching values, particularly of sulfates and heavy metals. These findings suggest that it is feasible to use calcium aluminate-containing NS in HSFA-based carbonated monoliths to immobilize sulfates without compromising the strength development derived from carbonation. This research contributes to the understanding of how accelerated carbonation and NS addition can enhance the performance of HSFA-based materials, providing valuable insights for the development of sustainable construction materials.

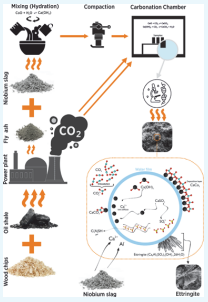

1. INTRODUCTION

The recycling of industrial alkaline solid waste is a key aspect of sustainable development which reduces the demand for natural resources and contributes to a lowering of greenhouse emissions in construction products. Thus, the utilization of industrial waste or byproducts can play a significant role in the cleaner production of construction materials. Evaluating the integration of secondary resources from various industrial sources is crucial to ensure these new materials meet the necessary technological and environmental standards. The quality of the potential supplementary cementitious materials can be evaluated with the chemical and mineralogical compositions of industrial wastes through various regulations and standards.[1−3] Fly ashes (FA) are widely known and utilized as supplementary and alternative cementitious materials.[4,5] Yet FA particle is only a few microns in thickness and can contain leachable toxic heavy metals and salts, which can limit the possibilities for the valorization of these materials. The SO_3 content in fly ashes (FAs) is a critical parameter, especially in high-sulfur fly ashes (HSFA), as a high sulfur content can lead to various adverse effects such as sulfate attack and reduced durability in cementitious systems.[6,7] These potential issues can significantly limit the utilization and applications of HSFA, despite its wide availability. Recycling of FAs or other types of out-of-furnace byproducts with high sulfur content[8−11] as supplementary cementitious materials requires compliance with legal standards,[12] which can be complex and costly once the sulfur removal treatments are considered.[13] Ashes from different fossil fuel (coal, oil shale, etc.) combustion processes as well as ashes of biomasses (wood, forestry waste, etc.), flue gas desulfurization waste, construction demolition wastes, slags from metal smelting, pulp, and paper mill waste, etc. can contain high amounts of sulfate.[14−21] Therefore, the utilization of these types of wastes especially HSFA in cementitious systems requires careful consideration and management to ensure that the negative effects of the high sulfur content are minimized for potential problems regarding deterioration and environmental safety of construction materials. Reduction of hazardous characteristics can be achieved using appropriate mix designs, washing

Received: May 16, 2023
Accepted: July 5, 2023
Published: July 31, 2023

https://doi.org/10.1021/acsomega.3c03286
ACS Omega 2023, 8, 29543−29557

techniques,[22,23] or the incorporation of additives such as hydraulic binders, i.e., amorphous calcium aluminate (CA).[8,24−26] Trincal et al. tested various experimental binders for their effectiveness in reducing sulfate leaching from soils with high gypsum content (maximum of 34 wt %).[27] The researchers found that the formation of ettringite partially immobilized the sulfates. The most successful binder was a hydraulic mixture consisting mainly of ye'elimite ($C_4A_3\overline{S}$) and belite (C2S), which decreased the leachable sulfate concentration by 50% in leaching tests. Further, Sadique et al.[28] investigated the hydration mechanism of a non-Portland binder (wastepaper sludge ash); during sulfate activation, demonstrating that the alumina phase in the ash reacts with the elevated SO_4^{2-} concentration to produce aluminosulfate, which mixes with Ca^{2+} to create ettringite.

CAs, and by extension the calcium sulfoaluminate (CAS) phases are known to be rapidly reactive hydraulic compounds that improve the strength of hardened mortars.[29] A major advantage of calcium sulfoaluminate phases or ettringite-based chemistry, as applied to the stabilization of residues, is the extremely low solubility of ettringite at alkaline pHs in the range of 10.4−13.7, thereby providing strong resistance to sulfate leaching.[30,31] The studies conducted by Rungchet et al. and Mrak et al. showed that the leaching of heavy metals and sulfates can be controlled via calcium sulfoaluminate phases[32,33] and similarly, Luo et al.[34] have found that sulfoaluminate cement can also effectively decrease the toxic leaching of heavy metals.

Recent research has pivoted toward accelerated carbonation of industrial alkaline wastes, a process that recycles carbon dioxide and reduces hazardous compounds.[35] This approach enhances the use of these wastes as alternative cementitious materials, fostering the creation of eco-friendly construction products and promoting a circular economy within the construction sector.[36,37] Experimental results have proven that the accelerated carbonation process improves the mechanical properties of the different test specimens (monoliths, pastes, granules, etc.) by altering physical characteristics like porosity and surface area.[38] Besides, the accelerated carbonation process lowers the mobility of hazardous compounds, encapsulating the toxic substance into the structure of the final product. Hence, stabilization of the industrial alkaline solid wastes can be achieved through accelerated carbonation, by creating stable precipitates that are insoluble to reduce the leachability of potentially harmful elements.[39−41] Lange et al. studied the leaching characteristics of cement-solidified waste forms upon carbonation.[42] Results showed that the carbonated solidified products had mean strength values increased by up to 70% and leachable metal concentrations reduced by up to 80%. Baciocchi et al. investigated the leaching behavior of refused derived fuel bottom ash through the accelerated carbonation method and concluded that a significant reduction of the mobility of most contaminants can be achieved.[38] However, studies regarding FAs in this field are rather limited, especially the utilization of HSFAs through accelerated carbonation in the construction industry remains understudied. Furthermore, a method of application incorporating accelerated carbonation can be challenging for HSFAs as the literature is rather ambiguous, and different leaching outcomes have been reported for the carbonation process in the past. Bergmans et al. found that as the pH of the leachate decreases, the sulfate concentration in the solution increases.[43] This pH-dependent behavior in sulfate leaching is consistent with the solubility of ettringite. Wang et al. concluded that there is no obvious correlation between reactivity during the carbonation of FA and the concentration of leachable sulfate, and the carbonation process did not influence the level of sulfates.[44] Li et al. however, claim that the release of soluble salts including SO_4^{2-} was reduced by the carbonation of FA.[45]

Therefore, the main objectives of this study are; first to evaluate the carbonation potential of oil shale FA and wood FA as targeted HSFA materials in carbonated structures for cement-free building material applications, second to characterize the sulfate leaching behavior of these cement-free monoliths and finally to investigate the effects of niobium slag as an additive to HSFAs for the evaluation of its role in possible immobilization of SO_4^{2-} and strength development in carbonated structures. This approach significantly deviates from conventional practices and has not been thoroughly investigated in prior research. A distinctive innovation of this study is the incorporation of niobium slag, a material enriched with amorphous CA, as an additive to HSFA, that could potentially augment the performance and sustainability of HSFA-based materials in the construction sector.

In essence, the significance of this study lies in the novel exploration of accelerated carbonation of HSFAs with a slag-based calcium aluminate additive.

2. MATERIALS AND METHODS

2.1. Materials. Three different types of industrial by-product samples (namely, oil shale fly ash (OSFA), wood fly ash (WFA), and niobium slag (NS)) were selected from the power and heat generation and metal sectors of Estonia, which represents the widely available low-grade fuel operated circulating fluidized bed (CFB) combustion residues as well as co-firing applications with biomass elsewhere. OSFA was obtained from Auvere Power Plant,[46] which is primarily operated by the direct combustion of OS with the ability to co-fire with up to 50% woodchips in CFB boilers for power production, and ash was collected from the electrostatic precipitators. WFA was obtained from AS Utilitas Tallinn,[47] which has a biofuel-based combined heat and power station supplied by mainly waste forestry wood and ash was collected from bag filters located in the postcombustion zones of the grate combustor. Calcium aluminate-bearing NS (as ground sample) is obtained from NPM Silmet. One of Europe's leading producers of rare metals (annual output of 700 t) and rare earth metals (annual production of 3000 tons) is NPM Silmet.[48] Niobium slag produced by the metallurgical process now amounts to 1000 tons or more annually. The major byproducts of the calcium aluminothermic reduction of niobium oxide (Nb_2O_5) are mostly calcium aluminate-containing slag and pure Nb. Niobium oxide Nb_2O_5 (3−7%) and pure Ni (perhaps up to 1%) remain in slag because of the non-full calcium aluminothermic reduction.[49]

2.2. Characterization of Materials and Methods. Mean samples were taken from each collected residue and a size fraction below 200 μm (by sieving) was used for material characterization and further sample preparation. The physical characterization of the selected waste streams included particle size distribution (PSD) measurements. Horiba Laser Scattering instrument (LA-950V2) was used for PSD measurement (with ethanol as a dispersant). The BET-N_2 sorption method was used to measure the specific surface area (SSA) with a Kelvin 1042 sorptiometer (Costech Microanalytical SC). Helium was

https://doi.org/10.1021/acsomega.3c03286
ACS Omega 2023, 8, 29543−29557

used as a carrier gas, while N_2 (purity 99.999%) was used as an adsorptive gas. N_2 adsorption data were collected at relative pressures (p/p_0) ranging from 0.05 to 0.2 at the liquid N_2 temperature of −196.15 °C. The SSA was calculated based on Brunauer−Emmett−Teller (BET) theory. The content of free lime and carbon (ELTRA CS 580 Carbon Sulfur Determinator) was determined in the solid phase. Pore size distribution and porosity measurements were obtained through a Mercury intrusion porosimeter (MIP) using a POREMASTER-60-17 porosimeter (Quantachrome Instruments). The total porosity was calculated by dividing the complete volume of mercury infiltrated at the highest experimental pressure by the overall volume of the sample being tested. The porosity measurements were performed at least twice and occasionally three times to ensure repeatability. The chemical and mineralogical characterization as well as the phase changes after different curing steps of the selected waste streams were analyzed by X-ray fluorescence (XRF) (Bruker S4 Pioneer) and X-ray diffraction (XRD) with Rigaku, SmartLab SE. The X-ray tube uses a Cu anode (wavelength 1.5406 Å). D/teX Ultra 250 1D detector was used for measurement. The measuring range was 9−60°, the step length was 0.04°, and the measuring speed was 3°/min. The ICDD PDF4 database was used for data processing. The thermogravimetric (TGA) analysis was also carried out to understand the thermal characterization of both carbonated and uncarbonated monoliths (mainly for the calculation of CO_2 uptake) by using a Setaram Labsys 2000 thermoanalyzer (10 K/min, sample mass: 20 ± 1 mg, 21% O_2/79% Ar) with alumina (Al_2O_3) crucible. The microstructures of the carbonated samples were analyzed by a scanning electron microscope (SEM) ZEISS Evo MA 15 with an EDX analyzer. The compressive strength measurements were performed with Toni TechnikD-13355.

Leaching tests were applied first to the initial ashes and later to both uncarbonated (UC) and carbonated (C) samples with NS additive according to the standard EN 12457-2. Crushed pieces were taken from initially hardened samples and were kept in sealed centrifuge tubes with distilled water for 24 ± 0.5 h in an overhead shaker (GFL 3025) with 34 rpm rotation speed at room temperature (20 ± 2 °C). The liquid-to-solid ratio (L/S) was 10 L/kg and the grain size of the crushed monoliths was between 0 and 4 mm. Later the suspension was vacuum filtered (standard filter paper, pore diameter 0.45 μm). Conductivity (EC) and pH values were measured using a Mettler Toledo SevenGo Duo Pro pH/Cond meter SG23. Cl^- and SO_4^{2-} ions were determined through Lovibond Spectro direct spectrometer, silver nitrate turbidity, and barium sulfate turbidity methods, respectively. The Agilent 4210 Microwave Plasma Atomic Emission Spectrometer (MP-AES) with nitrogen-based plasma generated from magnetically coupled microwave energy was used for the determination of heavy metals (Ba, Cr, Cu, Fe, Ni, Pb, Sr, Zn, Mn, Cd, etc.).

2.2.1. Sample Preparation and Experimental Setup. Samples are prepared in four different compositions including 100% OSFA, 100% WFA and 10% NS added to both OSFA and WFA (see Table 1). Each batch of samples included a minimum of four cylindrical samples and their average strength values are given in the results for each tested parameter. In the first step, the hydrated OSFA and WFA samples have been prepared with a liquid-to-solid ratio of 0.20 w/v. The moisture content has been measured using an MB23 moisture analyzer. The semibatch Eirich EL1 type intensive mixer was used for mixing. The samples were homogeneously mixed with deionized water at the fixed rotation speed (600 rpm) and time (20 min). Later, the samples were left to hydrate/cure in sealed and vacuumed containers at room temperature (10 ± 0.5 h) and were compacted in the next step using a hydraulic press into cylinders with a diameter of 20 mm and height of 20 ± 1 mm.

Table 1. Labeling of Monolithic Specimens (UC: Uncarbonated, C: Carbonated)

Composition	UC	C
OSFA (100%)	x 4	x 4
WFA (100%)	x 4	x 4
90% OSFA + 10% NS	x 4	x 4
90% WFA + 10% NS	x 4	x 4

NS (10 wt %) was incorporated into samples in a dry form after the first hydration period of ash samples and mixed for a fixed time (10 min) as calcium aluminate-bearing slags cause rapid hydration and hardening, which do not allow for a long waiting period before press forming. As press molding of samples was carried out with a manual (hand-operated) hydraulic press, serious attention was given to the uniform preparation of samples. NS powder has lower compressibility compared to the ash samples which affects the compaction ability of the sample based on the ratio of mix. The optimum compaction pressure of 300 ± 10 kg/cm^2 was selected based on the optimum workability, as lower compaction can result in low rigidity and effects the green strength of the samples before carbonation while higher compaction can inhibit carbonation as samples become less porous. Carbonation experiments were performed in an automated carbonation unit (stainless-steel 400 mL jacketed pressure vessel), consisting of apparatus controlling temperature (Circulator C-400). Furthermore, the carbonation experiments tests were performed under a controlled humidity environment using a potassium iodide saturated solution, which inhibits excessive humid conditions and maintains a relative humidity between 60 and 70% at room temperature. The optimum curing parameters (5 bar, 100% CO_2, 25 °C, 4 h) were selected based on previously conducted parametric studies.[5]

Samples for MIP tests were prepared after the curing stage by taking crushed pieces up to 5 mm × 5 mm × 5 mm from inside and outside the cylindrical samples making the selection as homogeneous as possible. To stop the hydration, these pieces were twice submerged in ethanol for 24 h. The samples were dried in an oven at 60 °C after being treated with ethanol to remove the solvent.

2.2.2. Physical Characterization. The carbonation efficiency and capacity tend to increase with decreasing particle size of fly ash due to two main reasons: first, smaller particles have a larger surface area which promotes carbonation reactions, and second, smaller particle size facilitates the release of metal ions such as Ca^{2+} and Mg^{2+}.[5050] PSD analysis of samples indicated that OSFA with a mean particle size of 17.97 μm has a smaller particle size compared to WFA, which has a mean particle size of 26.84 μm (Table 1). However, the surface area of WFA is 3 times higher than OSFA (Table 2) due to the presence of unburned carbon which potentially plays a role in increasing the specific surface area by providing more active sites for chemical reactions and adsorption.[51] NS has a much higher mean particle size compared to FAs (Figure

https://doi.org/10.1021/acsomega.3c03286
ACS Omega 2023, 8, 29543−29557

Table 2. D_{10}, D_{50}, and D_{90} Values of PSD and BET SSA of Samples

	D_{10} (μm)	D_{50} (μm)	D_{90} (μm)	BET SSA (m^2/g)
OSFA	8.63	17.97	36.23	3.18
WFA	9.65	26.84	65.68	9.81
NS	33.61	99.87	204.38	0.34

1) with lower SSA due to its high-temperature production process, which causes melting and pore blocking.[49]

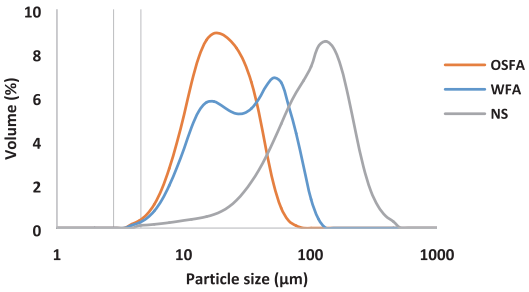

Figure 1. Particle size distribution (PSD) diagram of OSFA, WFA, and NS samples.

2.2.3. Chemical Characterization. The FAs generally showed a high sulfate content which is the primary focus of the selection of these ashes. The main phases in the powdered samples of both FAs included quartz, calcite, and lime. For OSFA, the main sulfate-containing phase is anhydrite while in WFA the main sulfate phase is arcanite. Moreover, free CaO content indicates their potential for CO_2 sequestration, as CaO is the optimal feedstock for CO_2 mineral carbonation (Table 3). OSFA exhibited slightly higher free CaO content compared to WFA which is another factor affecting the cementitious properties and CO_2 uptake. Organic contents of ashes are low as seen from total organic carbon (TOC) values which were calculated based on the values of total carbon (TC) and total inorganic carbon (TIC) (see Table 3). Most of the carbon in the ash belongs to the mineral CO_2. OSFA has a much higher SiO_2 content of 25.21% compared to WFA (3.38%) (Table 3). WFA contained apatite which was not in the OSFA sample. The initial phase composition is not reproduced here as XRD analysis of monoliths is discussed in Section 3.

The presence of quartz in fly ash can provide a surface for the amorphous silica and alumina to nucleate, which can enhance the pozzolanic activity of the fly ash.[52] A higher percentage of Al_2O_3 (9.41%) in OSFA can contribute to the formation of ettringite. The NS is mainly containing calcium aluminates with a small amount of NbO_5 staying in the slag. The unburned carbon content restriction for FA to be used in construction varies based on the intended use and local building codes. However, a common standard for the unburned carbon content in fly ash used in concrete is less than 3%.[53] Typically, WFA has a higher content of heavy metals compared to OSFA. Heavy metals such as Zn, Mn, Cu, and Ba are found in the WFA samples while NS is generally lacking in trace elements (Table 3). OSFA contained Zn, Pb, Ni, Cr, and Ba however in lower concentrations compared to WFA. The effect of carbonation on heavy-metal leaching is discussed in Section 3.2.

Table 3. Chemical Composition of OSFA, WFA, and NS (Including TIC, TOC, and Free CaO)[a]

sample	OSFA	WFA	NS
LOI (wt %)	12.85	21.87	–
MgO (wt %)	3.21	5.5	–
Al_2O_3 (wt %)	9.41	1.01	69.24
SiO_2 (wt %)	25.21	3.38	0.31
P_2O_5 (wt %)	0.22	5.4	–
SO_3 (wt %)	4.66	7.85	0.08
Cl (wt %)	0.43	0.87	0.1
K_2O (wt %)	3.13	7.66	–
CaO (wt %)	36.77	44.89	24.26
TiO_2 (wt %)	0.44	0.08	–
Fe_2O_3 (wt %)	3.2	0.63	1.19
F (wt %)	0.2	–	–
NbO_5 (wt %)	–	–	4.74
Zn (ppm)	160	2300	–
Sr (ppm)	330	530	370
Rb (ppm)	170	110	–
Pb (ppm)	160	–	–
Ni (ppm)	50	–	160
Mn (ppm)	–	2000	–
Cu (ppm)	–	220	–
Cr (ppm)	100	–	–
Ba (ppm)	480	890	–
TIC (%)	1.25	2.65	–
TC (%)	1.39	3.32	–
TOC (%)	0.14	0.67	–
free CaO (%)	20.37	18.84	–

[a]Note: The "–" symbol represents nonexistent or not applicable data.

3. RESULTS AND DISCUSSION

The mechanical, mineralogical, and microstructural features of the monoliths were examined using various techniques such as TGA, XRD, MIP, and SEM-EDS analysis to understand the effects of carbonation and NS addition (Section 3.1). The subsequent analysis focuses on the leaching properties, particularly sulfate leaching, which is the primary emphasis of this paper and is evaluated based on the results of the mineralogical and microstructural analysis (Section 3.2).

3.1. Effect of Carbonation and NS Addition on Mineralogy and Microstructure. *3.1.1. General Overview of Strength and CO_2 Uptake.* In the case of FAs, strength is partially created by the precipitation of carbonate minerals (mainly calcite (eq 1)), which fills the porous structures between the particles and bonds the individual glassy FA particles together.[54] OSFA and WFA monoliths had initial compressive strengths of 11.8 MPa and 9.8 MPa before curing (see Figure 2), respectively. Uibu et al. studied OSA-based concrete development resulting in strength development of up to 14 MPa for CFBC ash after 28 days which shows that the pozzolanic hydration process continues.[55] It is also known that due to the self-cementitious and pozzolanic capabilities of FAs, especially high-calcium FAs with calcium oxide contents higher than 15% in phase composition, an increase in compressive strength can occur as early as 3 days after mixing.[56]

$$Ca(OH)_2 + CO_2 \rightarrow CaCO_3 + H_2O \quad (1)$$

After 4 h carbonation curing it increases almost 4 times to 41.5 MPa for OSFA and 45.1 MPa for WFA monoliths. It should be kept in mind that strength development cannot be solely attributed to calcite formation during carbonation, the

https://doi.org/10.1021/acsomega.3c03286
ACS Omega 2023, 8, 29543−29557

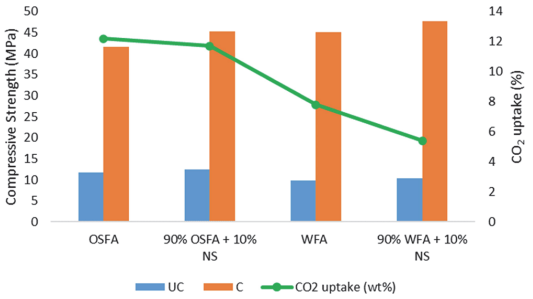

Figure 2. Compressive strength results of uncarbonated (UC) and carbonated (C) OSFA, WFA, and NS-added monoliths.

production of hydrated compounds such as CSH continues, contributing to an overall increase in strength. There is an overall higher strength increase in WFA monoliths compared to OSFA monoliths after carbonation despite a lower amount of CO_2 uptake.

NS as an additive further increased the strength to an average of 45.3 MPa for OSFA and 47.7 MPa for WFA. NS addition increases the strength of the UC sample up to 10% before curing and a further increase is followed by carbonation curing. NS introduces calcium aluminates which act as a supplier of aluminum that reacts during the alkaline activation of aluminosilicate materials, resulting in the creation of binding calcium (aluminate) silicate hydrate (CASH) gels that promote the rapid development of strength.[57−59]

According to the TGA/DTG curves of uncarbonated samples (Figure 3), the main steps in the mass loss process are as follows; the first step is related to water loss from evaporation and later dehydration of crystalline and amorphous components, such as ettringite (AFt) (up to 140 °C)[60,61] and calcium-silicate hydrate (CSH), or calcium aluminate hydrate (CAH), the second is the dehydration of $Ca(OH)_2$ (410−460 °C), and the third is CO_2 loss from the decomposition of $CaCO_3$ (600−800 °C). In UC OSFA, a slightly higher peak of ettringite decomposition is observed between 100 and 130 °C compared to C and NS-added samples. Similarly in WFA decomposition around 80 °C was lower in NS-added samples compared to C and UC samples. This finding suggests that CO_2 curing either slowed the formation of AFt, CSH, and CAH or caused their phase change. In both samples, mass loss between 200 and 370 °C can be attributed to CSH decomposition as well as continuing decomposition of monosulfate after ettringite decomposes.[60,62] In carbonated OSFA samples, the NS-added sample shows higher mass loss due to the decomposition of $Ca(OH)_2$ and lower mass loss in the decomposition of $CaCO_3$ compared to the carbonated sample which indicates a slight negative effect

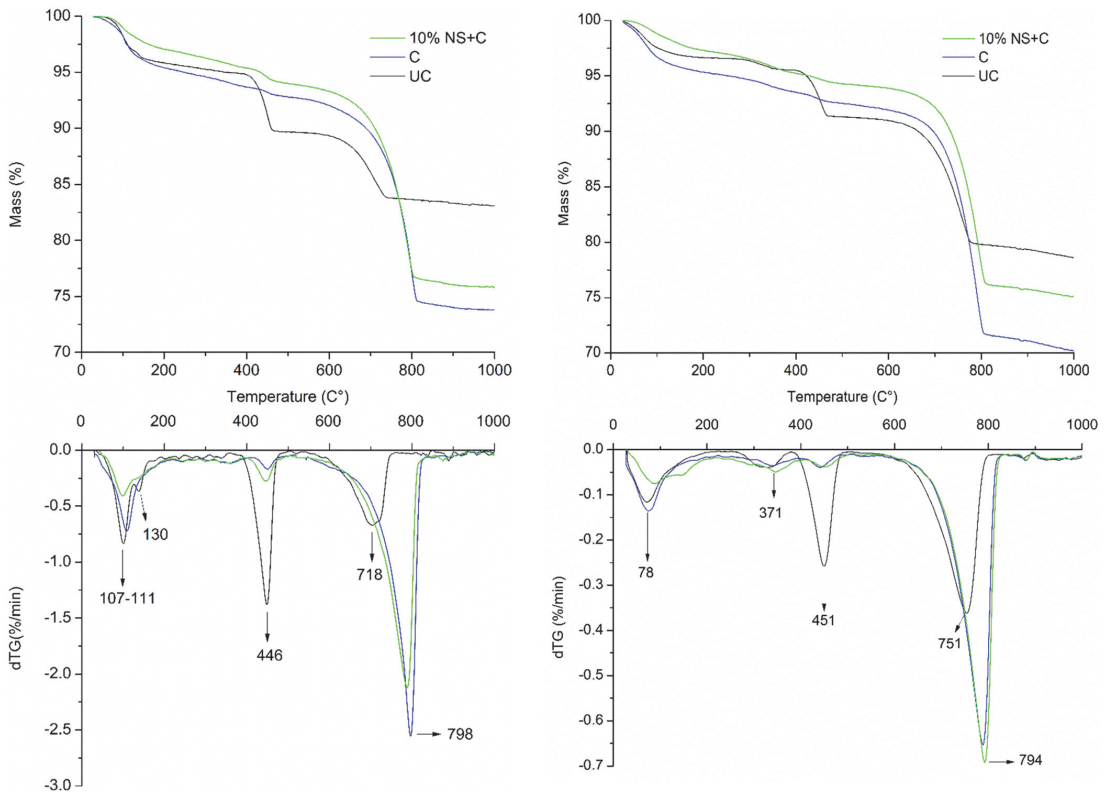

Figure 3. TGA and DTG patterns of OSFA (left) and WFA (right) compacts that are uncarbonated (UC), carbonated (C), and niobium slag-added (10% NS + C).

https://doi.org/10.1021/acsomega.3c03286
ACS Omega 2023, 8, 29543−29557

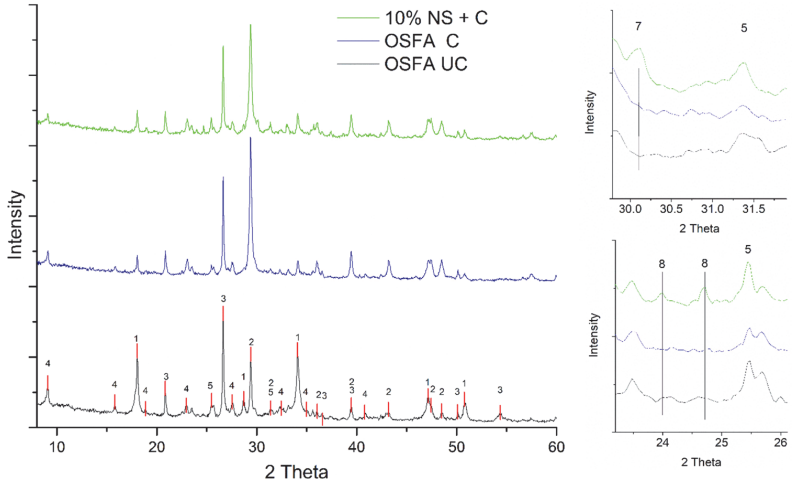

Figure 4. XRD patterns of OSFA samples (1—portlandite, 2—calcite, 3—quartz, 4—ettringite, 5—anhydrite, 7—CAH, 8—CAS).

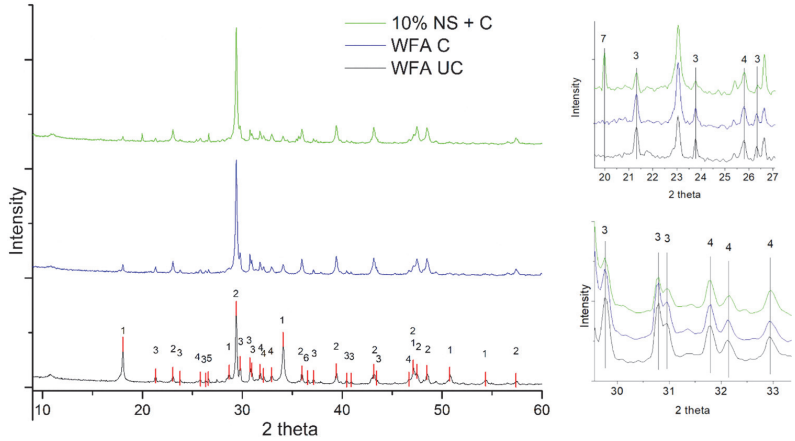

Figure 5. XRD patterns of WFA samples (1—portlandite, 2—calcite, 3—arcanite, 4—hydroxyapatite, 5—quartz, 6—periclase, 7—CAH).

of NS on carbonation. The initial (uncarbonated) mineral CO_2-associated mass loss is taken into consideration to determine the net CO_2 absorption. The net CO_2 uptake of the 100% OSFA sample is 12.2% and NS-added OSFA sample is 11.7%. 100% WFA sample and NS-added WFA samples are 7.8 and 5.4%, respectively. Lower CO_2 uptake of NS-added samples can be explained by the fast hydration of calcium aluminates changing pore structures causing less available surface area and a lower percentage of portlandite, which is the main phase contributing to carbonation, due to the replacement of ash with NS.

3.1.2. Mineralogical Characterization. 3.1.2.1. XRD Analysis. XRD analysis of monoliths made of OSFA and WFA together with NS-added monoliths is performed to see the changes in the phases after carbonation and NS addition. The main constituents in OSFA UC monoliths include portlandite, calcite, and quartz, while smaller peaks of ettringite, anhydrite, orthoclase, and hematite were identified (Figures 4 and 5). The main changes identified after the carbonation of OSFA monoliths included the intensity of portlandite as well as anhydrite peaks which are less intense in carbonated monoliths while showing higher intensity in NS-added monoliths. Ettringite formation (eq 2) occurs during the hydration period of samples which is supported by the XRD pattern as well as the TGA of the UC OSFA samples. It is created when calcium and alumina, both of which are present in cementitious matrices and supplementary cementitious materials (in this case NS), react with sulfate, which is either naturally present in the cement paste or is introduced into the system from an outside source[63−65] Delayed formation of ettringite can be harmful to ordinary cement systems; however, in calcium aluminate cement systems, ettringite formed during hydration is typically the most significant hydrate and is substantially in charge of these systems' unique characteristics, including quick setting, quick hardening, quick drying, and compensating for shrinkage.[66] Decomposition of ettringite is observed after carbonation which can form in addition to calcium carbonate, gypsum, and alumina gel.[67] In comparison to anhydrite and

https://doi.org/10.1021/acsomega.3c03286
ACS Omega 2023, 8, 29543−29557

ettringite, gypsum is more soluble, releasing more sulfates into the carbonated OSFA monolith's leachate.

$$3CaO{\cdot}Al_2O_3 + 26H_2O + 3CaSO_4{\cdot}2H_2O \rightarrow 3CaO{\cdot}Al_2O_3{\cdot}3CaSO_4{\cdot}32H_2O \quad (2)$$

$$3CaO{\cdot}Al_2O_3{\cdot}3CaSO_4{\cdot}32H_2O + 3CO_2 = 3CaCO_3 + 3(CaSO_4{\cdot}2H_2O) + Al_2O_3{\cdot}xH_2O + (26 - x)H_2O \quad (3)$$

In NS-added monoliths, calcium aluminate hydrate peaks as well as partial conversion of ettringite to amorphous phases are observed. The partial reduction of ettringite can also be observed in TGA patterns (Figure 3). The main sulfate-bearing phases are, namely, arcanite for WFA and anhydrite for OSFA. Ettringite formation in WFA monoliths during the hydration period is observed to be lower compared to OSFA. This can be explained by the lower Al content in WFA and the different behavior of sulfate-bearing phases (arcanite and anhydrite) in both ashes. In NS-added monoliths of WFA, the intensity of arcanite peaks is lower compared to UC and C monoliths which could indicate the binding of sulfates in amorphous calcium aluminate phases observed by SEM-EDS analysis (Figures 8 and 9). Hydroxyapatite which is also (Figure 5) observed in WFA monoliths can be partially responsible for high compressive strength values (Figure 2).[68] Changes in the CAS phases are discussed in Section 3.2 and explained in greater detail with the aid of additional figures, in conjunction with the sulfate leaching process. However, it can be difficult to determine the exact phases due to the amorphous nature and complex structure of the material.

3.1.3. Microstructural Characterization. 3.1.3.1. MIP Analysis. Pore structure and porosity are additional crucial elements that identify the physical strength of solidified structures. To investigate the impact of carbonation on the microstructure of the hardened monoliths, mercury intrusion porosimetry (MIP) was used to estimate the pore size distribution of the OSFA and WFA monoliths. A nonwetting liquid (one with a contact angle larger than 90°) will only infiltrate capillaries under pressure, according to the theory underlying MIP. Washburn as cited by Diamond[69] explains the relationship between pressure and capillary diameter (eq 4)

$$P = \frac{4\gamma \cos\theta}{d} \quad (4)$$

where P is the pressure, γ is the surface tension of the liquid, θ is the contact angle of the liquid (140° is selected), and d is the diameter of the capillary. The volume intruded at each pressure increment is used to calculate the pore size distribution. The entire volume of intruded pores is used to calculate total porosity. It should be noted that the MIP technique measures pore entrance size rather than pore size,[70] only the open porosity is determined using the MIP technique currently in use. The "ink-bottle effect" is a phenomenon that causes big pores to be underestimated and small pores to be overestimated.[71] The degree to which hydrated cementitious materials are porous depends mainly on the fineness of the particles, the water-to-solid ratio, the method of mixing, and the curing circumstances.

The MIP analysis revealed that OSFA monoliths exhibit a decline in macropores upon carbonation,[72] causing the associated compressive strength to rise from 11.8 to 41.5 MPa (Figures 6 and 7). Total porosity diminishes with increasing calcite deposition as well as the filling effect of

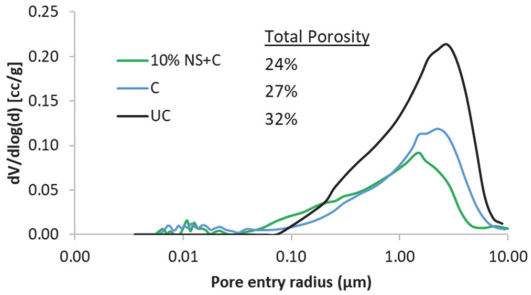

Figure 6. OSFA pore size distribution with total porosity values.

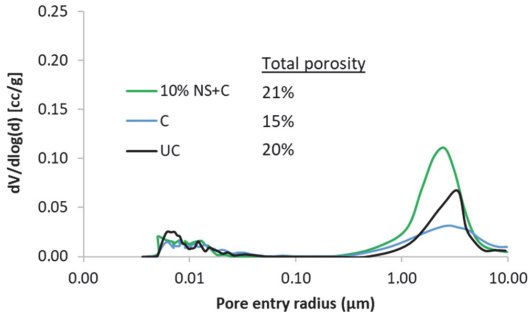

Figure 7. WFA pore size distribution with total porosity values.

hydrated phases, and the decline becomes more significant. Calcite is deposited on the inside of pores as well as at their entry during carbonation, obstructing some of these pores and blocking mercury infiltration. NS-added carbonated monoliths showed slightly lower macropores compared to carbonated OSFA monoliths. Upon carbonation, a partial decrease in ettringite can cause an overall increase in porosity due to its high molecular volume and low density. In the case of OSFA, this effect is mitigated by the subsequent formation of calcite polymorphs. In the case of WFA, the carbonation effect is also clear in the reduction of macropores. However, NS-added WFA monoliths showed higher macropores compared to 100% WFA monoliths which can be explained by the particle size difference between NS which has much coarser particles, and WFA, affecting pore mouth formations during hydration. The reason for the lower total porosity values in monoliths made from WFA compared to OSFA may be attributed to the different compaction properties of the ashes, which results in a denser structure upon compaction for WFA.

3.1.3.2. SEM-EDS Analysis. The morphological changes and chemical composition were identified by SEM images (1000–5000 times magnified) and EDS analysis of UC, C, and NS-added monoliths, which are reproduced in greater detail and attached as the Supporting Information to this publication. An image of the OSFA UC monolith with hexagonal lamellar portlandite crystals can be seen in Figure 8. The particles have a gritty appearance with some stubby laths and noticeable big pores. The EDS of UC monoliths reveals that the products are an amalgam of calcium and oxygen, validating the elemental

https://doi.org/10.1021/acsomega.3c03286
ACS Omega 2023, 8, 29543−29557

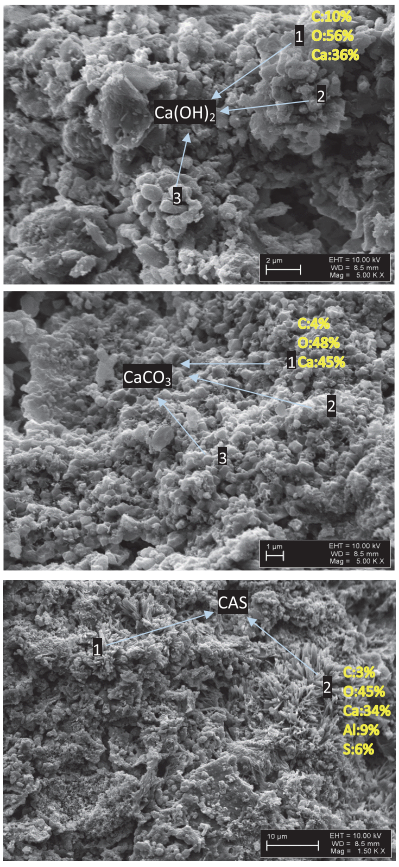

Figure 8. SEM images and numbered positions for quantitative EDS analysis of OSFA uncarbonated (top), carbonated (middle), and niobium slag-added (bottom).

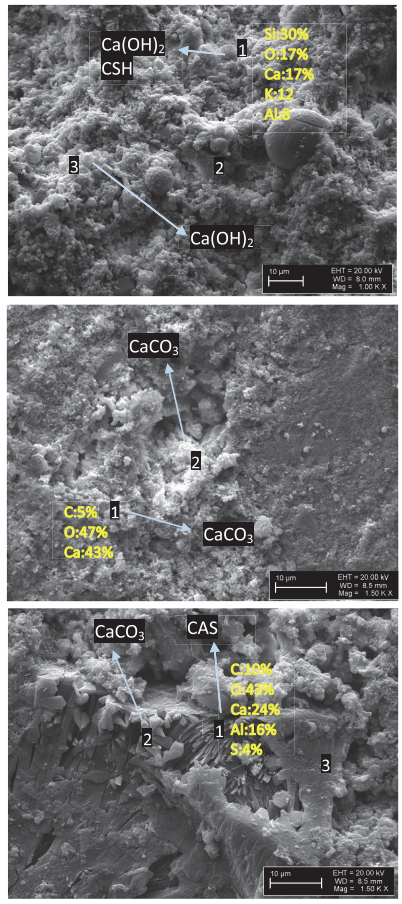

Figure 9. SEM images and numbered positions for quantitative EDS analysis of WFA uncarbonated (top), carbonated (middle), and niobium slag-added (bottom).

ratio for $Ca(OH)_2$ crystals. In the WFA UC image, spherical glassy FA particles surrounded by hydrated products can be clearly identified. In OSFA C monolith Polymorphs of calcium carbonate precipitated on carbonation in acicular and globular formation intermixed with decalcified C−S−H or silica gel. While carbonated WFA monoliths have shown Calcite formations like OSFA monoliths, smoother gel-like surfaces were more abundant with less porous structure (Figure 9) in WFA monoliths. EDS has shown, some of these areas include a mix of many elements in combined amorphous matrixes.

NS-added monoliths have exhibited needle-like CAS crystal growths in addition to calcite polymorphs (Figures 8 and 9). WFA monoliths were observed to be much denser in general and less porous compared to OSFA monoliths which are in line with MIP analysis results (Figures 6 and 7). SEM investigations along the sample depth of the carbonated monoliths have revealed that clusters of portlandite crystals are present only in the deeper part of the monolith. There are two tenable explanations for this imperfect conversion that work in tandem. The first is that the initial carbonated layer provides a macroscopic layer that inhibits the CO_2 gas diffusion to the portlandite crystals. Due to the pore closure brought on by the precipitation of bigger $CaCO_3$ crystals (36.9 cm^3/mol) than $Ca(OH)_2$ crystals (33.6 cm^3/mol) on the pore throats, it is anticipated that this carbonated layer will be less permeable.[73,74] The second reason can be due to the enhanced carbonation reaction's exothermic nature and the reduced hydrophilicity of $CaCO_3$ crystals compared to $Ca(OH)_2$ crystals, there is not enough water present for the reaction to take place.[75]

3.2. Effect of Carbonation and Niobium Slag Addition to Leaching Properties. *3.2.1. Sulfate Leaching.* The release of hazardous substances into the environment is one of the most crucial factors for waste disposal in landfills or reuse. The Criteria and Procedures for The Acceptance of Waste at Landfills established in the Council Directive 1999/31/EC of 26 April 1999[76] gives criteria for waste landfills, in which the wastes sent to landfill are classified into three categories, "inert," "nonhazardous" and "hazardous" in terms of their leachability and stability. For sulfates, leaching limits for these landfills are 1000, 20 000, and 50 000 mg/kg of waste, respectively.

https://doi.org/10.1021/acsomega.3c03286
ACS Omega 2023, 8, 29543−29557

As $Ca(OH)_2$ becomes depleted in the monoliths of OSFA, pH steadily declines from around 12.8 at the initial stage to around 11.4 as demonstrated by the pH measurements of the subsequent leachates (Figure 10). For WFA, a similar decrease

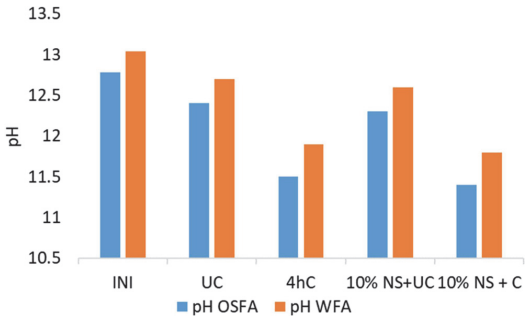

Figure 10. pH values of OSFA and WFA monoliths together with initial ash samples (INI).

in pH levels from an initial 13.1 to around 11.8 is observed. pH levels for OSFA and WFA UC monoliths are in the range of 12.3−12.7 which decreases after carbonation to the range of 11.4−11.9. It is noted that after NS addition pH still decreases compared to UC NS-added monolith, which supports that the carbonation reaction is not fully hindered. The stability domain for sulfate ettringite commonly lies between 10.5 and 13 at the various pH ranges described in the literature.[77,78]

Sulfate leaching tests revealed that for 100% OSFA sulfate concentration is increased from 2260 mg/kg to 6510 mg/kg after carbonation (Figure 11). However, 10% NS-added OSFA monoliths showed no detectable sulfate leaching for both uncarbonated and carbonated monoliths. Increased leaching of sulfates in carbonated OSFA monoliths was seen compared to uncarbonated ones due to the carbonation of ettringite. The addition of 10% NS reduced the leaching of sulfate to an undetectable range (less than 2 mg SO_4^{2-}/kg of ash) and it stayed in that range after carbonation as well, which shows the addition of NS is successful at curbing the negative effect of carbonation in sulfate leaching for OSFA monoliths. WFA exhibited much higher sulfate leaching levels compared to OSFA, which can be due to already higher initial concentration in WFA and higher solubility of arcanite compared to anhydrite.[79] Ettringite and other CAS formation in WFA monoliths during the hydration period is observed to be much lower compared to OSFA monoliths. In contrast to OSFA, WFA did not display an increase in leached sulfate upon carbonation which can be explained by the lack of ettringite formation which is the main cause of the increase in sulfate leaching in OSFA. Yet, in WFA monoliths slight decrease after carbonation is observed, which can be due to the physical encapsulation of sulfates with the formation of calcite. In WFA, NS addition significantly lowers sulfate leaching concentration before carbonation and a further decline is observed after carbonation. The decline of around 14 000 mg SO_4^{2-}/kg of ash with the addition of NS and carbonation compared to 100% WFA concentration is also considerably high in WFA.

The rapid hydration of calcium aluminates can provide an initial source of calcium ions, which can promote the carbonation of FA by providing a surface for the carbon dioxide to react. This can potentially enhance the carbonation potential of FAs and increase the sequestration of carbon dioxide in the cementitious system.[57] Additionally, it is important to note that the rapid hydration of calcium aluminates can also lead to the formation of CAS phases, which can consume sulfate ions and reduce the availability of these ions for sulfate mobility.

SEM images of NS-added monoliths together with mineralogical analysis are examined in connection with sulfate leaching. When niobium slag is added, the system's mineralogical state changes along with the chemistry of the hydrated phases, which can have a significant impact on the bound sulfate (Figures 12 and 13). In general, it can be deduced that both carbonation and NS addition have effects on the mobility of sulfates in OSFA and WFA which can be associated with chemical and physical changes in the monolith microstructure. This mechanism involves complex interrelated microstructural, mechanical, and CSH chemistry considerations.[80,81] According to clinker mineralogy, the hydrated phases include AFt, AFm, and CSH. Ettringite crystals fix SO_4, while AFm and CSH phases also help fix heavy metals in the matrix.[82,83] Figure 11 shows a SEM image of the NS-added OSFA monolith with sections of the XRD pattern including known peaks of CAS. Peaks of ettringite are still stable after carbonation however less in NS-added monoliths. Also, other peaks of different phase structures of CAS become more visible with NS addition. For OSFA, it can be deduced that different phases of CAS are seen along with anhydrite becoming more stable in the NS-added monoliths. According to Xu et al., the presence of anhydrite increases the stability of ettringite compared to other sources of calcium sulfate.[84] For WFA, a similar SEM image of NS-added monolith shows the clearer

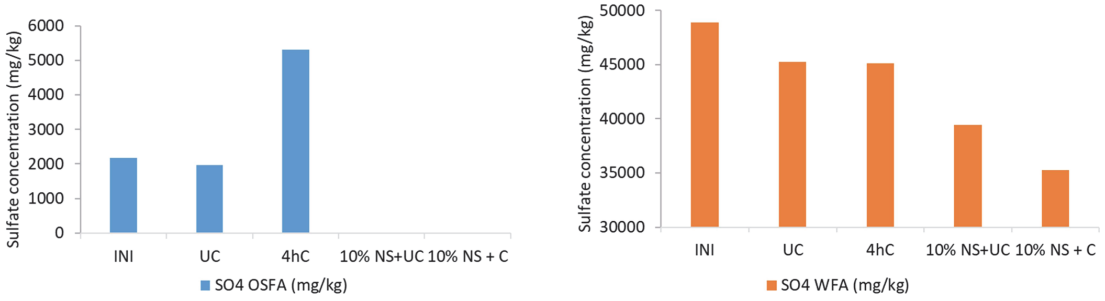

Figure 11. SO_4^{2-} Leaching values of OSFA (left) and WFA (right) monoliths together with initial ash samples (INI).

https://doi.org/10.1021/acsomega.3c03286
ACS Omega 2023, 8, 29543−29557

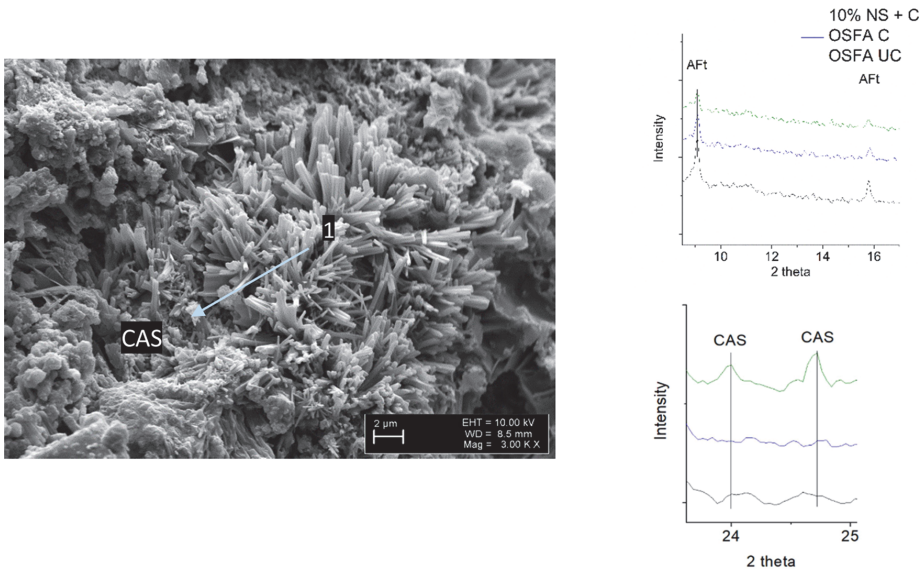

Figure 12. SEM image of NS-added OSFA with sections of XRD pattern detailing CAS peaks.

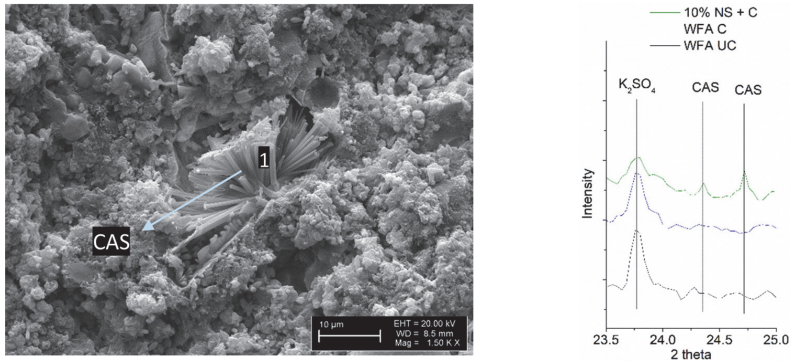

Figure 13. SEM image of NS-added WFA with sections of XRD pattern detailing K_2SO_4 and CAS peaks.

structure of needle-like formation, with sections of XRD pattern including arcanite and CAS phases. In WFA monoliths, sulfate-bearing arcanite seemed to be in less intensity and CAS phases are more distinguishable in the case of NS addition.

According to the mineralogical analysis, the highly soluble minerals halite and sylvite contain chloride ions. As a result, as indicated in Figure 14, the chloride release values from monoliths are lower than the landfill limits for nonhazardous wastes. Carbonation has slightly decreased Cl^- leaching concentrations for both OSFA and WFA monoliths. NS addition has decreased the mobility of Cl^- greatly for WFA and a further decrease occurred after the carbonation of NS-added monoliths. It can be said that both SO_4^{2-} and Cl^- mobility in WFA monoliths exhibited a similar trend after the NS addition and carbonation process. For OSFA Cl^- leaching values were not greatly affected by the NS addition or carbonation process. All Cl^- leaching levels are under the landfill limit for nonhazardous wastes which is 15 000 mg/kg of waste.

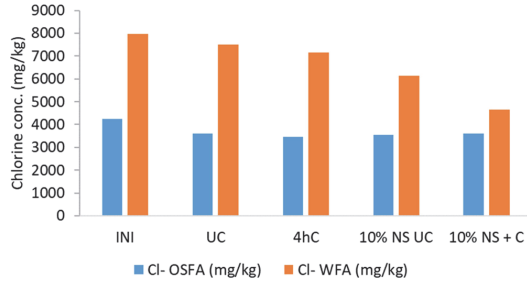

Figure 14. Cl^- leaching values of OSFA and WFA monoliths together with initial sample (INI).

Leaching results indicate that after carbonation curing, for OSFA the levels of Cr, Cu, and Zn, and for WFA the level of Ba slightly increased (Table 4). However, all of the heavy-metal leaching values were reduced with the addition of NS.

https://doi.org/10.1021/acsomega.3c03286
ACS Omega 2023, 8, 29543−29557

Table 4. Leaching Levels of Trace Elements in OSFA and WFA Ash and Monoliths with Landfill Limits (ppm)[a]

	OSFA				WFA					
	INI	UC	C	10% NS + C	INI	UC	C	10% NS + C	inert	nonhazardous
Ba	5.4	4.5	4.1	5.1	1.4	1	1.3	0.4	20	100
Cd	tr	tr	tr	tr	tr	tr	tr	tr	0.04	1
Cr	1	1.4	2	0	5.2	5.2	4.5	3.4	0.5	10
Cu	2.9	1	1.5	0.4	2.2	1.2	1	1	2	50
Mn	tr	tr	tr	tr	tr	tr	tr	tr	na	na
Ni	tr	tr	tr	tr	tr	tr	tr	tr	0.4	10
Pb	tr	tr	tr	tr	tr	tr	tr	tr	0.5	10
Rb	11.2	10.7	3.3	3	321.8	301.2	257.2	145.8	na	na
Sr	157.6	108.1	46.7	31.8	33.9	27.3	12.8	4.2	na	na
Zn	5.8	0.5	3.8	tr	4.7	tr	tr	tr	4	50

[a]tr = trace amount, na = not applicable.

For heavy metals, all of the leaching values are under the limit for landfills for nonhazardous waste. For OSFA, the limit values also for landfilling inert waste were not breached except for Cr, Cu, and Zn which were all under the limit in the NS-added monoliths. For WFA monoliths Cr was the only element that stayed above the inert landfill limit, while Zn and Cu were under the limit for uncarbonated samples. Mobility of Sr and Rb was greatly reduced after carbonation and NS addition for both WFA and OSFA monoliths. Irha et al.[85] and Uibu et al.[55] have addressed the leaching behaviors of various types of OSFA as well as OSFA-based mortars. Although the leachates under study were highly alkaline and saturated with various ions (the predominant ions were Ca^{2+}, K^{+}, Na^{+}, and SO_4^{2-}), their research shows that during the curing process, the fraction of readily soluble inorganic components reduced while the mobility of potentially hazardous Cd and Zn did not change. EC values exhibit a decrease with carbonation due to the carbonated layer reducing the availability of free ions in the material, which are responsible for conducting electricity (Figure 15). The formation of the carbonated layer also

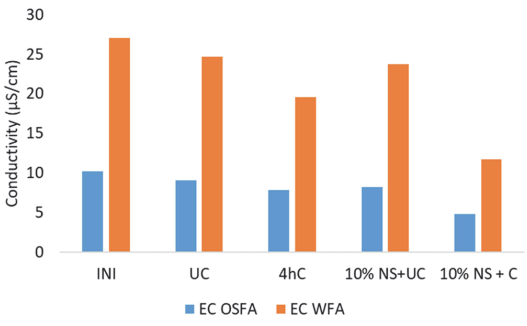

Figure 15. EC values of OSFA and WFA monoliths together with initial sample (INI).

reduces the porosity of the material, which can further limit the movement of ions and contribute to the reduction in EC. As a result of changes in the chemical composition and physical characteristics of the FA monoliths brought on by carbonation and the addition of NS, ions as well as heavy metals get immobilized, limiting the availability of these for EC.

4. DISCUSSION

Worldwide, there is a growing trend among industries to produce and apply cement-free or low-carbon building materials that are strengthened through carbonation. Despite the growing interest in the use of FA as an SCM or in general construction applications, the utilization of HSFA remains largely unexplored.[86] CO_2 mineralization processes could benefit from using alternative HSFA streams, particularly those not meeting the relevant standards (as per ASTM C618), as raw materials.[87]

A comparative analysis of CO_2 uptake across various studies reveals a broad spectrum of results, primarily contingent upon the specific material under investigation. For instance, Srivastava et al. reported CO_2 uptake values of ∼18 to 21% for Basic Oxygen Furnace slags after a reaction time of 4 h.[88] Conversely, electric arc furnace slag exhibited a more gradual increase in CO_2 uptake, ranging from 7 to 12% over the same duration. While Mo et al. reported that steel slag pastes carbonated at 0.1 MPa CO_2 for 24 h reached levels of CO_2 uptake between 11 and 17%.[89]

In the case of fly ash, Li et al. reported a substantial variation in CO_2 uptake, ranging from 6 to 21%, which was attributed to the different CaO contents in the Coal Fly Ash.[90] Class C Fly Ash, with a CaO content of 15−50%, carbonates rapidly and possesses sufficient strength for structural construction, thereby presenting a higher potential for CO_2 sequestration than Class F Fly Ash, which contains 1.5−5% CaO.[91,92] Zhang et al. developed an eco-cement from municipal solid waste residue and $Ca(OH)_2$, which demonstrated a CO_2 uptake of around 8%.[93] In a separate study, cement kiln dust, characterized by its high CaO content (20−60%), demonstrated a CO_2 uptake ranging from 4 to 8%.[94] The CO_2 sequestration potential of industrial solid wastes depends on their alkalinity content and various operating parameters associated with the carbonation process, as well as the waste production process affecting its physical and chemical characteristics.

In this context, the CO_2 uptake capacities achieved in this study are noteworthy. Specifically, the capacities range from 11.7 to 12.2% for OSFA and from 5.4 to 7.8% for WFA. These figures are not only comparable to those reported in other studies but are also crucial because the addition of niobium slag (NS) did not significantly hinder the carbonation potential of the residues, while it mitigated sulfate leaching. These findings highlight the feasibility of repurposing underutilized wastes such as HSFAs to produce construction materials

https://doi.org/10.1021/acsomega.3c03286
ACS Omega 2023, 8, 29543−29557

through accelerated carbonation. This approach aligns with broader goals of waste management and carbon sequestration, further emphasizing the importance of this study.

5. CONCLUSIONS

This study analyzes the environmental and microstructural properties of carbonate-bonded monoliths composed of HSFA and niobium slag NS enriched with calcium aluminate. A significant finding of our research is the considerable increase in the initial compressive strength of the monoliths post-carbonation (up to 41.5 MPa for OSFA and 45.1 MPa for WFA), which underlines the potential of this method for enhancing the structural integrity of HSFA-based construction materials. In addition, our findings reveal that the inclusion of NS leads to a further increase in strength without substantially impacting CO_2 uptake. This is a noteworthy discovery as it suggests that NS can be employed to bolster the mechanical properties of HSFA-based materials without impeding their carbon sequestration potential. Another key finding of our study is the general decline in leaching values, particularly sulfates and heavy metals, upon the introduction of NS. This suggests that the addition of NS can effectively immobilize harmful substances in HSFA. The experimental results of this study can be summarized as follows.

- The pH change is not solely dependent on the consumption of portlandite since carbonation curing slightly decreased the leachate pH due to the prolonged hydration reactions as well as the chemical and mineralogical composition of different FAs.
- MIP showed a decrease in macropores in carbonated and NS-added OSFA monoliths. In WFA monoliths the overall porosity was lower compared to OSFA, while NS addition did not decrease macropores due to particle size difference.
- For NS-added OSFA and WFA monoliths, all of the heavy-metal levels are reduced with the ion-stabilizing effect of hydrated calcium aluminate silicate gel.
- Anhydrite-bearing OSFA monoliths showed increased formation of ettringite compared to arcanite-bearing WFA monoliths.
- In NS-added monoliths, anhydrite, arcanite, ettringite, and different CAS phases are identified as main sulfate-bearing phases through SEM-EDS and XRD analyses.

Based on these findings, it can be concluded that the leaching of sulfates is effectively mitigated through a dual mechanism involving both the chemical binding to calcium aluminate silicate (CAS) phases and the physical entrapment within the structure of calcium aluminate silicate hydrate (CA(S)H) gels.

This research effectively showcases the potential of upcycling HSFAs through the outlined carbonation method incorporating calcium aluminate-rich NS. This process not only presents an opportunity to utilize these waste materials in the construction industry but also demonstrates significant sulfate immobilization as a key finding.

■ ASSOCIATED CONTENT

Supporting Information

The Supporting Information is available free of charge at https://pubs.acs.org/doi/10.1021/acsomega.3c03286.

Quantitative EDS analysis tables corresponding to Figures 8 and 9 (PDF)

■ AUTHOR INFORMATION

Corresponding Author

Mustafa Cem Usta − *Department of Materials and Environmental Technology, Tallinn University of Technology, 19086 Tallinn, Estonia;* orcid.org/0000-0003-3021-2656; Email: mustafa.usta@taltech.ee

Authors

Can Rüstü Yörük − *Department of Materials and Environmental Technology, Tallinn University of Technology, 19086 Tallinn, Estonia*

Mai Uibu − *Department of Materials and Environmental Technology, Tallinn University of Technology, 19086 Tallinn, Estonia*

Reiner Traksmaa − *Department of Mechanical and Industrial Engineering, Tallinn University of Technology, 19086 Tallinn, Estonia*

Tiina Hain − *Department of Civil Engineering and Architecture, Tallinn University of Technology, 19086 Tallinn, Estonia*

Andre Gregor − *Department of Materials and Environmental Technology, Tallinn University of Technology, 19086 Tallinn, Estonia*

Andres Trikkel − *Department of Materials and Environmental Technology, Tallinn University of Technology, 19086 Tallinn, Estonia*

Complete contact information is available at: https://pubs.acs.org/10.1021/acsomega.3c03286

Notes

The authors declare no competing financial interest.

■ ACKNOWLEDGMENTS

This work was carried out as part of a Ph.D. project supported by the Estonian Ministry of Education and Research (IUT33-19). This work was partially supported by ASTRA "TUT Institutional Development Program for 2016−2022" Graduate School of Functional Materials and Technologies. The help of Mart Viljus (SEM images) and Oliver Jarvik is gratefully acknowledged.

■ REFERENCES

(1) *ASTM C618: Standard Specification for Coal Fly Ash and Raw or Calcined Natural Pozzolan for Use in Concrete* ASTM International: West Conshohocken, PA; 2022.

(2) *EN 450-1: Fly Ash for Concrete − Definition, Specifications, and Conformity Criteria* British Standards Institution: London, U.K.; 2012.

(3) *JIS R 5213: Portland Fly-Ash Cement (Amendment 1)* Japanese Standards Association: Tokyo, Japan; 2009.

(4) Usta, M. C.; Yörük, C. R.; Hain, T.; Paaver, P.; Snellings, R.; Rozov, E.; Uibu, M.; et al. Evaluation of New Applications of Oil Shale Ashes in Building Materials. *Minerals* **2020**, *10*, 765.

(5) Usta, M. C.; Yörük, C. R.; Uibu, M.; Hain, T.; Gregor, A.; Trikkel, A. CO2 Curing of Ca-Rich Fly Ashes to Produce Cement-Free Building Materials. *Minerals* **2022**, *12*, 513.

(6) Socié, A.; Dubois, F.; Monerie, Y.; Neji, M.; Perales, F. Simulation of Internal and External Sulfate Attacks of Concrete with a Generic Reactive Transport-poromechanical Model. *Eur. J. Environ. Civ. Eng.* **2022**, 1−28.

(7) Neto, J. S. A.; Angeles, G.; Kirchheim, A. P. Effects of Sulfates on the Hydration of Portland Cement−A Review. *Constr. Build. Mater.* **2021**, *279*, No. 122428.

(8) Kaladharan, G.; Rajabipour, F. Evaluation and Beneficiation of High Sulfur and High Alkali Fly Ashes for Use as Supplementary

Cementitious Materials in Concrete. *Constr. Build. Mater.* **2022**, *339*, No. 127672.
(9) Papadakis, V. G.; Tsimas, S. Supplementary Cementing Materials in Concrete: Part I: Efficiency and Design. *Cem. Concr. Res.* **2002**, *32*, 1525−1532.
(10) Hou, P. K.; Qian, J. S.; Wang, Z.; Deng, C. Production of Quasi-sulfoaluminate Cementitious Materials with Electrolytic Manganese Residue. *Cem. Concr. Compos.* **2012**, *34*, 248−254.
(11) Zhang, Y.; Wang, J.; Zhang, L.; Li, C.; Jiang, H.; Ba, X.; Hou, D. Study on the Preparation and Properties of High-belite Cementitious Materials from Shield Slag and Calcium Carbide Slag. *Constr. Build. Mater.* **2022**, *355*, No. 129082.
(12) European Union. Regulation (EU) No 305/2011 of the European Parliament and of the Council of 9 March 2011. Laying Down Harmonised Conditions for the Marketing of Construction Products and Repealing Council Directive 89/106/EEC, 2011. http://data.europa.eu/eli/reg/2011/305/oj.
(13) Ragipani, R.; Escobar, E.; Prentice, D.; Bustillos, S.; Simonetti, D.; Sant, G.; Wang, B. Selective sulfur removal from semi-dry flue gas desulfurization coal fly ash for concrete and carbon dioxide capture applications. *Waste Manage.* **2021**, *121*, 117−126.
(14) Wang, W.; Luo, Z.; Shi, Z.; Cen, K. Thermodynamic analysis of ash mineral phases in combustion of high-sulfur coal with lime. *Ind. Eng. Chem. Res.* **2011**, *50*, 3064−3070.
(15) Duc, N. V. Experimental Water Quality Analysis from the Use of High Sulfuric Fly Ash as Base Course Material for Road Building. *Eng. Technol. Appl. Sci. Res.* **2019**, *9*, 4627−4630.
(16) Shin, J. H.; Park, J. H. Formation mechanism of oxide-sulfide complex inclusions in high-sulfur-containing steel melts. *Metall. Mater. Trans. B* **2018**, *49*, 311−324.
(17) Singh, A. K.; Chandra, R. Pollutants released from the pulp paper industry: Aquatic toxicity and their health hazards. *Aquat. Toxicol.* **2019**, *211*, 202−216.
(18) Luong, L. D.; Nguyen, D. V.; Luu, H. T.; Le, H. V.; Nguyen, T. M. Study on fluidized bed combustion fly ash with high sulfur from Cao Ngan coal-fired thermal power plant for production of construction materials. *Vietnamese J. Sci. Technol.* **2010**, *1*−*2*, 8−16.
(19) Shon, C. S.; Saylak, D.; Mishra, S. In *Evaluation of Manufactured Fluidized Bed Combustion Ash Aggregate as Road Base Coarse Material*, World of Coal Ash Conference, Denver, USA, May 9−12, 2011.
(20) Gazdič, D.; Fridrichova, M.; Kulisek, K.; Vehovska, L. The potential use of the FBC ash for the preparation of blended cements. *Procedia Eng.* **2017**, *180*, 1298−1305.
(21) Xie, X. M.; Guo, L. In *Study on Preparation and Properties of Fly Ash Concrete with High Sulfur and High-Calcium Fly*, 2nd IEEE International Conference on Information Management Engineering, Chengdu, China, April 16−18, 2010.
(22) Bogush, A. A.; Stegemann, J. A.; Roy, A. Changes in composition and lead speciation due to water washing of air pollution control residue from municipal waste incineration. *J. Hazard. Mater.* **2019**, *361*, 187−199.
(23) Yang, Z.; Tian, S.; Ji, R.; Liu, L.; Wang, X.; Zhang, Z. Effect of water-washing on the co-removal of chlorine and heavy metals in air pollution control residue from MSW incineration. *Waste Manage.* **2017**, *68*, 221−231.
(24) Martin, L. H. J.; Winnefeld, F.; Tschopp, E.; Müller, C. J.; Lothenbach, B. Influence of Fly Ash on the Hydration of Calcium Sulfoaluminate Cement. *Cem. Concr. Res.* **2017**, *95*, 152−163.
(25) Zhang, S.; Wang, R.; Xu, L.; Hecker, A.; Ludwig, H. M.; Wang, P. Properties of Calcium Sulfoaluminate Cement Mortar Modified by Hydroxyethyl Methyl Celluloses with Different Degrees of Substitution. *Molecules* **2021**, *26*, 2136.
(26) Skibsted, J.; Snellings, R. Reactivity of supplementary cementitious materials (SCMs) in cement blends. *Cem. Concr. Res.* **2019**, *124*, No. 105799.
(27) Trincal, V.; Thiéry, V.; Mamindy-Pajany, Y.; Hillier, S. Use of hydraulic binders for reducing sulphate leaching: application to gypsiferous soil sampled in Ile-de-France region (France). *Environ. Sci. Pollut. Res.* **2018**, *25*, 22977−22997.
(28) Sadique, M.; Al-Nageim, H.; Atherton, W.; Seton, L.; Dempster, N. Analytical investigation of hydration mechanism of a non-Portland binder with wastepaper sludge ash. *Constr. Build. Mater.* **2019**, *211*, 80−87.
(29) Bolaños-Vásquez, I.; Trauchessec, R.; Tobón, J. I.; Lecomte, A. Influence of the ye'elimite/anhydrite ratio on PC-CSA hybrid cements. *Mater. Today Commun.* **2020**, *22*, No. 100778.
(30) Bizzozero, J.; Gosselin, C.; Scrivener, K. L. Expansion mechanisms in calcium aluminate and sulfoaluminate systems with calcium sulfate. *Cem. Concr. Res.* **2014**, *56*, 190−202.
(31) Le Saoût, G.; Lothenbach, B.; Taquet, P.; Fryda, H.; Winnefeld, F. Hydration of calcium aluminate cement blended with anhydrite. *Adv. Cem. Res.* **2018**, *30*, 24−36.
(32) Rungchet, A.; Poon, C. S.; Chindaprasirt, P.; Pimraksa, K. Synthesis of Low-Temperature Calcium Sulfoaluminate-Belite Cements from Industrial Wastes and Their Hydration: Comparative Studies between Lignite Fly Ash and Bottom Ash. *Cem. Concr. Compos.* **2017**, *83*, 10−19.
(33) Mrak, M.; Winnefeld, F.; Lothenbach, B.; Dolenec, S. The Influence of Calcium Sulfate Content on the Hydration of Belite-Calcium Sulfoaluminate Cements with Different Clinker Phase Compositions. *Mater. Struct.* **2021**, *54*, 212.
(34) Luo, Z. T.; Ma, B. G.; Yu, Z. Q. Influence of heavy metal Pb on hydration and leaching toxicity of sulphoaluminate cement. *J. Qingdao Technol. Univ.* **2009**, *30*, 130−133.
(35) Liu, W.; Teng, L.; Rohani, S.; Qin, Z.; Zhao, B.; Xu, C. C.; Liang, B.; et al. CO2 Mineral Carbonation Using Industrial Solid Wastes: A Review of Recent Developments. *Chem. Eng. J.* **2021**, *416*, No. 129093.
(36) Roychand, R.; Li, J.; Kilmartin-Lynch, S.; Saberian, M.; Zhu, J.; Youssf, O.; Ngo, T. Carbon Sequestration from Waste and Carbon Dioxide Mineralisation in Concrete−A Stronger, Sustainable and Eco-Friendly Solution to Support Circular Economy. *Constr. Build. Mater.* **2023**, *379*, No. 131221.
(37) Van Gerven, T.; Van Keer, E.; Arickx, S.; Jaspers, M.; Wauters, G.; Vandecasteele, C. Carbonation of MSWI-bottom ash to decrease heavy metal leaching, in view of recycling. *Waste Manage.* **2005**, *25*, 291−300.
(38) Baciocchi, R.; Costa, G.; Lategano, E.; Marini, C.; Polettini, A.; Pomi, R.; Postorino, P.; Rocca, S. Accelerated carbonation of different size fractions of bottom ash from RDF incineration. *Waste Manage.* **2010**, *30*, 1310−1317.
(39) Ashraf, M. S.; Ghouleh, Z.; Shao, Y. Production of Eco-Cement Exclusively from Municipal Solid Waste Incineration Residues. *Resour. Conserv. Recycl.* **2019**, *149*, 332−342.
(40) Valls, S.; Vazquez, E. Accelerated carbonatation of sewage sludge−cement−sand mortars and its environmental impact. *Cem. Concr. Res.* **2001**, *31*, 1271−1276.
(41) Venhuis, M. A.; Reardon, E. J. Vacuum method for carbonation of cementitious wasteforms. *Environ. Sci. Technol.* **2001**, *35*, 4120−4125.
(42) Lange, L. C.; Hills, C. D.; Poole, A. B. Effect of carbonation on properties of blended and non-blended cement solidified waste forms. *J. Hazard. Mater.* **1997**, *52*, 193−212.
(43) Bergmans, J.; Nielsen, P.; Snellings, R.; Broos, K. Recycling of Autoclaved Aerated Concrete in Floor Screeds: Sulfate Leaching Reduction by Ettringite Formation. *Constr. Build. Mater.* **2016**, *111*, 9−14.
(44) Wang, L.; Jin, Y.; Nie, Y. Investigation of Accelerated and Natural Carbonation of MSWI Fly Ash with a High Content of Ca. *J. Hazard. Mater.* **2010**, *174*, 334−343.
(45) Li, X.; Bertos, M. F.; Hills, C. D.; Carey, P. J.; Simon, S. Accelerated Carbonation of Municipal Solid Waste Incineration Fly Ashes. *Waste Manage.* **2007**, *27*, 1200−1206.
(46) Auvere Power Plant. Affordable, Versatile, Sustainable. https://www.enefit.com/technology/power-production (accessed October 5, 2022).
(47) Utilitas Tallinn. https://www.utilitas.ee/en/company/as-utilitas-tallinn/ (accessed October 5, 2022).

https://doi.org/10.1021/acsomega.3c03286
ACS Omega 2023, 8, 29543−29557

(48) Neo Performance Materials https://www.neomaterials.com/ (accessed October 5, 2022).
(49) Gorkunov, V.; Munter, R. In *Possibilities of Utilization of Waste Slags from Niobium Production*, Proceedings of International Conference: Eco-Balt' 2007, Riga, May 10−11, 2007.
(50) Polettini, A.; Pomi, R.; Stramazzo, A. Carbon sequestration through accelerated carbonation of BOF slag: Influence of particle size characteristics. *Chem. Eng. J.* **2016**, *298*, 26−35.
(51) Kassahun, E.; Mekuria, S.; Beyan, S. M. Specific Surface Area Enhancement of Waste Tire-Based Activated Carbon by Demineralization Technique and Adsorption of Methylene Blue. *Int. J. Chem. Eng.* **2022**, *2022*, 1−15.
(52) Soutsos, M. N.; Tang, L. The effect of silica fume and fly ash on the hydration of calcium aluminate cement. *Cem. Concr. Res.* **2005**, *35*, 949−954.
(53) *ASTM C618: Standard Specification for Coal Fly Ash and Raw or Calcined Natural Pozzolan for Use in Concrete* ASTM International: West Conshohocken, PA; 2012.
(54) Van Gerven, T.; Moors, J.; Dutre, V.; Vandecasteele, C. Effect of CO2 on leaching from a cement-stabilized MSWI fly ash. *Cem. Concr. Res.* **2004**, *34*, 1103−1109.
(55) Uibu, M.; Somelar, P.; Raado, L.-M.; Irha, N.; Hain, T.; Koroljova, A.; Kuusik, R. Oil shale ash based backfilling concrete − strength development, mineral transformations and leachability. *Constr. Build. Mater.* **2016**, *102*, 620−630.
(56) Siddique, R.; Iqbal Khan, M. Fly Ash. In *Supplementary Cementing Materials. Engineering Materials*; Springer: Berlin, 2011; Vol. 37.
(57) Pyatina, T.; Sugama, T.; Moon, J.; James, S. Effect of tartaric acid on hydration of a sodium-metasilicate-activated blend of calcium aluminate cement and fly ash F. *Materials* **2016**, *9*, 422.
(58) Zhang, Y.; Zhang, H.; Zhang, X. Influence of calcined flue gas desulfurization gypsum and calcium aluminate on the strength and AFt evolution of fly ash blended concrete under steam curing. *Materials* **2021**, *14*, 7171.
(59) García-Maté, M.; De la Torre, A. G.; León-Reina, L.; Aranda, M. A. G.; Santacruz, I. Hydration studies of calcium sulfoaluminate cements blended with fly ash. *Cem. Concr. Res.* **2013**, *54*, 12−20.
(60) Scrivener, K.; Snellings, R.; Lothenbach, B. *A Practical Guide to Microstructural Analysis of Cementitious Materials*; CRC Press: Boca Raton, FL, 2016; Vol. *540*.
(61) Taylor, H. F. *Cement Chemistry*; Thomas Telford: London, 1997.
(62) Collier, N. C.; Sharp, J. H.; Milestone, N. B.; Hill, J.; Godfrey, I. H. The Influence of Water Removal Techniques on the Composition and Microstructure of Hardened Cement Pastes. *Cem. Concr. Res.* **2008**, *38*, 737−744.
(63) Chrysochoou, M.; Dermatas, D. Evaluation of Ettringite and Hydrocalumite Formation for Heavy Metal Immobilization: Literature Review and Experimental Study. *J. Hazard. Mater.* **2006**, *136*, 20−33.
(64) Xu, L.; Wang, P.; Zhang, G. Formation of Ettringite in Portland Cement/Calcium Aluminate Cement/Calcium Sulfate Ternary System Hydrates at Lower Temperatures. *Constr. Build. Mater.* **2012**, *31*, 347−352.
(65) Hou, W.; Liu, J.; Liu, Z.; He, F.; Zhu, J.; Cui, Y.; Jinyang, W. Calcium Transfer Process of Cement Paste for Ettringite Formation under Different Sulfate Concentrations. *Constr. Build. Mater.* **2022**, *348*, No. 128706.
(66) Amathieu, L.; Touzo, B. Ettringite Binder for Dense Mortar, Comprising Calcium Sulphates and a Mineral Compound of Calcium Aluminates. U.S. Patent US20070094919A1, 2007.
(67) Chen, B.; Horgnies, M.; Huet, B.; Morin, V.; Johannes, K.; Kuznik, F. Comparative Kinetics Study on Carbonation of Ettringite and Meta-Ettringite Based Materials. *Cem. Concr. Res.* **2020**, *137*, No. 106209.
(68) Chung, C. W.; Lee, J. Y.; Kim, J. H. Formation of Hydroxyapatite in Portland Cement Paste. *J. Korea Inst. Build. Constr.* **2014**, *14*, 68−75.
(69) Diamond, S. Mercury Porosimetry: An Inappropriate Method for the Measurement of Pore Size Distributions in Cement-Based Materials. *Cem. Concr. Res.* **2000**, *30*, 1517−1525.
(70) Abell, A. B.; Willis, K. L.; Lange, D. A. Mercury Intrusion Porosimetry and Image Analysis of Cement-Based Materials. *J. Colloid Interface Sci.* **1999**, *211*, 39−44.
(71) Cizer, Ö.; Van Balen, K.; Elsen, J.; Van Gemert, D. Real-time Investigation of Reaction Rate and Mineral Phase Modifications of Lime Carbonation. *Constr. Build. Mater.* **2012**, *35*, 741−751.
(72) Pham, S. T.; Prince, W. Effects of Carbonation on the Microstructure of Cement Materials: Influence of Measuring Methods and of Types of Cement. *Int. J. Concr. Struct. Mater.* **2014**, *8*, 327−333.
(73) Chen, B.; Laucks, M. L.; Davis, E. J. Carbon Dioxide Uptake by Hydrated Lime Aerosol Particles. *Aerosol Sci. Technol.* **2004**, *38*, 588−597.
(74) Uibu, M.; Kuusik, R. Main Physicochemical Factors Affecting the Aqueous Carbonation of Oil Shale Ash. *Miner. Eng.* **2014**, *59*, 64−70.
(75) Matschei, T.; Lothenbach, B.; Glasser, F. P. Thermodynamic Properties of Portland Cement Hydrates in the System CaO−Al2O3−SiO2−CaSO4−CaCO3−H2O. *Cem. Concr. Res.* **2007**, *37*, 1379−1410.
(76) Nair, K. S.; Kumar, S. Sulfate Induced Heave: Addressing Ettringite Behavior in Lime Treated Soils and in Cementitious Materials, Ph.D. Thesis, Texas A&M University, 2010.
(77) Baquerizo, L. G.; Matschei, T.; Scrivener, K. L. Impact of Water Activity on the Stability of Ettringite. *Cem. Concr. Res.* **2016**, *79*, 31−44.
(78) Bertos, M. F.; Li, X.; Simons, S. J. R.; Hills, C. D.; Carey, P. J. Investigation of Accelerated Carbonation for the Stabilization of MSW Incinerator Ashes and the Sequestration of CO2. *Green Chem.* **2004**, *6*, 428−436.
(79) Ptacek, C.; Blowes, D. Predicting Sulfate-mineral Solubility in Concentrated Waters. *Rev. Mineral. Geochem.* **2000**, *40*, 513−540.
(80) Xu, L.; Wu, K.; Rößler, C.; Wang, P.; Ludwig, H. M. Influence of Curing Temperatures on the Hydration of Calcium Aluminate Cement/Portland Cement/Calcium Sulfate Blends. *Cem. Concr. Compos.* **2017**, *80*, 298−306.
(81) Telesca, A.; Marroccoli, M.; Pace, M. L.; Tomasulo, M.; Valenti, G. L.; Monteiro, P. J. M. A Hydration Study of Various Calcium Sulfoaluminate Cements. *Cem. Concr. Compos.* **2014**, *53*, 224−232.
(82) Pelletier-Chaignat, L.; Winnefeld, F.; Lothenbach, B.; Le Saout, G.; Müller, C. J.; Famy, C. Influence of the Calcium Sulfate Source on the Hydration Mechanism of Portland Cement−Calcium Sulphoaluminate Clinker−Calcium Sulfate Binders. *Cem. Concr. Compos.* **2011**, *33*, 551−561.
(83) Seo, J.; Nawaz, A.; Jang, J. G.; Lee, H. K. Modifications in Hydration Kinetics and Characteristics of Calcium Aluminate Cement upon Blending with Calcium Sulfoaluminate Cement. *Constr. Build. Mater.* **2022**, *342*, No. 127958.
(84) Xu, L.; Wang, P.; Zhang, G. Calorimetric Study on the Influence of Calcium Sulfate on the Hydration of Portland Cement−Calcium Aluminate Cement Mixtures. *J. Therm. Anal. Calorim.* **2012**, *110*, 725−731.
(85) Irha, N.; Uibu, M.; Jefimova, J.; Raado, L.-M.; Hain, T.; Kuusik, R. Leaching Behaviour of Estonian Oil Shale Ash-based Construction Mortars. *Oil Shale* **2014**, *31*, 394.
(86) Nawaz, M.; Indraratna, B.; Sivakumar, M. Geopolymers in construction - recent developments. *Constr. Build. Mater.* **2020**, *260*, No. 120472.
(87) Ragipani, R.; Escobar, E.; Prentice, D. P.; Bustillos, S.; Simonetti, D. A.; Sant, G.; Wang, B. Selective sulfur removal from semi-dry flue gas desulfurization coal fly ash for concrete and carbon dioxide capture applications. *Waste Manage.* **2021**, *121*, 391−403.
(88) Srivastava, S.; Snellings, R.; Cool, P. Clinker-free Carbonate-bonded (CFCB) Products Prepared by Accelerated Carbonation of

Steel Furnace Slags: A Parametric Overview of the Process Development. *Constr. Build. Mater.* **2021**, *303*, No. 124556.
(89) Mo, L.; Zhang, F.; Deng, M. Mechanical Performance and Microstructure of the Calcium Carbonate Binders Produced by Carbonating Steel Slag Paste under CO2 Curing. *Cem. Concr. Res.* **2016**, *88*, 217−226.
(90) Li, N.; Mo, L.; Unluer, C. Emerging CO2 Utilization Technologies for Construction Materials: A Review. *J. CO_2 Util.* **2022**, *65*, No. 102237.
(91) Wei, Z.; Wang, B.; Falzone, G.; La Plante, E. C.; Okoronkwo, M. U.; She, Z.; et al. Clinkering-free Cementation by Fly Ash Carbonation. *J. CO_2 Util.* **2018**, *23*, 117−127.
(92) Meng, J.; Liao, W.; Zhang, G. Emerging CO2-mineralization Technologies for Co-utilization of Industrial Solid Waste and Carbon Resources in China. *Minerals* **2021**, *11*, 274.
(93) Zhang, S.; Ghouleh, Z.; Shao, Y. Green Concrete Made from MSWI Residues Derived Eco-cement and Bottom Ash Aggregates. *Constr. Build. Mater.* **2021**, *297*, No. 123818.
(94) Kaliyavaradhan, S. K.; Ling, T. C.; Mo, K. H. Valorization of Waste Powders from Cement-concrete Life Cycle: A Pathway to Circular Future. *J. Cleaner Prod.* **2020**, *268*, No. 122358.

https://doi.org/10.1021/acsomega.3c03286
ACS Omega 2023, 8, 29543−29557

Appendix 4

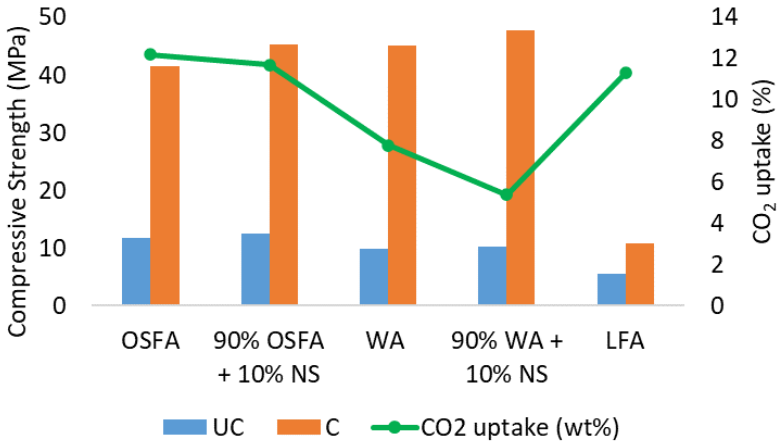

Figure 13. Compressive strength and CO_2 uptake values for monoliths that are uncarbonated (UC) and carbonated (C), incorporating OSA, WA, and added NS as well as LFA.

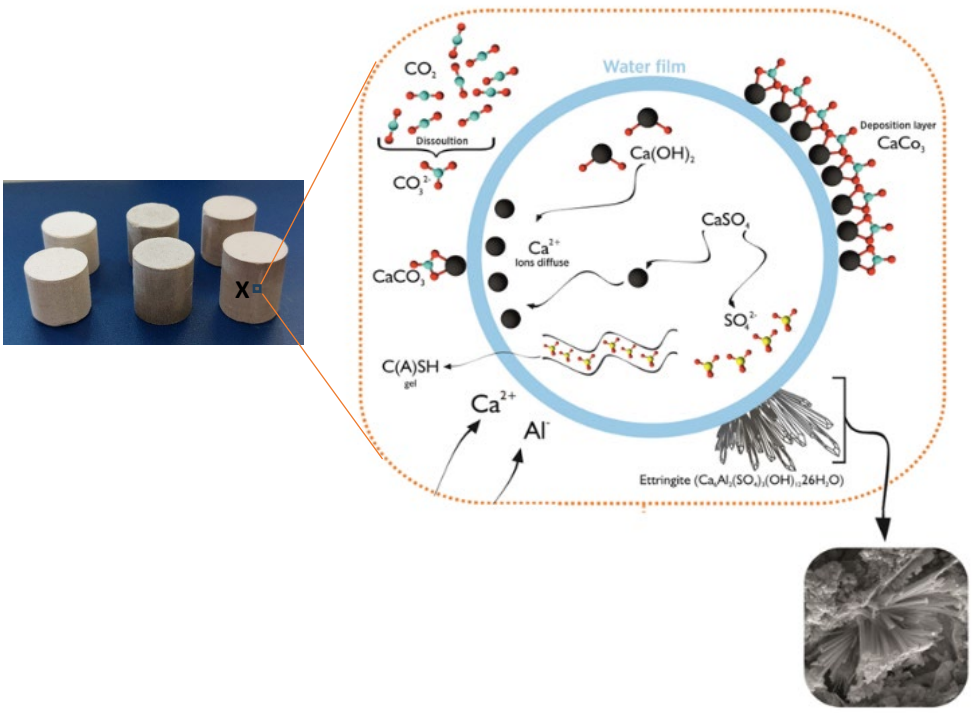

Figure 14. Schematic representation of mechanism during accelerated carbonation process of prepared monoliths.

Curriculum vitae

Personal data

Name:	Mustafa Cem Usta
Date of birth:	15/12/1990
Place of birth:	Kayseri/Turkey
Citizenship:	Turkish

Contact data

E-mail: ustacem@gmail.com

Education

2019–2023	Tallinn University of Technology, Chemical and Materials Technology – PhD
2017–2019	Tallinn University of Technology, Environmental Engineering and Management – MSc, *summa cum laude*
2010–2016	Middle East Technical University, Mining Engineering – BSc
2005–2009	Sami Yangin Anatolian High School – High School Degree

Language competence

Turkish	Native
English	Fluent
German	Intermediate
Estonian	Basic

Professional employment

2019–Ongoing	Junior Researcher	Laboratory of Inorganic Materials, Tallinn University of Technology

Conference Participation

2019–2022	Graduate School of Functional Materials and Technologies (GSFMT), Tallinn University of Technology and Tartu University, Estonia. Oral and poster presentations
2021	17th International Conference on Environmental Science and Technology CEST2021, Athens, Greece. Springer
2021	International Conference on Accelerated Carbonation for Environmental and Material Engineering (ACEME), Tallinn, Estonia
2019	2nd Journal of Thermal Analysis and Calorimetry Conference and 7th V4 (Joint Czech-Hungarian-Polish-Slovakian) Thermoanalytical Conference, Budapest, Hungary

Defended Dissertations

2019	*MSc thesis:* Experimental Study of CO_2 Mineralization in Burnt Oil Shale and Cement Bypass Dust Based Systems. Supervisors: Dr. Can Rüştü Yörük, Dr. Mai Uibu

Research projects

VFP17114EK	"CLEAN clinKER production by Calcium looping process"
LEKEE23002	"Testing of masonry units based on carbonated bottom ashes"
IUT33-19	"Fundamentals of multicomponent mineral-organic systems: Chemistry, modelling and sustainable processing"

Supervised dissertations

2021	Ademola Michael Adegbile, Master's Degree, (supervisors: Dr. Can Rüstü Yörük; Mustafa Cem Usta), Performance evaluation of flue gas/CO_2 cured calcium-rich fly ash based building blocks/materials, Tallinn University of Technology School of Engineering, Department of Materials and Environmental Technology

List of publications

Usta, M. C., Yörük, C. R., Uibu, M., Traksmaa, R., Hain, T., Gregor, A., & Trikkel, A. (2023). Carbonation and Leaching Behaviors of Cement-Free Monoliths Based on High-Sulphur Fly Ashes with the Incorporation of Amorphous Calcium Aluminate. *ACS omega*, *8*(32), 29543–29557. https://doi.org/10.1021/acsomega.3c03286

Usta, M. C., Yörük, C. R., Uibu, M., Hain, T., Gregor, A., & Trikkel, A. (2022). CO_2 Curing of Ca-Rich Fly Ashes to Produce Cement-Free Building Materials. *Minerals*, *12*(5), 513. https://doi.org/10.3390/min12050513

Usta, M. C., Yörük, C. R., Hain, T., Paaver, P., Snellings, R., Rozov, E., ... & Uibu, M. (2020). Evaluation of new applications of oil shale ashes in building materials. *Minerals*, *10*(9), 765. https://doi.org/10.3390/min10090765

Yörük, C. R., Uibu, M., Usta, M. C., Kaljuvee, T., & Trikkel, A. (2020). CO_2 mineralization by burnt oil shale and cement bypass dust: effect of operating temperature and pre-treatment. *Journal of Thermal Analysis and Calorimetry*, *142*, 991–999. https://doi.org/10.1007/s10973-020-09349-9

Usta, M. C., Uibu, M., Yörük, C. R., Tamm, K., Kuusik, R., Trikkel, A., ... & Canonico, F. (2021, March). Mineral sequestration of CO2 from Vernasca Ca-looping demo system: scale up to a pilot. In *Proceedings of the 15th Greenhouse Gas Control Technologies Conference* (pp. 15–18). https://dx.doi.org/10.2139/ssrn.3812245

Usta, M. C., Adegbile, A. M., Gregor, A., Paaver, P., Hain, T., Yörük, C. R., Uibu, M., & Trikkel, A. (2021). Performance evaluation of flue gas cured calcium rich fly ash based building blocks. Proceedings of the 17th International Conference on Environmental Science and Technology CEST2021. Springer. https://doi.org/10.30955/gnc2021.00333

Elulookirjeldus

Isiklikud andmed

Nimi:	Mustafa Cem Usta
Sünnikuupäev:	15.12.1990
Sünnikoht:	Kayseri/Türgi
Kodakondsus:	Türgi

Kontaktandmed

E-post:	ustacem@gmail.com

Hariduskäik

2019–2023	Tallinna Tehnikaülikool, Keemilise ja Materjalitehnoloogia – PhD
2017–2019	Tallinna Tehnikaülikool, Keskkonnatehnika ja -juhtimine – MSc, *summa cum laude*
2010–2016	Middle East Technical University, Kaevandusinsener – BSc
2005–2009	Sami Yangin Anatolian Highschool – Gümnaasiumi lõputunnistus

Keelteoskus

Türgi	Emakeel
Inglise	Väga hea
Saksa	Kesktase
Eesti	Algaja

Professionaalne töökogemus

2019–jätkub	Nooremteadur Anorgaaniliste Materjalide Labor, Tallinna Tehnikaülikool

Konverentside osalemine

2019–2022	Doktorikool Funktsionaalsed Materjalid ja Tehnoloogiad (GSFMT), Tallinna Tehnikaülikool ja Tartu Ülikool, Eesti. Suulised ja postriettekanded
2021	17. Rahvusvaheline Keskkonnateaduste ja -tehnoloogia Konverents CEST2021, Ateena, Kreeka. Springer
2021	Rahvusvaheline Konverents Kiirendatud Karboniseerimise kohta Keskkonna- ja Materjalitehnika jaoks (ACEME), Tallinn, Eesti
2019	2. Soojusanalüüsi ja Kalorimeetria Ajakirja Konverents ja 7. V4 (Ühine Tšehhi-Ungari-Poola-Slovakkia) Termoanalüütiline Konverents, Budapest, Ungari

Kaitstud lõputööd

2019	Magistritöö: CO_2 Mineraalimise Eksperimentaalne Uuring Põletatud Põlevkivi ja Tsemendi Kõrvalsaaduste Baasil. Juhendajad: Dr. Can Rüştü Yörük, Dr. Mai Uibu

Teadusprojektid

VFP17114EK	“CLEAN clinKER tootmine Calcium looping protsessi abil”
LEKEE23002	“Karboniseeritud põhjatuha baasil müüritise ühikute testimine”
IUT33-19	“Mitmekomponentsete mineraal-orgaaniliste süsteemide alused: Keemia, modelleerimine ja jätkusuutlik töötlemine”

Juhendatud lõputööd

2021	Ademola Michael Adegbile, Magistrikraad, (juhendajad: Dr. Can Rüştü Yörük; Mustafa Cem Usta), Heitgaasi/CO_2 kõvastunud kaltsiumirikaste lendtuha baasil ehitusmaterjalide jõudluse hindamine, Tallinna Tehnikaülikooli Inseneriteaduskond, Materjalide ja Keskkonnatehnoloogia Instituut

ISSN 2585-6901 (PDF)
ISBN 978-9916-80-068-3 (PDF)